SCHOOL OF CHEMISTRY
CARDIFF UNIVERSITY

Organic Molecules, Dendrimers and Sulfur-based Polymers of Intrinsic Microporosity

Thesis submitted for the degree of Doctor of Philosophy by:

Rupert George Drummond Taylor

Supervisor: Neil B. McKeown   2013

Declaration

This work has not been submitted in substance for any other degree or award at this or any other university or place of learning, nor is it being submitted concurrently in candidature for any degree or other award.

Signed …………………………………… (candidate)   Date …………………………

Statement 1

This thesis is being submitted in partial fulfilment of the requirements for the degree of Doctor of Philosophy.

Signed …………………………………… (candidate)   Date …………………………

Statement 2

This thesis is the result of my own independent work/investigation, except where otherwise stated. Other sources are acknowledged by explicit references. Any views expressed are my own.

Signed …………………………………… (candidate)   Date …………………………

Statement 3

I hereby give consent for my thesis, if accepted, to be available for photocopying and for inter-library loan, and for the title and summary to be made available to outside organisations.

Signed …………………………………… (candidate)   Date …………………………

Acknowledgements

First and foremost, I would like to thank my supervisor, Professor Neil McKeown, for giving me the opportunity to join his research group and for his constant guidance and support throughout my PhD.

Special thanks should also go Lino and Grazia, for sharing their practical and mental expertise and for assisting me wherever possible throughout my time in the lab and during the preparation of this thesis.

I would also like to thank everyone else who has worked in lab 1.107A over the past four years: Kadhum, Rhys, Egg, Jono, Alaa, Mo, James, Matt, Heulyn, Evans, Yulia, Mike, Sabeeha, Ian, Rhodri, Sadiq and Ali, for making it a friendly and enjoyable place to work.

I would like to thank Dr. Rob Jenkins, Robin Hicks, Dave Walker, Gaz Coleman, Simon James and all of the technical staff within the School of Chemistry, for their expertise and willingness to help at any given moment. Particularly thanks should also go to Dr. Benson Kariuki for measuring and solving countless crystal structures featured in this thesis.

Thanks also to those who featured on the *Materials World Network* collaboration, our monthly Skype conferences served as a great asset to develop my understanding of different areas of material chemistry research. Special thanks to Professor Coray Colina and Professor James Runt for allowing me to visit their respective research groups at Pennsylvania State University during May 2011.

Finally, I would like to thank my family and friends, without whom none of this could have been possible.

Abstract

The research in this thesis is centred on the synthesis of novel organic molecules of intrinsic microporosity (OMIMs), dendrimers of intrinsic microporosity (DIMs) and sulfur-based polymers of intrinsic microporosity (sPIMs).

OMIMs are a new class of discretely amorphous microporous materials, synthesised by the combination of functionalised cores and termini that share awkward molecular geometries exploited to generate microporosity in polymers of intrinsic microporosity (PIMs). OMIMs presented in this thesis are prepared by the combination of fluorinated biphenyl or terphenyl cores with dihydroxy (catechol) based benzene, naphthalene or triptycene termini. Through a systematic study of substituted termini, a structure-property relationship is established and applied to generate highly soluble OMIMs possessing apparent BET surface areas within the range of $7 - 726$ m^2 g^{-1}, as measured by nitrogen sorption at 77 K.

The second section on DIMs is an expansion of the work on OMIMs. By isolating tri-substituted biphenyl cores (branch units), first generation dendrimers are afforded by the reaction of a branch unit with a suitably functionalised core. DIMs in this thesis centre around the 9,10-diethyltriptycene-2,3,6,7,13,14-hexaol core, and give rise to apparent BET surface areas within the range of $300 - 722$ m^2 g^{-1}, as measured by nitrogen sorption at 77 K.

The final section of this thesis focuses around the monomer synthesis and subsequent polymerisations of three spirobisindane based sPIMs (sPIM-0, sPIM-1 and sPIM-2). Whereas typical PIMs exploit catechol containing monomers to generate dibenzodioxane containing polymers, sPIMs employ dithiol containing monomers to generate thianthrene containing polymers. These thianthrene units could lead to enhanced gas separation properties of the polymer before or after post-polymerisation oxidation to sulfones or sulfoxides. All three sPIMs were found to be microporous, possessing apparent BET surface areas within the range $438 - 510$ m^2 g^{-1}, as measured by nitrogen sorption at 77 K.

Abbreviations

Å	Angstrom(s)
Ac$_2$O	Acetic Anhydride
Ad	Adamantyl
AIBN	Azobisisobutyronitrile
ASAP	Accelerated Surface Area and Porosimetry
BET	Brunauer, Emmett and Teller
br.	Broad
calc.	Calculated
COD	Cyclooctadiene
COF	Covalent Organic Framework
CTC	Cyclotricatechylene
Cy6	2,2',5,5'-Tetramethylcyclohexane, (Cycle-6)
d	Diameter
DBDHSBI	5,5'-Dibromo-6,6'-dihydroxy-3,3,3',3'-tetramethyl-1,1'-spirobisindane
DBDTSBI	5,5'-Dibromo-6,6'-dithiol-3,3,3',3'-tetramethyl-1,1'-spirobisindane
DCB	1,2-Dichlorobenzene
DCDMB	1,4-Dichloro-2,5-di(4'-methylbenzoyl)benzene
DCE	1,2-Dichloroethane
DCM	Dichloromethane
DEF	Diethylformamide
DHSBI	6,6'-Dihydroxy-3,3,3',3'-tetramethyl-1,1'-spirobisindane
DIM	Dendrimer of Intrinsic Microporosity
DMAC	N,N-Dimethylacetamide
DMF	N,N-Dimethylformamide
DMSO	Dimethylsulfoxide
DTSBI	6,6'-Dithiol-3,3,3',3'-tetramethyl-1,1'-spirobisindane
EI	Electron Impact
eq.	Equivalent(s)
ES	Electrospray
Et	Ethyl
Et$_2$O	Diethyl ether
EtOH	Ethanol
f	Functionality
g	Gram(s)

GPC	Gel Permeation Chromatography
HATN	Hexachlorohexaazatrinaphthylene
HCP	Hyper-Cross-linked Polymer
hr	Hour(s)
HRMS	High Resolution Mass Spectrometry
Hz	Hertz
^{i}Pr	Iso-propyl
IR	Infra-Red
ISAACS	Interactive Structure Analysis of Amorphous and Crystalline Systems
IUPAC	International Union of Pure and Applied Chemistry
J	Coupling constant (in Hz)
K	Kelvin
lit.	Literature
LRMS	Low Resolution Mass Spectrometry
m	Multiplet
m^2	Square meter
M	Molar
m/z	Mass to charge ratio
MALDI	Matrix Assisted Laser Desorption Ionisation
***m*CPBA**	*meta*-Chloroperoxybenzoic acid
Me	Methyl
MeCN	Acetonitrile
MeOH	Methanol
min	Minute(s)
ml	Millilitre(s)
MMC	Microporous Molecular Crystal
mmol	Millimole(s)
M_n	Number-average molecular weight
MOF	Metal Organic Framework
mp	Melting point
MS	Mass Spectrometry
M_w	Mass-average molecular weight
N	Normal
N,N-DMA	N,N-Dimethylaniline
NBS	N-Bromosuccinimide
***n*-BuLi**	*n*-Butyllithium

nm	Nanometer(s)
NMR	Nuclear Magnetic Resonance
o	*ortho*
OMIM	Organic Molecule of Intrinsic Microporosity
p	*para*
PAF	Porous Aromatic Framework
PDI	Polydispersity index
PEPPSI[TM]	Pyridine-Enhanced Precatalyst Preparation Stabilization and Initiation
Ph	Phenyl
PHBPB	Pyridinium Hydrobromide Perbromide
PIM	Polymer of Intrinsic Microporosity
Pr	Propyl
q	Quartet
RT	Room Temperature
s	Singlet
S$_N$Ar	Nucleophilic Aromatic Substitution
sPIM	Sulfur-PIM
t	Triplet
TBSBI	5,5',6,6'-Tetrabromo-3,3,3',3'-tetramethyl-1,1'-spirobisindane
TBTQ	Tribenzotriquinacene
^{t}Bu/*tert*-Bu	Tertiary butyl
TFA	Trifluoroacetic acid
TCTPN	2,3,5,6-Tetrachloroterephthalonitrile
TFTPN	2,3,5,6-Tetrafluoroterephthalonitrile
TGA	Thermogravimetric Analysis
THF	Tetrahydrofuran
THSBI	5,5',6,6'-Tetrahydroxy-3,3,3',3'-tetramethyl-1,1'-spirobisindane
TLC	Thin Layer Chromatography
TMEDA	Tetramethylethylenediamine
T*n*BTSBI	5,5',6,6'-Tetrakis(*n*-butylsulfane)-3,3,3',3'-tetramethyl-1,1'-spirobisindane
TTSBI	5,5',6,6'-Tetrathiol-3,3,3',3'-tetramethyl-1,1'-spirobisindane
uCy6	Unsymmetrical 2,2',5,5'-tetramethylcyclohexane, (uCycle-6)

Table of Contents

1. Introduction

1.1 Porous Materials

In materials science, a pore can take the form of a void, cavity or interstice that is at least partially surrounded by the component material. Pore structure can vary significantly depending upon the material, but can largely be defined by three factors: size, shape and accessibility, all of which influence the properties, and hence applications of, porous materials.

Size is perhaps the most apparent property a pore can possess, and consequently there are three well-defined classes of pore-size as define by *IUPAC*[1] (International Union of Pure and Applied Chemistry). These are: *macropores* (pores with a width of greater than 50 nm), *mesopores* (pore width of 2 – 50 nm) and *micropores* (pore width less than 2 nm). All porous materials can be assigned to at least one of these pore sizes, allowing for simple classification. However, the unfortunate over popularisation of the *nano-* prefix in popular science has led to the rather confusing class of *nanopores* that encompass any pores of width under 1000 nm.
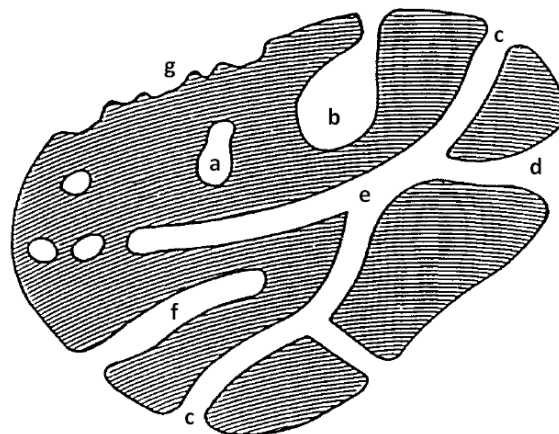

Figure 1.1 Classification of pores.

Pore accessibility can also be easily defined, although this time into just two categories: *closed* or *open*. A closed pore (*a* in **Figure 1.1**) is inaccessible to external fluids and as such, influences only macroscopic properties such as bulk density and mechanical strength. Open pores (*b*, *c*, *d*, *e* and *f* in **Figure 1.1**) emanate from the surface of the material and as such,

are accessible to external fluids, and therefore influence microscopic properties such as porosity and surface area.[1]

Open pores may be further classified by their shape (**Figure 1.1**: *c* and *f* are *cylindrical*, whereas *b* is said to be *ink-bottled* shaped), and whether they are only open at one end (*b* and *f*) or penetrate the entire material (*e*). For a surface to be considered porous, any irregularities must be deeper than they are wide, thus *g* is considered a rough surface rather than a porous surface.

1.2 Quantifying Surface Area

When referring to how porous a material is, it is commonplace to talk about the materials *surface area* (i.e. the total area of the material that is accessible to a probe). There are several known methods for quantifying the surface area of a material. These include: optical methods,[2] studying the material under a microscope and comparing the total area to the area of accessible pores, porosimetry methods,[3] forcing a non-wetting liquid, often mercury,[4] into a porous material and using the external pressure required to do so to estimate pore size, and computational methods,[5,6] involving the simulation of a porous material followed by subsequent analysis of the void space. However, by far the most common technique for estimating the surface area of a material is gas sorption, specifically physisorption (rather than chemisorption) as these processes are reversible. By '*showing*' a clean surface a known amount of an inert gas, and measuring how much of that gas is taken up by the sample, either by change in sample weight (*gravimetric analysis*) or by change in volume of the probe gas (*volumetric analysis*), one can determine how many gas molecules are required to cover the available surface, and hence estimate the surface area.

Currently, the most widely used method is a volumetric technique referred to as BET (named after the co-inventors: Brunauer, Emmett and Teller).[7] The theory is an extension of the Langmuir model (developed by Irving Langmuir in 1916),[8] which considers the equilibrium between a gas molecule (*A*), a surface site (*S*) and an adsorbed molecule (*AS*).

$$A + S \rightleftharpoons AS \qquad\qquad K = \frac{[AS]}{[A][S]}$$

The equilibrium constant for this system (*K*, shown above) can expressed in more useful terms by referring to the concentration of adsorbed gas molecules *[AS]*, as a fraction of occupied sites (*Θ*) and the concentration of available sites, [*S*] as (1 − *Θ*) to give:

$$K = \frac{\Theta}{(1 - \Theta)P}$$

Where '*P*' represents the concentration of a gas [*A*], or as it's more typically known *partial pressure*. Rearranging for *Θ* and equating it to the volume of gas adsorbed (*V$_A$*), divided by the total monolayer volume (*V$_M$*), we find:

$$\Theta = \frac{KP}{1 + KP} = \frac{V_A}{V_M}$$

This equation is generally presented in the *y = mx + c* form such that measureable data (volume of gas adsorbed, *V$_A$* and partial pressure, *P*) can be plotted to allow *V$_M$* to be calculated by extrapolation of a straight line plot:

$$\frac{1}{V_A} = \frac{1}{KV_M}\left[\frac{1}{P}\right] + \frac{1}{V_M}$$

BET theory builds on these ideas but accounts for multilayer adsorption (an assumption of the Langmuir model is that only a single 'monolayer' of gas will adsorb on to a surface). The equivalent equation for gas sorption using the BET model is:

$$\frac{P_S}{V_A(P_S - P_0)} = \frac{C - 1}{CV_M}\left[\frac{P_S}{P_0}\right] + \frac{1}{CV_M}$$

Where; '*P$_S$*' represents sample pressure, '*P$_0$*' saturation pressure, '*V$_A$*' volume adsorbed, '*V$_M$*' monolayer volume and '*C*' is the BET constant. A *y = mx + c* plot of *P$_S$*/[*V$_A$*(*P$_S$* − *P$_0$*)] against *P$_S$*/*P$_0$* has been shown experimentally[7] to give a linear plot over the range 0.05 ≤ *P*/*P$_0$* ≤ 0.35. Thus, after some rearrangement, the gradient (*A*) and intercept (*I*) of said linear plot within this region allows for calculation of *V$_M$* as follows:

$$V_M = \frac{1}{A + I}$$

Knowing the monolayer volume (*V$_M$*) in moles, one can then simply calculate the BET surface area, (*S$_{BET}$*) in m^2 g^{-1} using: Avogadro's number (*N$_A$*), the molar volume of adsorbate gas at

STP (M_V) (22.4 L), the sample weight in grams (W_S) and the cross-sectional area of the probe molecule (σ) (16.2 Å^2 for nitrogen)[9] as follows:

$$S_{BET} = \frac{N_A V_M \sigma}{W_S M_V}$$

BET analysis is typically performed using nitrogen as the probe gas and at low pressure and temperature (77 K). The evacuated sample is dosed with a small quantity of nitrogen, allowed to reach equilibrium with the surrounding vessel, and then the pressure of the vessel measured (this measurement is converted into a volume using the ideal gas equation). Once equilibrium is achieved, more nitrogen is added and the process repeated until saturation pressure is reached. Thus, a plot of adsorbed volume versus partial pressure can be constructed to give an *adsorption isotherm*. Six types of adsorption isotherms have been classified by IUPAC[10] (**Figure 1.2**)[11] and give an accurate indication of the average pore size of the sample.
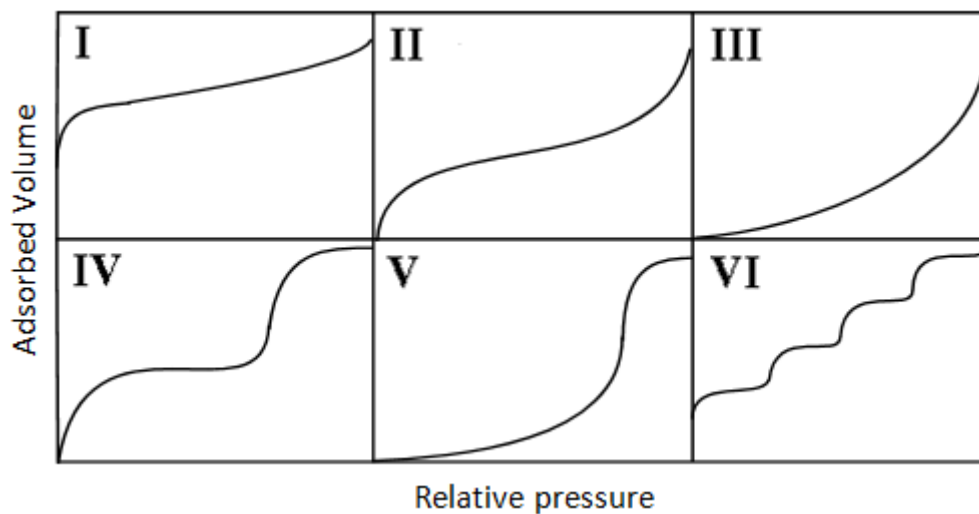

Figure 1.2 IUPAC defined isotherms: *Type I*: Microporous, *Type II*: Non-porous/Macroporous, *Type III, V*: Non-porous, *Type IV, VI*: Mesoporous.

1.3 Microporous Materials

Over the past decade there has been increasing interest in the study of microporous materials for applications in hydrogen storage,[12-14] selective gas separation membranes,[15-17] heterogeneous catalysis[15,16,18] and ion exchange resins[19] to name but a few. Such wide

range of application arises from the diverse range of microporous materials present in the literature, which can be broadly subdivided into two classes: *structured crystalline networks* and *amorphous powders*. Structured crystalline networks are materials that have long range order and as such, possess well defined pore sizes. Typical examples include: zeolites, metal-organic frameworks (MOFs), covalent organic frameworks (COFs) and molecular crystals. Amorphous powders are much more random structures that possess little or no long-range order, typical examples include: hyper-cross-linked polymers (HCPs), activated carbons and polymers of intrinsic microporosity (PIMs). Each material has its own unique compliment of properties, applications and synthetic challenges, which are discussed in the following sections.

1.4 Structured Crystalline Networks

1.4.1 Zeolites

The term zeolite is derived from the Greek words *zein* (meaning 'to boil') and *líthos* (meaning 'stone') after Swedish Mineralogist Axel F. Cronstedt noted in 1756 that a sample of stilbite produced steam upon heating with a blowpipe.[20,21] The term now encompasses any naturally occurring or synthetically produced hydrated aluminosilicate. The unique structure of zeolites arises from the combination of tetrahedral MO_4 units (M is generally a mixture of Si or Al, however many other elemental compositions are known)[22] in which each oxygen atom bridges two M atoms to form clusters of tetrahedral units. These clusters are further combined to form an extended, three-dimensional framework containing well defined pores of roughly molecular dimension (1 – 20 Å). The presence of $[AlO_4]^-$ units gives the framework a net negative charge and hence small alkali earth metal counter ions reside within the pores of the structure along with the adsorbed water molecules (**Figure 1.3**).

Upon removal of the adsorbed water molecules, zeolites remain as highly stable frameworks,[23] allowing them to act as '*molecular sieves*' in which external molecules are selectively adsorbed based on their size.[20] This, combined with the net negative charge gives zeolites excellent properties in the fields of ion-exchange,[24-26] water[27] and gas purification,[28,29] regioselective chemistry[30,31] and catalysis.[32,33]
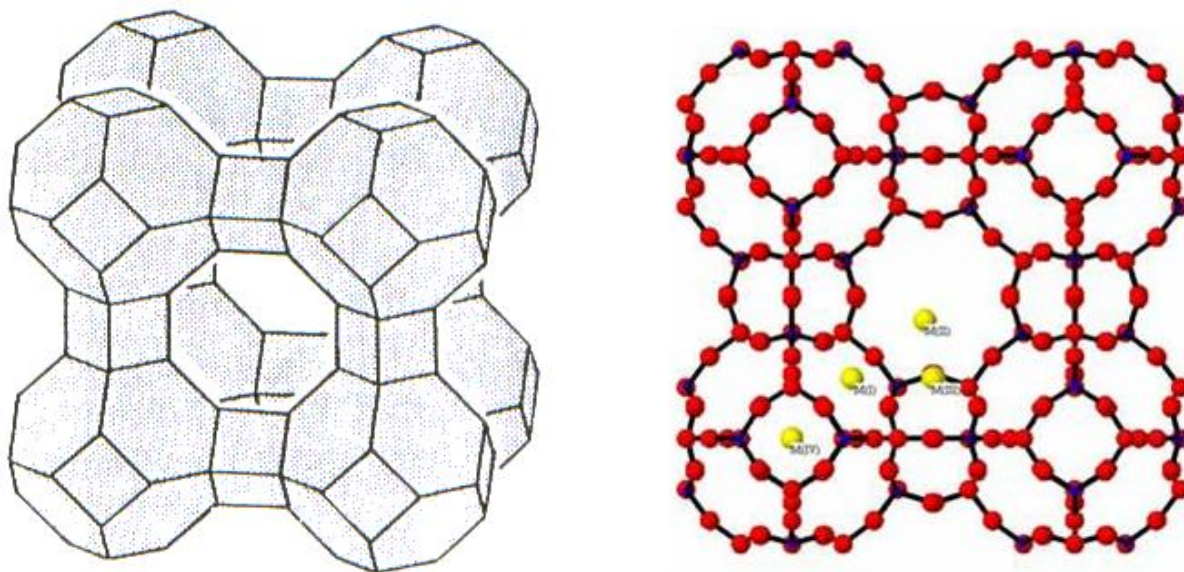
Figure 1.3 Block (left) and atomistic (right) structures of *Zeolite A* showing the internal channel (approximately 4 Å in diameter) and potential cation position (yellow dots).

Furthermore, acidic zeolites (H$^+$ counter ions) are commonly used in the petrochemical industry in the catalytic cracking of long chain hydrocarbons.[22,34,35] Their high thermal stability and large internal surface areas allow zeolites to act as self-supporting catalysts which can selectively catalyse the cracking of various hydrocarbons based on their size (owing to the narrow pore size distribution of the selected zeolite).

## 1.4.2 Metal Organic Frameworks (MOFs)

As the name suggests MOFs are a hybrid material, formed by the self-assembly of inorganic metal centres and organic 'linker' molecules to give an ordered three-dimensional structure. The organic linkers contain two or more donor groups (e.g. carboxylic acids or amines) that can coordinate the chosen metal centre. The wide range of potential metal centres and organic linkers gives rise to a large synthetic diversity within the field of MOFs (in contrast to zeolites), which has attracted much interest in scientific literature.[36] Most notably due to the impressively high surface areas (some in excess of 5000 m^2 g^{-1})[37,38] that can be achieved. **Scheme 1.1** shows the typical synthesis and structure of a MOF (*MOF-5*) from hexaaqua zinc (II) nitrate and benzene-1,4-dicarboxylic acid.[36]
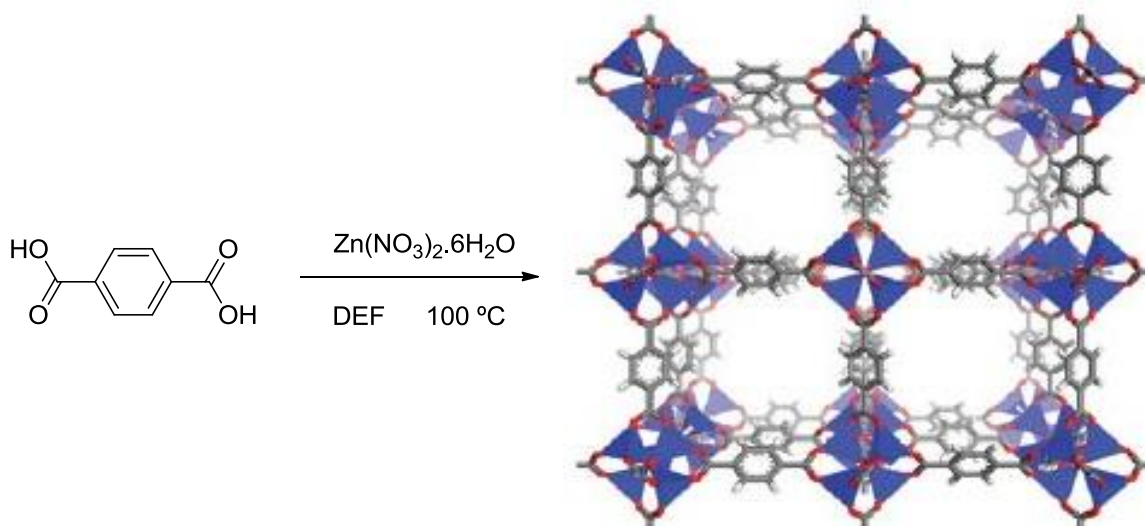
Scheme 1.1 MOF-5 synthesis and structure. X-ray diffraction studies revealed a pore size of 18.5 Å and an overall void space of 80 % of the crystal volume.

MOF-5 was somewhat of a breakthrough in the field, as it was the first reported MOF to remain stable at high temperatures (up to 300 °C).[36] Previously, the large cavities created were subject to collapsing upon removal of host solvent molecules.[39,40] The stability was demonstrated by comparing single crystal X-ray diffraction data on samples of MOF-5 that had been desolvated at room temperature and at 300 °C. The cell parameters measured were found to be identical, indicating no change in the morphology or crystallinity of the material. MOF-5 was also shown to have an extremely low density (0.59 g cm^{-3}), which combined with its stability, led to an impressive surface area, estimated by gravimetric analysis to be at least 3000 m^2 g^{-1}.[36]

Since the publication of MOF-5, the number of papers published per year on MOFs has increased dramatically from 11 in 1999 to 2496 in 2012,[41] and applications have been uncovered in fields including: gas storage (hydrogen[42] as well as small hydrocarbons),[43] gas separation,[44] heterogeneous catalysis,[45] molecular recognition[46] and even drug delivery.[47] Surface areas have also improved substantially; to date the highest apparent BET surface area reported for a MOF is 7140 m^2 g^{-1}, belonging to material dubbed *NU-110*[38] (**Scheme 1.2**). The authors attribute the ultrahigh surface area to the employment of 'space efficient' ethynyl groups within the organic linkers and the use of supercritical CO$_2$ towards MOF activation[48] (removal of guest solvent molecules without loss of porosity). They also speculate that by replacing all but the central and terminal phenyl units of the linker with ethynyl units, MOFs with surface areas in excess of 14,000 m^2 g^{-1} are achievable.
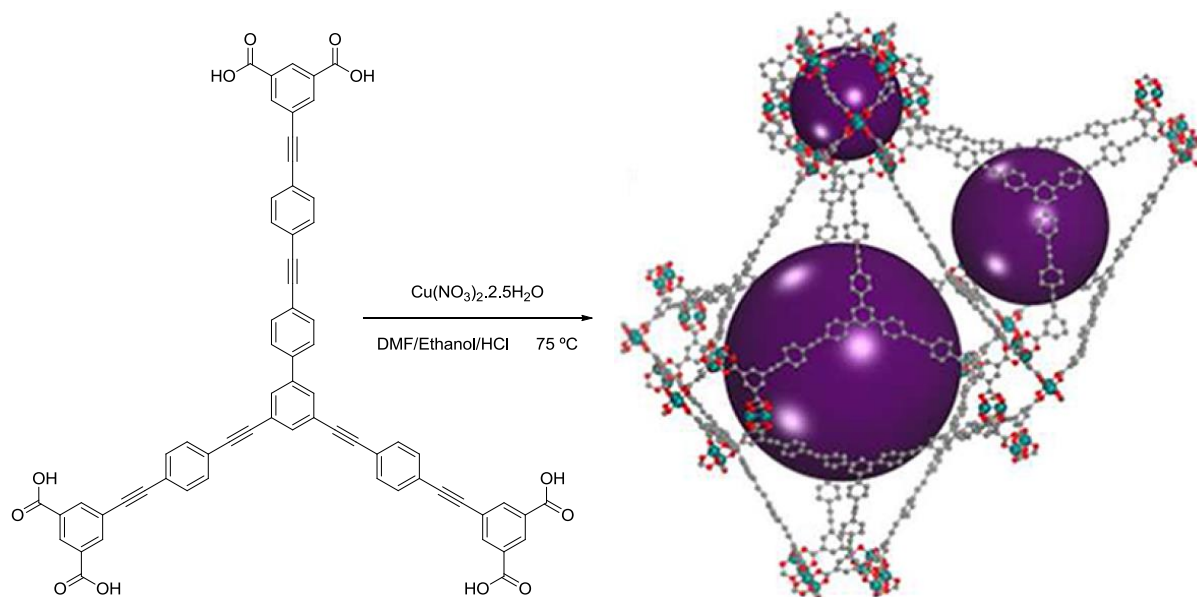
Scheme 1.2 *NU-110* synthesis and partial structure indicating the largest accessible pores in purple, the largest of which were measured to be approximately 35 Å in diameter.

1.4.3 Covalent Organic Frameworks (COFs)

COFs are a more recent extension to the work on MOFs and are similar in structure, but, as the name suggests they do not contain any metal centres. Instead, the organic linkers are functionalised with groups that allow the formation of covalent bonds between themselves (e.g. boronic acids,[49] catechols,[50] nitriles[51] or amines),[52] hence the name. Generally, COFs are solely made from light elements (H, B, C, N and O) which are known to form strong covalent bonds (diamond, graphene,[53] boron nitride)[54] and possess very low mass densities, which, coupled with very high thermal stabilities (up to 600 °C), gives rise to permanently porous materials.[55] Application of COFs are understandably similar to those of MOFs, (gas sorption[49,56,57] and catalysis),[58] but those constructed as layered two dimensional structures generate ordered π systems which can possess additional electronic[55,59] and optical properties.[55,60]

One of the first reported COFs by Yaghi and co-workers[61] in 2005 was *COF-5*, produced from the reaction between benzene-1,4-diboronic acid and hexahydroxytriphenylene (**Scheme 1.3**).
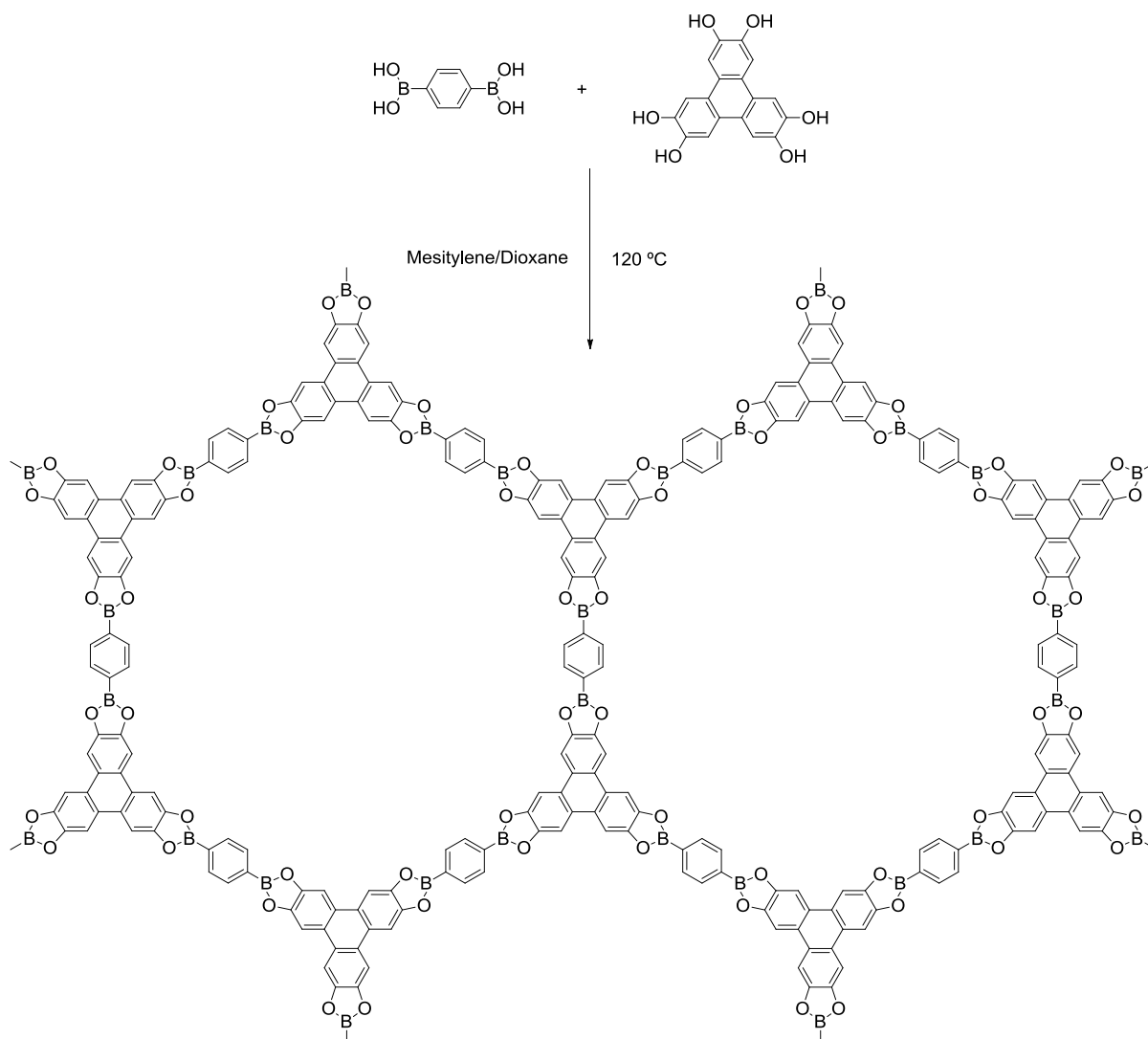
Scheme 1.3 COF-5 synthesis and structure fragment. Pore size approximately 27 Å.

The BET surface area of the two dimensional COF-5 was measured by nitrogen sorption to be 1590 $m^2 g^{-1}$, which whilst fairly unimpressive in comparison to those achieved by three dimensional MOFs, is impressive compared to other two dimensional layered structures: graphite (10 $m^2 g^{-1}$),[61] powdered graphene (156 $m^2 g^{-1}$)[62] and pillared clays (up to 400 $m^2 g^{-1}$).[63] Powder X-ray diffraction studies revealed the purity and crystallinity of COF-5, the latter of which has been previously thought to be impossible due to the required microscopic reversibility of crystallisation in similar polymeric solids.[64] Using so called '*reticular chemistry*' COFs can be expanded into the third dimension through the use of tetrahedral shaped boronic acids (such as tetra(4-dihydroxyborylphenyl)methane used in the synthesis of COF-102,[50] **Scheme 1.4**)
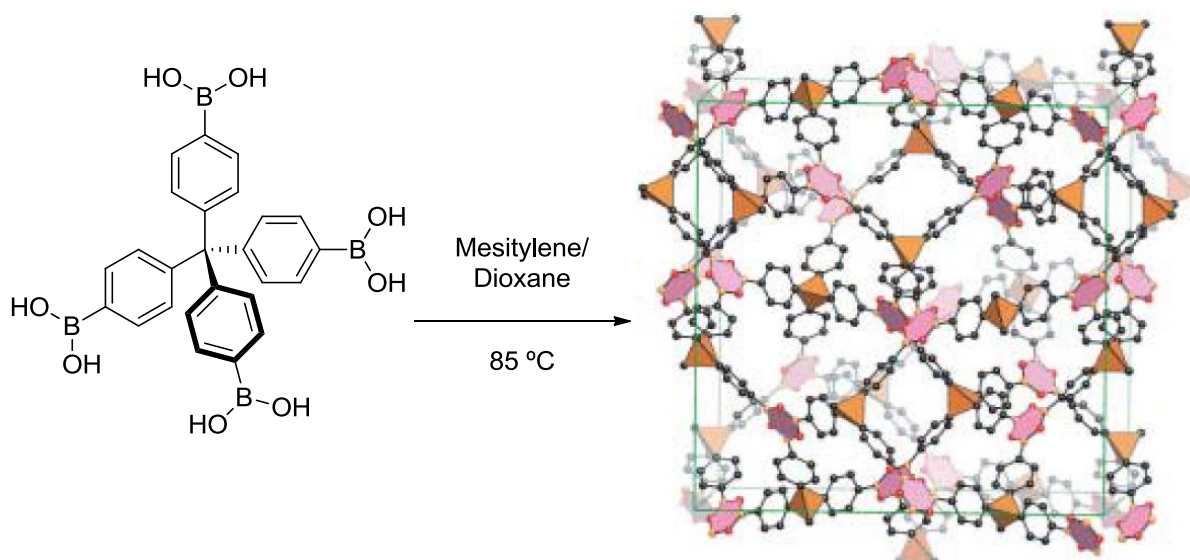
Scheme 1.4 COF-102 synthesis and structure. Pore size approximately 9 Å.

COF-102 was again found to be crystalline through powder X-ray diffraction studies and reported to have an apparent BET surface area of 3620 $m^2 g^{-1}$ as measured by argon sorption at 87 K. Clearly, when allowed to propagate into all three special dimensions, COFs could well become as an impressive a class of material as MOFs in the very near future, given that they have only been studied for a relatively short time.

1.4.4 Microporous Molecular Crystals (MMCs)

So far, all porous materials discussed have been derived from an extended or polymeric network. However, within the past decade a number of discrete (i.e. molecular, non-networked) crystalline porous materials (dubbed '*microporous molecular crystals*' or MMCs) have been reported. Held together only by weak, non-covalent interactions, MMCs are created *via* the removal of guest molecules from within inclusion compounds (a process that often causes collapse of the open structure).

One of the first reported MMCs, *tris(o-phenylenedioxy)cyclotriphosphazene* (TPP) (**Figure 1.4**) was shown to have a surface area of 240 $m^2 g^{-1}$ (as measured by nitrogen sorption)[65] as well as impressively high CO_2 uptake at low pressures.[66] However, the hexagonal open-pore structure was shown to only be stable to temperatures of about 50 °C, at which point the zeolite-like structure collapsed into a denser, non-porous structure.[67]
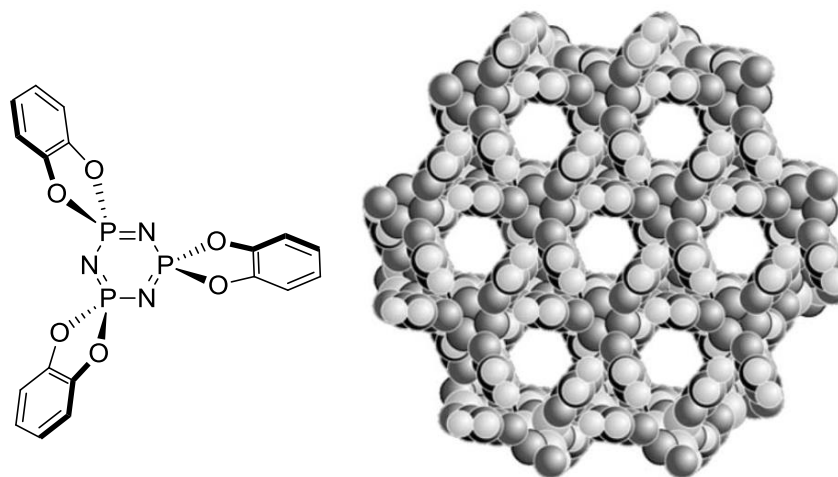
Figure 1.4 Tris(*o-phenylenedioxy)cyclotriphosphazene* (TPP) and hexagonal crystal structure viewed along channel axis. Pore size approximately 4.8 Å.

In 2009, Cooper's group first reported '*porous organic cages*', materials that are microporous due to both the molecular voids contained within the cages (intrinsic porosity), and their inefficient packing in the solid state (extrinsic porosity).[68,69] '*Cage 2*' (**Scheme 1.5**) is formed by the Schiff base condensation reaction between 1,3,5-triformylbenzene and 1,2-propylenediamine under relatively mild conditions. The material was found to possess an apparent BET surface area of 533 $m^2 g^{-1}$ (as measured by nitrogen sorption), and to be stable at temperatures over 300 °C. This is impressive considering that it is widely accepted that most molecules pack space as efficiently as possible resulting in minimal void volume.[70]

The molecular (rather than framework) nature of these porous organic cages was demonstrated through studies of '*Cage 1*' (synthesised from 1,3,5-triformylbenzene and 1,2-ethylenediamine, resulting in a structure much like Cage 2 (**Scheme 1.5**) but lacking the methyl groups). This formally non-porous material (apparent BET surface area 24 $m^2 g^{-1}$) was recrystallised from a mixture of DCM and *o*-xylene to produce a permanently porous polymorph (apparent BET surface area 550 $m^2 g^{-1}$).
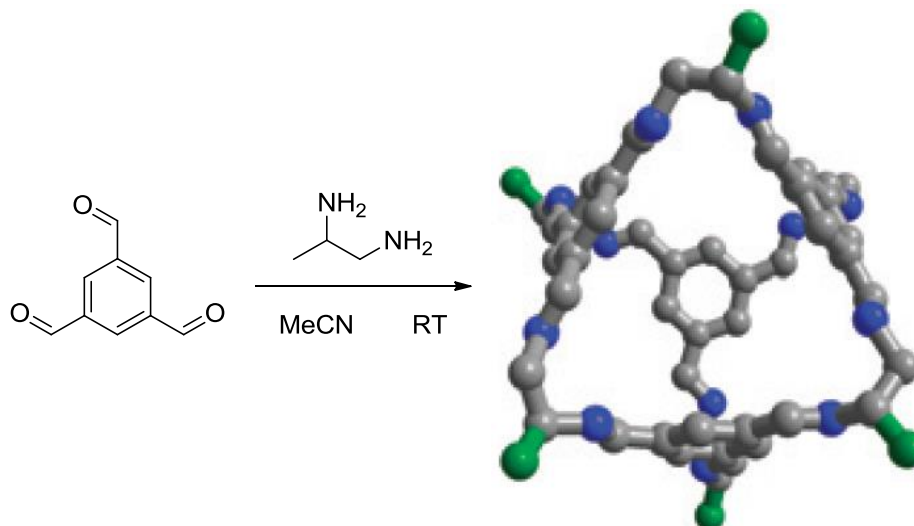
Scheme 1.5 Cage 2 synthesis and crystal structure. Pore size up to 6.1 Å.
Methyl groups (green) not present in Cage 1.

In 2011, the Mastalerz group[71] expanded upon this work reporting a new, stable, porous organic cage with a BET surface area of 1375 $m^2\,g^{-1}$. The material, *'cage compound 3'* (**Scheme 1.6**) is made using the same amine/aldehyde Schiff base condensation reaction, but this time utilises triptycene; a molecular fragment of high internal free volume[72] that has been utilised in the synthesis of many highly porous materials[5,13,73-75] and will feature heavily throughout this thesis. In addition to the high surface area, cage compound 3 was shown to have good gas separation properties, with a selectivity ratio of 10:1 for CO_2 over CH_4. The authors attribute this selectivity to interactions of polar hydroxy groups (contained within the internal cavities) with polar gases (e.g. CO_2).
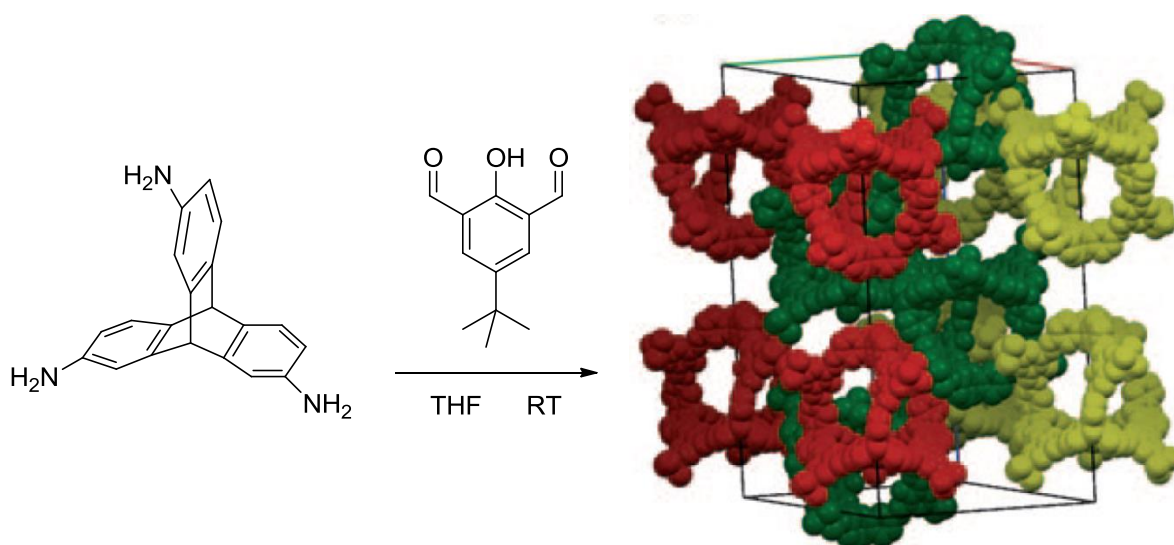
Scheme 1.6 '*Cage compound 3***'** synthesis and unit cell packing. Pore size up to 8.8 Å.

Phthalocyanine and porphyrin based microporous crystals (PMCs) offer a unique advantage to discrete porous materials as they are able to coordinate metal ions for use in catalysis.[76] In 2005 McKeown *et al.*[77] reported the synthesis of large (up to 1 mm^3) cubic crystals of 2,3,9,10,16,17,23,24-octa(2',6'-diisopropylphenoxy)phthalocyanine (**Figure 1.5**) which contained up to 35 % void space within the crystal structure. However, X-ray diffraction studies revealed the instability of the structure upon solvent removal at room temperature, making it impossible to accurately estimate the surface area *via* gas sorption. The problem was solved in 2010 by the introduction of bidentate ligands (e.g. bipyridine) to act as '*wall ties*' between metal centres to reinforce the highly symmetrical structure. Now, the dimeric microporous structure remains stable to temperatures over 100 °C allowing for the removal of recrystallisation solvents and BET analysis (up to 1000 m^2 g^{-1} depending on the metal ion and ligands).
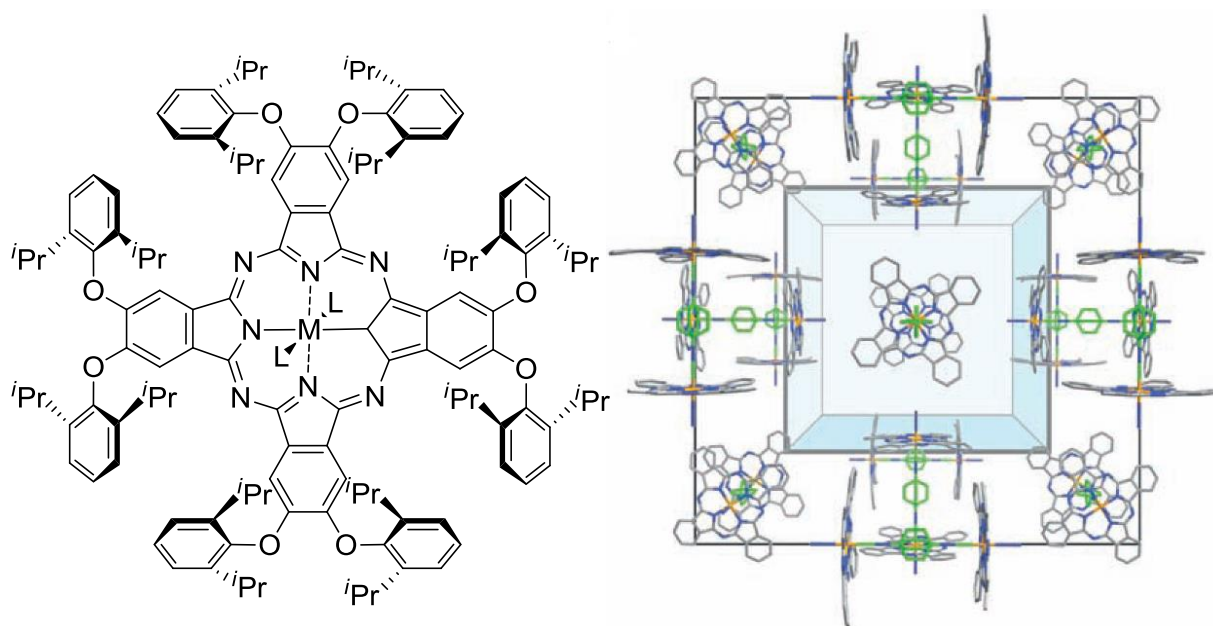

Figure 1.5 2,3,9,10,16,17,23,24-octa(2',6'-diisopropylphenoxy)phthalocyanine structure (left) and crystal structure with '*wall-tie*' ligands in green (right).

PMCs and MMCs demonstrate well that the extended network structures shown in MOFs, COFs and zeolites are *not* required to create a porous material. Furthermore, they often possess the advantage of solution processability, leading to applications in spin coating[78] and tailoring of polymeric membrane properties through the creation of so-called '*mixed-matrix membranes*' (MMMs).[79]

1.5 Networked Amorphous Microporous Materials

1.5.1 Activated Carbon

Also known as '*activated charcoal*', activated carbon can be simply defined as '*porosity enclosed by carbon atoms*'.[80] They are generally believed to consist of disordered graphene-like sheets linked by non-graphitised aliphatic units. However, their actual structure is not fully understood and likely to be highly random,[81] consisting of fragments of various known allotropes of carbon (**Figure 1.6**). Most naturally occurring carbonaceous materials (wood, coal, peat etc…) can be pyrolyzed (heated to a high temperature in an inert atmosphere) into *carbons*. Subsequent activation *via* either; *gasification* of individual carbons atoms by means of heating in the presence of oxidising gases (*thermal activation*), or dehydration/oxidation of the bulk material with impregnated chemicals (*chemical oxidation*), enlarges the diameters of pores previously created during carbonisation to create *activated carbon*.[81] Due to the somewhat random structures and varying degrees of activation, activated carbons have pore sizes and shapes scattered over a very wide range (micropores to macropores),[81] and consequently, surfaces areas can vary significantly (300 – 3000 $m^2 g^{-1}$).[82,83]
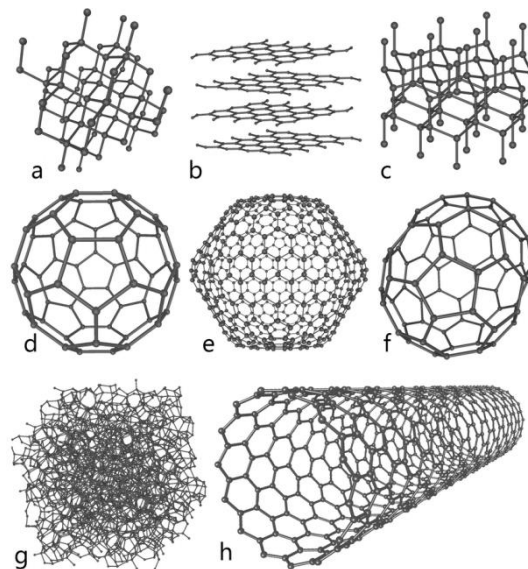

Figure 1.6 Allotropes of carbon: *a*) Diamond, *b*) Graphite (layered), Graphene (single sheet), *c*) Lonsdaleite, *d*) C_{60}, Buckminsterfullerene, *e*) C_{240}, *f*) C_{70}, *g*) Amorphous carbon, *h*) Carbon nanotube.

Applications of activated carbons date back to the time of ancient Greeks where they were employed as medicine to relieve digestion problems, a practice that continues today.[80] They were also notably employed as filters in gas masks during World War II for protection against chlorine, phosgene and mustard gas. More recently, activated carbons have found use in the removal of small organic pollutants from wastewater *via* filtration,[84] deodorisation of oils[85] and decolourisation.[86] The ability of activated carbons to adsorb a wide range of organic compounds is often attributed to the chemically ill-defined surface boasting a large variety of oxygen and nitrogen containing functional groups.[87,88]

1.5.2 Hyper-Cross-Linked Polymers (HCPs)

Work on hyper-cross-linked polymers was first published in 1983 by Davankov[89] in the form of *hyper-cross-linked polystyrenes*, prepared *via* post-polymerisation cross-linking of gel-type polystyrenes. The cross-linking was achieved by mixing a swollen polystyrene gel, with a methylene supplier (typically chloromethyl methyl ether) and a Lewis acid, such that Friedel-Crafts alkylation followed by electrophilic aromatic substation would introduce a number of -CH_2- bridges. These bridges then fix the polymer in its swollen state thus forming pores that persist upon solvent removal (**Figure 1.7**).[19,90,91]
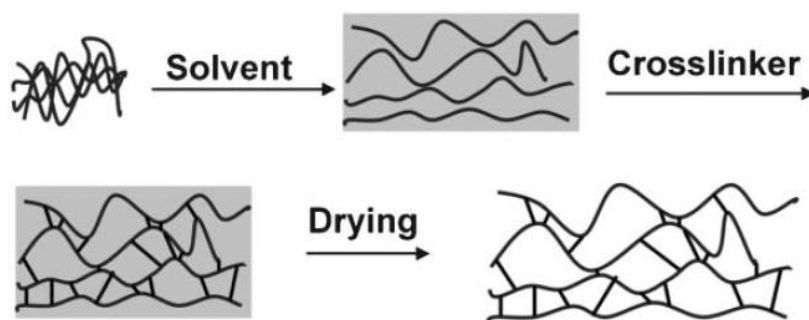

Figure 1.7 Illustration of polymer swelling and cross-linking to generate a permanently porous material.

More recently, procedures have been developed that eliminate the need to introduce an external methylene supplier by utilising a benzyl chloride functionalised monomer, allowing for cross-linking to proceed *via* an internal, Lewis acid mediated Friedel-Crafts alkylation

(**Scheme 1.7**).[90,92] By manipulating the reaction conditions of the intra-molecular cross-linking step, Ahn *et al*.[92] were able to selectively prepare hyper-cross-linked polystyrenes with surface areas ranging from 300 – 2000 $m^2 g^{-1}$ and well defined bimodal pore size distributions (original macropores present in the non-cross-linked polymer and micropores formed during cross-linking).[92]
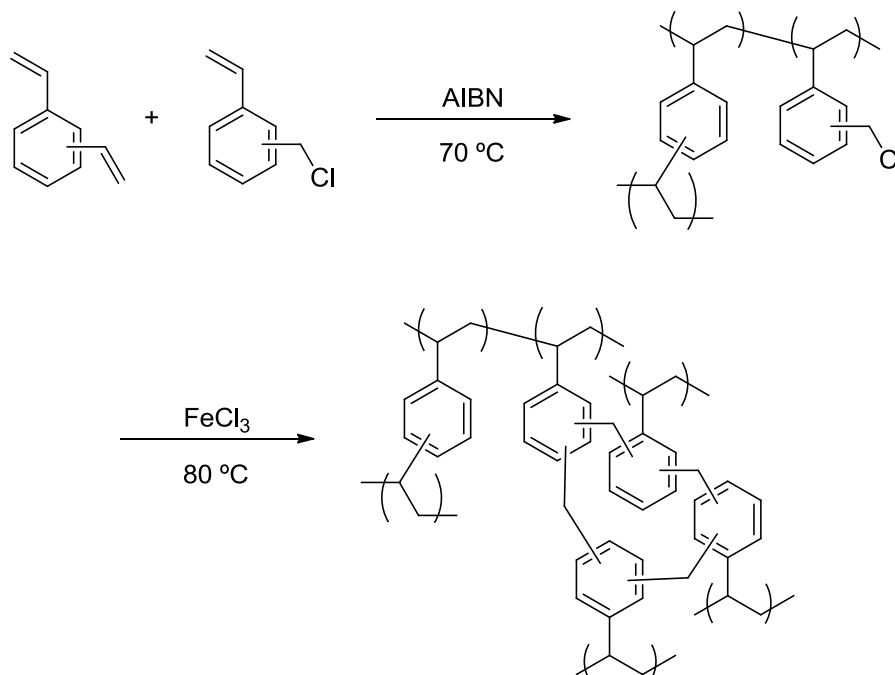
Scheme 1.7 Preparation of poly(vinylbenzyl) chloride partially cross-linked with divinylbenzene *via* radical initiation, and subsequent hyper-cross-linking *via* intra-molecular Friedel-Crafts alkylation.

First introduced in 2007, *hyper-cross-linked polyanilines* demonstrate a different class of HCPs. Formed by the cross-linking of polyanilines with bifunctional N-alkylating agents (**Scheme 1.8**), hyper-cross-linked polyanilines have been shown to possess good BET surface areas (630 $m^2 g^{-1}$ as measured by nitrogen sorption) and potential application as sensors,[93] super capacitors[94] and in hydrogen storage.[91] In the original 2007 paper, Germain *et al*.[91] investigated the use of diiodoalkanes and paraformaldehyde as cross-linking agents. Of the three diiodoalkanes tested, diiodomethane was found to be by far the best, generating surface areas up to 630 $m^2 g^{-1}$. Longer alkanes (diiodoethane, diiodopropane) gave much lower surface areas (47 and 20 $m^2 g^{-1}$ respectively), likely due to the increased flexibility of the ethyl and propyl bridges. Paraformaldehyde was also shown to be a successful cross-linking agent, generating hyper-cross-linked polyanilines with surface areas up to 480 $m^2 g^{-1}$.
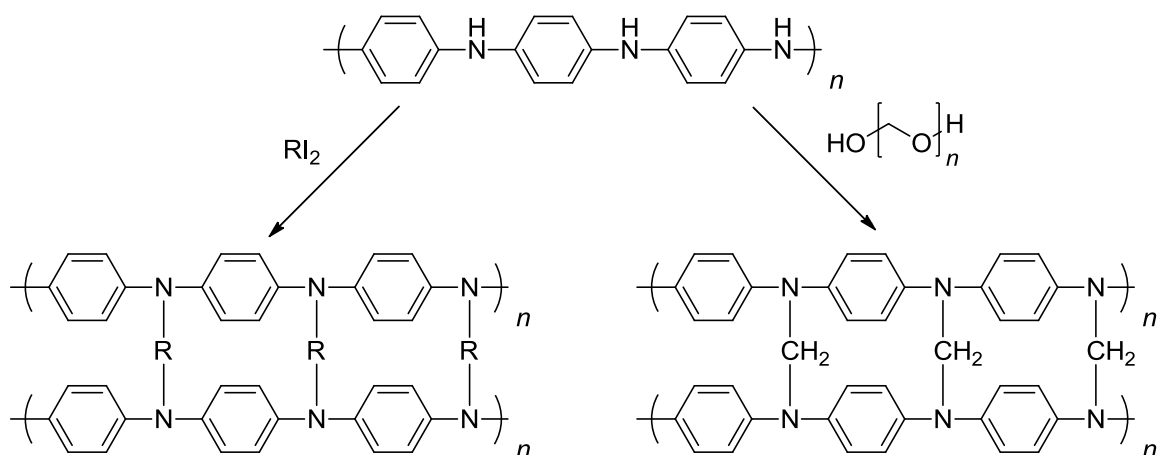
Scheme 1.8 Hyper-cross-linking of polyaniline with a diiodoalkane (left) or paraformaldehyde (right).

1.5.3 Porous Aromatic Frameworks (PAFs)

Porous aromatic frameworks (PAFs) are a very new class of porous material, first introduced by Ben *et al.* in 2009.[95] *PAF-1*, synthesised from tetrakis(4-bromophenyl)methane *via* a Yamamoto-type[96] Ullmann cross-coupling reaction (**Scheme 1.9**), was found to have a BET surface area of 5640 $m^2 g^{-1}$ (the highest of any porous material at the time of publishing),[97] and exceptional thermal stability (up to 520 °C, attributed to its diamond-like tetrahedral structure).[95] At first glance, PAF-1 may appear to be a crystalline material, owing to its framework based structure and highly symmetrical building unit. However, through a combination of powder X-ray diffraction and transmission electron microscopy, the authors established that PAF-1 is in fact a largely amorphous material[95] with very small pockets of crystallinity.[98] Despite the lack of long range order, PAF-1 possess a relatively uniform pore diameter of approximately 11 Å,[99] which has generated many studies into the use of PAFs for the selective sorption of organic pollutants[99,100] as well as hydrogen storage.[101]
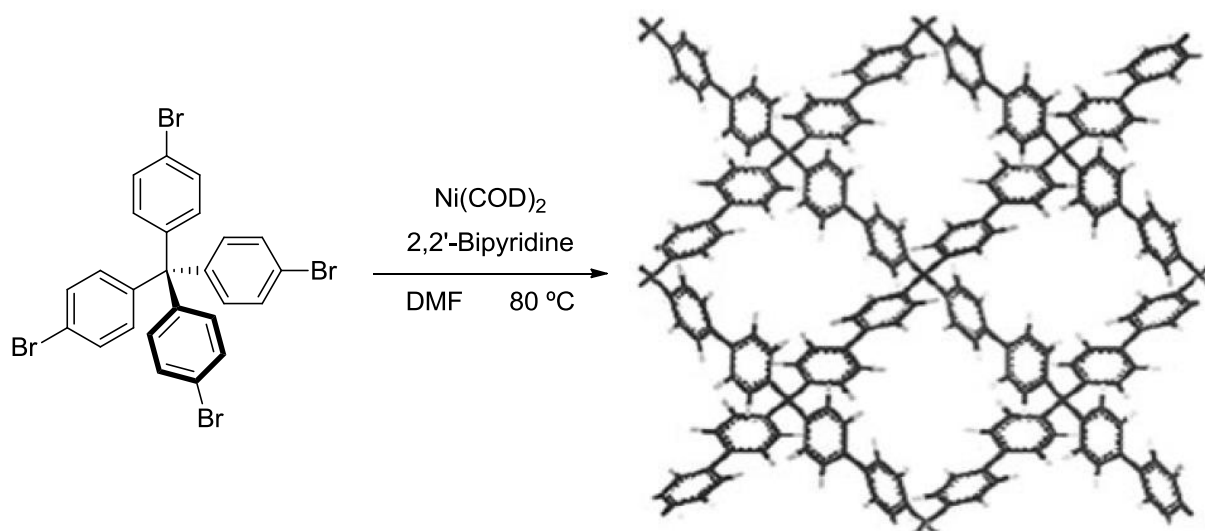
Scheme 1.9 PAF-1 synthesis and simulated structure.

More recently Yuan *et al*.[102] reported the synthesis of three new PAFs, each made from an analogue of tetrakis(4-bromophenyl)methane whereby the central carbon atom was replaced with either: an adamantane unit (*PPN-3*), a silicon atom (*PPN-4*), or a germanium atom (*PPN-5*) (**Scheme 1.10**). All three materials were found to possess impressively high surface areas (over 4200 $m^2 g^{-1}$), but PPN-4 was found to have an exceptionally high surface area of 6460 $m^2 g^{-1}$ (again, the highest known of any material at the time of publishing).[97]
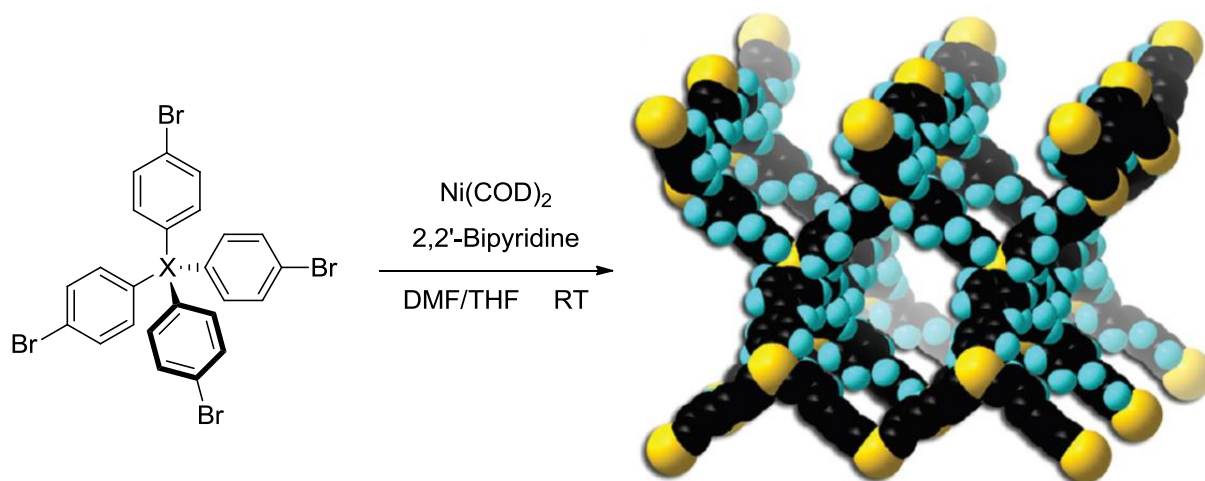
Scheme 1.10 Synthesis of PPN-3 (X = adamantane), PPN-4 (X = Si), PPN-5 (X = Ge), and representation of the diamondoid network of PPN-4 (black, C; blue, H; yellow, Si).

Little insight is offered to explain why varying just the central atom has such a noticeable impact on the apparent BET surface areas of PPN-4 and PPN-5. Though the authors do suggest that residual 2,2'-bipyridine ligand (speculated due to trace amounts of nitrogen detected by elemental analysis) could cause an underestimation of surface areas for PPN-3 and PPN-5. Regardless, the study of PAFs, in their largely amorphous state, has helped to break the notion that exceptionally high surface areas arise only from highly ordered molecular networks.[98]

1.6 Polymers of Intrinsic Microporosity (PIMs)

Whereas the structure of hyper-cross-linked polymers (HCPs) had to be manipulated (swollen and then locked in place with bridges)[19] to form highly porous materials, Polymers of Intrinsic Microporosity or '*PIMs*' do so without the need for any post polymerisation modification. This is achieved through the utilisation of monomers containing either *awkward molecular geometry* (e.g. triptycenes)[73] or a *site of contortion* (e.g. spirobisindanes),[103] that link together to form rigid, contorted structures which cannot pack space efficiently (hence porosity). The monomers are typically functionalised with *ortho*-dihydroxy (catechol) or *ortho*-dihalo (typically fluorine but on occasion chlorine)[104] groups, such that polymerisation is achieved *via* an efficient double nucleophilic aromatic substitution reaction between monomers of opposing functionality, to form rigid dibenzodioxane units throughout the polymer backbone. Since their discovery in 2004[103] two classes of PIMs have emerged: *Ladder* and *Network* PIMs (**Figure 1.8**). Ladder PIMs are pseudo-linear structures, formed by the reaction of two difunctional ($f = 2$) monomers, often leading to solution processable products. Network PIMs are two/three dimensional structures that arise from the reaction between two multi-functional monomers (one $f \geq 2$ and one $f > 2$), resulting in insoluble products that generally possess higher surface areas than their ladder counterparts.
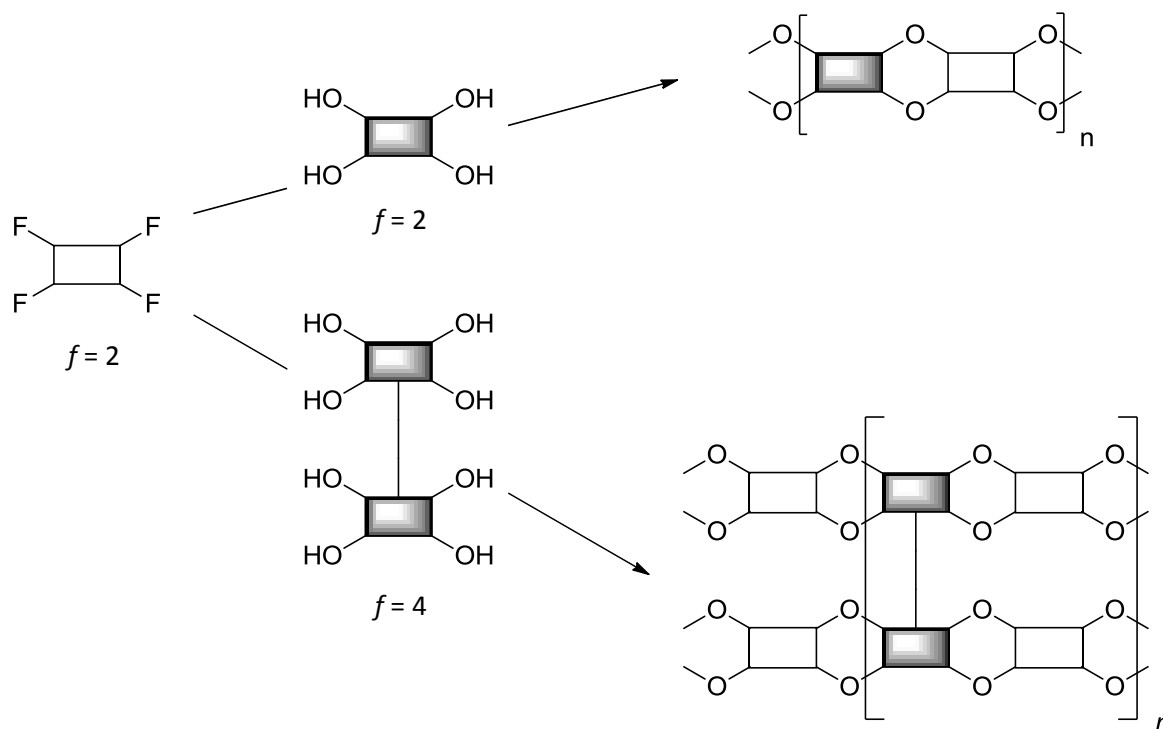
Figure 1.8 Ladder (top) and network (bottom) PIM formation.

1.6.1 Ladder PIMs

Whilst some porous phthalocyanine and porphyrin based network polymers (that are now classed as network PIMs) were published in 2002,[105,106] the term *Polymer of Intrinsic Microporosity* or *PIM* was not coined until the publication of the soluble ladder polymer *PIM-1* in 2004.

PIM-1 is produced from the efficient dibenzodioxane forming reaction between two commercial monomers: 5,5',6,6'-tetrahydroxy-3,3,3',3'-tetramethyl-1,1'-spirobisindane (THSBI) and 2,3,5,6-tetrafluoroterephthalonitrile (TFTPN) (**Scheme 1.11**). The resulting fluorescent yellow polymer is fully soluble in chloroform and THF, of very high molecular weight (M_W over 200,000 g mol^{-1} as measured by GPC compared to polystyrene standards) and has an apparent BET surface area of 760 m^2 g^{-1} as measured by nitrogen sorption.[103]
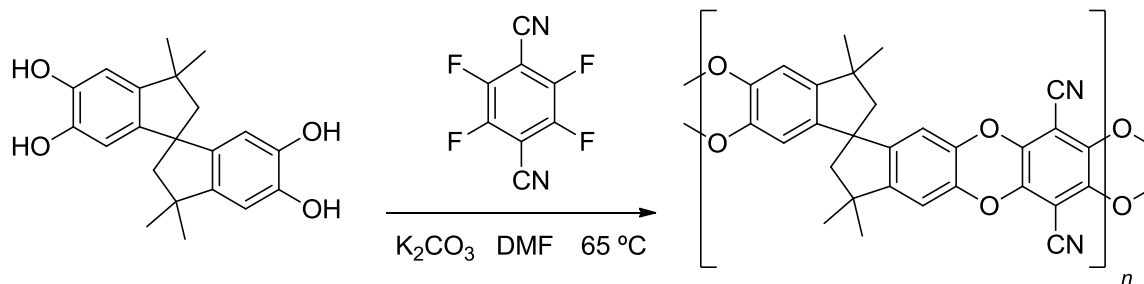
Scheme 1.11 PIM-1 synthesis.

Generally, non-networked polymers such as PIM-1 pack space efficiently as the constituent polymer chains are able to bend and flex to maximise intermolecular interactions (as far as molecules are concerned, *empty space is wasted space*).[70] However, as the backbone of PIM-1 comprises of entirely fused five and six membered rings, the flexibility of the constituent chains is severely limited. This unique property, combined with the sites of contortion (provided by the single carbon atom linking the two five membered rings of the THSBI monomer), leads to a highly rigid and contorted structure that cannot pack space efficiently (**Figure 1.9**), thus leaving voids of free space that create porosity.[15] The microporosity in PIMs is termed *intrinsic* as it arises solely from their molecular structure, and is not dependent on any thermal or processing history[103] (as is required for other porous polymers such as HCPs).
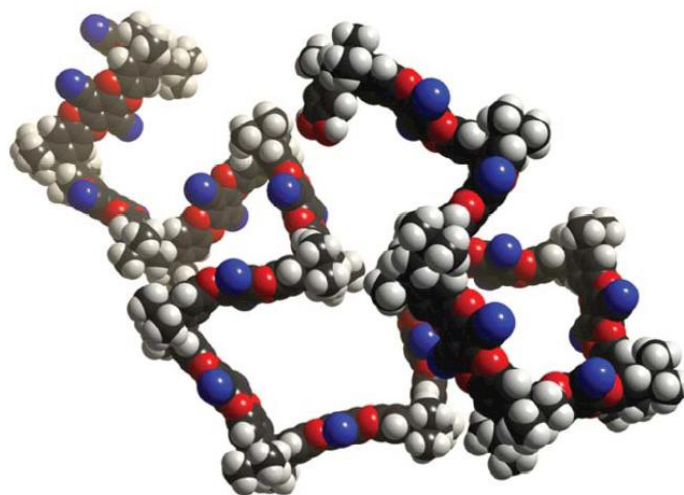

Figure 1.9 Modelled structure of a PIM-1 fragment showing voids created by inefficient packing.

PIM-7 (**Scheme 1.12**) is an alternative ladder PIM in which both monomers contain a site of contortion courtesy of a spirobisindane unit. Despite the added complexity of the constituent monomers, the macromolecular structures of PIM-1 and PIM-7 are very similar (each having five fused six membered rings between spirocentres), and therefore possess a very similar degree of porosity (BET surface areas: PIM-1 – 760 $m^2 g^{-1}$, PIM-7 – 750 $m^2 g^{-1}$).[16] However, whilst the replacement of the nitrile groups of PIM-1 with the phenazine units of PIM-7 does not have considerable impact on the structure of the polymer backbone, it does facilitate the coordination of metal ions. This was demonstrated by addition of bis(benzonitrile)palladium (II) chloride to a solution of PIM-7 resulting in an immediate precipitation of a red powder. The insoluble material was found to contain over 20 % by mass of Pd^{2+} and remained highly microporous (BET surface are 650 $m^2 g^{-1}$), inferring that a palladium cross-linked polymer had been formed.[16] Similar palladium containing microporous materials have been shown to act as efficient heterogeneous catalysts in carbon cross-coupling reactions.[107]
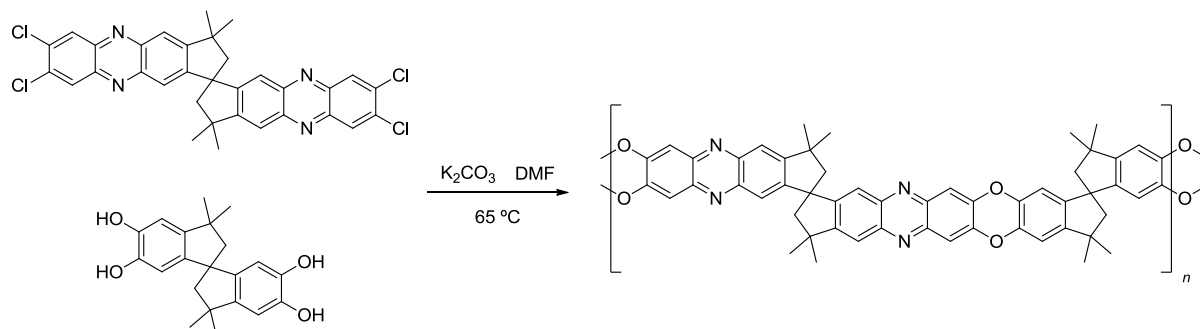
Scheme 1.12 Synthesis of PIM-7.

Ladder polymers such as PIM-1 and PIM-7 possess all of the properties (and hence application) of regular microporous polymers, however what sets them apart from others is their solubility in common organic solvents. This allows them to be cast into robust, free-standing membranes that can potentially be used for industrial gas separation applications depending on their properties. Simply put, an effective gas separation membrane must be highly permeable and highly selective for one gas over another. Unfortunately, many highly permeable polymers show low selectivity and *vice versa*, a relationship that was demonstrated in 1991 by Robeson's double-logarithmic plots of selectivity against permeability (**Figure 1.10**).[108] From these plots, Robeson was able to identify an *upper-*

bound that illustrated the observed trade-off between the two factors in all known polymer membranes to date. Promisingly, the data obtained for both PIM-1 and PIM-7 lay above the upper-bound for many gas pairs, demonstrating the excellent potential of PIMs for gas separation membranes and prompting Robeson to re-calculate his upper-bound.[109] A feat which may well be repeated, as the very recently developed class of ladder PIMs dubbed *Trögers Base PIMs*[110] lay well above the re-calculated upper-bound for many gas pairs. For the sake of brevity, this new class of ladder PIMs will not be discussed at further length, but the interested reader is referred to the Science paper referenced above.
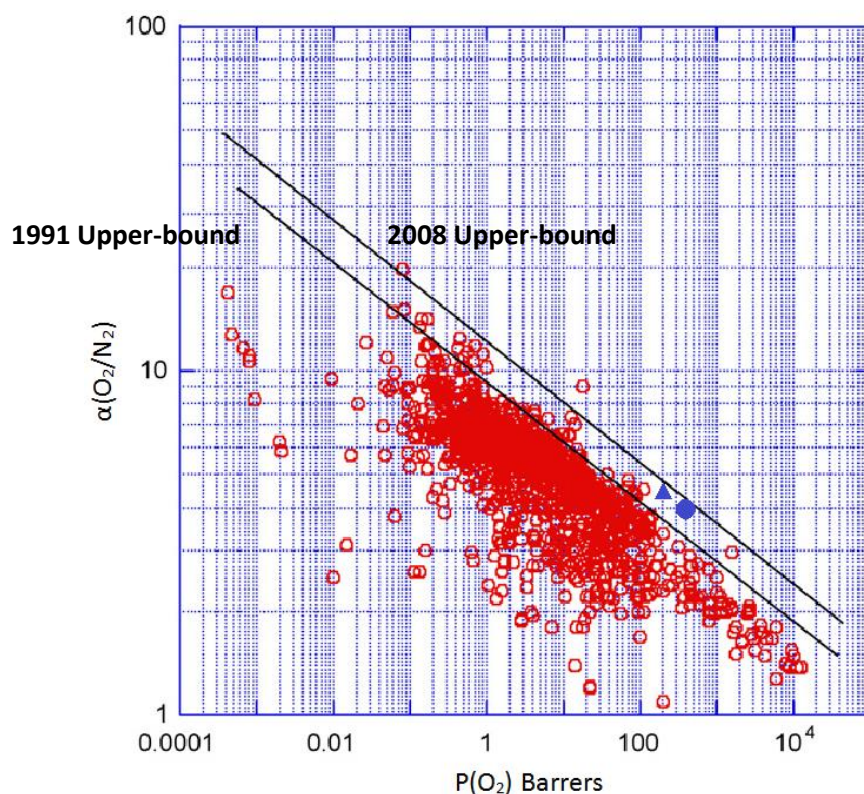

Figure 1.10 Double log plot of permeability (*P*) against ideal selectivity (*α*) for O_2/N_2. PIM-1 (blue circle), PIM-7 (blue triangle).
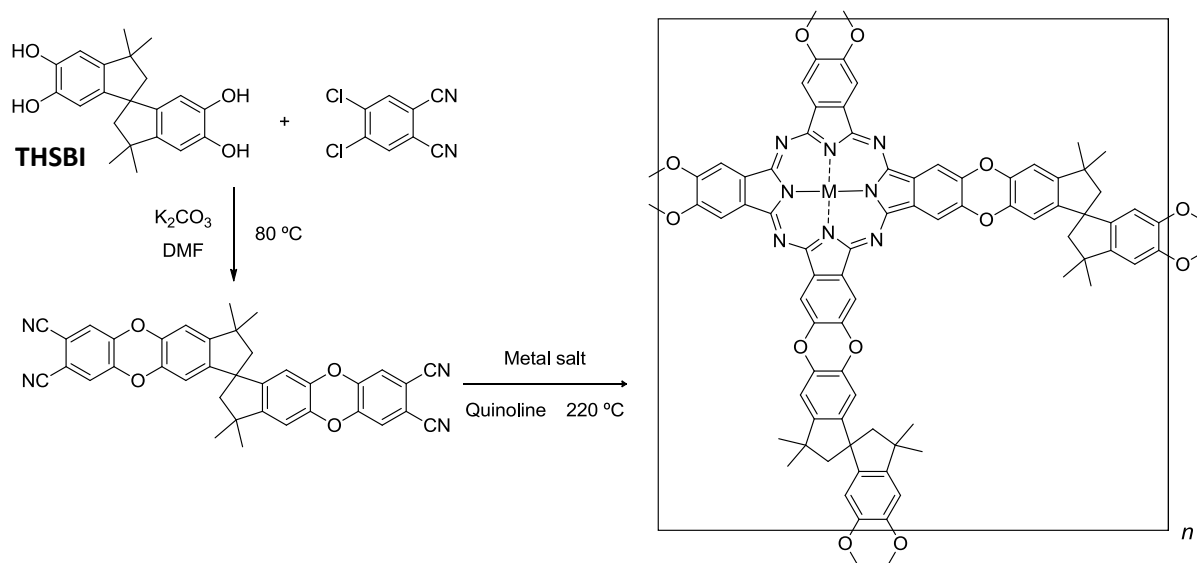
1.6.2 Network PIMs

1.6.2.1 Phthalocyanine Network PIMs

The application of discrete phthalocyanines (e.g. PMCs) as homogeneous catalysts has been well documented,[111,112] however much research has been directed towards incorporating

phthalocyanine centres into networked systems. These *heterogeneous* systems would benefit from increased ease of recovery and diminished degradation/deactivation when employed as catalysts.[113] Furthermore, a porous phthalocyanine network with a high surface area would eliminate the need to load the catalyst onto a suitable support.[114,115]

Many of the phthalocyanine networks known in the literature do not form porous materials,[116] likely due to their planarity and tendency to form dense solids (composed of columnar stacks) in order to maximise intermolecular interactions.[105] However, McKeown *et al*. have shown that by using THSBI as a rigid spirocyclic linker (**Scheme 1.13**), an orthogonal relationship between adjacent phthalocyanine units can be enforced, thus diminishing intermolecular interactions and inducing porosity.[105] The same effect was later observed through the use of bulky triptycene units as linkers between the phthalocyanine centres.[117]

Scheme 1.13 Synthesis of a phthalocyanine network PIM containing rigid spirocyclic linkers.

Analysis of the phthalocyanine network PIMs by nitrogen sorption revealed BET surface areas ranging from $450 - 950$ $m^2 g^{-1}$ depending on the metal cation (or lack of).[105] Their stability at low pressures, elevated temperatures and to a wide range of solvents reinforces the potential of phthalocyanine network PIMs as excellent candidates for heterogeneous catalysis.[113]

1.6.2.2 Porphyrin Network PIMs

Given the promising results achieved with phthalocyanine network PIMs, research was undertaken to determine if similar rigid, metal-coordinating structures could be incorporated into polymer networks. One such example is that of porphyrins: aromatic compounds, which like phthalocyanines possess four nitrogen atoms able to coordinate a metal centre, generating similar scope for catalytic activity.[113,118]

It is well known that the formation of porphyrins from pyrrole and a suitable aldehyde is far less efficient than the corresponding formation of a phthalocyanine,[119] therefore porphyrin formation is not a suitable route to network formation. A much more efficient route was revealed by McKeown *et al*. who showed how a pre-formed, fluorine-functionalised porphyrin (5,10,15,20-tetrakis(pentafluorophenyl)porphyrin) could be reacted with THSBI to form a porous porphyrin network (**Scheme 1.14**).[106]
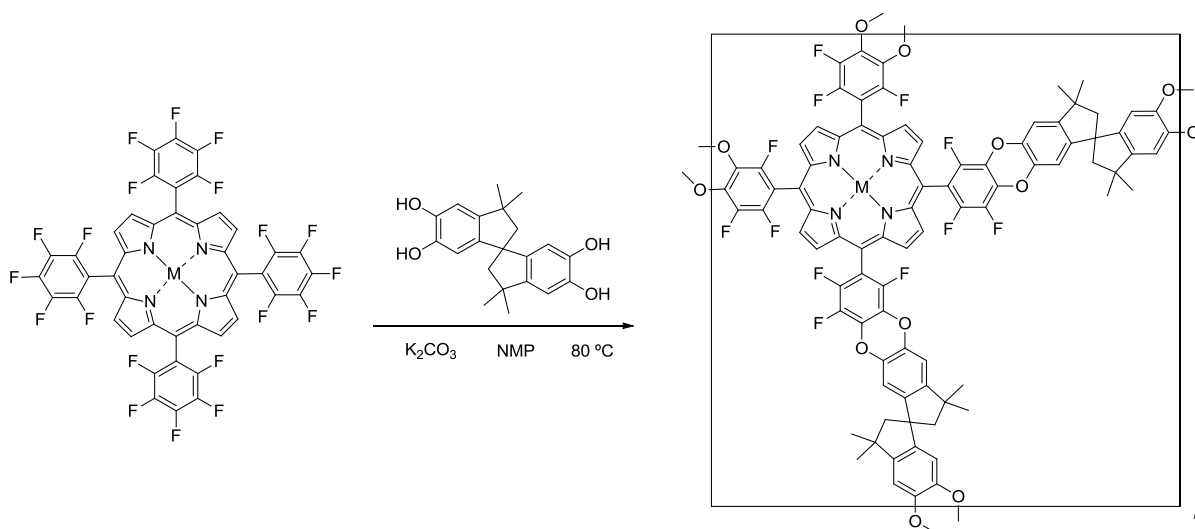
Scheme 1.14 Porphyrin network PIM formation.

Previous studies indicated that the *para* fluorine atom of the porphyrin is the most activated towards nucleophilic substitution,[120] leading to the hypothetical structure shown in **Scheme 1.14**, containing twelve residual fluorine atoms per repeat unit. This structure was confirmed by both elemental analysis, and isolation of a tetra-substituted porphyrin in 90 % yield upon reaction of the same porphyrin with catechol (**Figure 1.11**).
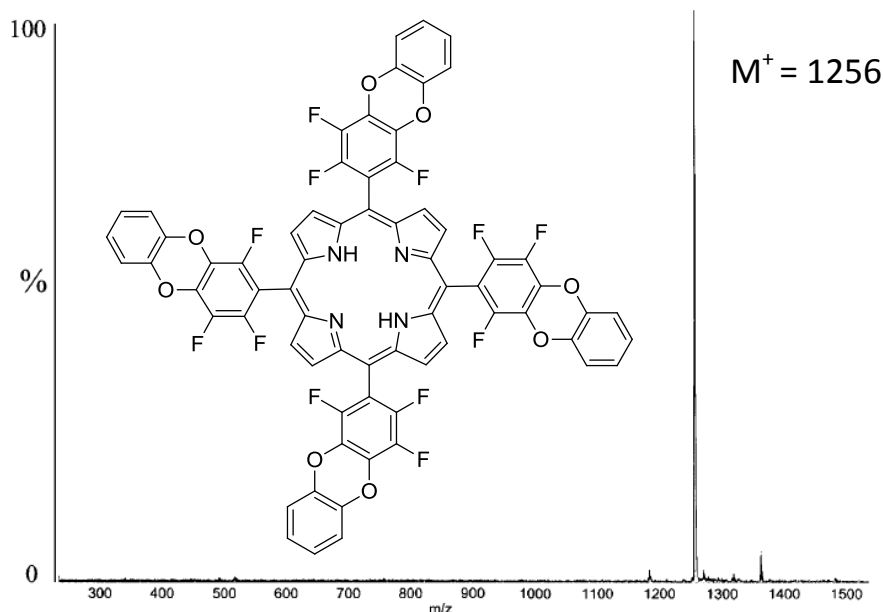
Figure 1.11 MALDI mass spectrum of the tetra-catechol-substituted porphyrin (inset).

Nitrogen sorption studies showed these porphyrin network PIMs to have BET surface areas of close to 1000 $m^2 g^{-1}$, demonstrating that despite the presence of C-C single bonds (at the *meso* positions of the porphyrin), there is sufficiently restricted rotation to prohibit structural relaxation, and maintain the open pore structure.[113]

1.6.2.3 HATN Network PIM

The hexaazatrinaphthylene (HATN) unit (**Scheme 1.15**) is an appealing component for the manufacture of network PIMs due its three-fold symmetry, rigid planarity and phenanthroline-like binding sites for metal ion complexation. The hexachloro HATN monomer can be simply obtained *via* the efficient condensation of 1,2,3,4,5,6-cyclohexanehexone with 4,5-dichlorobenzene-1,2-diamine in high yield.[121] Once formed, the monomer is reacted with the ever popular THSBI monomer to form a highly stable (thermal degradation above 420 °C), highly porous (BET surface area 750 – 850 $m^2 g^{-1}$, as measured by nitrogen sorption) network polymer (**Scheme 1.15**).[104]
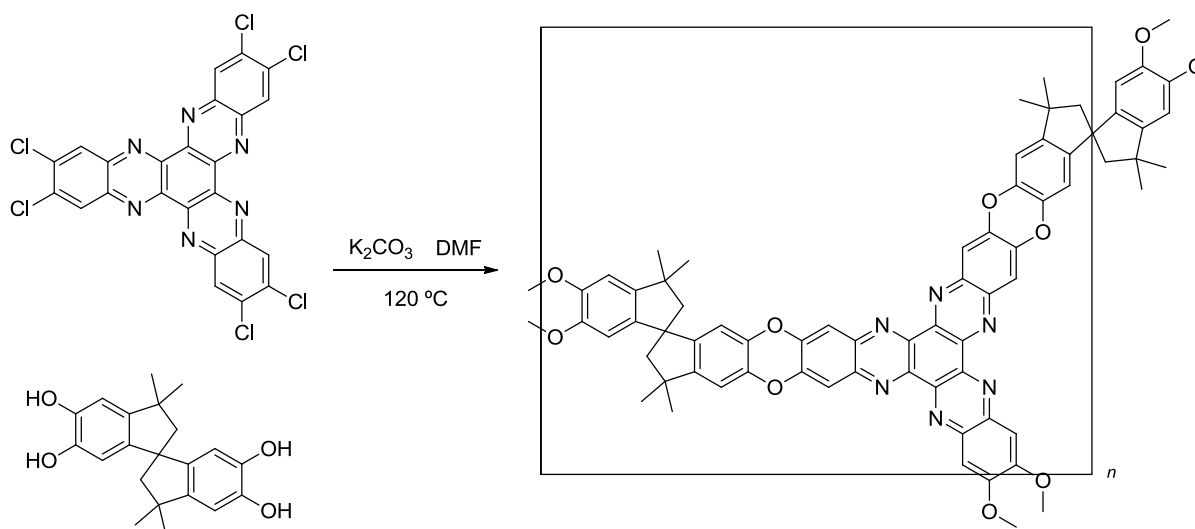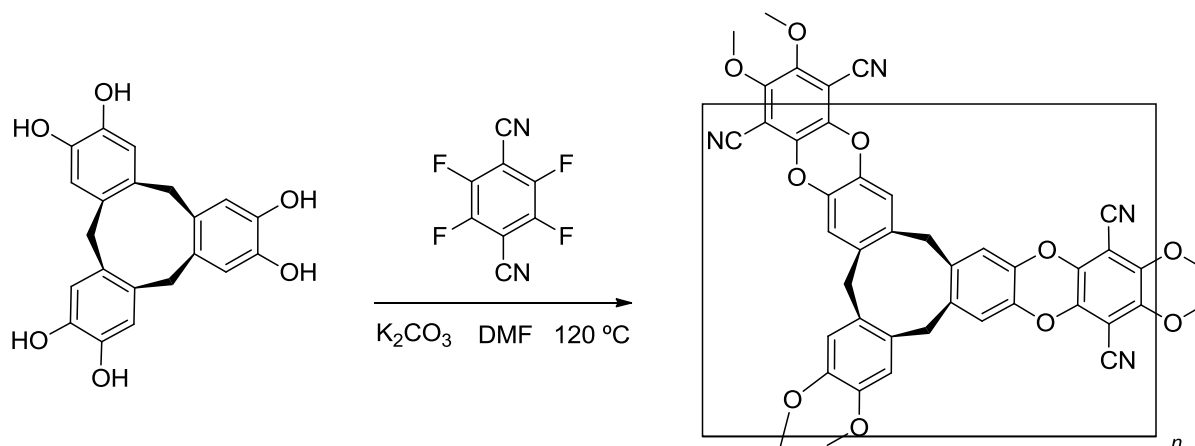
Scheme 1.15 HATN Network PIM synthesis.

Treating a sample of the HATN network PIM with a chloroform solution containing excess bis(benzonitrile) palladium(II) chloride, generated a new material that was shown to have roughly three complexed palladium (II) moieties per HATN unit. The palladium doped polymer was measured by nitrogen sorption to retain a BET surface area of 350 $m^2 g^{-1}$, which whilst substantially lower than the un-complexed polymer, can be largely assigned to a gain in mass rather than a loss of porosity.[104]

1.6.2.4 CTC and TBTQ Network PIMs

The microporosity in all of the ladder and network PIMs discussed so far has been exclusively due to the presence of a *site of contortion*, contributed by a spirobisindane based monomer. The following examples demonstrate an alternative way of generating microporosity; through the use *awkward molecular geometry*.

The first PIM to show a high degree of porosity without containing a site of contortion was the network derived from the cyclotricatechylene (CTC) unit whose structure was first determined in 1965.[122] The central, bowl-shaped[123] nine-membered ring in CTC offers the unique advantage of producing porous materials containing pre-formed cavities of known diameter. By exploiting this property, one can envisage how materials could be prepared to possess a desired pore size distribution that favours adsorption of specific gases.

The hexahydroxy CTC PIM monomer (formed by the acid mediated cyclic trimerisation of verataldehyde and subsequent demethylation)[123] is reacted with TFTPN to give a network polymer with a BET surface area of 830 $m^2 g^{-1}$ as measured by nitrogen sorption (**Scheme 1.16**).[124]

Scheme 1.16 CTC network PIM synthesis.

A second bowl-shaped monomer: tribenzotriquinacene (TBTQ)[125] whose structure is similar to that of CTC (but with the addition of a central carbon atom which splits the central nine-membered into three fused five-membered rings) has since been incorporated into network PIMs by Vile *et al*. (**Scheme 1.17**).[126] It was anticipated that the fused ring structure should enforce greater rigidity of the polymer and that substitution of the apical carbon with bulky substituents would hinder columnar stacking of the bowl-shaped units, thus enhancing porosity. Suitably functionalised hexahydroxy TBTQ monomers were synthesised containing either methyl or isopropyl substituents at the apical carbon position. Reaction of these monomers with TFTPN in standard PIM forming conditions yielded network PIMs with BET surface areas of 565 $m^2 g^{-1}$ (methyl) and 673 $m^2 g^{-1}$ (isopropyl).[126]
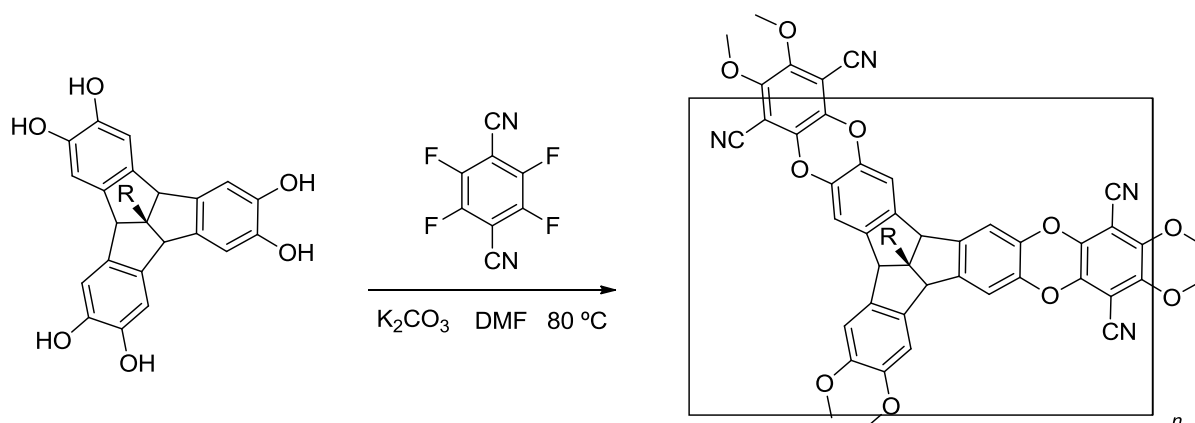
Scheme 1.17 TBTQ network PIM synthesis. R = Me or ^{i}Pr.

The diminished surface areas (in comparison to the CTC network PIM) were attributed to two factors: firstly, that once incorporated into a polymer network, the anticipated flexibility of the CTC unit is not seen, thus no advantage is gained from further rigidity and secondly, the concavity of the bowl in a TBTQ unit is less than that of a CTC unit. This was demonstrated by comparison of crystal structures measured by single crystal X-ray diffraction of the CTC and TBTQ monomers (**Figure 1.12**). Encouragingly however, the desired effect of adding a bulkier apical carbon substituent was observed, as the isopropyl TBTQ network PIM had a surface area over 100 $m^2 g^{-1}$ higher that the methyl TBTQ PIM.
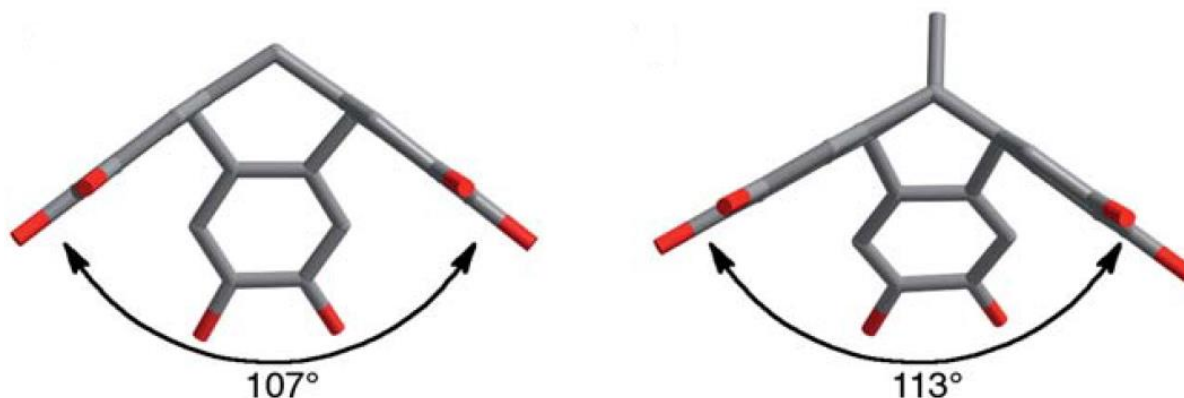

Figure 1.12 Crystal structures of CTC (left) and TBTQ-Me (right) monomers, showing increased concavity in CTC.

1.6.2.5 Triptycene Network PIMs

As discussed previously, *triptycene* (the first in a series of aromatic hydrocarbons dubbed '*iptycenes*')[127] is a well-studied unit in the field of porous materials, largely due to its high internal free volume.[72] Its three-fold symmetry also lends itself well to the formation of network polymers *via* a suitably tri-functionalised monomer. For example, triptycenes functionalised with three catechol units can be reacted with TFTPN to form highly porous network PIMs (**Scheme 1.18**).[73,74]
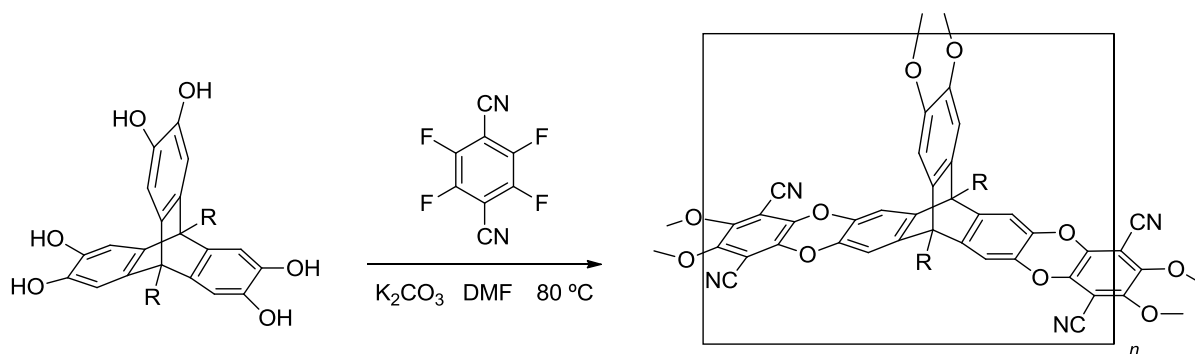
Scheme 1.18 Synthesis of triptycene network PIMs.
R = H, Me, Et, Pr, ^{i}Pr, Bu, ^{i}Bu, Pent, Oct, Bz.

A series of triptycene network PIMs were prepared with alkyl chains of varying length attached to the bridgehead position of the triptycene monomer. It was found that short alkyl chains (H, Me, Et, Pr) led to highly porous materials (BET surface areas of 1343 – 1760 m^2g^{-1}), but increasing the length of the alkyl chains further led to a decrease in porosity in a fairly constant manner (**Figure 1.13**). The high degree of porosity is attributed to the perpendicular orientation of the plane of polymer growth and the faces of the ribbon-like 'struts' linking triptycene units. This arrangement is surmised to block any face-to-face association of the planar struts, and thus further frustrate space efficient packing and produce more/larger cavities.[73]
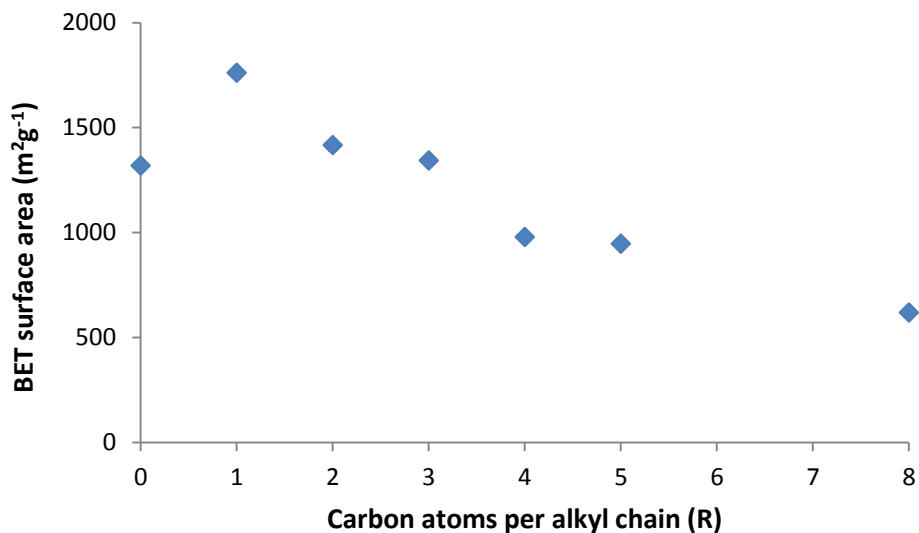
Figure 1.13 BET surface area vs. bridgehead alkyl chain length in triptycene network PIMs (0 = H, 1 = Me, 2 = Et, 3 = Pr...).

1.7 Discrete Amorphous Microporous Materials

The use of discretely amorphous materials as a medium for gas sorption was, until recently, a completely unexplored area of research.[128] In 2009 Tian *et al.*[129] published the first example of such materials based on *noria* macrocycles (named after the Latin for *waterwheel* in accordance with their structure, **Scheme 1.19**).[130]
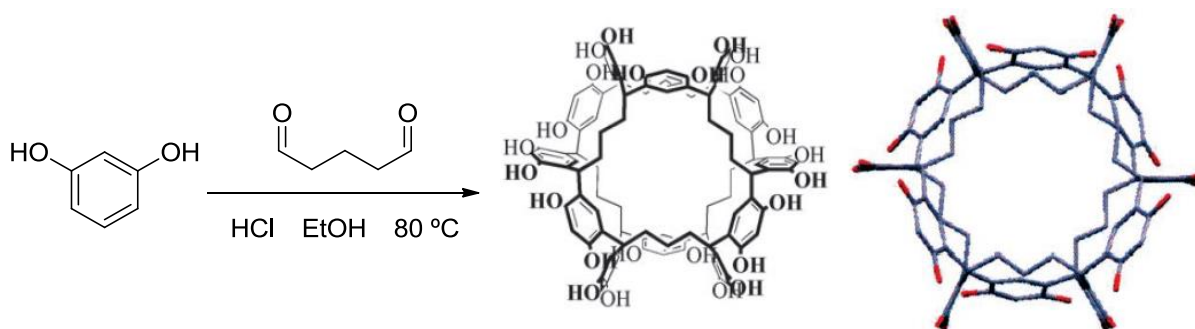
Scheme 1.19 Synthesis of a noria macrocycle and crystal structure (right). The central cavity is approximately 7 Å in diameter.

These finely ground materials were shown to be fully amorphous by powder X-ray diffraction studies and although their affinity for nitrogen was poor (apparent BET surface area of 40 $m^2 g^{-1}$ as measured by nitrogen sorption), surface areas of up to 350 $m^2 g^{-1}$ were obtained using CO_2 as the adsorbate. The authors speculate that the inherent microporosity

is due to a combination of the large central cavity and inefficient packing of the constituent macrocycles.

Since 2009, further examples of discretely microporous amorphous materials have been published,[131-133] including a series of triptycene-based nickel salphens (**Scheme 1.20**).[131] These largely amorphous materials, produced *via* the Schiff base condensation of primary amines with salicylaldehyde derivatives (much like the Mastalerz group's cage compounds, **Scheme 1.6**),[71] were shown to possess apparent BET surfaces areas up to 500 m^2 g^{-1}.
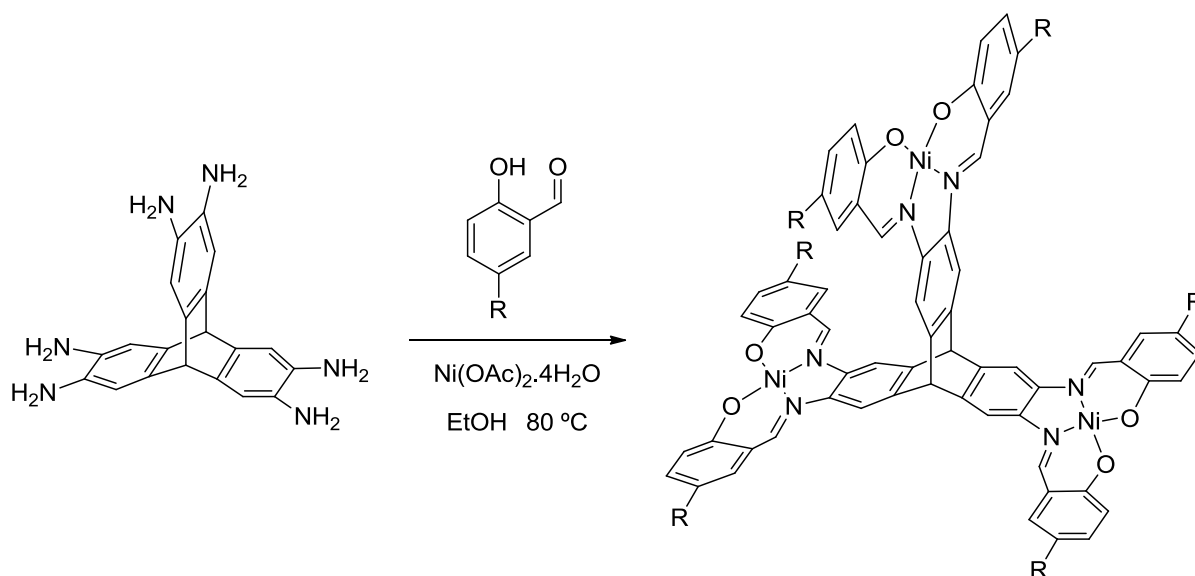
Scheme 1.20 Synthesis of a triptycene based nickel salphen.
R = H, ^{t}Bu.

Unlike cage compounds (**Scheme 1.6**) and noria macrocycles (**Scheme 1.19**), porosity in nickel salphens arises solely from inefficient packing of the awkwardly shaped molecules, rather than from in-built molecular cavities. Single crystal X-ray diffraction studies of the metal salphen shown in **Scheme 1.20** (R = H), reveal how the triptycene moieties prevent close packing of constituent molecules leading to substantial void space (**Figure 1.14**). Furthermore, the authors demonstrate how appending bulky tertiary butyl groups to the extremities of these structures leads to an increase in their apparent porosity, a structure-property relationship that will be explored in the work presented in this thesis.
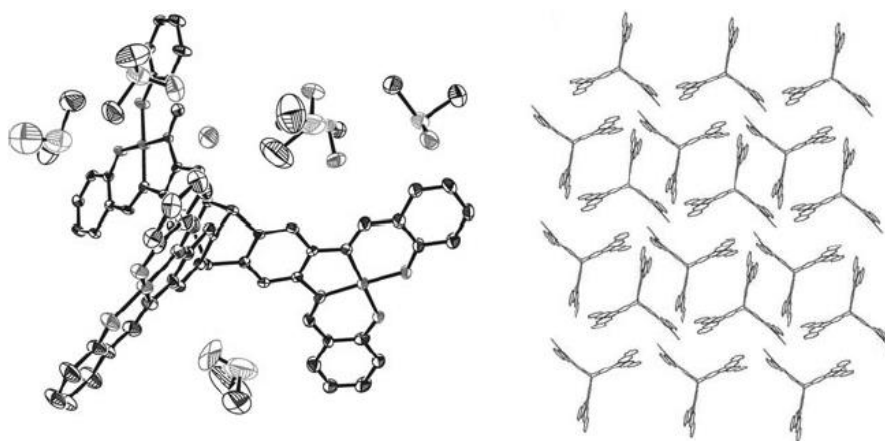
Figure 1.14 Crystal structure (left) and packing (right) of a triptycene based metal salphen showing significant void space. Protons and solvent molecules (packing) removed for clarity.

Expanding upon their previous work on porous crystalline organic cages (Chapter 1.4.4),[68] Cooper's group recently published a series of predominantly amorphous organic cages synthesised through the Schiff base condensation of triformylbenzene (TFB) with ethane-1,2-diamine (EDA) and cyclohexane-1,2-diamine (CHDA) (**Scheme 1.21**).[132]
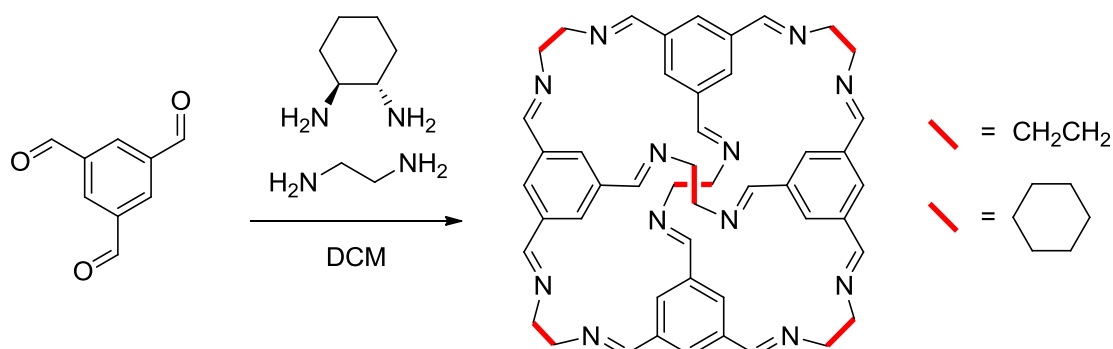
Scheme 1.21 Synthesis of amorphous cages.

By varying the ratio of EDA to CHDA (**Scheme 1.21**), highly stable amorphous materials (as demonstrated by thermogravametric and X-ray diffraction analyses) with apparent BET surface areas up to 704 $m^2 g^{-1}$ were produced. Through further exploitation of the dynamic nature of imine bonds,[134,135] the authors were able to *scramble* crystalline samples of cage compounds produced *via* the reaction of TFB with either EDA or CHDA.[68] This *cage-cage interchange* reaction produced an amorphous material with an apparent BET surface area of 818 m^2g^{-1}, the highest of any discrete amorphous material to date.[132]

2. Organic Molecules of Intrinsic Microporosity

2.1 Background

As established in the previous chapter, there are two well-studied classes of porous materials: *crystalline ordered structures*, whose porosity arises from in-built molecular voids (e.g. zeolites,[32] MOFs,[38] COFs[55] and MMCs),[136] and *amorphous structures*, whose porosity arises from their inability to pack space efficiently in the solid state (e.g. PIMs[137] and HCPs).[19] Within these two classes, the vast majority of materials are based on networked or polymeric structures, with substantially fewer examples of discretely porous materials published to date. Porosity in most discretely porous materials is often attributed solely to in-built molecular voids,[65] or to these voids in combination with frustrated packing in the solid state,[69,133] meaning that to date, there are only a few literature examples of discretely microporous materials (crystalline or amorphous) whose porosity arises solely from frustrated amorphous packing.[131] Organic Molecules of Intrinsic Microporosity (*OMIMs*) offer themselves as a potential candidate for this relatively unexplored area of porous material research.

When typical discrete molecules come together to form crystalline solids, the constituent molecules do so in such a way that intermolecular interactions are maximised and hence the amount of void space is minimised (this can be viewed as efficient packing).[138] To maximise the amount of void space and create a porous material, intermolecular interactions need to be inhibited, such that when the constituent molecules come together to form solids, they do so in an inefficient manner and hence create voids. Research by Jiao *et al*. has shown that for both two[139] and three dimensional[70] shapes, packing efficiency (Φ) will be at its lowest when the shapes possess highly concave faces (**Figure 2.1**). The authors studied various octahedra of varying degrees of concavity/convexity as measured by their *deformation parameter*, p (p = 0.5 represents a regular octahedron, p < 0.5 represents a concave octahedron reaching the limit of three dimensional cross at p = 0 and p > 0.5 represents a convex octahedron, reaching a perfect sphere at p = 1 and a perfect cube at p = ∞, **Figure 2.1**). It was shown that although convex octahedra reach a minimum packing efficiency (Φ) of around 0.75 for a sphere (p = 1), concave octahedra are capable of exhibiting much lower

packing efficiencies, an observation that gives rise to the research hypothesis that: '*organic molecules possessing strongly concave faces will pack space inefficiently in the solid state thus giving rise to porous materials*'.
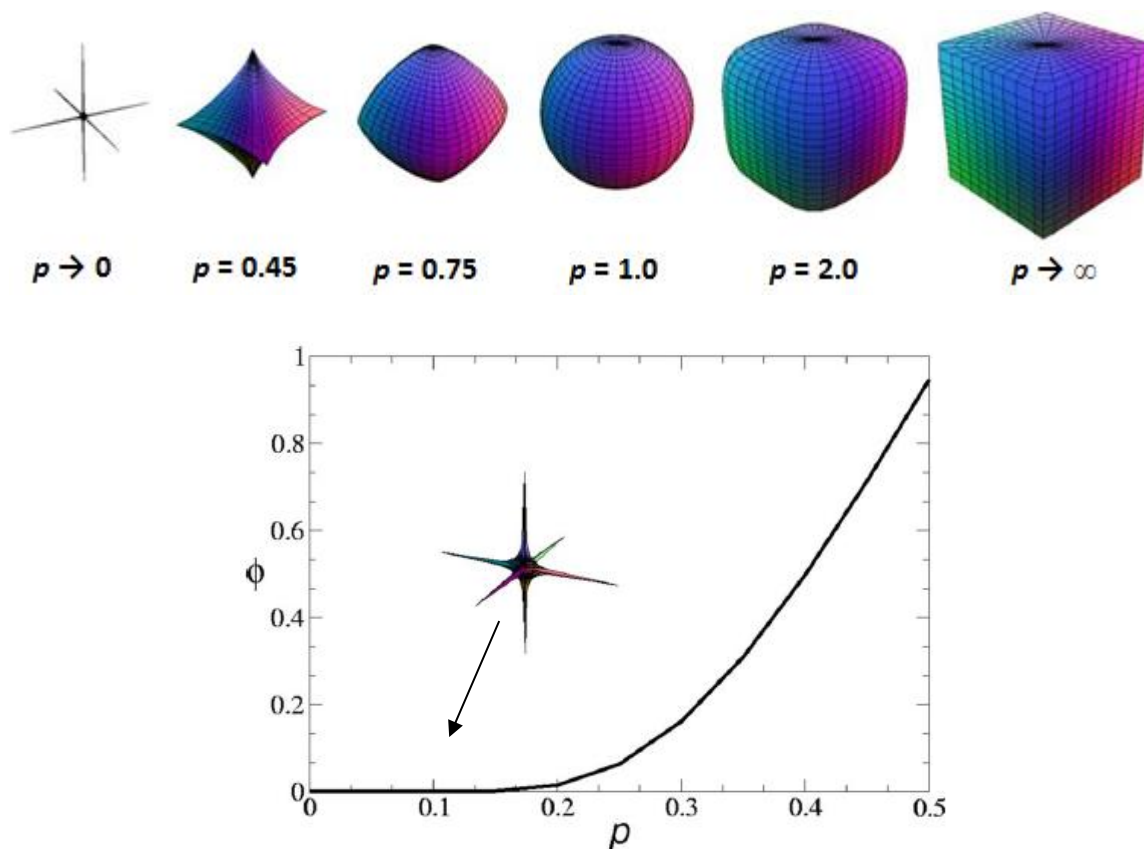
Figure 2.1 Various three-dimensional shapes as defined by their deformation parameter (*p*) (top), and packing efficiency (*Φ*) vs. deformation parameter (*p*) for concave octahedra (bottom) with inset p = 0.1 octahedra.

With the above hypothesis established, eleven potential precursors to organic molecules of intrinsic microporosity (OMIMs) with highly concave faces were proposed (**Figure 2.2**). Each precursor possesses either awkward molecular geometry (triptycenes, propellanes), or enforced orthogonality (biphenyls, spirobisfluorenes) such that when a core and terminus are combined a large, three dimensional, awkwardly shaped molecule is produced in the form of an OMIM.
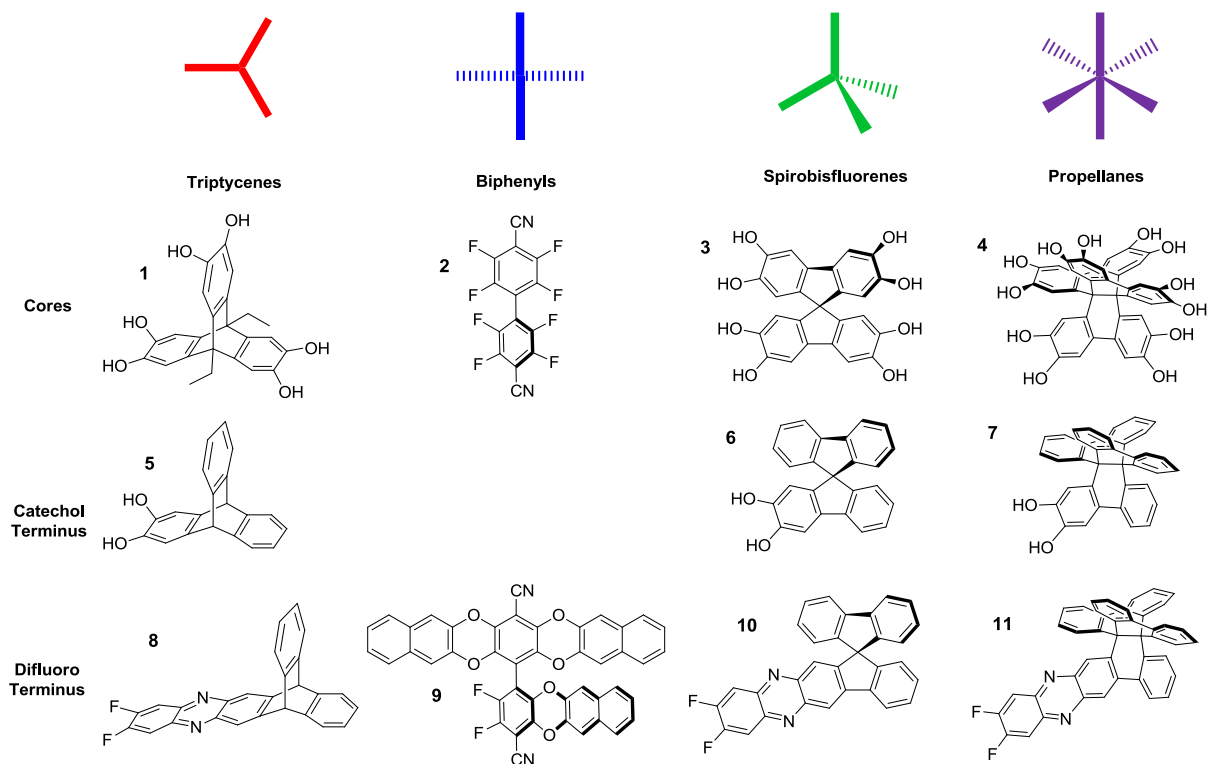
Figure 2.2 Potential OMIM precursors.

These precursors can be sub-divided into two categories: *cores* (**1 – 4**) and *termini* (**5 – 11**). Both are functionalised with either pairs of *ortho*-fluorine or *ortho*-hydroxy (catechol) groups, such that when combining a core with a terminus of opposing functionality, a double nucleophilic aromatic substitution reaction will occur to form a rigid, six membered dibenzodioxane linking unit (as previously utilised in PIMs).[103] Naturally, all termini precursors are functionalised with just one pair of reactive groups (*functionality* or *f* = 1). However, cores must possess a functionality of at least three (*f* ≥ 3) to ensure a three-dimensional structure is formed when reacted with a chosen terminus (a core with *f* = 2 could give rise to a porous material, but it opens up one spatial dimension to efficient packing).

Several of the precursors in **Figure 2.2** have already been synthesised by colleagues either as cores for network PIMs,[73,74,140] or to establish a proof of concept for this work.[5,141] Much of the content of this chapter will demonstrate a more systematic approach to OMIM precursors, through the study of the structure-property relationship of smaller termini,

which will then be applied to some of the above precursors in an effort to test the limits of these materials.

2.2 Synthesis of octafluoro

Many of the OMIMs discussed in this thesis are based around biphenyl core **2**: 4,4-dicyano-2,2',3,3',5,5',6,6'-octafluorobiphenyl, or *"octafluoro"*). The compound, whilst commercially available at great expense[142] can be synthesised in one step from relatively cheap commercial materials (**Scheme 2.1**). Hence, 2,3,4,5,6-pentaflurorobenzonitrile was reacted with tris(diethylamino)phosphine in anhydrous diethyl ether based on the literature procedure by Kaneko *et al.*.[143]
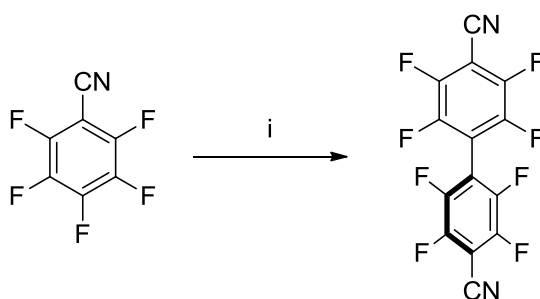
Scheme 2.1 Synthesis of octafluoro.
Reagents and conditions: i) P(NEt$_2$)$_3$, Et$_2$O, 3 hrs, RT.

After three hours, the reaction was adjudged to be complete owing to total consumption of the *pentafluoro* starting material, as observed by thin layer chromatography. Purification was achieved using column chromatography over silica gel to yield the desired product in 35 % yield. Subsequent recrystallisation from methanol yielded large, white needle-like crystals whose X-ray diffraction analysis (**Figure 2.3**), combined with ^{19}F NMR, ^{13}C NMR and high resolution mass spectrometry, confirmed the purity and structure of the desired product.
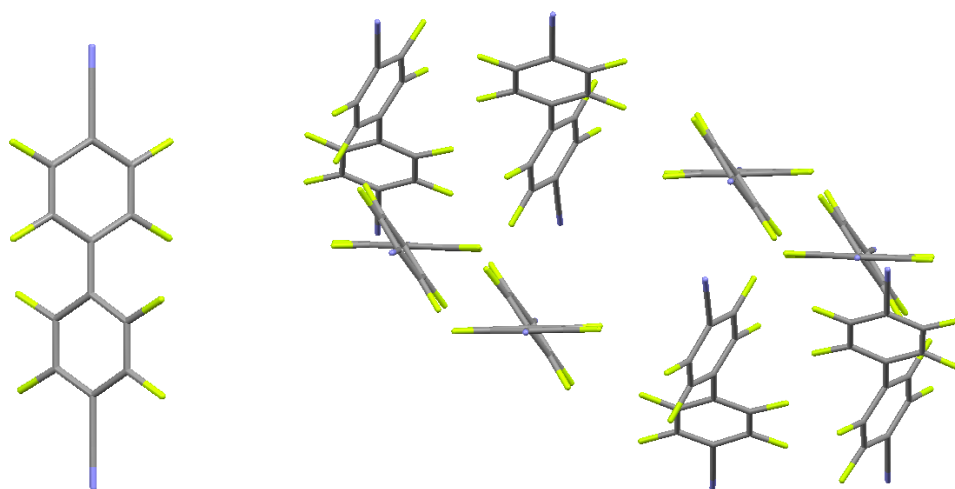
Figure 2.3 Biphenyl core **2** (octafluoro) crystal structure (left), and packing (right). Solvent molecules removed for clarity.

Owing to the relatively modest yield and complete consumption of starting material, efforts were made to isolate some of the other reaction by-products visible in the crude TLC (at least four by-products, as well as some baseline material). A second column afforded small quantities of the first two unknown by-products for analysis. The first gave more complicated ^{19}F and ^{13}C NMR spectra (than the previously isolated octafluoro), likely indicating the presence of a larger/less symmetrical product. Mass spectrometry confirmed this, revealing a molecular ion peak at *m/z* = 503, which was coincident with the inclusion of a third molecule of 2,3,4,5,6-pentafluorobenzonitrile (with the corresponding loss of two fluorine atoms). This led to the proposed structure (dubbed *undecafluoro*) shown in **Figure 2.4** which was subsequently proved *via* X-ray diffraction studies on a sample recrystallised from propan-2-ol.
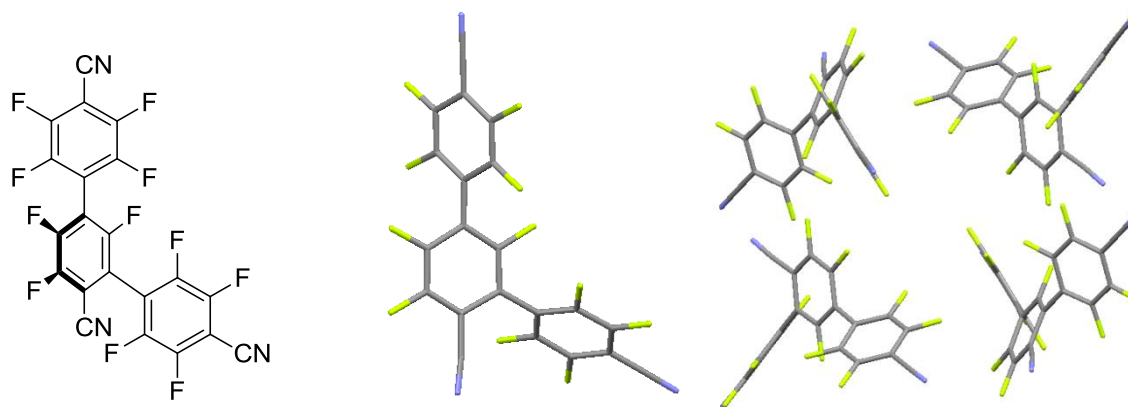
Figure 2.4 Isolated by-product '*undecafluoro*' structure (left), crystal structure (centre) and packing (right), solvent molecules removed for clarity.

Characterisation of the first unknown product as a *'trimer'* of 2,3,4,5,6-pentafluorobeznonitrile naturally led to the assumption that the second would be a tetramer, and indeed this was found to be the case as mass spectrometry showed a peak at *m/z* = 658. The ^{19}F NMR of this tetramer proved significantly more complex than that of the dimer or trimer, suggesting the presence of regioisomers (**Figure 2.5**). Attempts to crystallise any further products were unsuccessful, however with the evidence already collected it seems reasonable to suggest that higher order (pentamers, hexamers etc...) and perhaps even oligomeric/polymeric structures are being formed during the reaction and thus diminishing the overall yield of the octafluoro dimer.
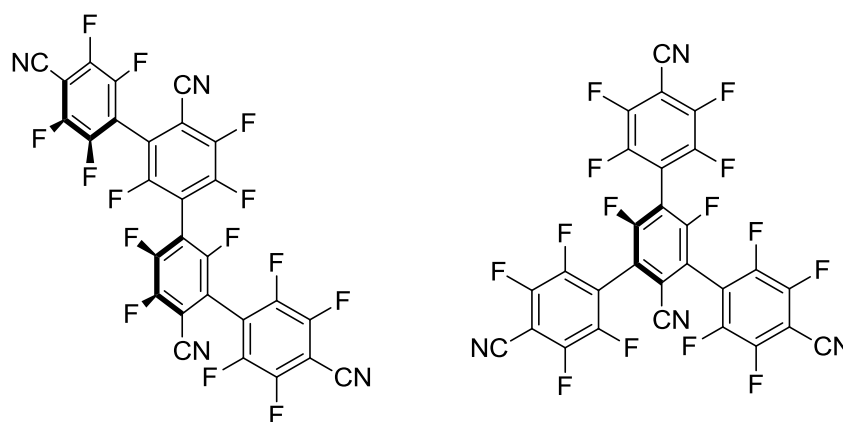
Figure 2.5 Isolated *'tetramer'* by-product showing two possible regioisomers.

A brief amount of time was spent trying to optimise the reaction conditions for octafluoro formation but no significant and repeatable improvement on 35 % was made.

2.3 Biphenyl OMIMs

2.3.1 Catechol based biphenyl adducts

With a synthetic route to multi-gram quantities of the biphenyl core, octafluoro, established, its reactivity with catechol based termini was investigated by first reacting it with catechol (**Scheme 2.2**). Reaction condition optimization proved difficult (due to the issues discussed below), however it was found that using a slight excess (4.2 equivalents) of catechol under PIM forming conditions[144] gave the best results.
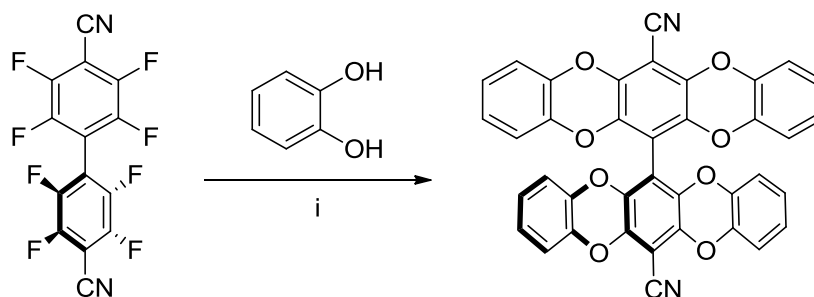
Scheme 2.2 Synthesis of the tetra-[catechol] biphenyl adduct.
Reagents and conditions: i) K_2CO_3, DMF, 65 °C, 72 hrs.

Following an aqueous work up, TLC analysis of the crude yellow powder revealed total consumption of the octafluoro starting material and that multiple products had formed. *Gel Permeation Chromatography*, GPC, analysis confirmed this showing two peaks (**Figure 2.6**), one of which corresponded to material with a molecular weight of roughly 600 g mol^{-1}, and another to a material of double that (roughly 1200 g mol^{-1}).

Peak RV - (ml)	20.033	20.550
Mn - (Daltons)	1,134	558
Mw - (Daltons)	1,175	592
Mz - (Daltons)	1,226	623
Mp - (Daltons)	1,021	599
Mw / Mn	1.036	1.060
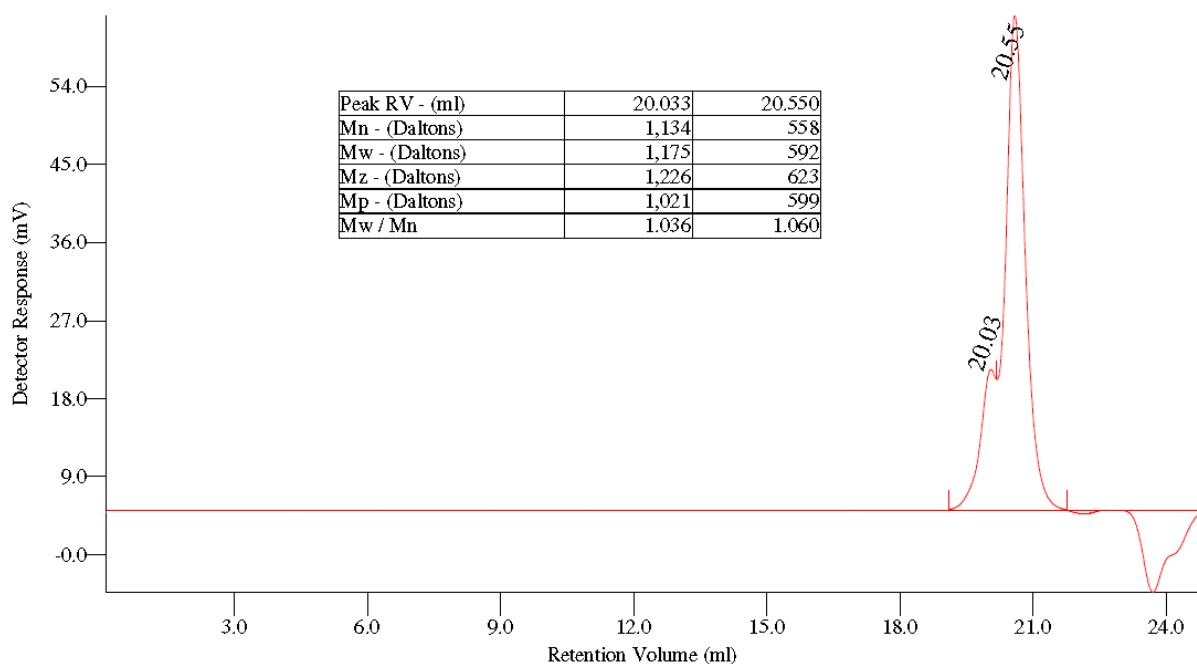
Figure 2.6 GPC trace and relevant data (inset) of the crude reaction products from the synthesis of the tetra-[catechol] biphenyl adduct.

Attempts were made to recrystallise the crude material from toluene but these yielded only equally impure precipitates. Accordingly, the material was purified by column

chromatography to give three fractions. Mass spectrometry, ^{1}H NMR and ^{19}F NMR showed the first fraction to be the tri-substituted analogue of the desired product (**Figure 2.7**), a surprising result considering that excess catechol had been added to the reaction with the sole purpose of avoiding the formation of this by-product. However, only a trace amount of this tri-substituted material was recovered.
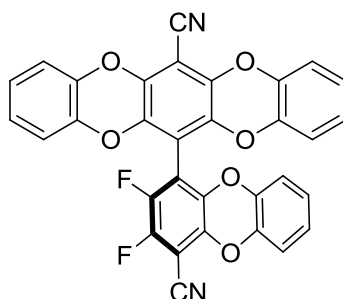
Figure 2.7 Isolated by-product, tri-[catechol] biphenyl adduct.

Thankfully, the same analyses revealed the second fraction to be the desired tetra-substituted product (no peaks visible in the ^{19}F spectrum), which was isolated in a 74 % yield. Subsequent crystallisation *via* slow diffusion of methanol into chloroform solution yielded small crystals whose analysis revealed the anticipated structure (**Figure 2.8**).
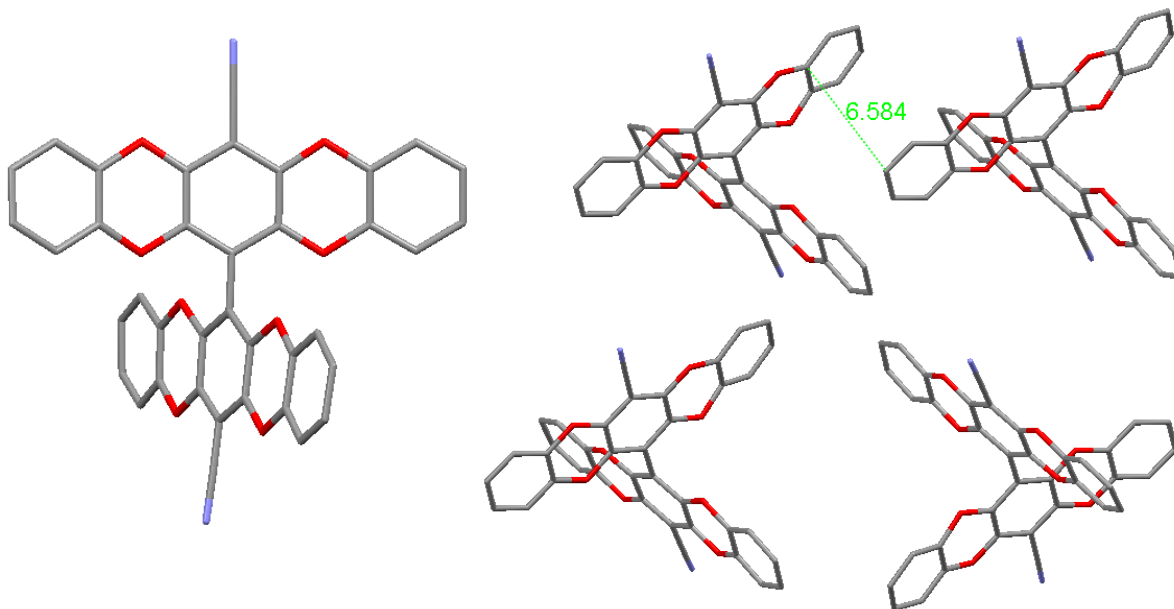
Figure 2.8 Crystal structure (left) and packing (right) for the tetra-[catechol] biphenyl adduct. Protons and solvent molecules removed for clarity, distances in Å.

The relatively similar molecular weights of the tri and tetra substituted compounds, combined with the presence of a large excess of one in the crude reaction mixture, are likely to have caused them to elute from a GPC column together as a single peak. It was therefore assumed that the second (left hand) peak of the GPC trace was due to the third fraction.

Analysis of the third fraction using matrix-assisted laser desorption ionisation mass spectrometry (MALDI-MS) revealed it to comprise of a multitude of *bridged compounds* in which a single catechol molecule bridged two biphenyl cores (**Figure 2.9**). Indeed, TLC analysis using more polar eluents displayed a large number of spots; however attempts to isolate a reasonable quantity of any pure bridged compound were unsuccessful. Again, given the lack of distinctly different molecular weights, these bridged compounds are likely to have eluted from a GPC column with very similar retention times (hence as a single peak), resulting in only two distinct peaks visible in the crude GPC trace.
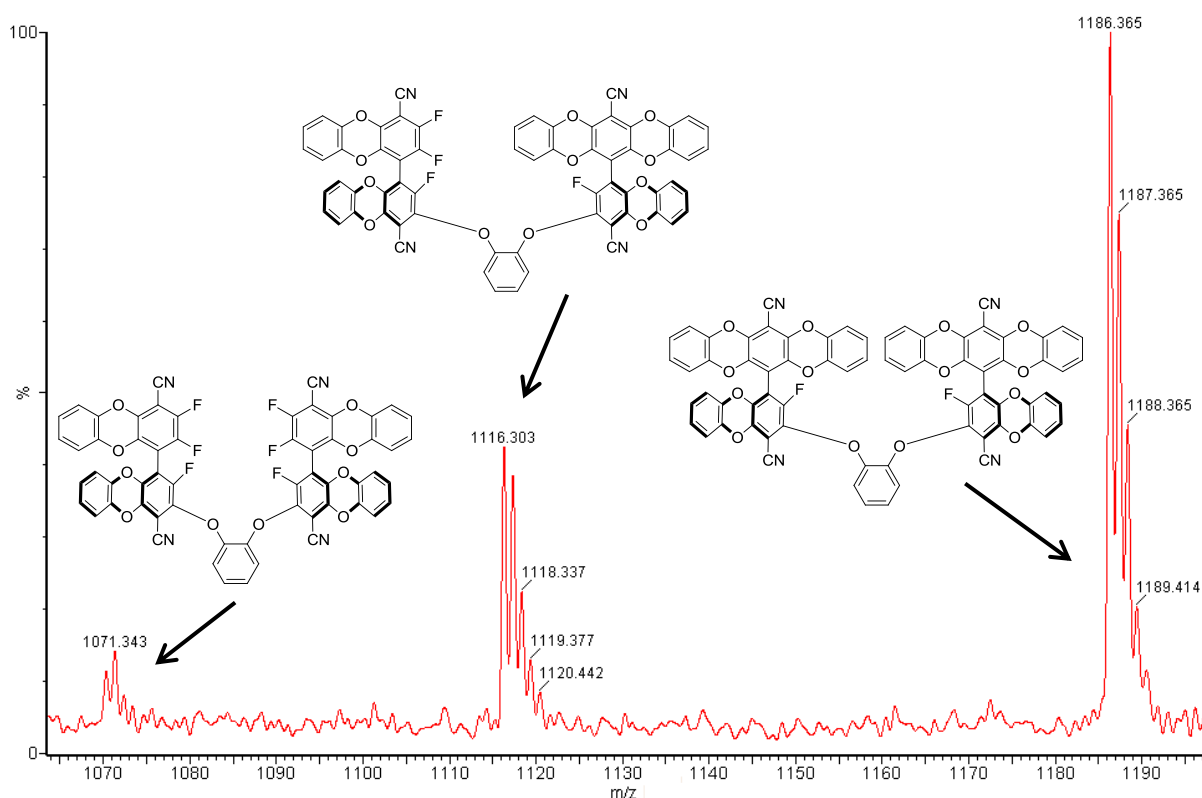
Figure 2.9 MALDI mass spectrum showing presence of bridged compounds. Larger multi-bridge compounds were also visible.

The reaction was repeated and monitored by TLC, which unfortunately demonstrated that bridged compounds formed simultaneously with the desired un-bridged products and as such, no further improvement on a yield of 74 % was seen. BET analysis (using nitrogen sorption at 77 K) of the pure tetra-substituted compound indicated the material to be non-porous with an apparent BET surface area and pore volume of 7 $m^2\,g^{-1}$ and 0.03 $cm^3\,g^{-1}$ respectively. As well as being non-porous, the tetra-substituted adduct was also poorly soluble, a property that is likely due to the rigid planarity of the flat aromatic termini. In an effort to overcome this, two analogues of the tetra-substituted product were prepared using 4-*tert*-butylcatechol and 3,5-di-*tert*-butylcatechol (**Scheme 2.3**). It was anticipated that the resulting structures would be more soluble, due to the flexible nature of the *tert*-butyl groups and perhaps also more porous, due to the additional cavities generated by the presence of the bulky groups.
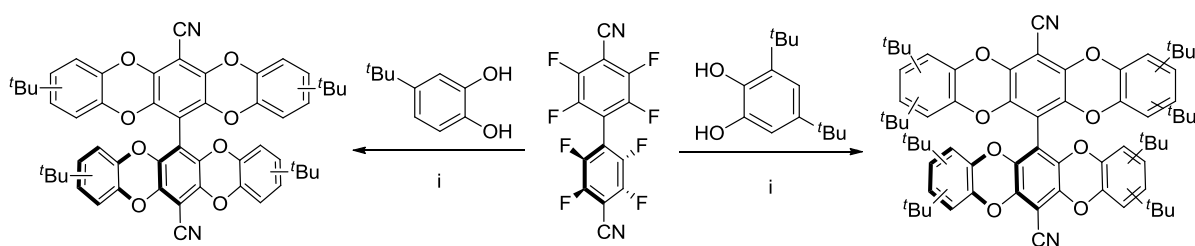
Scheme 2.3 Syntheses of the tetra-[4-*tert*-butylcatechol] and [3,5-di-*tert*-butylcatechol] biphenyl adducts.
Reagents and conditions: i) K_2CO_3, DMF, 65 °C, 72 hrs.

In both cases, reactions between a *tert*-butylcatechol and octafluoro led to the formation of bridged compounds as seen in the catechol adduct (**Figure 2.9**), leading to slightly diminished yields (80 % for 4-*tert*-butylcatechol and 70 % for 3,5-di-*tert*-butylcatechol). However, these impurities were readily removed *via* column chromatography along with any trace amounts of tri-substituted material that was still present in the crude reaction mixture. Due to the unsymmetrical nature of both *tert*-butylcatechols, both the tetra-substituted biphenyl adducts were isolated as mixtures of regioisomers. Partial separation of regioisomers could be achieved in an efficiently run column, owing to their very slightly different retention times, however overlap was unavoidable so no single regioisomer could be isolated in this manner. Purity of both the highly soluble compounds was established using ^{1}H, ^{13}C and ^{19}F NMR combined with MALDI-MS and GPC.

BET analysis of the two new compounds showed a subtle improvement over the catechol adduct, with the mono and di-*tert*-butyl compounds both demonstrating enhanced surface areas (41 and 67 m^2 g^{-1} respectively). **Figure 2.10** shows the nitrogen sorption isotherms of the three tetra-[catechol] biphenyl adducts as measured at 77 K. The increasing size of the hysteresis (gap between the adsorption and desorption plots) seen for the *tert*-butyl containing compounds indicates that more of the adsorbed nitrogen is being 'held on to' after saturation. This has previously been attributed to a molecular rearrangement, or *swelling*, during adsorption,[74] suggesting the more flexible *tert*-butyl containing compounds are able to move slightly during adsorption.
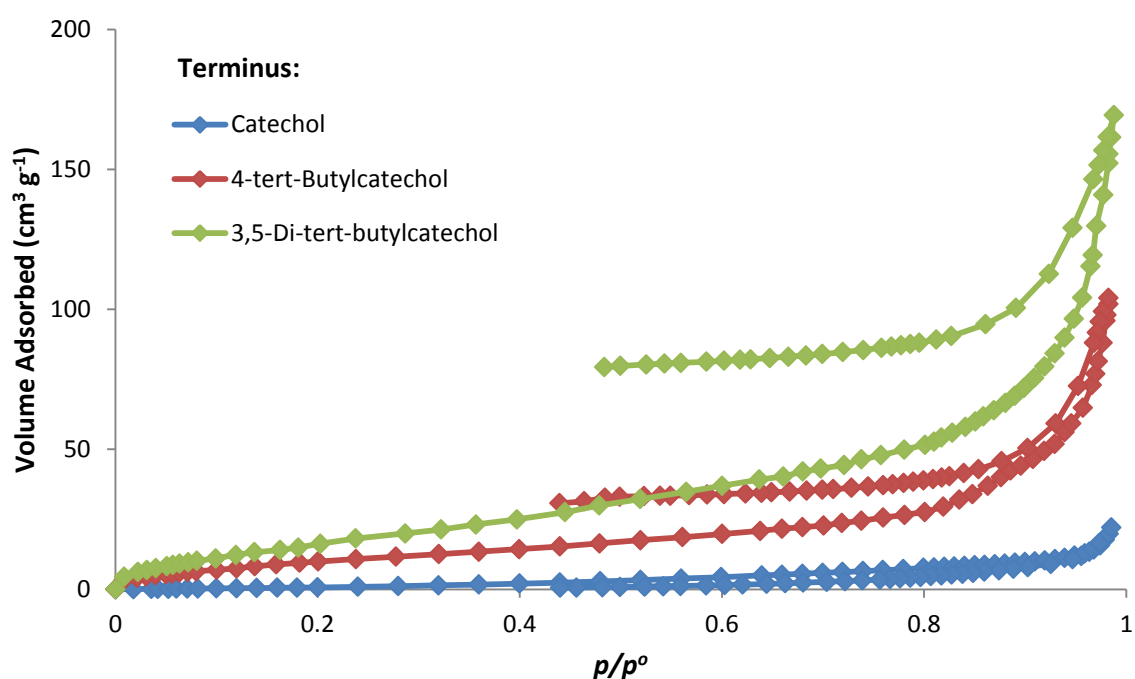
Figure 2.10 BET nitrogen sorption isotherms of the three tetra-[catechol] biphenyl adducts.

Terminus	BET surface area (m^2 g^{-1})	Total pore volume (cm^3 g^{-1})
Catechol	7	0.03
4-*tert*-Butylcatechol	41	0.15
3,5-Di-*tert*-butylcatechol	67	0.23

Table 2.1 Nitrogen sorption data for the three tetra-catechol biphenyl adducts.

Cleary, the introduction of *tert*-butyl groups succeeded in improving the solubility and increasing the surface area of catechol based biphenyl adducts. The latter of which is more impressive when one considers how the large increase in weight associated with an extra *tert*-butyl group, still produces a material with a higher surface area per gram. This effect becomes more apparent when examining the total pore volumes for the three materials (**Table 2.1**), as the di-*tert*-butyl adduct possesses a total pore volume that is nearly an order of magnitude larger than the catechol analogue.

2.3.2 Naphthalene-2,3-diol based biphenyl adducts

With only modest surface areas obtained for catechol based biphenyl adducts, investigations were made into the synthesis of potential OMIMs comprising of larger termini (e.g. naphthalene-2,3-diol), with hopes that the longer *arms* would inhibit packing of the constituent molecules. The first in the series was synthesised by reacting octafluoro with commercially available naphthalene-2,3-diol in analogous reactions conditions to those used in the catechol based biphenyl adducts.
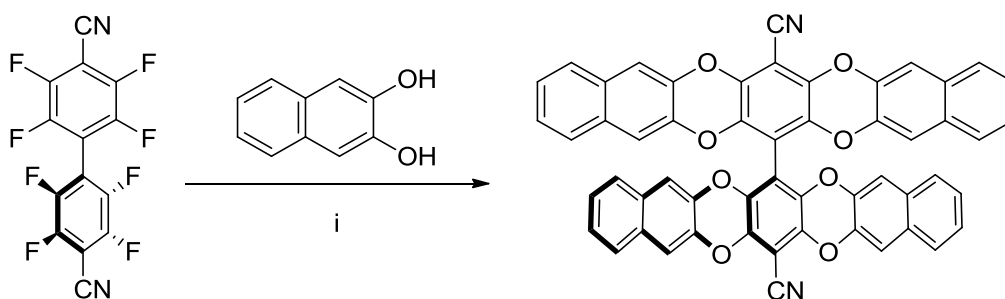
Scheme 2.4 Synthesis of the tetra-[naphthalene-2,3-diol] biphenyl adduct.
Reagents and conditions: i) K_2CO_3, DMF, 65 °C, 72 hrs.

The crude reaction products of this reaction were found to be even less soluble than the catechol analogue, likely due to the presence of extended planar aromatic groups, but were sufficiently soluble in toluene and THF to enable purification by column chromatography (traces of tri-substituted material and bridged compounds were removed). The tetra-substituted product was isolated in only modest yield (44 %) owing to its poor solubility and confirmed pure by ^{1}H NMR, ^{19}F NMR, MALDI-MS and GPC. However, BET analysis

demonstrated it to be similarly non-porous to the tetra-[catechol] adduct, possessing a surface area of only 25 m^2 g^{-1} and a total pore volume of 0.05 cm^3 g^{-1}.

The tetra-[naphthalene-2,3-diol] adducts partial solubility in THF was exploited in an effort to grow crystals so that the nature of the packing and arrangement of the four '*arm*' naphthalene groups about the biphenyl core may be better understood. Crystals were grown by slow evaporation of a THF solution (kept at approximately 40 °C) to generate the structure shown in **Figure 2.11**. Inspection of the packing of the constituent molecules shows the arrangement of the naphthalene arms in over-lapping parallel lines with inter-molecular distances of approximately 6.8 Å. Whilst these interactions are too long range to be considered typical $\pi - \pi$ interactions,[145] such interactions may exist in the solid state, which would offer further explanation for the poor solubility of the material.
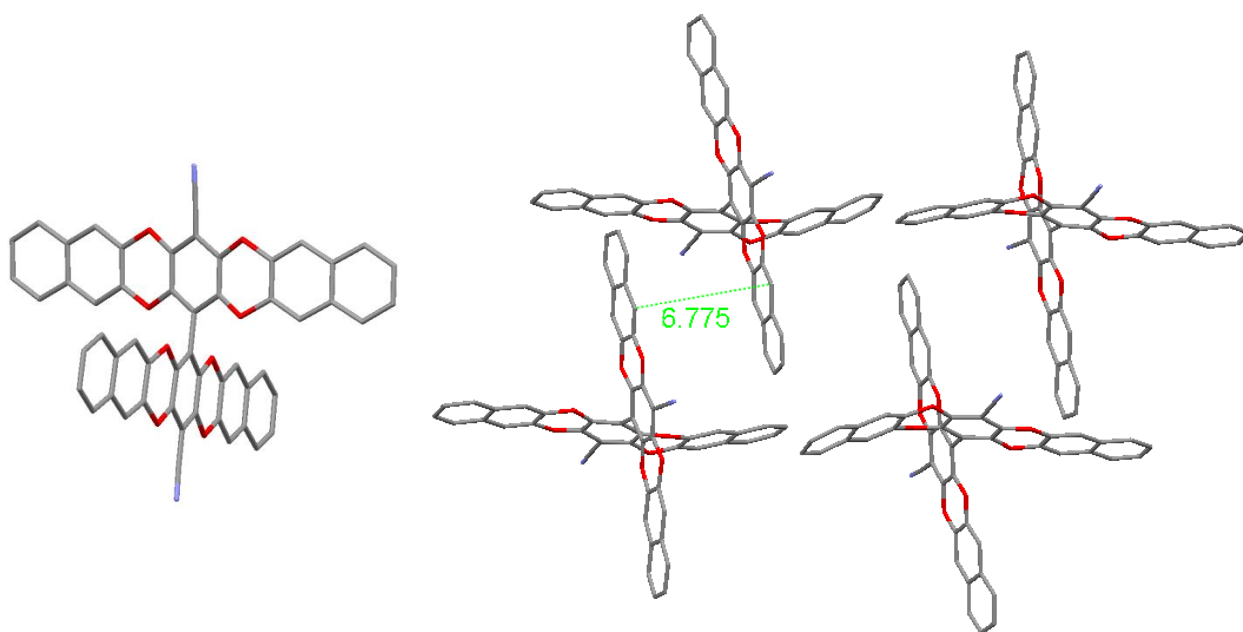
Figure 2.11 Crystal structure (left) and packing (right) for the tetra-[naphthalene-2,3-diol] biphenyl adduct. Protons and solvent molecules removed for clarity, distances in Å.

In a similar vein to the series of catechol based biphenyl adducts, efforts were made to create substituted analogues of the tetra-[naphthalene-2,3-diol] adduct through the use of substituted naphthalene-2,3-diols. No such commercial materials exist, but a simple procedure outlined by Stepakov *et al.*[146] provided an efficient route to two such diols: 6-*tert*-butylnaphthalene-2,3-diol and 6(1-adamantyl)naphthalene-2,3-diol, **Scheme 2.5**.
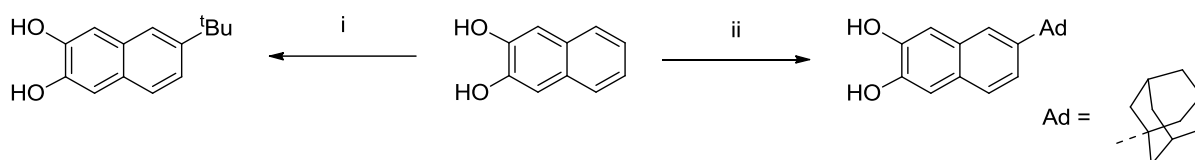
Scheme 2.5 Syntheses of 6-*tert*-butylnaphthalene-2,3-diol and 6-(1-adamantyl)naphthalene-2,3-diol.
Reagents and conditions: i) *tert*-Butanol, TFA, 72 hrs, RT ii) 1-Adamantol, TFA, 12 hrs, RT.

The procedure by Stepakov *et al.*[146] was followed to produce the adamantyl substituted compound in excellent yield (91 %) after 12 hours and adapted for the less stable carbocation of *tert*-butanol to produce the *tert*-butyl substituted compound in equally impressive yield (84 %) after 72 hours. Both compounds required no further purification as confirmed by ^{1}H NMR, ^{13}C NMR and low resolution mass spectrometry, so were subsequently dried and reacted with octafluoro in identical reaction conditions to those used previously.
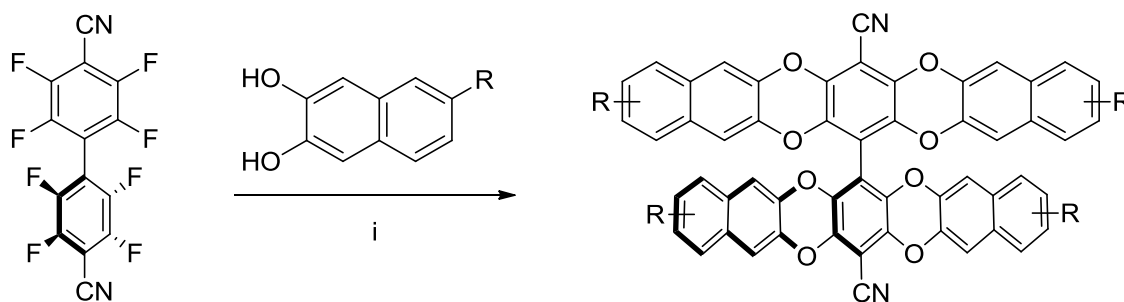
Scheme 2.6 Syntheses of the two substituted tetra-[naphthalene-2,3-diol] biphenyl adducts. R = ^{t}Bu, Ad.
Reagents and conditions: i) K$_2$CO$_3$, DMF, 65 °C, 72 hrs.

After purification by column chromatography, both tetra-substituted adducts were isolated as highly soluble mixtures of regioisomers and their purity established using ^{1}H, ^{13}C and ^{19}F NMR (no peaks in ^{19}F NMR) combined with MALDI-MS and GPC. BET analysis revealed that the introduction of the bulky substituents had had a marked impact on the porosity of the material, as in both cases the apparent BET surface area increased (**Table 2.2**). However, the increased porosity came at a cost, as both compounds gave rise to slow sorption kinetics as indicated by the unusually shaped isotherms (**Figure 2.12)** and longer than normal equilibration times between nitrogen doses during the early stages of adsorption. This phenomenon is discussed in more detail in the following pages.
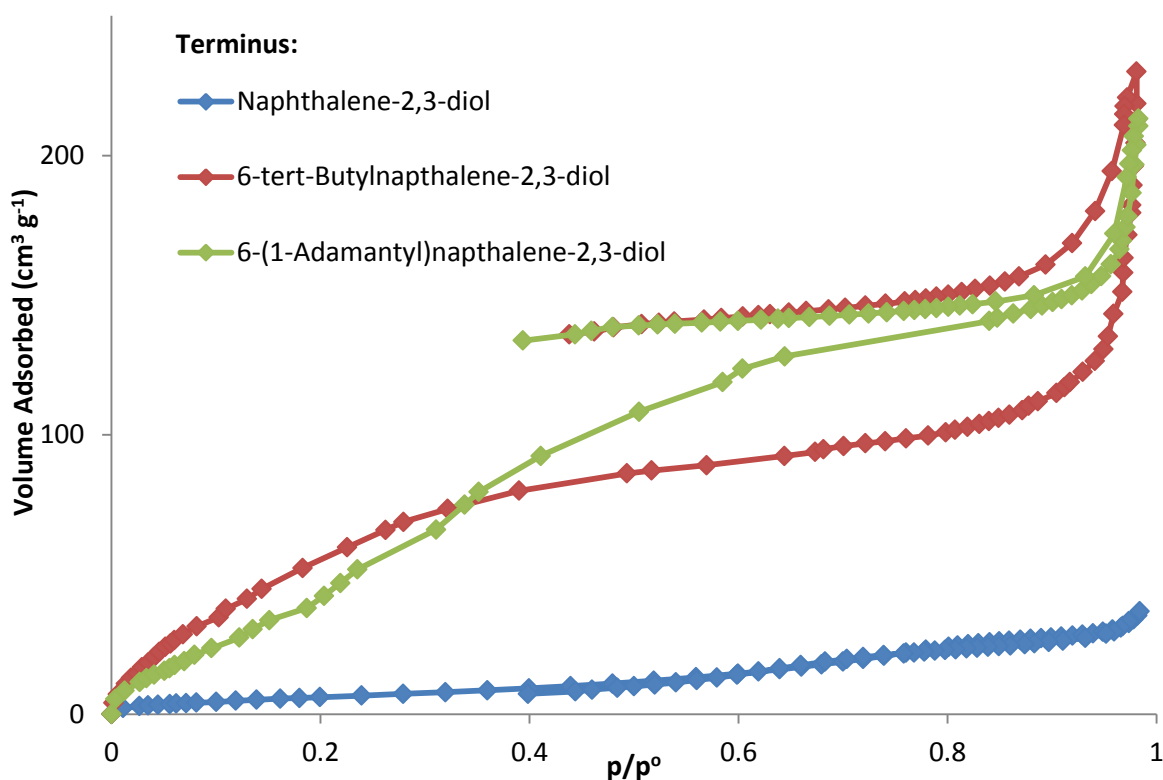
Figure 2.12 BET nitrogen sorption isotherms of the three tetra-[naphthalene-2,3-diol] biphenyl adducts.

Terminus	BET surface area $(m^2 g^{-1})$	Total pore volume $(cm^3 g^{-1})$
Naphthalene-2,3-diol	25	0.05
6-*tert*-Butylnaphthalene-2,3-diol	260	0.33
6-(1-Adamantyl)-naphthalene-2,3-diol	132	0.25

Table 2.2 BET nitrogen sorption data of the three tetra-[naphthalene-2,3-diol] biphenyl adducts.

2.3.3 Triptycene-2,3-diol based biphenyl adducts

2.3.3.1 OMIM-1

As demonstrated in the previous two sections, a biphenyl core substituted with flat, unsubstituted aromatic termini does not produce a highly porous material. Improvements in porosity were observed through appending bulky groups (*tert*-butyl or adamantyl) to the termini, but significant porosity was still not observed. In an attempt to overcome this, the

use of triptycene (a bulky, aromatic compound of high internal free volume[72] that has shown much potential in similar porous materials)[5,13,72,74] as a terminus was investigated. Catechol functionalised triptycene (triptycene-2,3-diol) was prepared *via* a Diels-Alder reaction[147] between anthracene and a freshly prepared dimethoxybenzyne precursor,[148] followed by demethylation with boron tribromide.[147] Subsequent reaction with octafluoro led to the formation of the compound dubbed *OMIM-1*, first synthesised by Dr. Kadhum Msayib.
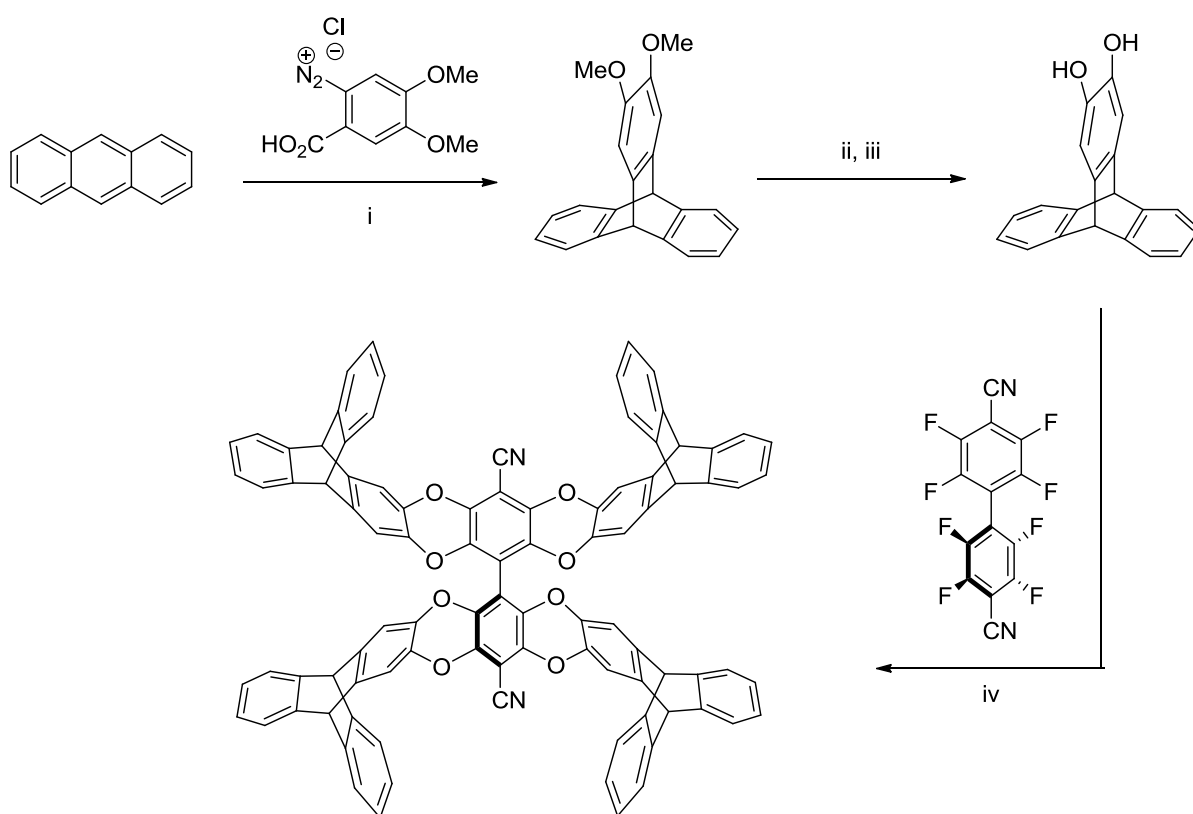
Scheme 2.7 Synthesis of OMIM-1.
Reagents and conditions: i) 1,2-Epoxypropane, DCE, 12 hrs, reflux ii) BBr$_3$, DCM, 3 hrs, RT iii) H$_2$O iv) K$_2$CO$_3$, DMF, 65 °C, 72 hrs.

After purification, *OMIM-1* was found to possess an apparent BET surface area of 480 m^2 g^{-1} as measured by nitrogen sorption, making it one of the first highly microporous materials of this nature, hence the name. Further inspection of the OMIM-1 isotherm (**Figure 2.13**) revealed, that unlike a classic type I isotherm,[10] it had deviated from the y-axis almost immediately, indicating that not all of the dosed nitrogen had been adsorbed before the partial pressure of the analysis tube was measured (given more time, all of the dosed nitrogen may fully adsorb to the surface). The fact that OMIM-1 then continued to adsorb

most of the dosed nitrogen, led to the conclusion that it suffers from slow sorption kinetics. To prove this hypothesis, a sample of OMIM-1 was measured on an ASAP (Accelerated Surface Area and Porosimetry) BET analyser, which allows for full equilibration between each nitrogen dose. As expected, the isotherm took much longer (23 days) to acquire, and produced a typical type I isotherm (**Figure 2.13**), confirming the presence of (very) slow sorption kinetics. Analysis of the ASAP isotherm gave an increased apparent BET surface area of 601 m^2 g^{-1}, demonstrating that slow sorption kinetics can lead to underestimation of apparent BET surface areas (**Table 2.3**). However, given the vastly longer analysis time, it was considered unfeasible to measure all samples in this way.
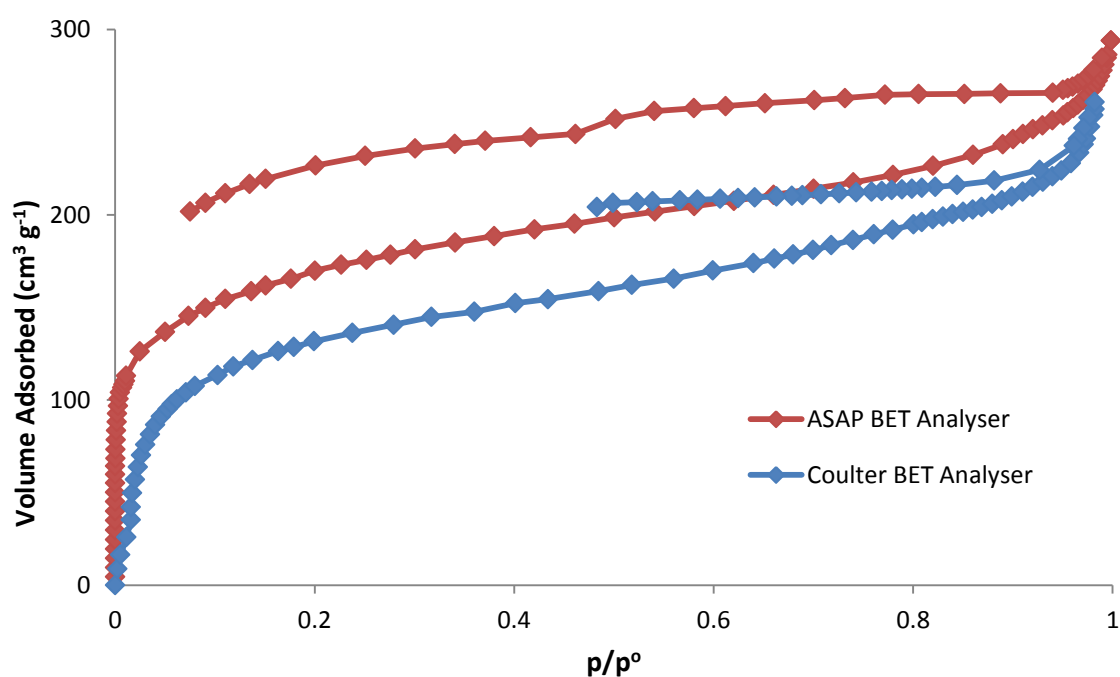
Figure 2.13 BET nitrogen sorption isotherms of OMIM-1 measured in Cardiff (Coulter analyser, measured by Dr. Grazia Bezzu) and Manchester (ASAP analyser, measured by Louise Maynard-Atem).

BET analyser	BET surface area (m^2 g^{-1})	Analysis runtime (hours)
Coulter SA 3100	485	8
ASAP	601	542

Table 2.3 Measured BET surface areas and analysis run times for OMIM-1.

2.3.3.2 Synthesis of alternative triptycene-2,3-diols

Given the vast improvements in porosity achieved when utilising a triptycene based terminus in OMIM-1, the synthesis and use of alternative triptycene-2,3-diols as termini was investigated. It was of interest to see how the structure-property relationships observed thus far would contribute to the porosity and sorption kinetics of new triptycene-2,3-diol based OMIMs. A series of three substituted 2,3-dimethoxytriptycenes were prepared as outlined below, with the intent to convert each into a triptycene-2,3-diol *via* boron tribromide assisted demethylation.
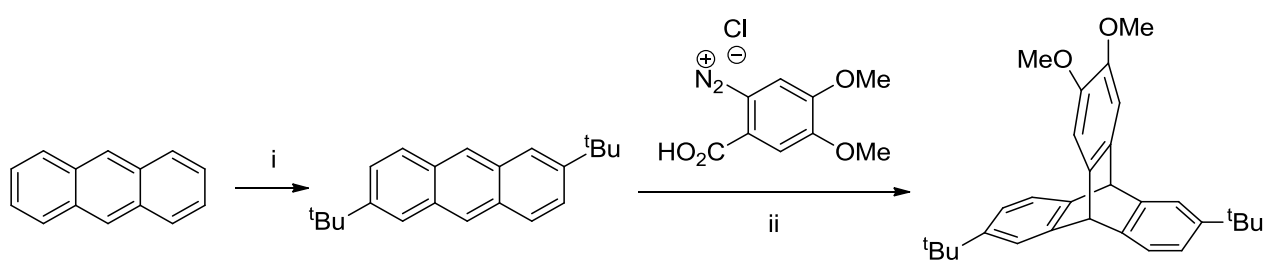
Scheme 2.8 Synthesis of 2,3-dimethoxy-7,14-di-*tert*-butyltriptycene
Reagents and conditions: i) *tert*-Butanol, TFA, 24 hrs, reflux ii) 1,2-Epoxypropane, DCE, 12 hrs, reflux.

2,6-Di-*tert*-butylanthracene (**Scheme 2.8**) was prepared according to the literature procedure by Herron *et al.*,[149] and confirmed pure by ^{1}H NMR, ^{13}C NMR and low resolution mass spectrometry. The anthracene was then reacted with a dimethoxybenzyne precursor in analogous reactions conditions to those outlined by Peng *et al.*[147] to give the corresponding dimethoxytriptycene (**Scheme 2.8**). The novel compound's structure was confirmed by single crystal X-ray diffraction (on a crystal grown *via* slow diffusion of methanol into chloroform solution, **Figure 2.14**) combined with the expected spectra obtained from ^{1}H NMR, ^{13}C NMR and high resolution mass spectrometry.
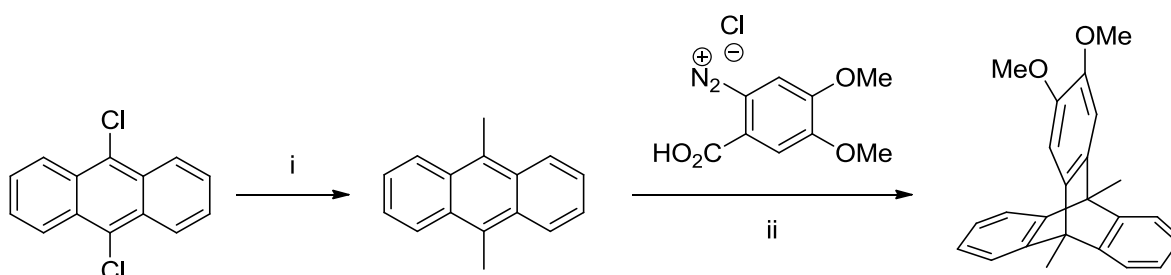
Scheme 2.9 Synthesis of 2,3-dimethoxy-9,10-dimethyltriptycene.
Reagents and conditions: i) MeMgBr, PEPPSI[TM]-[i]Pr catalyst, 1,4-dioxane, 24 hrs, RT ii) 1,2-Epoxypropane, DCE, 12 hrs, reflux.

9,10-Dimethylanthracene (**Scheme 2.9**) was prepared according to the literature procedure by Yagodkin *et al.*,[150] and isolated in excellent yield (98 %) without the need for further purification (as established by ^{1}H NMR, ^{13}C NMR and low resolution mass spectrometry). The anthracene was subsequently converted into the corresponding dimethoxytriptycene *via* reaction with a dimethoxybenzyne precursor in analogous reaction conditions to those outline by Peng *et al.*[147] (**Scheme 2.9**). The structure of the novel compound was confirmed by ^{1}H NMR, ^{13}C NMR, high resolution mass spectrometry and single crystal X-ray diffraction (**Figure 2.14**).
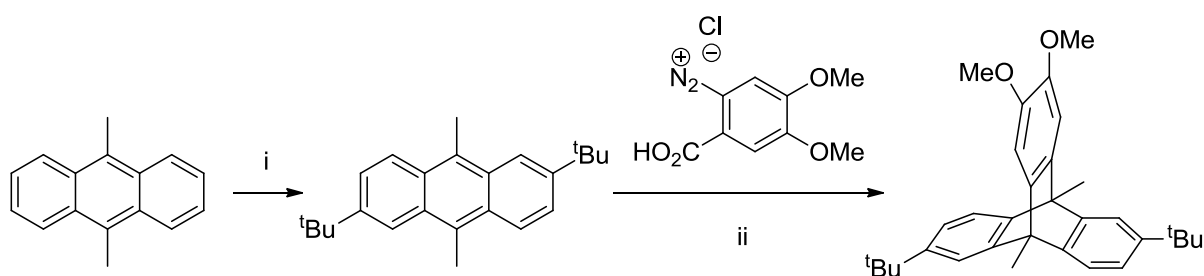
Scheme 2.10 Synthesis of 2,3-dimethoxy-7,14-di-*tert*-butyl-9,10-dimethyltriptycene
Reagents and conditions: i) *tert*-Butanol, TFA, 24 hrs, reflux ii) 1,2-Epoxypropane, DCE, 12 hrs, reflux

9,10-Dimethylanthracene (**Scheme 2.10**) was further substituted with *tert*-butyl groups according to the literature procedure by Fu and Harvey[151] to give 2,6-di-*tert*-butyl-9,10-dimethylanthracene (**Scheme 2.10**). This anthracene was subsequently reacted with a dimethoxybenzyne precursor under analogous reaction condition to those outlined by Peng *et al.*[147] to give the corresponding dimethoxytriptycene (**Scheme 2.10**). Purity and structure were again confirmed by ^{1}H NMR, ^{13}C NMR, high resolution mass spectrometry and single crystal X-ray diffraction (**Figure 2.14**).
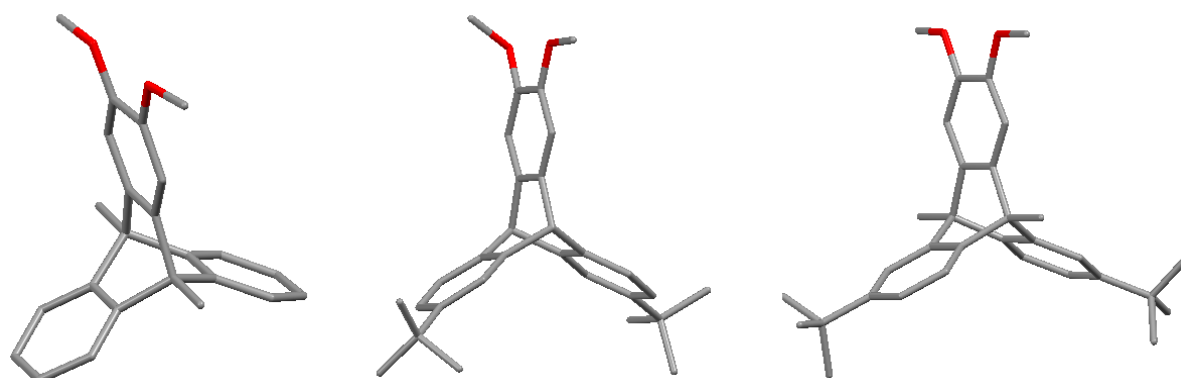
Figure 2.14 Crystal structures of the three alternative 2.3-dimethoxytriptycenes: 2,3-dimethoxy-9,10-dimethyltriptycene (left), 2,3-dimethoxy-7,14-di-*tert*-butyltriptycene (centre), 2,3-dimethoxy-7,14-di-*tert*-butyl-9,10-dimethyltriptycene (right). Protons and solvent molecules removed for clarity.

Once isolated and thoroughly dried, each 2,3-dimethoxytriptycene was demethylated using boron tribromide under similar anhydrous reactions conditions to those outlined by Zhu *et al.*[152] (**Scheme 2.11**). Each of the triptycene-2,3-diols were isolated in excellent yield (82 – 97 %, **Table 2.4**), and found to be relatively stable in air at modest temperatures, allowing for efficient drying under vacuum. Each was fully characterised by ^{1}H NMR, ^{13}C NMR, IR and high resolution mass spectrometry. A summary of the yields for the formation of the four 2,3-dimethoxytriptycenes and triptycene-2,3-diols is given in **Table 2.4**.
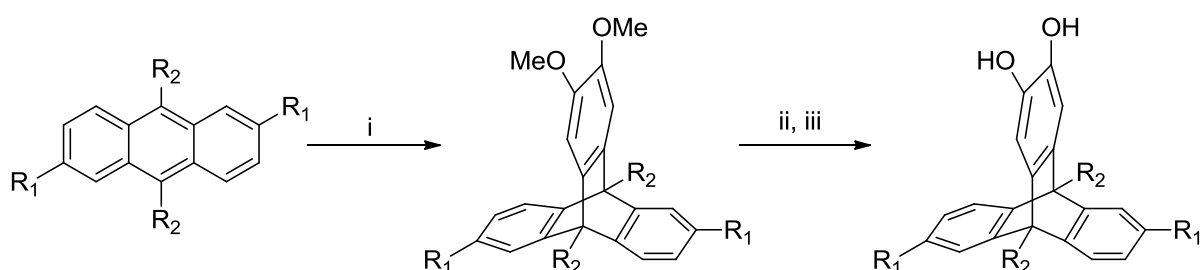
Scheme 2.11 Synthesis of triptycene-2,3-diols.
Reagents and conditions: i) 4,5-dimethoxybenzenediazonium-2-carboxylate chloride, 1,2-epoxypropane, DCE, 12 hrs, reflux ii) BBr$_3$, DCM, 3 hrs, RT iii) H$_2$O.

Anthracene	2,3-Dimethoxytriptycene yield (%)	Triptycene-2,3-diol yield (%)
R$_1$ = H, R$_2$ = H	35	82
R$_1$ = H, R$_2$ = Me	62	97
R$_1$ = ^{t}Bu, R$_2$ = H	16	86
R$_1$ = ^{t}Bu, R$_2$ = Me	45	95

Table 2.4 Yields of 2,3-dimethoxytriptycene formation and subsequent demethylation.

A final substituted anthracene was also prepared in the form of octamethyloctahydropentacene (**Scheme 2.12**) using a double Friedel-Crafts alkylation of 2,5-dichloro-2,5-dimethylhexane (prepared from 2,5-dihydroxy-2,5-dimethylhexane)[153] on 9,10-dihydroanthracene in accordance with the literature procedure by Bouffard *et al.*.[154]
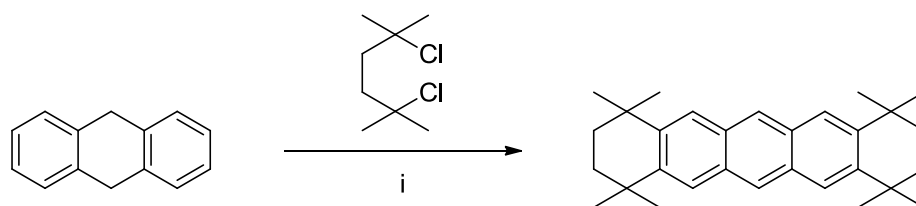
Scheme 2.12 Synthesis of octamethyloctahydropentacene
Reagents and conditions: i) TiCl$_4$, DCM, 30 mins, -78 °C, 16 hrs, RT

Octamethyloctahydropentacene was then reacted with a dimethoxybenzyne precursor in analogous reaction conditions to those outlined by Peng *et al.*[147] in an attempt to synthesise the corresponding 2,3-dimethoxytriptycene. However, during the purification of the crude reaction products it was observed that the isolated material, thought to be the expected dimethoxytriptycene, in fact contained two different compounds. Both products had (almost) identical retention times under the chromatographic procedures used for the initial purification, but could be separated using less polar solvent as eluent. Care was taken to isolate both compounds through further column chromatography so that their structures could be elucidated. Low and high resolution mass spectrometry revealed both compounds to have identical molecular weights demonstrating that they were regioisomers of the desired product. ^{1}H and ^{13}C NMR studies revealed the second fraction to be the expected symmetrical product, whilst the first was an unsymmetrical regioisomer, in which the dimethoxybenzyne had undergone a Diels-Alder reaction with one of the outer (rather than inner) benzene rings of the anthracene (**Scheme 2.13**).
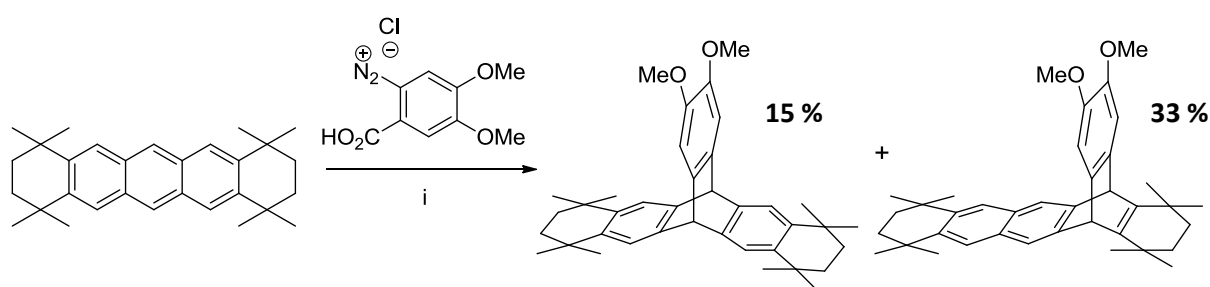
Scheme 2.13 Synthesis and yields of the two cy6-2,3-dimethoxytriptycenes.
Reagents and conditions: i) 1,2-Epoxypropane, DCE, 12 hrs, reflux.

Crystals of both triptycenes were grown by slow diffusion of methanol into chloroform solution and measured by single crystal X-ray diffraction to confirm these proposed structures (**Figure 2.15**). The yields of the two compounds (15 and 33 % for the symmetrical and unsymmetrical products respectively) suggest that each of the three aromatic rings of

the highly substituted anthracene is almost equally activated towards a Diels-Alder reaction with a benzyne. Examples of similar unsymmetrical products obtained from analogous reactions are present in the literature, although they are generally reported as trace or low yield by-products, or not isolated due to their difficult separation from the symmetrical regioisomer.[148,155-157]
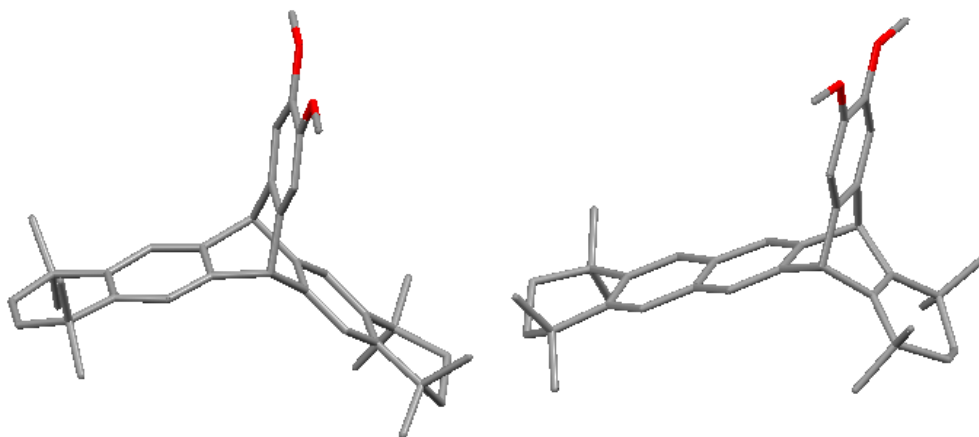
Figure 2.15 Crystal structures of symmetrical (left) and unsymmetrical (right) cy6-2,3-dimethoxytriptycenes. Protons and solvent molecules removed for clarity.

Once isolated and thoroughly dried, both cy6-2,3-dimethoxytriptycenes were demethylated using boron tribromide under similar reactions conditions to those outlined by Zhu *et al*.[152] to give the corresponding cy6-triptycene-2,3-diols in excellent yields (**Scheme 2.14**). Both were found to be relatively stable in air at modest temperatures, allowing for efficient drying under vacuum, and fully characterised by ^{1}H NMR, ^{13}C NMR, IR and high resolution mass spectrometry.
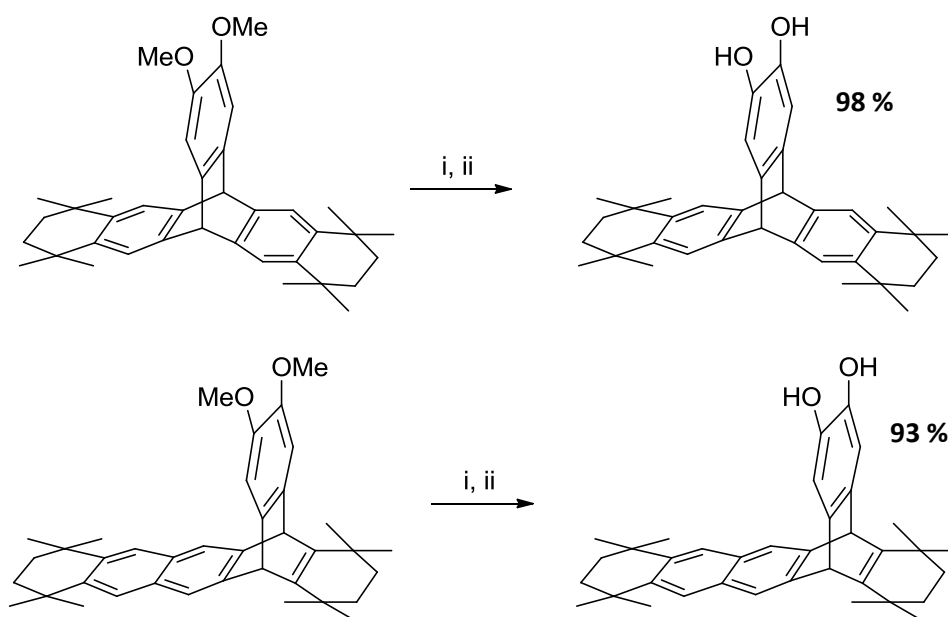
Scheme 2.14 Demethylation of the symmetrical (top) and unsymmetrical (bottom) 2,3-dimethoxytriptycenes.
Reagents and conditions: i) BBr_3, DCM, 3 hrs, RT ii) H_2O.

2.3.3.3 Alternative triptycene-2,3-diol based biphenyl adducts

Using identical reaction conditions to those used to produce catechol and naphthalene based biphenyl adducts, a series of tetra-substituted triptycene based OMIMs were prepared using the triptycene-2,3-diols and cy6-triptycene-2,3-diols detailed in the previous section (**Scheme 2.15**). Each was isolated following purification *via* column chromatography and characterised by: ^{1}H, ^{13}C and ^{19}F NMR (lack of peaks in ^{19}F NMR data indicates no presence of under-substituted materials), MALDI-MS and GPC. Yields of the reactions and shorthand names of the corresponding OMIMs are summarised in **Table 2.5**.
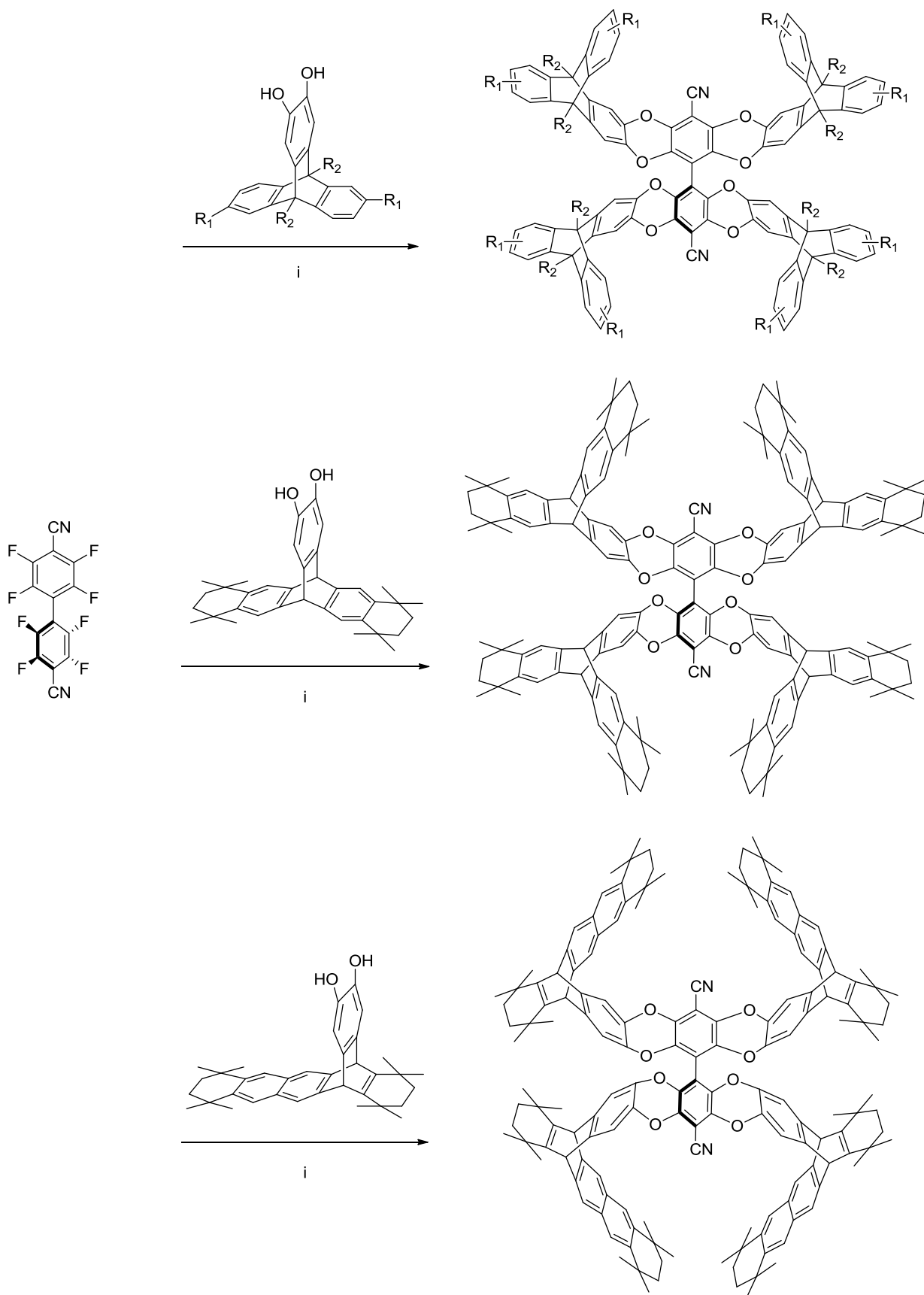
Scheme 2.15 Synthesis of triptycene based OMIMs (top) [R$_1$ = H, ^{t}Bu, R$_2$ = H, Me] and symmetrical (middle) and unsymmetrical (bottom, structure is one possible regioisomer) cy6-triptycene based OMIMs.
Reagents and conditions: i) K$_2$CO$_3$, DMF, 65 °C, 72 hrs.

Triptycene-2,3-diol	Corresponding OMIM name	Isolated yield (%)
R_1 = H, R_2 = H	OMIM-1	73
R_1 = H, R_2 = Me	OMIM-1-Me	71
R_1 = ^{t}Bu, R_2 = H	OMIM-1-*t*Bu	69
R_1 = ^{t}Bu, R_2 = Me	OMIM-1-Me-*t*Bu	47
Symmetrical cy6	OMIM-1-Cy6	83
Unsymmetrical cy6	OMIM-1-uCy6	86

Table 2.5 Yields and short hand names of triptycene-2,3-diol and cy6-triptycene-2,3-diol based OMIMs.

Surface areas of each new triptycene based OMIM were then measured by nitrogen sorption at 77 K. Their resultant adsorption isotherms (**Figure 2.16**) and data (**Table 2.6**) are shown below:
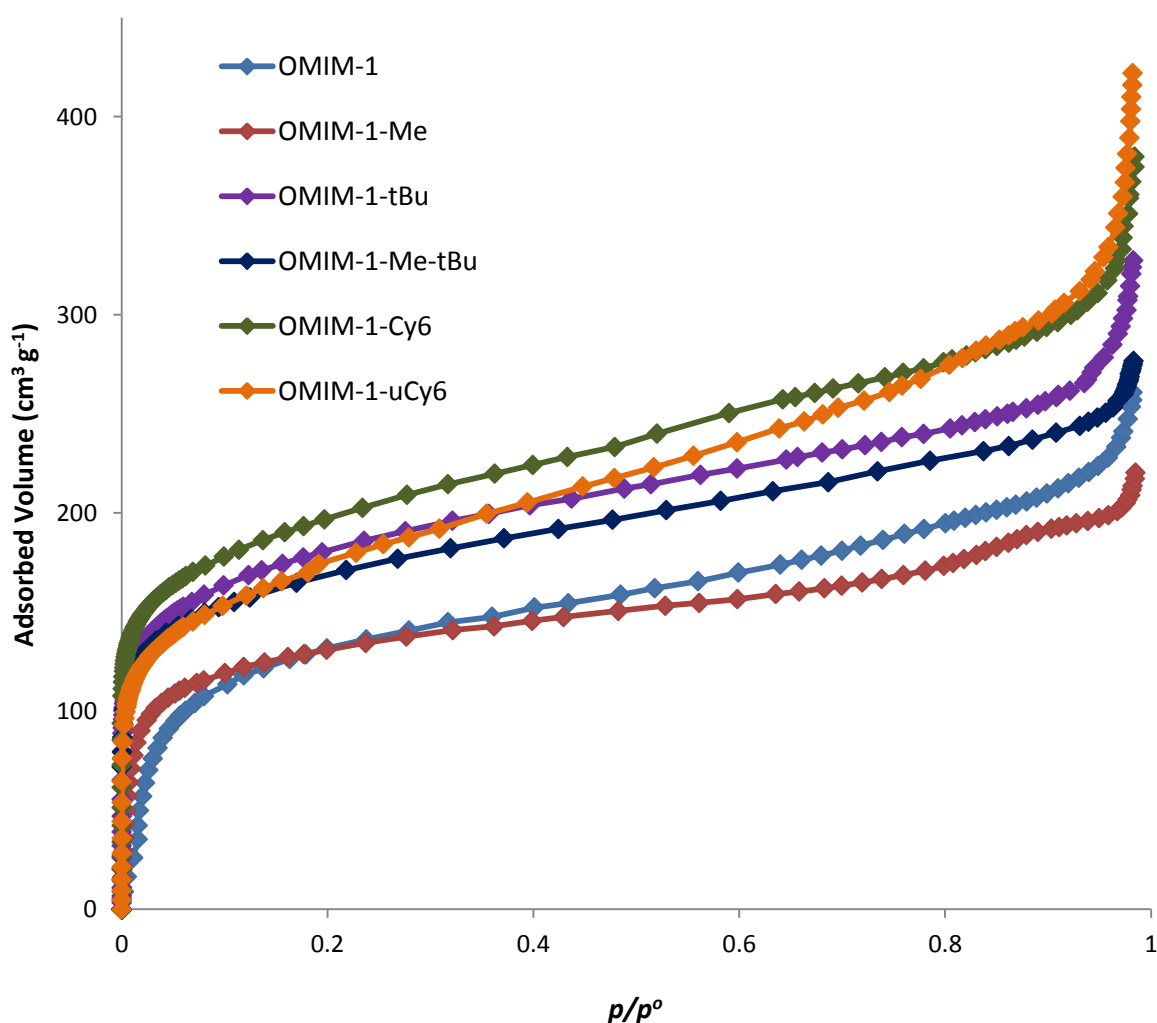
Figure 2.16 BET nitrogen adsorption isotherms for all six triptycene based OMIMs, desorption plots removed for clarity.

OMIM	BET surface area (m^2 g^{-1})	Total pore volume (cm^3 g^{-1})
1	485	0.40
1-Me	462	0.33
1-*t*Bu	654	0.54
1-Me-*t*Bu	599	0.42
1-Cy6	702	0.60
1-uCy6	622	0.64

Table 2.6 Nitrogen sorption data for the six triptycene based OMIMs.

The results clearly indicate, through the wide range of observed surface areas, 462 – 702 m^2 g^{-1}, the large effects introducing substituents can have on triptycene based OMIMs. Comparison of **OMIM-1** and **OMIM-1-Me** shows that addition of methyl groups to the bridgehead (R$_2$) positions of the triptycene termini lowers the apparent surface area of the OMIM. This can be explained either by the increase in weight due to the extra methyl groups lowering the surface area per gram, or by the methyl groups partially filling a concavity that would otherwise be available for gas adsorption. Regular sorption kinetics for **OMIM 1-Me** further emphasises this difference in porosity, as the measured surface area of **OMIM-1** (485 m^2 g^{-1}) is likely to be under-estimated due to its very slow adsorption kinetics, so the actual drop in surface area due to addition of methyl groups may be closer to 100 m^2 g^{-1}. Similar effects can be seen when comparing **OMIM-1-*t*Bu** and **OMIM-1-Me-*t*Bu**, again the introduction of bridgehead methyl groups lowers the apparent BET surface area (by 55 m^2 g^{-1}). Further discussion on these differences is offered in the following section on OMIM crystal structures.

Conversely, comparison of **OMIM-1** and **OMIM-1-*t*Bu** indicates that addition of *tert*-butyl groups to the R$_1$ positions greatly improves the surface area of the OMIM (by over 150 m^2 g^{-1}), possibly due to the bulky groups holding the *arms* of the molecule apart. Similar effects can be observed when comparing **OMIM-1-Me** with **OMIM-1-Me-*t*Bu**, or **OMIM-1** with **OMIM-1-Cy6**. In both cases, the addition of bulky groups to the R$_1$ positions had a twofold effect: increasing the apparent surface area and improving the adsorption kinetics, though the two may be intrinsically linked, as slow sorption kinetics have been shown previously to result in underestimated surface areas.

2.3.3.4 Triptycene-2,3-diol based OMIMs: crystal structure discussion

In an effort to ascertain what effects the addition of substituents to the R_1 or R_2 positions of triptycene termini have on the overall structure of triptycene based OMIMs, a series of crystals were grown (*via* slow diffusion of methanol into a chloroform solution) of the mono-regioisomeric triptycene-2,3-diol based OMIMs. **Figure 2.17** shows the structures of individual OMIM molecules, with some intramolecular distances and angles labelled (summarised in **Table 2.7**).
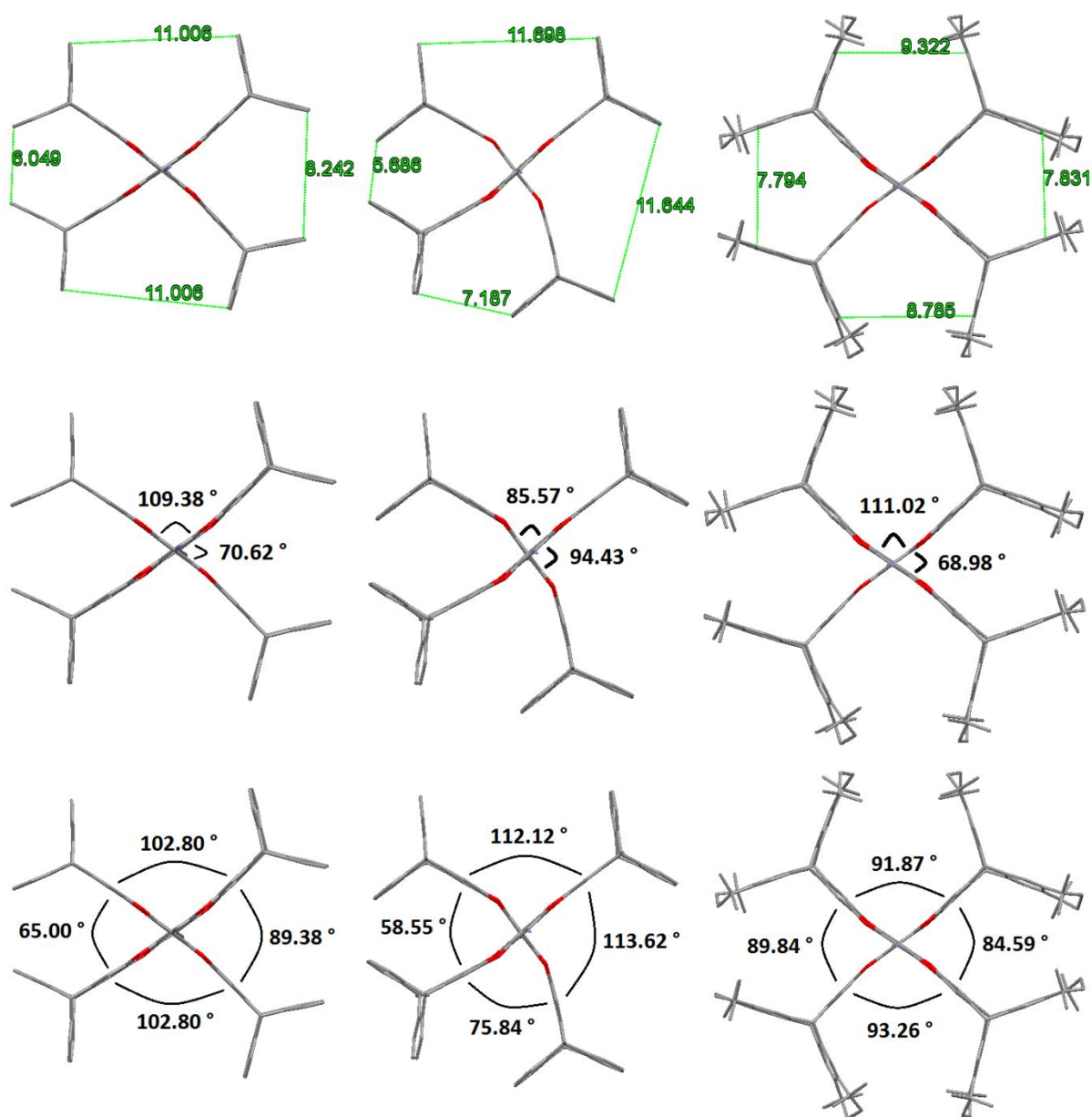
Figure 2.17 Crystal structures (and relevant detail) for **OMIM-1** (left), **OMIM-1-Me** (centre) and **OMIM-1-Cy6** (right). Distances in Å, protons and solvent molecules removed for clarity.

OMIM	Biphenyl Angles (°)	Triptycene Angles (°)	Triptycene -Triptycene distances [average] (Å)
OMIM-1	70.62, 109.38	65.00, 89.38, 102.80, 102.80	6.05, 8.24, 11.01, 11.01 [9.08]
OMIM-1-Me	85.57, 94.43	58.55, 75.84, 112.12, 113.62	5.69, 7.19, 11.64, 11.70 [9.06]
OMIM-1-Cy6	68.98, 111.02	84.59, 89.84, 91.87, 93.26	7.80, 7.83, 8.79, 9.32 [8.44]

Table 2.7 Summary of crystal structure intramolecular distances and angles.

Before discussing the relationship of these crystal structures with the observed properties of OMIMs, it must first be emphasised that all BET measurements were performed on *amorphous* powdered samples. It would be incorrect to universally attribute any observed property of an amorphous material to a feature seen in its crystalline state; however comparisons may be drawn as a point of discussion or to offer suggestions as to the observed differences. Furthermore, all porosity data were collected at 77 K, whilst diffraction studies were carried out at 150 K, so, when subjected to BET analysis, the amorphous structures would be at very low energy, and so perhaps closer to their crystalline state than usual.

Analysis of **Figure 2.17** demonstrates that the addition of methyl groups to the triptycene termini distorts the displaced cruciform arrangement relative to that observed in the unsubstituted **OMIM-1**, giving rise to a much larger range of intramolecular triptycene-triptycene distances and internal angles. Closer inspection of the intermolecular interactions (**Figure 2.18**) reveals that **OMIM-1** molecules pack much closer together (than **OMIM-1-Me**) with intermolecular interactions (shown in blue) between multiple protons and carbons of the triptycene groups, as well as nitrile-nitrile interactions. **OMIM-1-Me** molecules by comparison, pack less efficiently in a different arrangement that favours multiple intermolecular interactions between the bridgehead methyl groups and neighbouring molecules. These different arrangements offer a possible explanation as to why the two compounds possess different sorption properties, as one can envisage the stronger intermolecular interactions of OMIM-1 maintaining a more open structure upon removal of solvent.
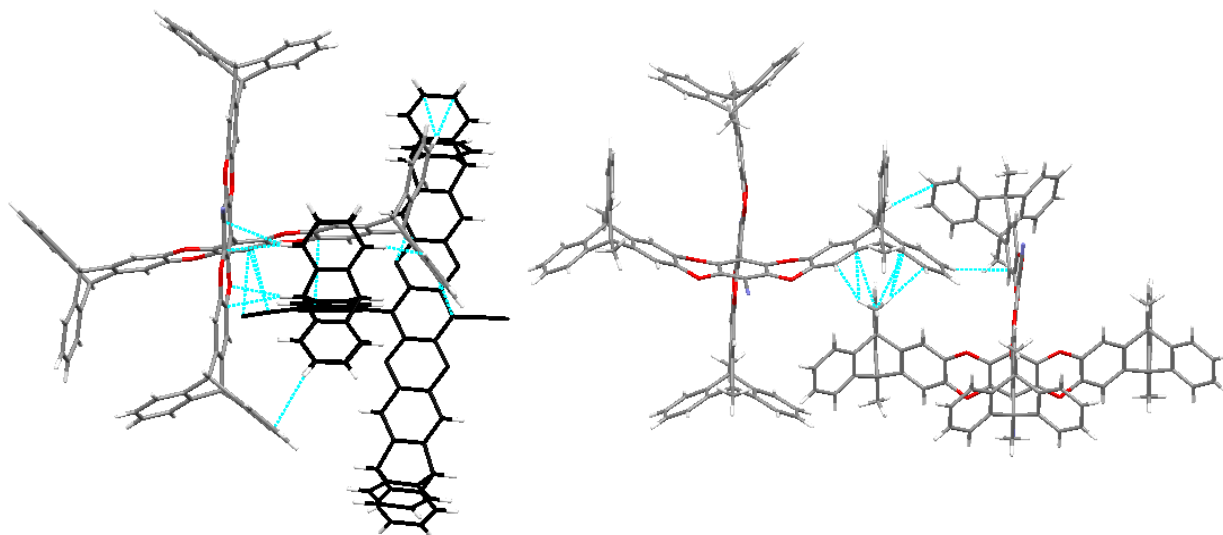
Figure 2.18 Interactions (blue) of neighbouring molecules in crystal structures of **OMIM-1** (left), and **OMIM-1-Me** (right). Solvent molecules removed for clarity.

When examining the packing of *space filling* **OMIM-1** molecules, channels running through the entire length of the structure are visible (**Figure 2.19**). Whilst these channels are unlikely to be solely responsible for the porosity observed in amorphous **OMIM-1**, it is possible that similar local ordering occurs. The expanded image in **Figure 2.19** shows that these large pores, with a minimum width of 8.6 Å, are surrounded by four bridgehead positions of triptycene termini, indicating that this area of the molecule plays a part in the porosity of the bulk material. This may help to explain why **OMIM-1-Me** has a slightly lower surface area than **OMIM-1**, on top of their different packing arrangements, as any cavities around the bridgehead positions in **OMIM-1-Me** are now partially filled with methyl groups.
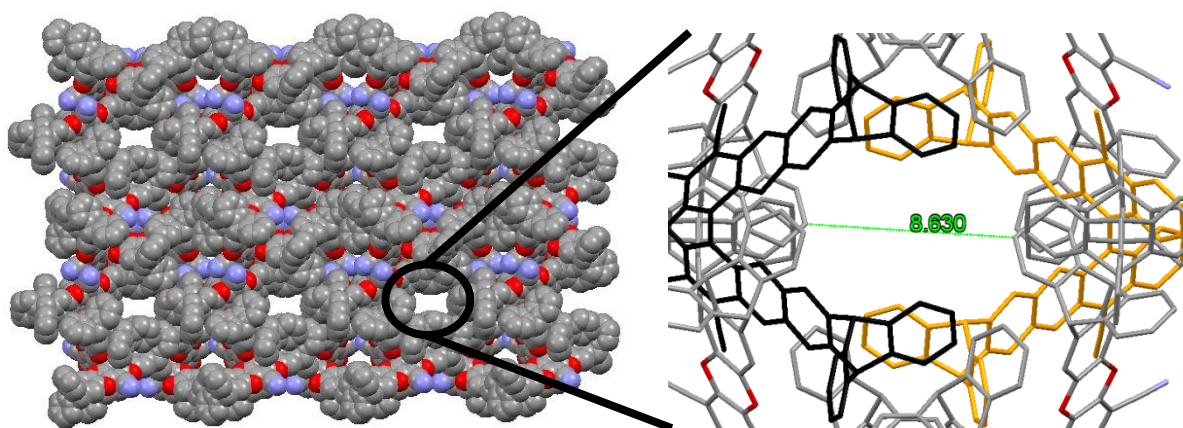
Figure 2.19 Packing of **OMIM-1** molecules. Space filling display (left) showing channels and expanded view (right) showing relative location and size of channel. Distances in Å, protons and solvent molecules removed for clarity.

Indeed the packing of space filling **OMIM-1-Me** molecules is quite different to **OMIM-1**, however small channels that penetrate the entire material are again visible (**Figure 2.20**). Closer inspection of these channels shows that they are located between the voids created by the displaced cruciform nature of the biphenyl cores. The actual width of the channels is difficult to estimate due to the angle at which they are visible; however they appear to be of a similar size to those observed in **OMIM-1** (**Figure 2.19**).
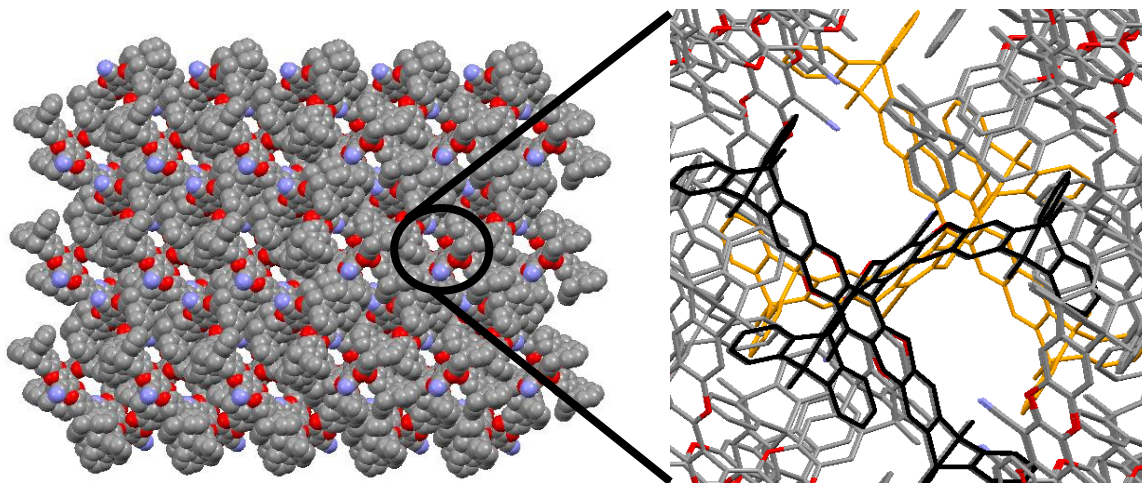
Figure 2.20 Packing of **OMIM-1-Me** molecules. Space filling display (left) showing channels and expanded view (right) showing relative location and size of channel. Protons and solvent molecules removed for clarity.

Figure 2.17 shows that the molecular structures of **OMIM-1** and **OMIM-1-Cy6** within their respective crystals are very similar. However, the similarities end there, as the packing arrangement of **OMIM-1-Cy6** molecules is vastly different. Instead of neighbouring molecules sharing a somewhat orthogonal relationship as seen in **OMIM-1** and **OMIM-1-Me** (**Figure 2.18**), **OMIM-1-Cy6** molecules arrange themselves in a parallel manner in a series of layers with no inter-penetration of neighbouring molecules (**Figures 2.21** and **2.22**). This inefficient packing is likely to be due to the large size, up to 7 Å, of the bulky cy6 groups appending each triptycene arm, prohibiting any inter-penetration of neighbouring molecules, and consequently responsible for the improved surface area.
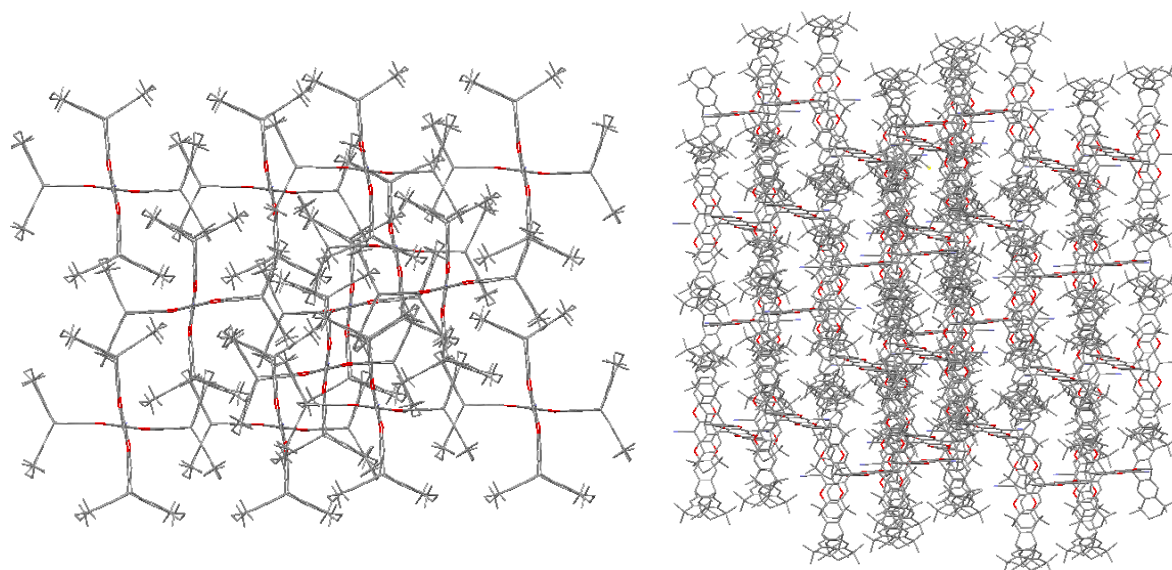
Figure 2.21 Arrangement of **OMIM-1-Cy6** molecules from above (left) showing their parallel relationship and from the side (right) showing the layered structure. Solvent molecules removed for clarity.
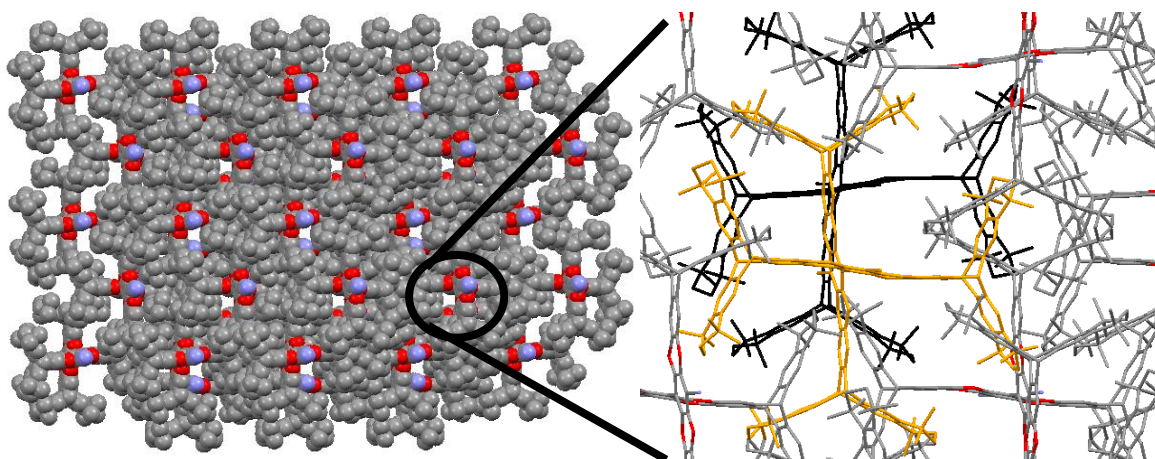
Figure 2.22 Packing of **OMIM-1-Cy6** molecules. Space filling display (left) showing channels and expanded view (right) showing relative location of the channels. Protons and solvent molecules removed for clarity.

2.3.3.5 Unsymmetrical biphenyl adducts

During the synthesis of tetra-substituted biphenyl adducts, it was commonplace for a slight excess of catechol to be used in an effort to force the reaction to produce only the tetra-substituted product (as well as bridged compound by-products). However, when attempting to synthesise and isolate the tri-substituted adducts (this will be discussed in detail in

Chapter 3), reactions were carried out in a simple three to one stoichiometric ratio, which often resulted in the formation of some di-substituted adducts as well as tri- and tetra-substituted products (**Scheme 2.16**).
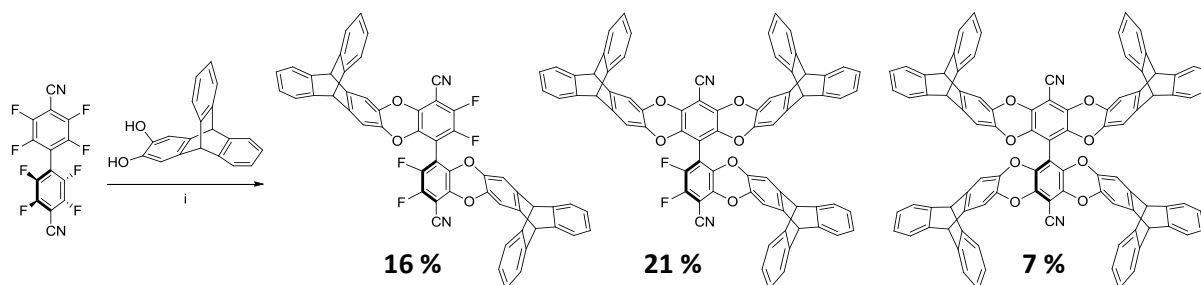
Scheme 2.16 Synthesis and isolated yields of the di, tri and tetra-[triptycene-2,3-diol] biphenyl adducts.
Reagents and conditions: i) K$_2$CO$_3$, DMF, 65 °C, 72 hrs.

With the of help column chromatography all three adducts, di, tri and tetra, could be isolated, leading to the possibility of creating *unsymmetrical OMIMs*, comprising of two or more different termini, through reacting di-substituted adducts with a different catechol. It was hypothesised that the lower symmetry of these *unsymmetrical OMIMs* could lead to less efficient packing and therefore higher surface areas. The first such compound produced was prepared from the reaction of the di-[triptycene-2,3-diol] biphenyl adduct with a propellane-2,3-diol (supplied by Dr. Grazia Bezzu) (**Scheme 2.17**).
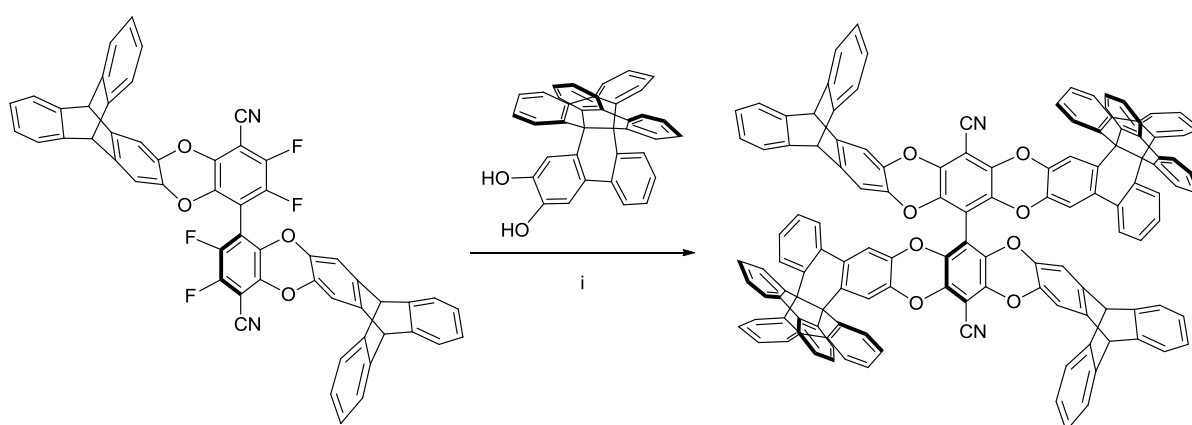
Scheme 2.17 Synthesis of the di-[triptycene-2,3-diol]-di-[propellane-2,3-diol] biphenyl adduct.
Reagents and conditions: i) K$_2$CO$_3$, DMF, 65 °C, 72 hrs.

65

The resultant unsymmetrical OMIM was isolated in good yield (84 %) and characterised by the usual techniques to confirm its purity. BET analysis (**Figure 2.23**, **Table 2.8**) revealed a surface area of 481 m^2 g^{-1}, rendering it almost identical to the tetra-[triptycene-2,3-diol] biphenyl adduct (**OMIM-1**).
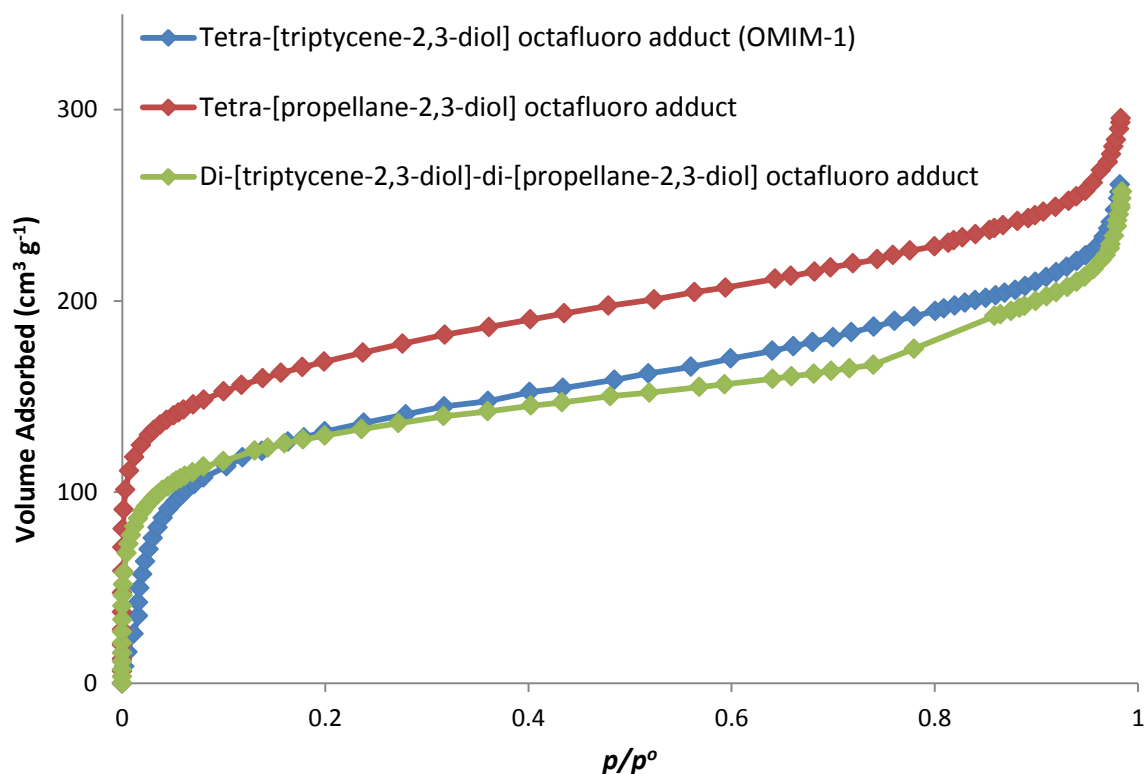
Figure 2.23 BET nitrogen adsorption isotherms of the *unsymmetrical* OMIM and both its corresponding *symmetrical* counterparts. Desorption plots removed for clarity.

OMIM	BET surface area (m^2 g^{-1})	Total pore volume (cm^3 g^{-1})
Tetra-[triptycene-2,3-diol] – OMIM-1	485	0.40
Tetra-[propellane-2,3-diol][a]	594	0.45
Di-[triptycene-2,3-diol]-di-[propellane-2,3-diol]	481	0.38

Table 2.8 BET nitrogen sorption data of the *unsymmetrical* OMIM and both its corresponding *symmetrical* counterparts.
a) Sample synthesised and analysed by Dr. Grazia Bezzu

It seems strange that the *hybrid* compound has porosity properties so close to one of its *pure* counterparts (as opposed to being a mixture or higher/lower than both). A possible explanation can be offered given that the observed surface area of **OMIM-1** may be

underestimated due to slow sorption kinetics. Therefore, the actual effect of mixing these termini is to remove the slow sorption kinetics and decrease the surface area, likely resulting from more efficient packing due to the different shapes of the termini allowing for more intermolecular interactions.

A second *unsymmetrical OMIM* was synthesised after isolating a suitable quantity of the di-[cy6-triptycene-2,3-diol] biphenyl adduct, which was then subsequently reacted with unsubstituted triptycene-2,3-diol (**Scheme 2.18**).
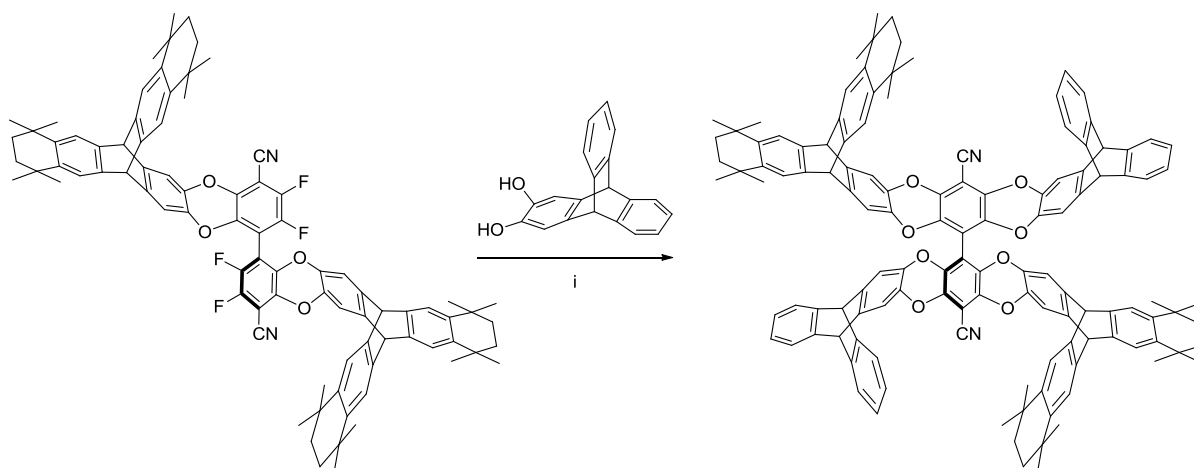
Scheme 2.18 Synthesis of the di-[triptycene-2,3-diol]-di-[cy6-triptycene-2,3-diol] biphenyl adduct.
Reagents and conditions: i) K$_2$CO$_3$, DMF, 65 °C, 72 hrs.

After the compound was isolated and its purity established *via* the usual techniques, BET analysis revealed a surprisingly low apparent surface area of 179 m^2 g^{-1} (much lower than both of its symmetrical counterparts, **Figure 2.24** and **Table 2.9**). In a similar vein to the previous unsymmetrical OMIM, it seems that the use of two different termini in triptycene based OMIMs produces a compound that is able to pack space more efficiently, and thus is less porous.
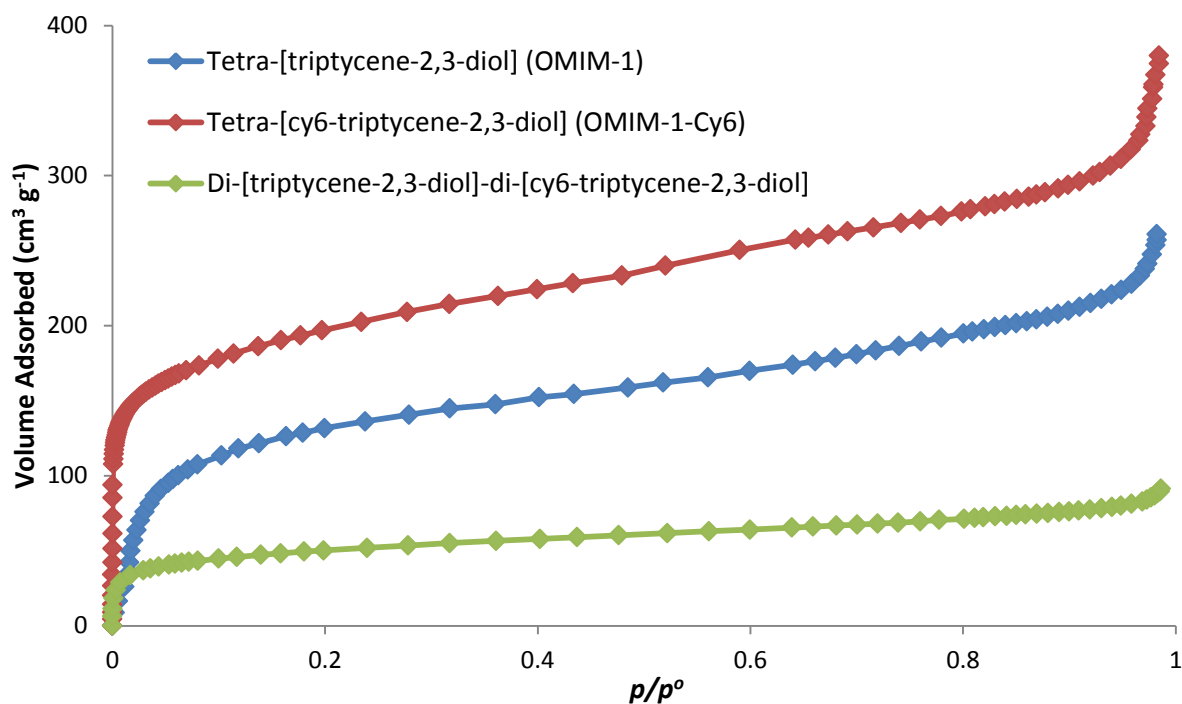
Figure 2.24 BET nitrogen adsorption isotherms of the second *unsymmetrical* OMIM and both its corresponding *symmetrical* counterparts. Desorption plots removed for clarity.

OMIM	BET surface area ($m^2\,g^{-1}$)	Total pore volume ($cm^3\,g^{-1}$)
Tetra-[triptycene-2,3-diol] (OMIM-1)	485	0.40
Tetra-[cy6-triptycene-2,3-diol] (OMIM-1-Cy6)	702	0.50
Di-[triptycene-2,3-diol]-di-[cy6-triptycene-2,3-diol)	179	0.14

Table 2.9 BET nitrogen sorption data of the second *unsymmetrical* OMIM and both its corresponding *symmetrical* counterparts.

No further unsymmetrical OMIMs were produced due to lack of isolated di-substituted biphenyl adducts. However both the obtained results suggest that they are inferior to their symmetrical counterparts for two reasons: their elongated synthesis and there decreased porosity.

2.4 Terphenyl OMIMs

As previously discussed in Chapter 2.2, when synthesising *octafluoro*, multiple by-products were also produced, one of which: 4,4',4''-tricyano-2,2',2'',3,3'',5,5',5'',6,6',6''-undecafluoro-[1,1':3',1''-terphenyl] (**Scheme 2.19**) or *undecafluoro*, could be isolated in a repeatable yield of approximately 6 %, meaning that sufficient quantity could be collected, and thus its reactivity with catechol functionalised molecules explored.
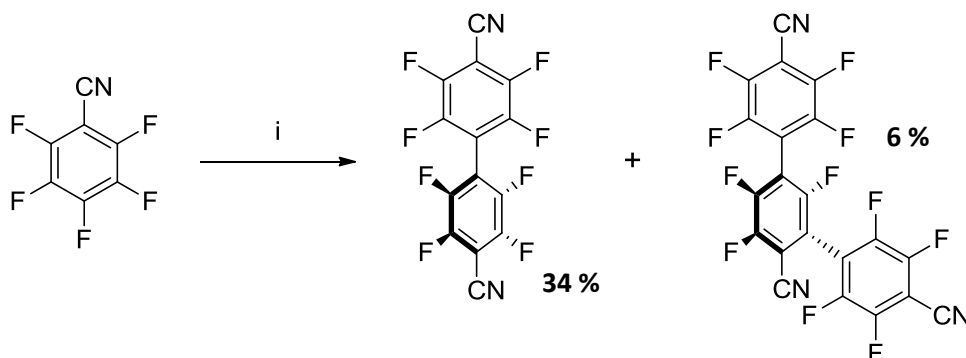
Scheme 2.19 Synthesis of octafluoro and undecafluoro by-product.
Reagents and conditions: i) P(NEt$_2$)$_3$, Et$_2$O, 3 hrs, RT.

Of particular interest was what impact the addition of extra catechols around the central *terphenyl* core would have on the apparent surface areas (compared with the previously produced biphenyl adducts), and what substitution pattern would be adopted given the uneven (eleven) number of reactive fluorine groups.

2.4.1 Catechol based terphenyl adducts

Undecafluoro was first reacted with five equivalents (plus a slight excess) of catechol (**Scheme 2.20**) under standard conditions to probe the reactivity of the molecule. It seemed likely that the products could contain a mixture of the penta adduct (with one residual fluorine atom, **Scheme 2.20**), the hexa adduct (with a dangling hydroxyl group) and any number of bridged compounds. Despite TLC analysis indicating the presence of at least two products in the crude reaction mixture, only the molecular ion peak for the penta-[catechol] terphenyl adduct could be seen in the crude mass spectrum (no evidence of the over

substituted hexa or under substituted tetra adducts), suggesting that the eleventh fluorine atom is too sterically hindered to react.
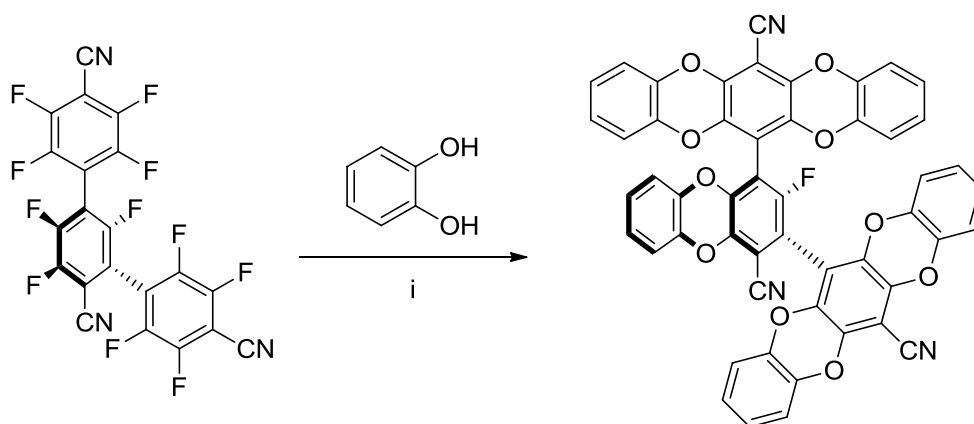
Scheme 2.20 Synthesis of the penta-[catechol] terphenyl adduct.
Reagents and conditions: i) K$_2$CO$_3$, DMF, 65 °C, 72 hrs.

A slight shoulder in the crude GPC trace (**Figure 2.25**) indicated the presence of a small amount of higher molecular weight material (likely to be evidence of bridged compounds), so the material was purified using column chromatography.

Peak RV - (ml)	19.317
Mn - (Daltons)	640
Mw - (Daltons)	668
Mz - (Daltons)	705
Mp - (Daltons)	637
Mw / Mn	1.045
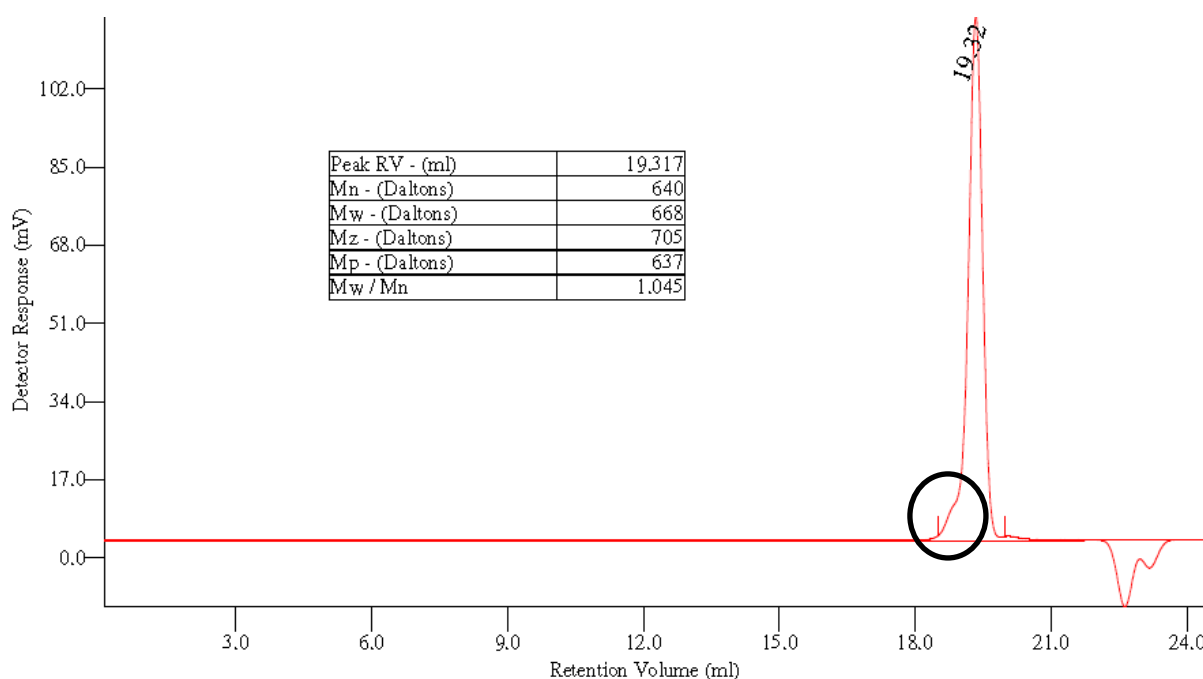
Figure 2.25 GPC trace and relevant data (inset) of the crude penta-[catechol] terphenyl adduct showing slight impurity (shoulder).

Once purified, the penta-[catechol] adduct was isolated in excellent yield (87 %) and fully characterised by ^{1}H, ^{13}C and ^{19}F NMR, low resolution MS, GPC and X-ray crystallography. ^{19}F NMR studies showed just a solitary singlet, confirming the presence of a single residual

fluorine atom, and complete substitution of the five fluorine pairs with catechol moieties. X-ray crystallography studies later confirmed the hypothesised structure (**Figure 2.26**).
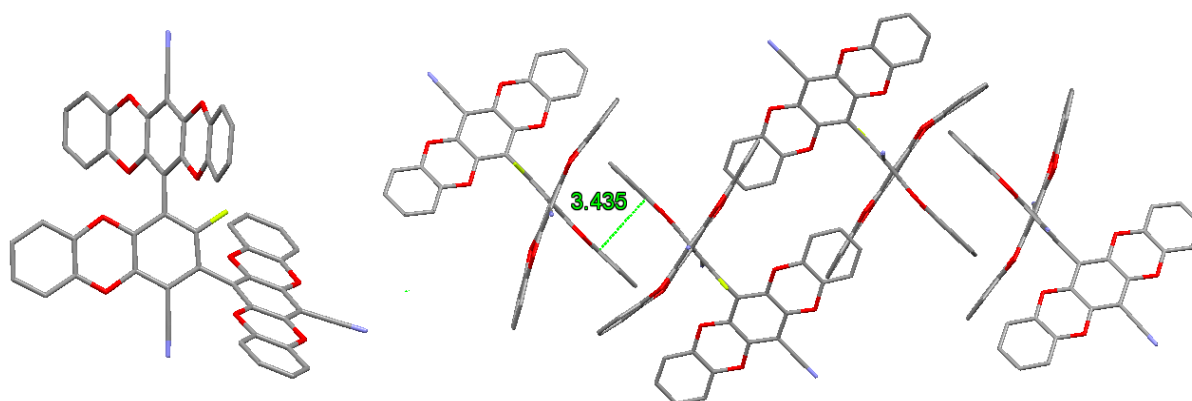
Figure 2.26 Crystal structure (left) and packing (right) of the penta-[catechol] terphenyl adduct. Crystals obtained *via* slow diffusion of methanol into chloroform solution. Protons and solvent molecules removed for clarity. Distances in Å.

The compound was significantly more soluble in common organic solvents than the corresponding biphenyl adduct, likely due to its more awkward shape limiting intermolecular ($\pi - \pi$) interactions. Unfortunately, these diminished interactions did not yield a significant improvement in surface area, as BET analysis revealed an apparent surface area of only 13 $m^2 g^{-1}$.

Given the evidence (that *tert*-butyl substituted catechols give rise to more porous structures) gathered in Chapter 2.2, undecafluoro was subsequently reacted with the same two *tert*-butyl containing catechols (4-*tert*-butylcatechol and 3,5-di-*tert*-butylcatechol) to give the corresponding penta substituted terphenyl adducts (**Scheme 2.21**).
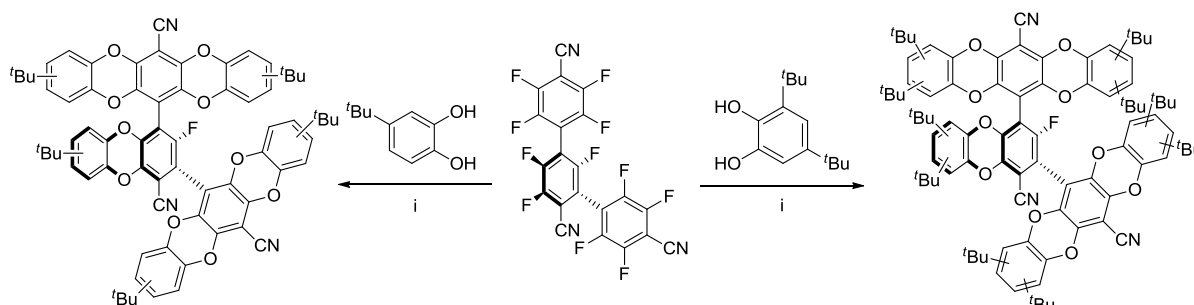
Scheme 2.21 Synthesis of the penta-[4-*tert*-butylcatechol] and [3,5-di-*tert*-butylcatechol] terphenyl adducts.
Reagents and conditions: i) K$_2$CO$_3$, DMF, 65 °C, 72 hrs.

Both adducts were isolated as mixtures of regioisomers following purification *via* column chromatography and characterised *via* the usual techniques (NMR, MALDI-MS and GPC). BET nitrogen sorption data for the three penta-[catechol] terphenyl adducts (and their tetra-[catechol] biphenyl analogues for comparison) are shown in **Figure 2.27** and **Table 2.10**.
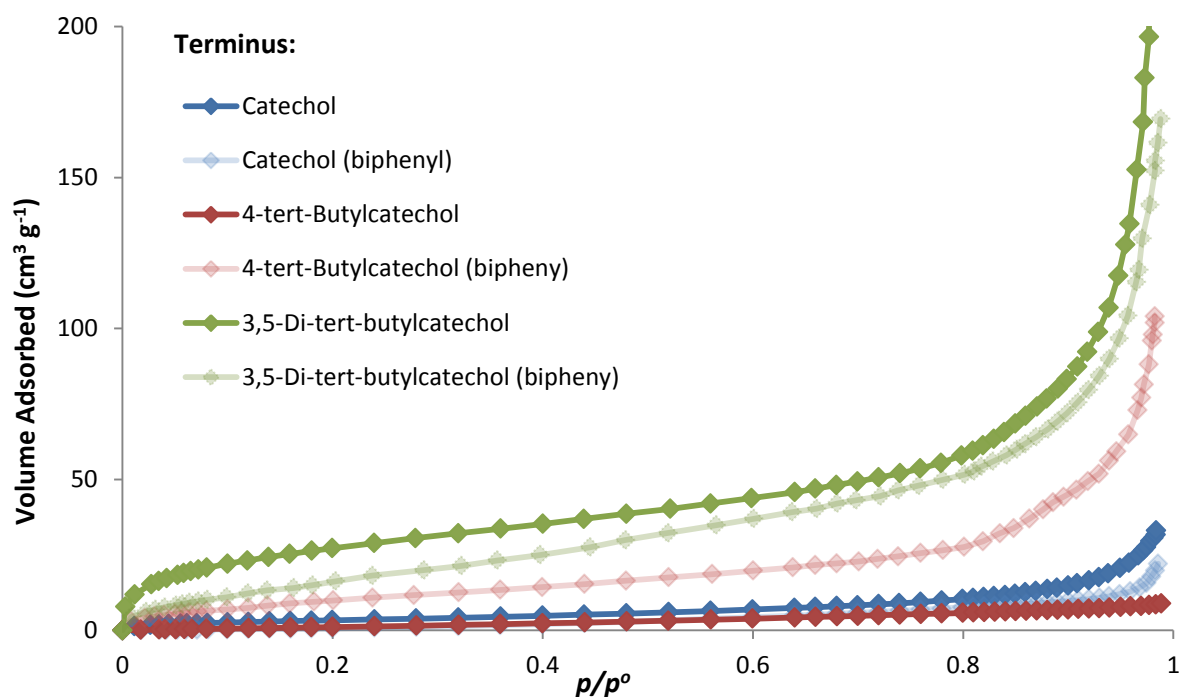
Figure 2.27 BET nitrogen adsorption isotherms for the three penta-[catechol] terphenyl adducts (bold) and their tetra-[catechol] biphenyl adducts (faint).

Terminus	BET surface area (m² g⁻¹) [biphenyl adduct]	Total pore volume (cm³ g⁻¹) [biphenyl adduct]
Catechol	13 [7]	0.05 [0.03]
4-*tert*-Butylcatechol	7 [41]	0.01 [0.15]
3,5-Di-*tert*-butylcatechol	102 [67]	0.37 [0.23]

Table 2.10 BET nitrogen sorption data for the three penta-[catechol] terphenyl adducts and their tetra-[catechol] biphenyl counterparts in square brackets.

These data show virtually no improvement in porosity for the unsubstituted catechol adducts when increasing the size of the fluorinated core, suggesting that regardless of the size of the core, catechol is not a sufficiently large terminus to promote awkward/frustrated packing in discrete molecules of this nature. The penta-[4-*tert*-butylcatechol] terphenyl

adduct gave a lower surface area than the corresponding biphenyl adduct, a result which breaks the trend seen thus far of increasing surface areas with terminus bulk. Given the decreased intermolecular interactions seen in the biphenyl catechol adduct (compared to the terphenyl adducts), it is suggested that, while *tert*-butyl groups hold the arms of the biphenyl adduct apart (thus increasing the surface area), the catechol arms of the terphenyl adduct are already held sufficiently apart (due to the added complexity of the structure). Therefore, addition of bulky groups has much less of an impact on the porosity of the structure, such that the extra weight associated with them negates any increase in surface area per gram. Some evidence for this can be seen in the adsorption isotherms (**Figure 2.27**), as the catechol terphenyl adduct shows a slight increase in adsorption at high relative pressure, whereas the 4-*tert*-butylcatechol terphenyl adduct does not. Something is responsible for this small drop in porosity and given that the only variation between the two adducts is the addition of *tert*-butyl groups it seem logical to assign such a feature to their presence.

Conversely, when comparing the two 3,5-di-*tert*-butylcatehcol adducts (biphenyl and terphenyl), an increase in surface area is seen for the terphenyl adduct, suggesting that the addition of a second *tert*-butyl group to each catechol terminus is sufficient to further frustrate the packing around the terphenyl core. When comparing the isotherms of both 3,5-di-*tert*-butylcatehcol adducts, it becomes apparent that they follow very similar plots, suggesting that the bulk structure (and subsequent porosity) of the two adducts are fairly similar (**Figure 2.27**). However, at low relative pressure the terphenyl adduct adsorbs more nitrogen (hence the higher surface area) suggesting that the increased number of bulky groups around the central core are creating more cavities that are within the micropore range.

2.4.2 Naphthalene-2,3-diol based terphenyl adducts

To further the comparison of biphenyl and terphenyl cores, a series of naphthalene-2,3-diol terphenyl adducts were synthesised (**Scheme 2.22**), using the same naphthalene-2,3-diols and reaction conditions discussed in Chapter 2.3.2.
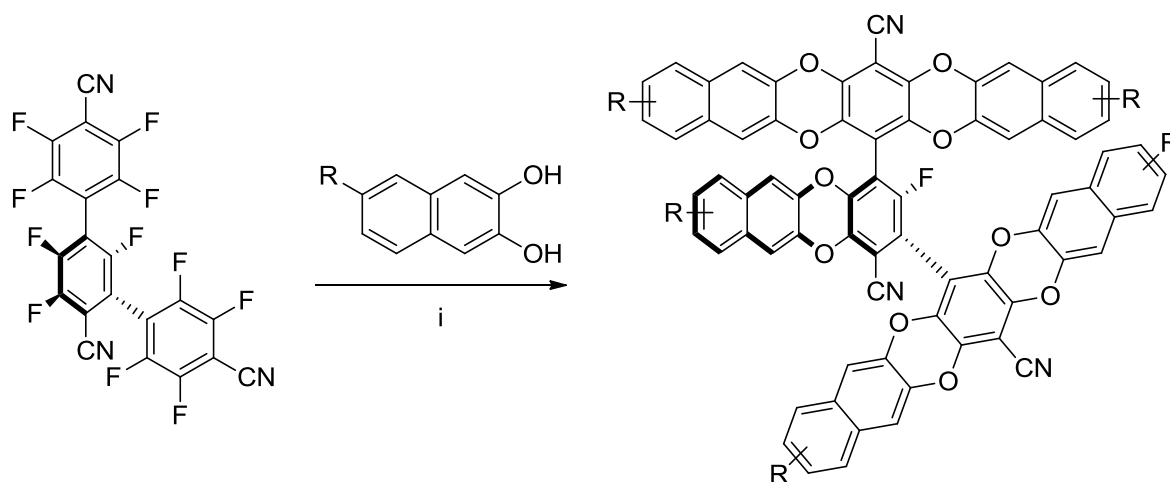
Scheme 2.22 Synthesis of the three penta-[naphthalene-2,3-diol] terphenyl adducts. R = H, ^{t}Bu or Ad.
Reagents and conditions: i) K_2CO_3, DMF, 65 °C, 72 hrs.

Purification of each adduct was achieved *via* column chromatography to remove bridged compounds (**Figure 2.28**), the products isolated (as mixtures of regioisomers for the *tert*-butyl and adamantyl substituted adducts) and subsequently characterised *via* the usual techniques.
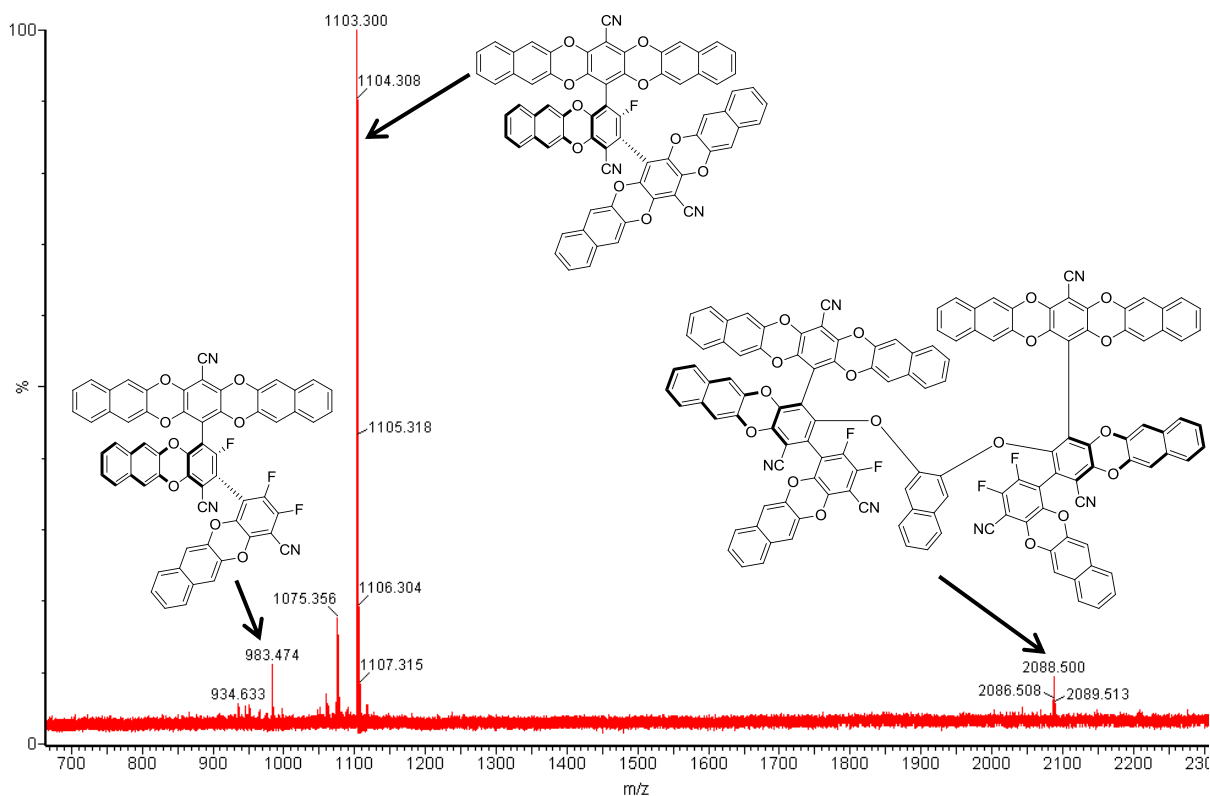
Figure 2.28 MALDI mass spectrum of the crude reaction products of the penta-[naphthalene-2,3-diol] terphenyl adduct showing the presence of the under substituted tetra adduct and a bridged compound.

BET nitrogen sorption data for the three naphthalene terphenyl adducts (and their biphenyl analogues) are shown in **Figure 2.29** and **Table 2.11**.
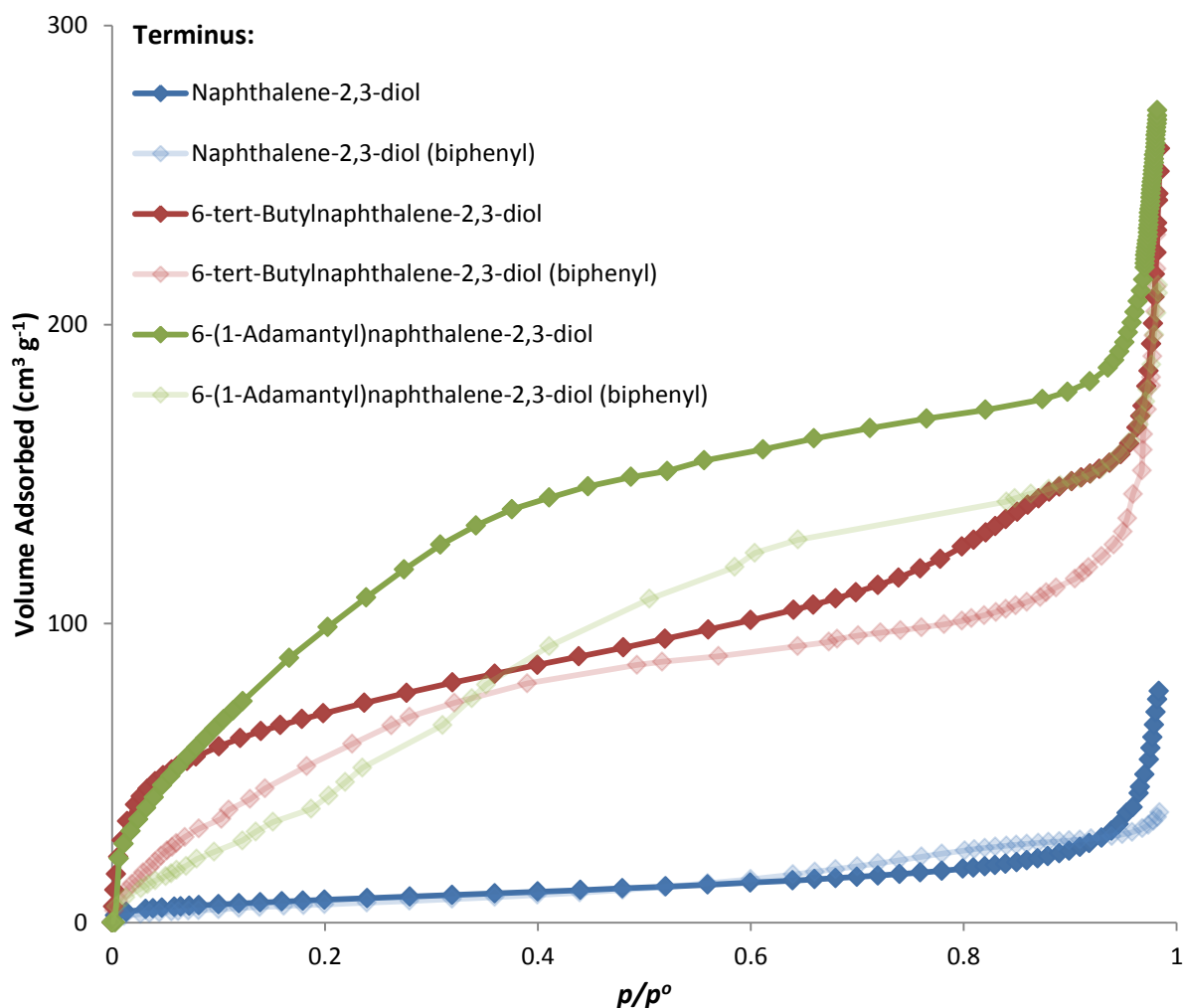
Figure 2.29 BET nitrogen adsorption isotherms for the three penta-[naphthalene-2,3-diol] terphenyl adducts (bold) and their tetra-[naphthalene-2,3-diol] biphenyl adducts (faint). Desorption plots removed for clarity.

Terminus	BET surface area (m^2 g^{-1}) [biphenyl adduct]	Total pore volume (cm^3 g^{-1}) [biphenyl adduct]
Naphthalene-2,3-diol	29 [25]	0.11 [0.05]
6-*tert*-Butylnaphthalene-2,3-diol	259 [260]	0.35 [0.33]
6-(1-Adamantyl)naphthalene-2,3-diol	347 [132]	0.41 [0.25]

Table 2.11 BET nitrogen sorption data for the three penta-[naphthalene-2,3-diol] terphenyl adducts and their tetra-[naphthalene-2,3-diol] biphenyl counterparts.

These data indicate a similar relationship (between terphenyl and biphenyl cores) for the unsubstituted termini as was seen for the catechol adducts discussed in the previous section. That is, that very little change in surface area is evident, but the terphenyl adduct adsorbs more nitrogen at higher relative pressure, leading to a larger total pore volume. It is likely that this extra void space is manifested only during *swelling* of the material in the course of nitrogen adsorption, hence increasing the apparent total pore volume. The data suggests that the penta-[naphthalene-2,3-diol] terphenyl adduct *swells* more than the corresponding biphenyl adduct, possibly due to the extended structure allowing for additional internal movement of the termini.

Concerning the two 4-*tert*-butylcatechol adducts, a drop in surface area (and total pore volume) was observed when using the larger terphenyl core. This was attributed to the *tert*-butyl groups not having a significant effect on the termini of the terphenyl adduct, due to the already awkward molecular geometry. When using an extended terminus (6-*tert*-butylnaphthalene-2,3-diol) a different relationship is observed, the two cores now give almost identical surface areas and total pore volumes. However, inspection of the adsorption isotherms in **Figure 2.29** reveals that this may not be the complete picture, as the adsorption kinetics are much slower for the biphenyl adduct, meaning that its surface area may be underestimated. The same can be said for the adamantyl substituted adducts: use of the terphenyl core creates an adduct with an improved surface area and sorption kinetics, compared with the smaller biphenyl adduct.

2.4.3 Triptycene-2,3-diol based terphenyl adducts

Reaction of the undecafluoro core with the set of triptycenes-2,3-diols synthesised in Chapter 2.3.3.3 under similar reaction conditions to those used previously for terphenyl based OMIMs, produced a series of six triptycene-2,3-diol based terphenyl OMIMs (**Scheme 2.23**).
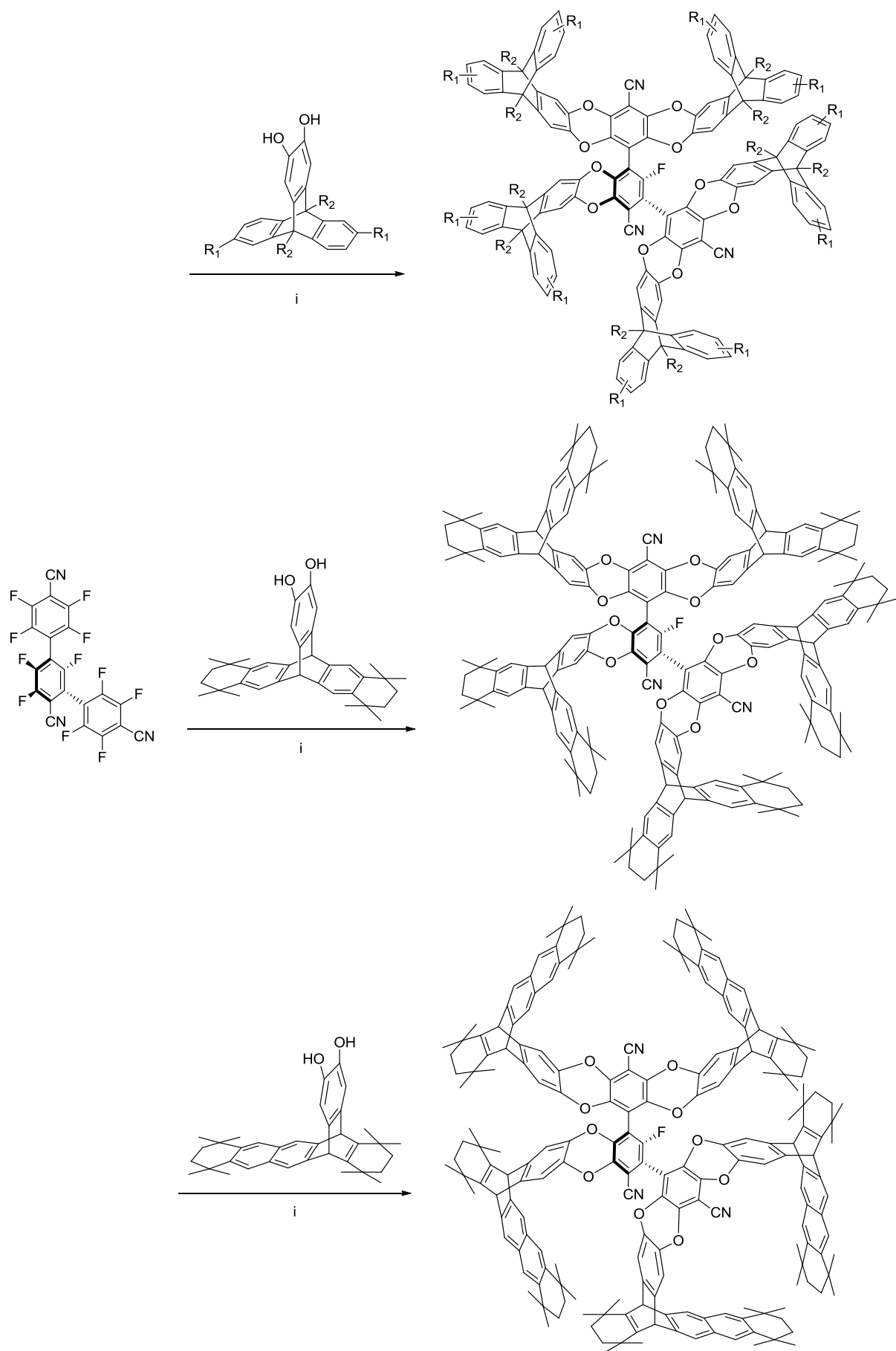
Scheme 2.25 Synthesis of the penta-[triptycene-2,3-diol] terphenyl adducts (top) [R₁ = H, ᵗBu, R₂ = H, Me] and the symmetrical (middle) and unsymmetrical (bottom, one possible regioisomer) penta-[cy6-triptycene-2,3-diol] terphenyl adducts.
Reagents and conditions: i) K₂CO₃, DMF, 65 °C, 72 hrs.

All six adducts were purified *via* column chromatography (removal of bridged and under-substituted products) to give the pure penta adducts (as mixtures of regioisomers for the *tert*-butyl substituted and unsymmetrical cy6-triptycene-2,3-diol adducts), which were subsequently characterised by the usual techniques (NMR combined with MALDI-MS and GPC). BET nitrogen sorption data for the penta-[triptycene-2,3-diol] terphenyl adducts (and their biphenyl analogues) are shown in **Figures 2.30**, **2.31** and **Table 2.12**.
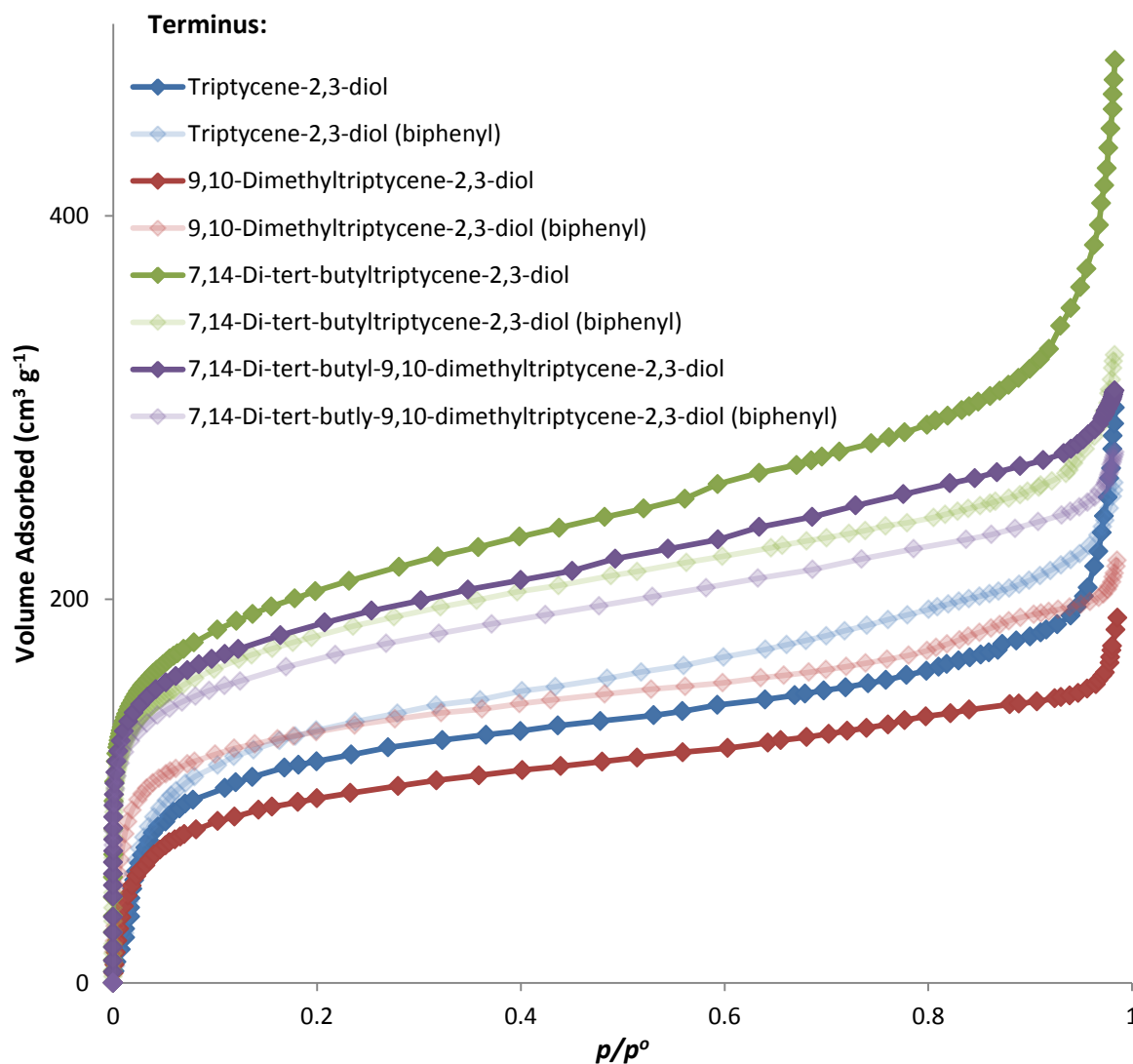
Figure 2.30 BET nitrogen adsorption isotherms for the four penta-[triptycene-2,3-diol] terphenyl adducts (bold) and their tetra-[triptycene-2,3-diol] biphenyl adducts (faint).
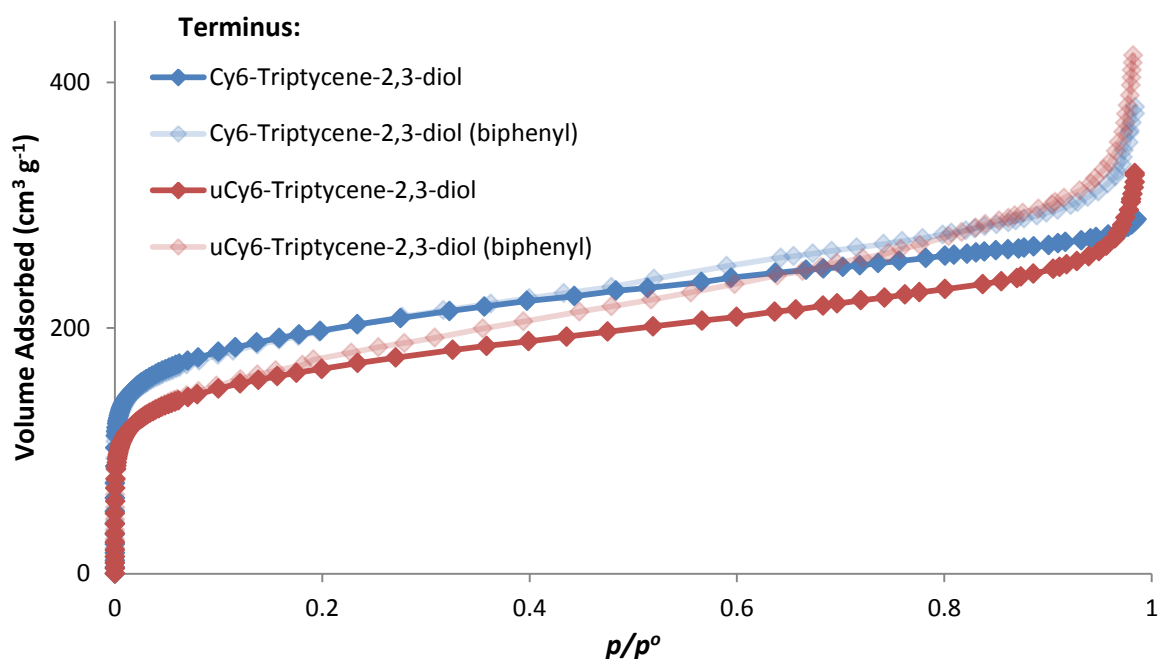
Figure 2.31 BET nitrogen adsorption isotherms for the two penta-[cy6-triptycene-2,3-diol] terphenyl adducts (bold) and their tetra-[cy6-triptycene-2,3-diol] biphenyl adducts (faint).

Terminus	BET surface area ($m^2\ g^{-1}$) [biphenyl adduct]	Total pore volume ($cm^3\ g^{-1}$) [biphenyl adduct]
Triptycene-2,3-diol	423 [485]	0.44 [0.40]
9,10-Dimethyltriptycene-2,3-diol	351 [462]	0.30 [0.33]
7,14-Di-*tert*-butyltriptycene-2,3-diol	726 [654]	0.72 [0.54]
7,14-Di-*tert*-butyl-9,10-dimethyltriptycene-2,3-diol	651 [599]	0.47 [0.42]
Symmetrical cy6-triptycene-2,3-diol	698 [702]	0.44 [0.50]
Unsymmetrical cy6-triptycene-2,3-diol	591 [622]	0.49 [0.64]

Table 2.12 BET nitrogen sorption data for the six-[triptycene-2,3-diol] terphenyl adducts and their tetra-[triptycene-2,3-diol] biphenyl adduct counterparts.

These results further demonstrate that when using an unsubstituted terminus (e.g. triptycene-2,3-diol), there is very little change in the surface area of the adduct when increasing the size of the core (biphenyl to terphenyl), as was also observed for catechol and naphthalene-2,3-diol based adducts.

Comparing the penta-[triptycene-2,3-diol] and penta-[9,10-dimethyltriptycene-2,3-diol] terphenyl adducts, it is apparent that the addition of methyl groups to the bridgehead (R_2) position results in an OMIM with a lower surface area, as was seen when comparing the corresponding biphenyl adducts in Chapter 2.3.3.3. The same hypothesis is offered as an explanation: the area around the bridgehead position of triptycene-2,3-diol based OMIMs plays a significant part in the porosity of the material (Chapter 2.3.3.4), and as such, filling this area with substituents blocks/partially fills cavities that would otherwise be accessible to adsorbing gases. The same relationship (as seen for the biphenyl adducts) is also observable for the *tert*-butylated terphenyl adducts, as the extra methyl groups on the penta-[7,14-di-*tert*-butyl-9,10-dimethyltriptycene-2,3-diol] adduct yielded a lower surface area than the non-methylated penta-[7,14-di-*tert*-butyltriptycene-2,3-diol] adduct.

Comparison of the biphenyl and terphenyl-[7,14-di-*tert*-butyltriptycene-2,3-diol] adducts shows a subtle improvement in the already impressive surface area for the larger terphenyl adduct, which consequently led to the highest surface area (726 m^2 g^{-1}) achieved for any OMIM produced thus far. As with the 3,5-di-*tert*-butylcatechol adducts (Chapter 2.4.1), it seems that introduction of significant bulk (multiple *tert*-butyl groups per terminus), can yield an improved surface area for the larger terphenyl adduct, suggesting that there is some room to *spread the arms* of the terphenyl adducts further apart despite their already somewhat awkward geometric shape. A similar effect can be observed when comparing the biphenyl and terphenyl-[7,14-di-*tert*-butyl-9,10-dimethyltriptycene-2,3-diol] adducts (**Table 2.12**). Conversely, when evaluating the properties of the biphenyl and terphenyl-[9,10-dimethyltriptycene-2,3-diol] adducts, a significant drop in surface area for the larger terphenyl adduct is observed. This suggests that without the presence of bulky *tert*-butyl groups *on the ends* of the termini, the adducts cannot create such an open structure, and so adding more substituents around a similarly shaped core serves only to decrease the porosity of the material.

Both the penta-[cy6-triptycene-2,3-diol] terphenyl adducts (symmetrical and unsymmetrical) show little change when compared to their biphenyl adducts, suggesting a potential limit to the amount of bulk that can be placed around a triptycene-2,3-diol based terminus. It is feasible that excessive bulk could either fill pores (thus decrease surface

area), or not contribute to a significant increase in porosity such that their extra molecular weight results in a lower surface area per gram.

2.5 OMIM simulations

In an effort to further understand their structure-property relationship, computational simulations of several OMIMs were performed so that their properties could be estimated and compared to those obtained from experimental samples. These simulations were performed at Pennsylvania State University using Materials Studio software and the LionXI computational cluster.[158]

2.5.1 Simulation technique

Geometry optimised OMIM structures were packed into low density (approximately 0.5 g cm^{-3}) periodic boxes and compressed, using a 21 step compression scheme,[6] to more realistic densities (approximately 1.0 g cm^{-3}, **Figure 2.32**). Boxes were packed at low densities to avoid packing errors (overlaps or ring spearing), and also to allow them to independently arrive at realistic densities upon compression, that are representative of a favourable packing arrangement, without the need for prior knowledge of an experimental density.
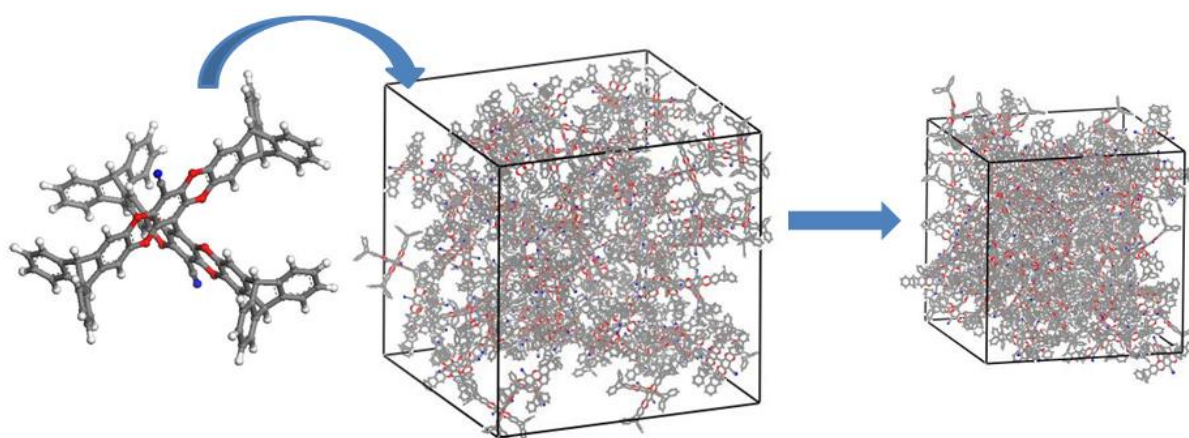
Figure 2.32 Simulation method: geometry optimised OMIM (left) packed into low density periodic box (centre, approximately 100 molecules per box) and compressed (right).

Once obtained, the *accessible surface area* (**Figure 3.33**)[159] and total pore volume of each compressed box was estimated using a probe equal in size to the kinetic diameter of a nitrogen molecule (d_{N2} = 3.681 Å). Results were then converted into per gram measurements and averaged across at least three independently constructed and compressed boxes, to give simulated accessible surface areas and total pore volumes.
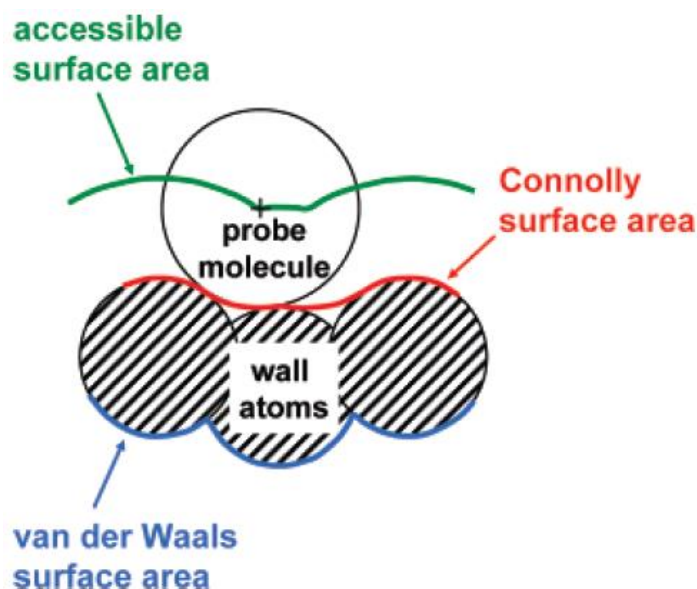
Figure 2.33 Definition of various estimations of surface areas.

The validity of each compressed box could be studied by comparing simulated scattering data to experimentally measured powder X-ray diffraction data of a corresponding sample. To generate simulated scattering, three dimensional Cartesian coordinates of each atom within a compressed box were mapped to a .xyz file, which was then used in conjunction with ISAACS software[160] to generate a simulated radial distribution function from which simulated scattering plots could be estimated. Briefly, for homogeneous materials, the radial distribution function measures the probability of finding an atom within a particular shell (of width *dr*) at distance *r* from another atom. Once averaged across every atom in the box, an approximate picture of intra-atomic distances is built up that can be used to estimate X-ray scattering patterns. A comparison of simulated and experimental scattering for **OMIM-1** is shown in **Figure 2.34**.[5]
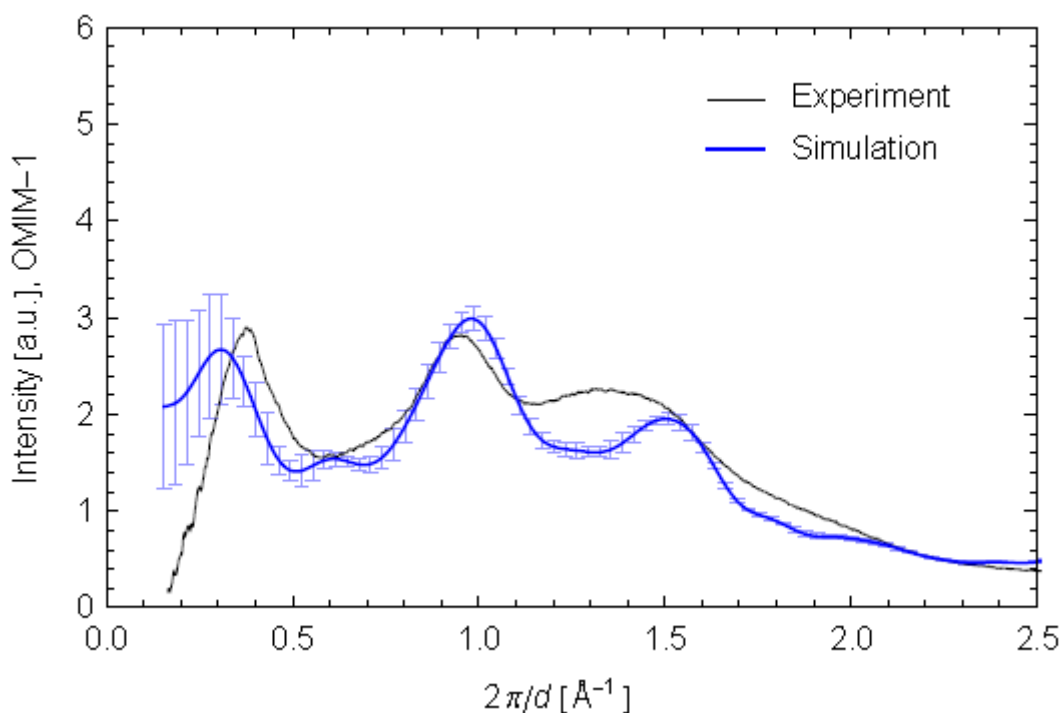
Figure 2.34 Simulated (blue) and experimentally measured powder (black) X-ray scattering of OMIM-1.

Generally, good agreement is observed between the simulated and experimental samples, validating the method of simulation. Significant variations between independent simulations in the long range interaction region, indicated by the error bars, may account for the slight shifting of the left hand peak.[5]

2.5.1 Simulation results

Many OMIM structures detailed in the thesis have been the subject of simulation studies, but two, **OMIM-1** and **OMIM-1-tBu,** have been studied in much detail along with two further OMIMs produced by Dr. Grazia Bezzu: **OMIM-2** and **OMIM-3** (**Figure 2.35**). The results obtained from simulations show good compatibility between the experimentally measured and simulated data[5] (**Table 2.13**). Details of further simulated OMIMs are also presented in **Table 2.13** alongside their experimentally measured data for comparison.
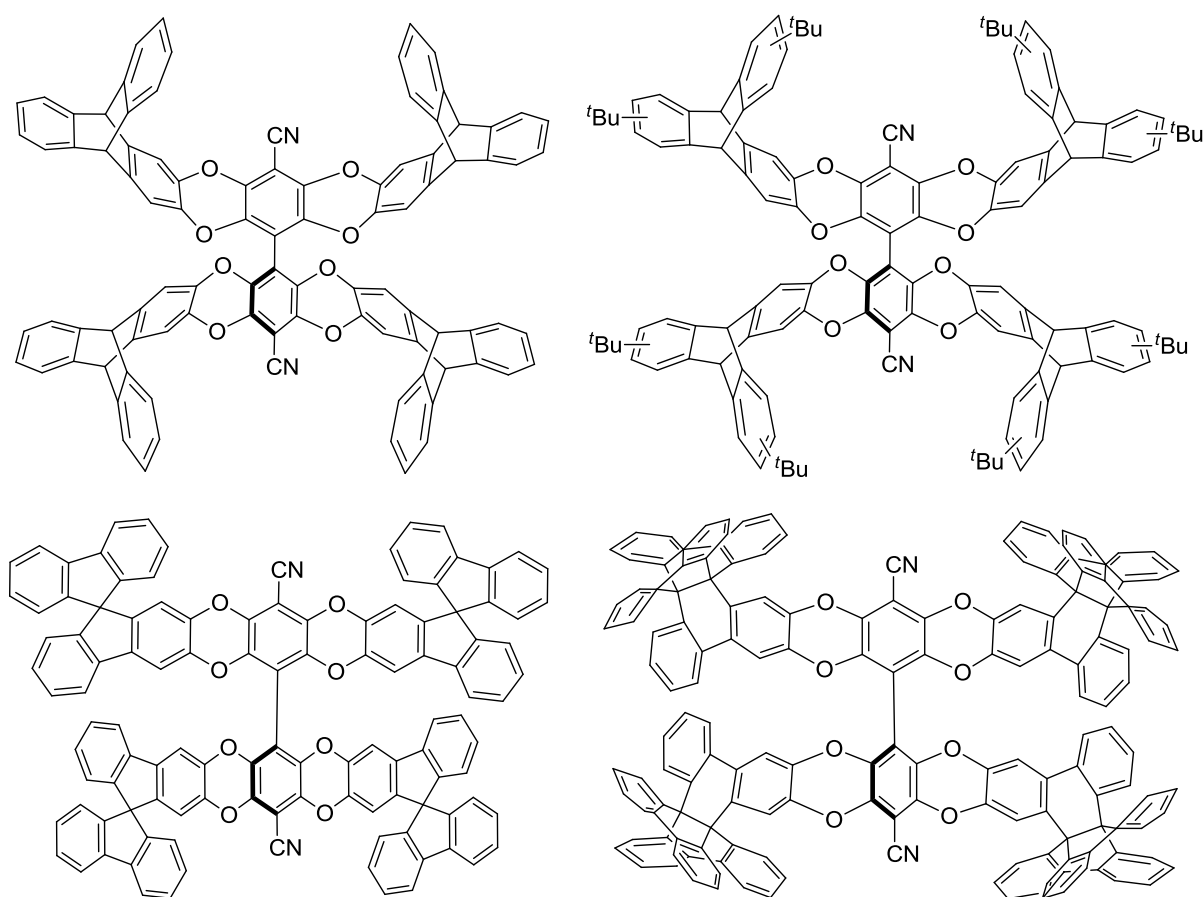
Figure 2.35 Simulated OMIMs: **OMIM-1**, **OMIM-1-tBu**, **OMIM-2** and **OMIM-3** (top left to bottom right).

OMIM	Simulated		BET	
	Surface area (m^2 g^{-1})	Total pore volume (cm^3 g^{-1})	Surface area (m^2 g^{-1})	Total pore volume (cm^3 g^{-1})
Biphenyl OMIMs				
OMIM-1	155 (21)[a]	0.158(8)[a]	485	0.40
OMIM-1-*t*Bu	286 (21)[a]	0.24(1)[a]	654	0.54
OMIM-1-Cy6	321 (75)[b]	0.245(29)[b]	702	0.60
OMIM-2	92 (19)[a]	0.131(8)[a]	477	0.06
OMIM-3	194 (26)[a]	0.184(9)[a]	595	0.22
Terphenyl OMIMs				
Tripycene-2,3-diol	140 (22)[b]	0.152 (8)[b]	423	0.44
*t*Bu-tripycene-2,3-diol	237 (32)[b]	0.227 (8)[b]	726	0.72
Cy6-tripycene-2,3-diol	283 (34)[b]	0.228 (13)[b]	698	0.44

Table 2.13 Simulated and experimental surface areas and total pore volumes for selected OMIMs, standard deviations shown in parentheses.
a) Data from Abbott *et al.*[5] averaged over 5 boxes.
b) Data from research visit to Pennsylvania State University averaged over 3 boxes.

Whilst the results show that the simulations universally give rise to underestimated surface areas and total pores volumes, the trend of both agrees with experimentally measured data. **OMIM-1-Cy6** has the highest experimentally measured surface area (702 m^2 g^{-1}) for the biphenyl based OMIMs and simulations predict it to have the highest surface area; the same is true for **OMIM-2**, which is measured and predicted to have the lowest surface area. The trend for the terphenyl based OMIMs is not as accurate however, as the simulations predict the symmetrical penta-[cy6-triptycene-2,3-diol] adduct to have the highest surface area, whilst experimental data suggests that the penta-[7,14-di-*tert*-butyltriptycene-2,3-diol] adduct has the highest.

Despite some anomalies, the process of OMIM simulation has proved itself as a valid means of screening potential structures without the need for synthesis, which as demonstrated in this chapter, can be a lengthy procedure. Further advancements in this field are currently being made, and better comparisons to known OMIM porosity data are being achieved, however the details are beyond the scope of this thesis. The interested reader is referred to the publication in preparation.[161]

2.6 Summary and conclusions (OMIMs)

Thirteen novel biphenyl based and twelve novel terphenyl based OMIMs were prepared, fully characterised using typical techniques and found to possess apparent BET surface areas in the range 7 – 726 m^2 g^{-1}. OMIMs comprising of two different termini (unsymmetrical OMIMs) were found be less porous than either of their symmetrical counterparts, though more research is needed to verify this discovery. Computational simulations of OMIMs have proved that they are able to predict their relative porosity, although again, more research in needed to improve the simulation technique such that quantitative prediction of surface areas can be made.

Comparing the OMIMs discussed in this chapter, it is clear to see that those based on small, planar units possessing no substituents, are poor at establishing a high degree of microporosity in the resultant OMIM. This is most evident in **Figures 2.27** and **2.29**, as the catechol and naphthalene-2,3-diol biphenyl and terphenyl adducts all gave rise to apparent

BET surface areas under 30 m^2 g^{-1}. Substitution of these termini with bulky groups (*tert*-butyl, adamantyl) gave rise to materials of higher microporosity, with apparent BET surface areas of up to 102 and 347 m^2 g^{-1} for catechol and naphthalene based OMIMs respectively, however, this often came at the cost of introducing slow sorption kinetics.

When utilising the triptycene moiety as a terminus, materials of even greater microporosity were obtained. The unsubstituted triptycene terminus generated OMIMs with apparent BET surface areas of over 420 m^2 g^{-1} when combined with both the biphenyl and terphenyl cores. Substitution of the bridgehead protons with a methyl groups led to decreased surface areas in OMIMs centred around either core, suggesting that this area of space plays a key role in the porosity of the material, an effect that has been previously observed in similar materials.[73] Conversely, substitution with bulky groups at the extremities of the termini led to a large increase in apparent BET surface areas, reaching 726 m^2 g^{-1} for the di-*tert*-butyltriptycene-2,3-diol terphenyl adduct. Unlike smaller termini, the introduction these substituents *improved* the sorption kinetics in the resultant OMIM, verifying triptycene's status as an excellent component for microporous materials.

3. Dendrimers of Intrinsic Microporosity

3.1 Background

The term *dendrimer* is derived from the Greek word for *tree – δένδρον* (pronounced *dendron*), and refers to large, highly branched molecules with a monodisperse molecular weight. Whilst their history can be traced back as far as 1941 to the work by Flory on size distribution in three dimensional polymers,[162,163] the first use of the term in scientific literature was as recently as 1985 regarding the synthesis of *PAMAM* (poly(amidoamine)) dendrimers.[164] These dendrimers are formed by the sequential exhaustive Michael addition between ethylenediamine and methyl acrylate, followed by amidation of the resulting esters with ethylenediamine (**Scheme 3.1**). By repeating these steps, sequentially larger dendrimers can be grown and defined by their *generation number* (the number of branch units between the core and terminal groups).[165]
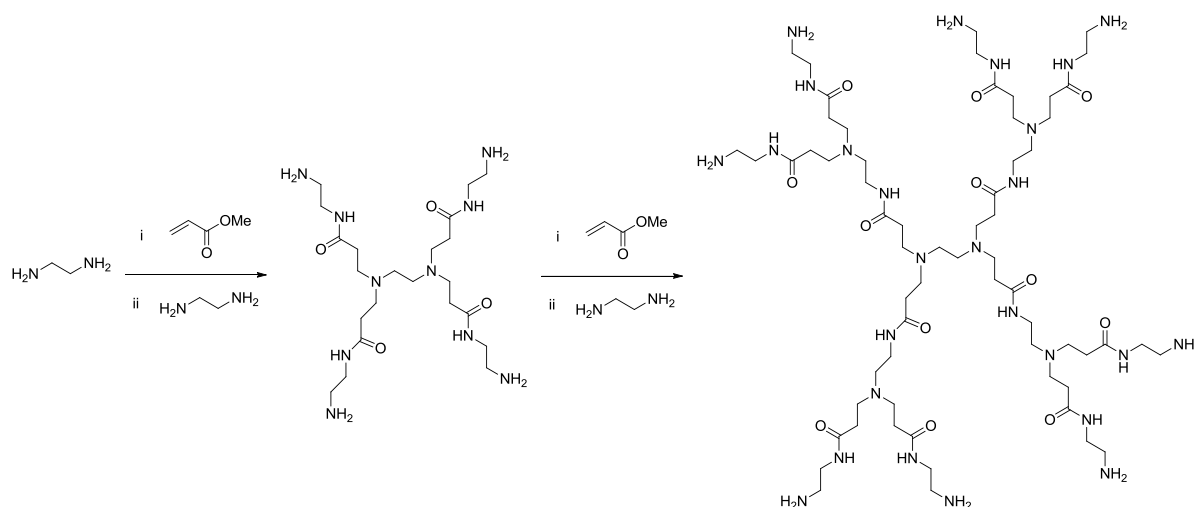
Scheme 3.1 Synthesis of a first and second generation *PAMAM* dendrimer.

This synthesis of a *PAMAM* dendrimer is an example of a *divergent* dendrimer synthesis (**Figure 3.1**),[166] one which begins with the core and successively branches outwards until the steric limit is reached. Although this approach has been successfully employed in the synthesis of many dendrimers,[164,167] it has often led to the production of imperfect samples,[168] due to the exponentially increasing number of functional terminal groups leading to unavoidable structural defects (even with the addition of a large excess of

reactants). Separation of these imperfect samples is then problematic, due to the very similar chemical properties of the perfect and imperfect dendrimers.

Convergent synthesis (**Figure 3.1**)[166] uses the opposite strategy: beginning with what will be the terminus of the completed dendrimer and working inwards.[169] Once a sufficient generation of *dendron* (branch unit) is reached, a non-functional group is activated and subsequently reacted with a core to produce the desired dendrimer. Due to the small number of functional terminal groups involved in each step, convergent synthesis does not produce the structural defects associated with divergent synthesis. Furthermore, large excesses of reagents, often necessary in divergent synthesis, are not required, allowing for easier purification after each step.
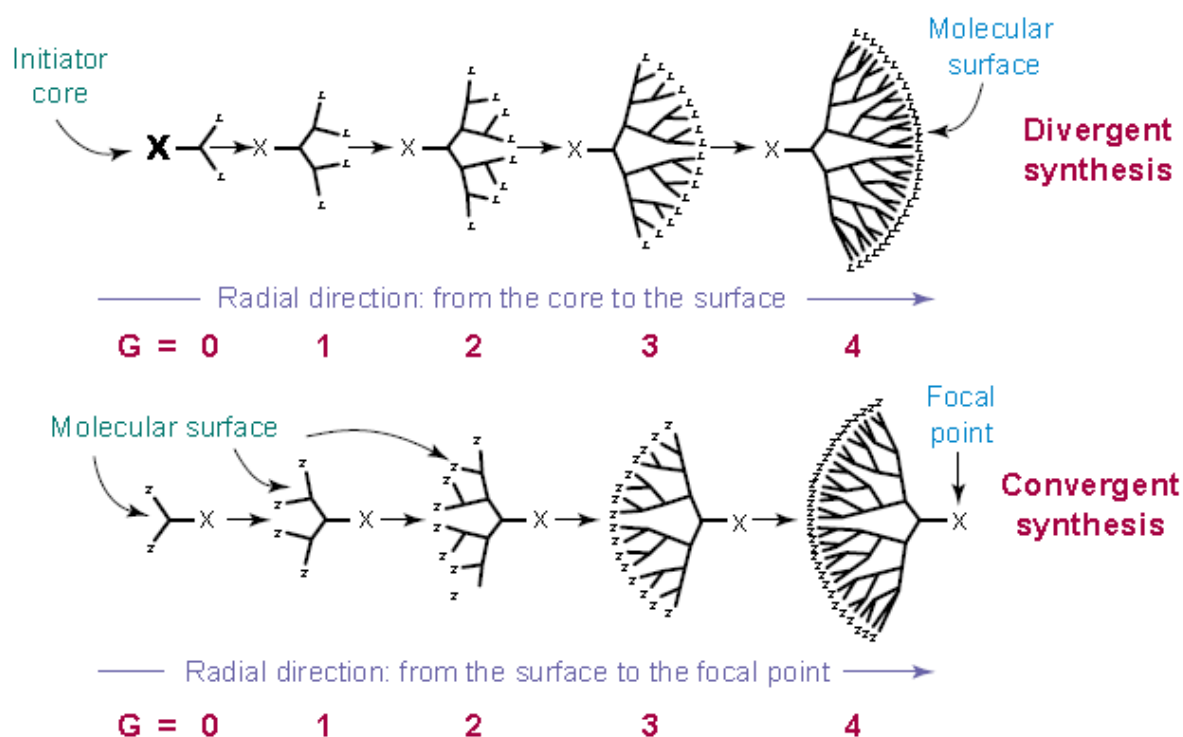
Figure 3.1 Comparison of divergent (top) and convergent (bottom) dendrimer synthesis. G = Generation number.

It is the aim of this chapter to expand upon the results obtained for Organic Molecules of Intrinsic Microporosity (*OMIMs*) by producing a series of Dendrimers of Intrinsic Microporosity (*DIMs*) comprised of similar components. Isolation of tri-substituted biphenyl branch units, will allow for the convergent synthesis of first generation dendrimers by reaction with a catechol functionalised core (**Scheme 3.2**). The alternative divergent

synthesis (**Scheme 3.3**), would call for reaction of a suitable catechol functionalised core with octafluoro to produce a compound with nine reactive fluorine pairs. Given the reactive nature of both reactants and their reported polymer forming properties,[74] it was decided not to attempt this approach, and instead, focus on the more realistic convergent route (**Scheme 3.2**).
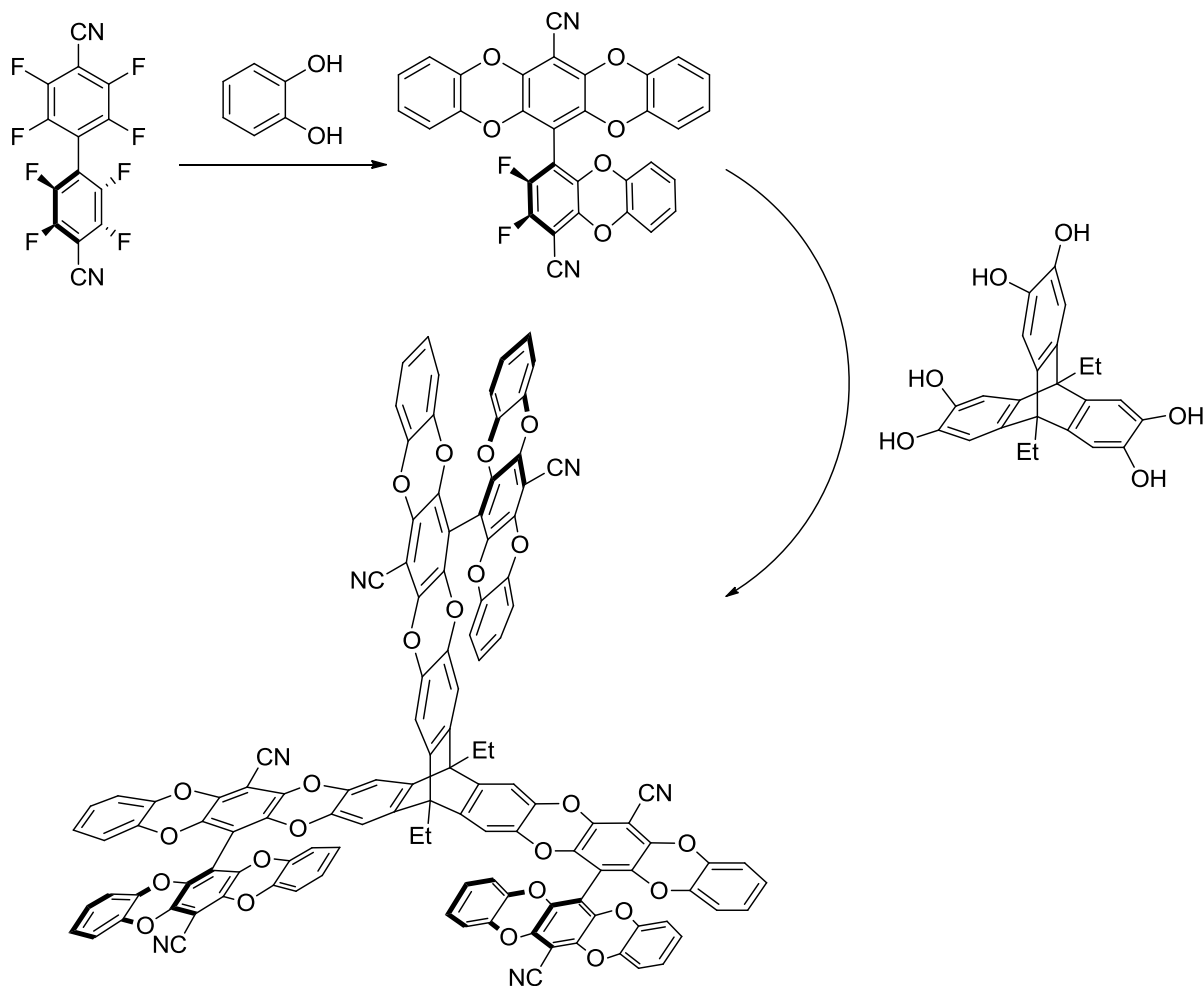
Scheme 3.2 Example of a convergent DIM synthesis.
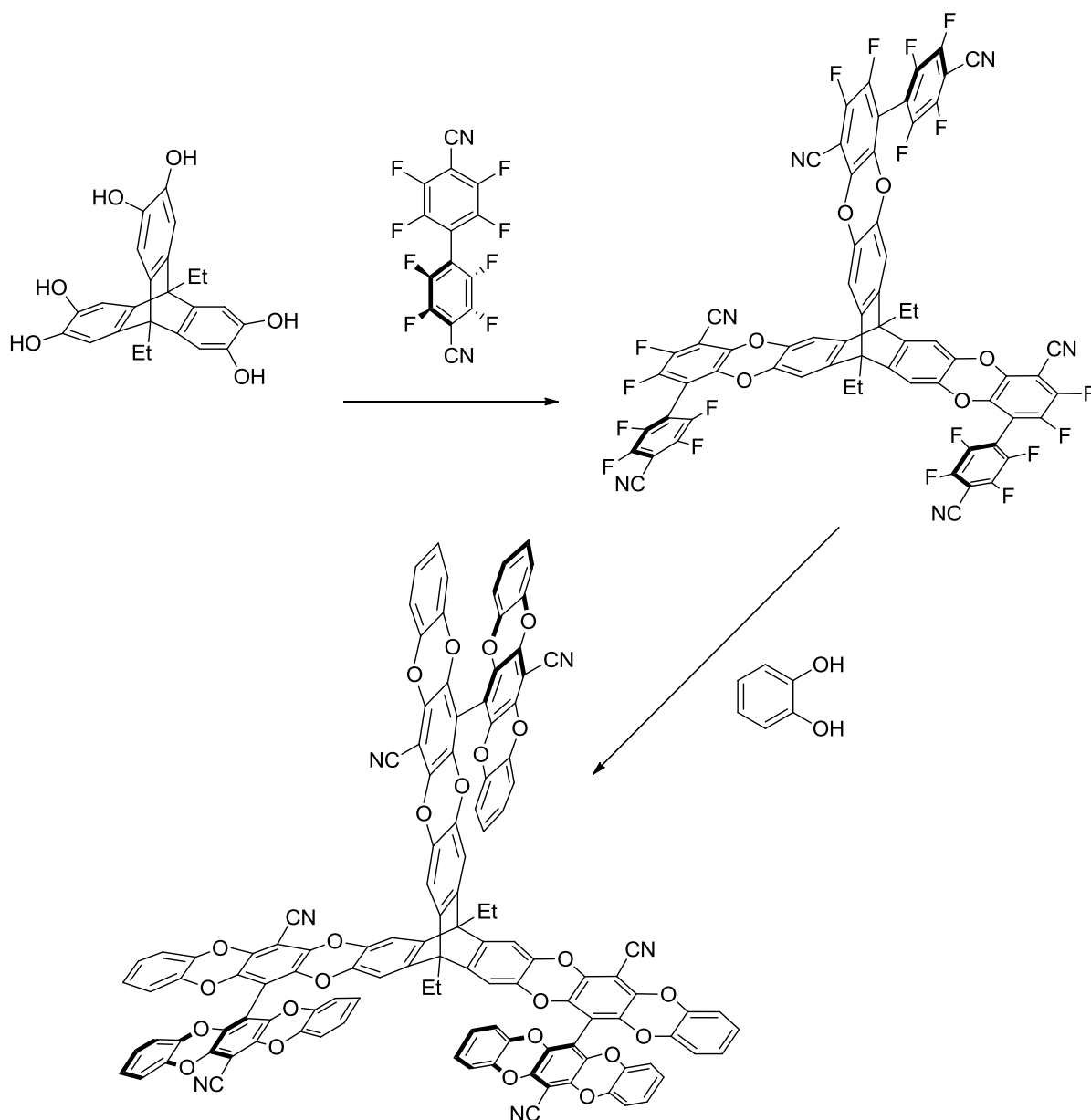
Scheme 3.3 Example of a divergent DIM synthesis.
It was proposed that the *octodecafluoro* compound (top right) would be too reactive to isolate in suitable yield

3.2 Synthesis of 9,10-diethyltriptycene-2,3,6,7,13,14-hexaol

Owing to its ease of synthesis and previous exploitation in highly porous materials,[73,74] 9,10-diethyltriptycene-2,3,6,7,13,14-hexaol was chosen as the core from which to synthesise a systematic series of DIMs. In accordance with literature procedures[73,148,170] 2,3,6,7-tetramethoxy-9,10-diethylanthracene was first produced by reaction of veratrole and propanal under acidic conditions (**Scheme 3.4**).[170] Once isolated, the anthracene was

subjected to a Diels-Alder reaction with a freshly prepared dimethoxybenzyne intermediate[148] to afford 2,3,6,7,13,14-hexamethoxy-9,10-diethyltriptycene, which was subsequently demethylated with boron tribromide to give the desired 9,10-diethyltriptycene-2,3,6,7,13,14-hexaol (**Scheme 3.4**).[73] Given its poor stability in air[171] and ease of deprotection, 9,10-diethyltriptycene-2,3,6,7,13,14-hexaol was stored in its protected methoxy state and deprotected only immediately prior to use.
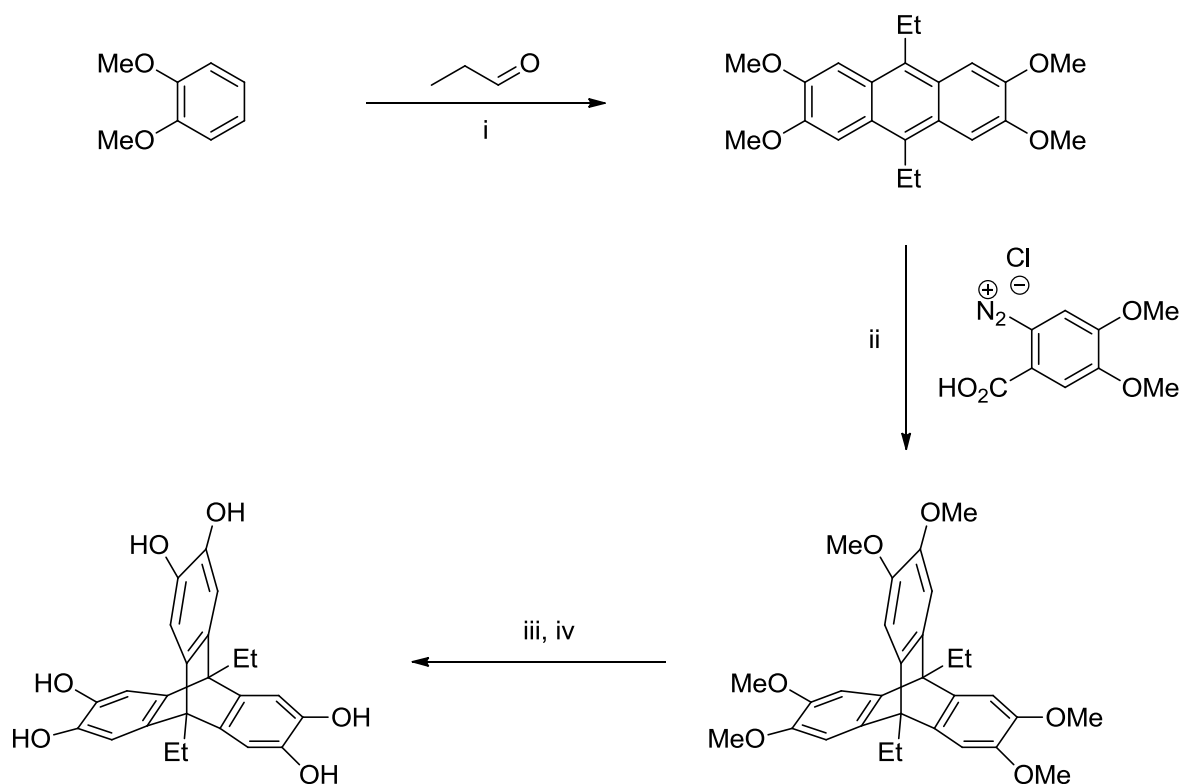
Scheme 3.4 Synthesis of 9,10-diethyltriptycene-2,3,6,7,13,14-hexaol.
Reagents and Conditions: i) H_2SO_4, 5 °C, 3 hrs ii) 1,2-Epoxypropane, DCE, 12 hrs, reflux iii) BBr_3, DCM, 3 hrs, RT iv) H_2O.

3.3 Catechol based DIMs

With a synthetic route to a potential core established, investigations were made into the synthesis of branch units in the form of tri-substituted biphenyl adducts (**Scheme 3.5**). Using the same reaction conditions employed to produce the tetra-[catechol] biphenyl adduct in Chapter 2.3.1, the tri-[catechol] biphenyl adduct was prepared by reaction of octafluoro with three equivalents of catechol (**Scheme 3.5**).
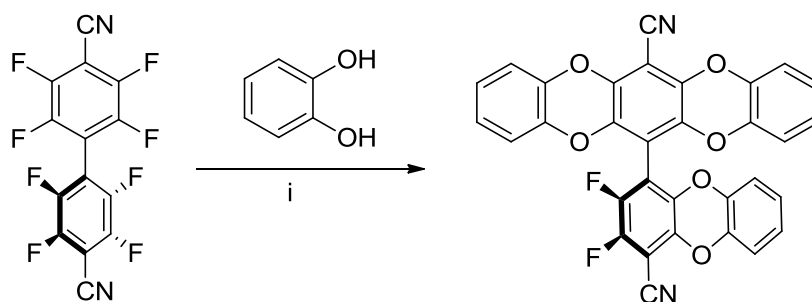
Scheme 3.5 Synthesis the tri-[catechol] biphenyl adduct.
Reagents and conditions: i) K$_2$CO$_3$, DMF, 65 °C, 72 hrs.

Purification of the crude reaction mixture *via* column chromatography was required, as the reactive nature of the octafluoro unit led to the formation of some of the tetra-[catechol] biphenyl adduct (**Scheme 2.2**). This in turn resulted in some di-substituted material remaining in the crude reaction products due to over consumption of catechol. Bridged compounds, discussed in Chapter 2.3.1, were also produced and removed in the same process. Once isolated, the tri-[catechol] biphenyl adduct was characterised by ^{1}H, ^{13}C and ^{19}F NMR, combined with GPC and high resolution MS to confirm its purity.

The combined effects of the non-selectivity of the reaction, the poor solubility of the crude reaction products and the minimal separation attainable on a silica (or alumina) column, led to a relatively low isolated yield of the tri-[catechol] biphenyl adduct (29 %). However, sufficient quantity could still be synthesised in a single reaction to allow for formation of a dendrimer by reaction with freshly prepared 9,10-diethyltriptycene-2,3,6,7,13,14-hexaol (**Scheme 3.6**).
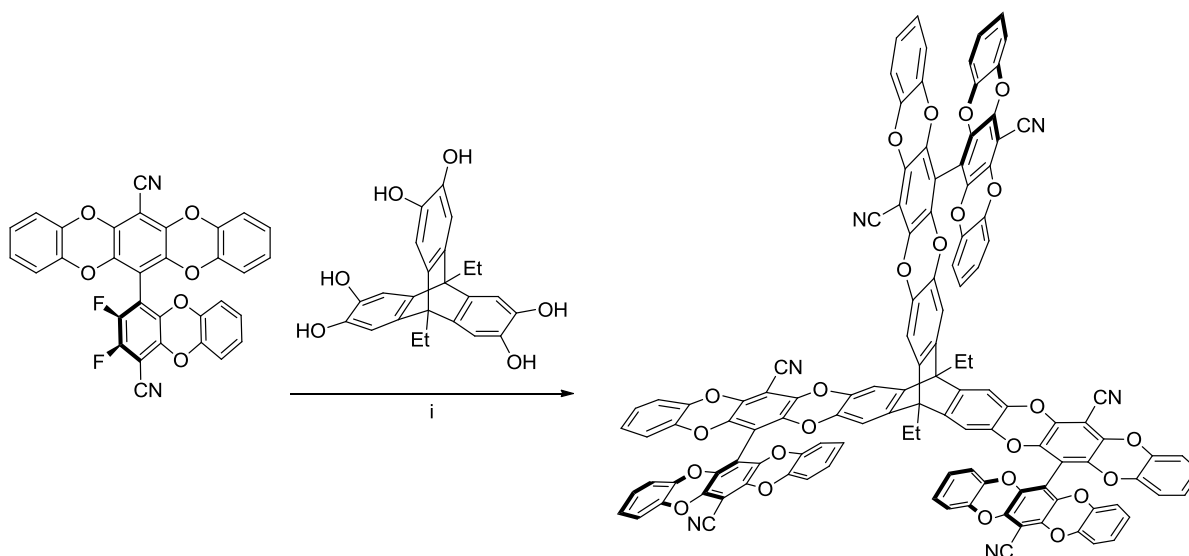
Scheme 3.6 Synthesis of the tri-[catechol]-9,10-diethyltriptycene dendrimer.
Reagents and conditions: i) K$_2$CO$_3$, DMF, 65 °C, 72 hrs.

The isolated tri-[catechol] biphenyl adduct was reacted in just over three to one stoichiometry with freshly prepared 9,10-diethyltriptycene-2,3,6,7,13,14-hexaol under similar reaction conditions to those used for the formation of biphenyl adducts. After 72 hrs, GPC analysis (**Figure 3.2**) of the crude reaction products revealed a small expected amount of unreacted branch unit, and the fact that the fully substituted dendrimer had formed selectively, no evidence of mono or di substituted cores was seen.

Peak RV - (ml)	18.600	19.667
Mn - (Daltons)	1,355	400
Mw - (Daltons)	1,403	424
Mz - (Daltons)	1,457	448
Mp - (Daltons)	1,382	426
Mw / Mn	1.035	1.062
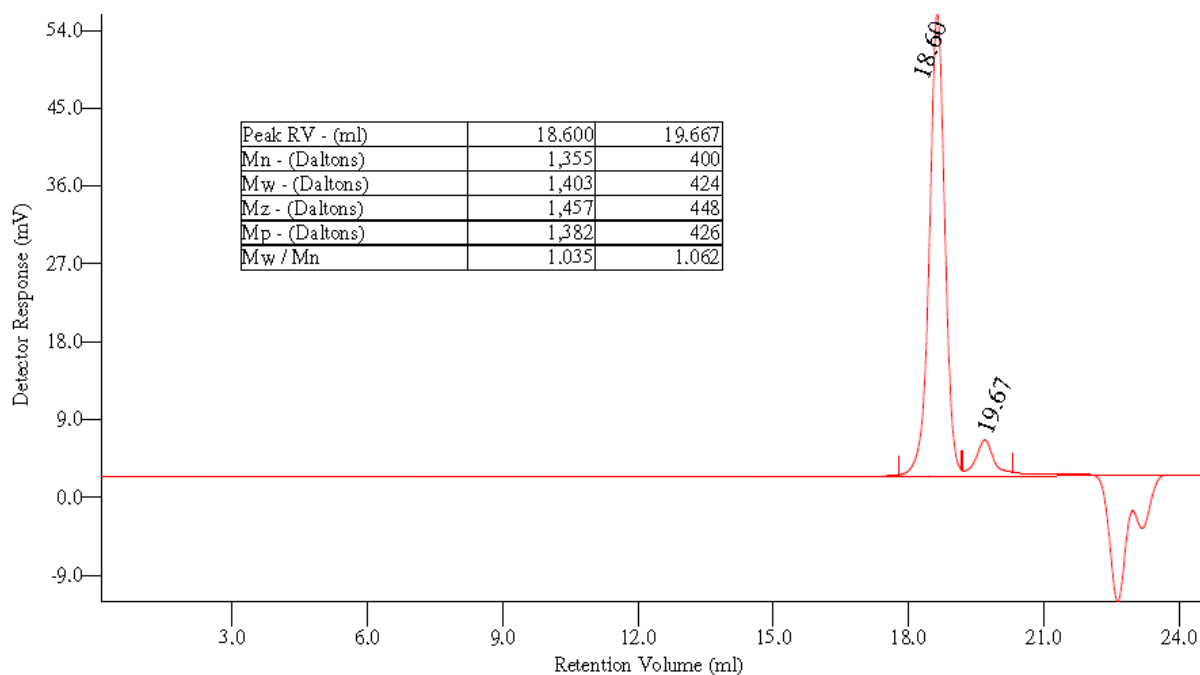
Figure 3.2 Crude GPC trace for the tri-[catechol]-9,10-diethyltriptycene dendrimer showing residual excess branch unit (right-hand peak), dendrimer (left-hand peak) and relevant data (inset).

Given the very poor solubility of the resultant dendrimer, purification could be achieved simply by chloroform treatment, which removed the more soluble branch unit. Once isolated, as a mixture of regioisomers, since each branch unit has two possible orientations in which to approach the triptycene core, the dendrimer was further characterised by ^{1}H NMR, MALDI-MS and nitrogen sorption, the latter of which revealed an apparent BET surface area of 330 m^2 g^{-1} and total pore volume of 0.44 cm^3 g^{-1}. Clearly, expansion of the tetra-[catechol] biphenyl adduct (apparent BET surface area of 7 m^2 g^{-1}) to the corresponding DIM had a marked impact on porosity of the material, a property that once again confirms how triptycene units can enhance the formation of porous materials.

In an effort to create soluble catechol based DIMs and further study the effects of bulky substituents on discrete porous materials, dendrimers were prepared from branch units containing 4-*tert*-butylcatechol and 3,5-di-*tert*-butylcatechol termini (**Scheme 3.7**).
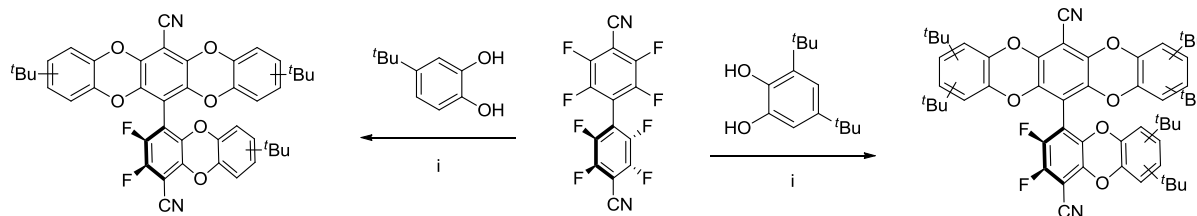
Scheme 3.7 Synthesis of the tri-[4-*tert*-butylcatechol] and tri-[3,5-di-*tert*-butylcatechol] biphenyl adducts.
Reagents and conditions: i) K$_2$CO$_3$, DMF, 65 °C, 72 hrs.

Both the *tert*-butyl containing branch units were prepared under analogous reaction conditions to those used to produce the catechol branch unit (**Scheme 3.5**). Analysis of the crude reaction products revealed the same impurities (di and tetra substituted adducts, as well as branched compounds), which were removed *via* column chromatography. The presence of regioisomers for each product (and impurities) made for difficult separation on silica (due to the broadening of bands), meaning that the isolated yields were again fairly low (57 and 39 % for the mono and di-*tert*-butyl compounds respectively). Once isolated as mixtures of regioisomers, both were characterised and confirmed pure by ^{1}H, ^{13}C and ^{19}F NMR combined with MALDI-MS and GPC. Reaction with freshly prepared 9,10-diethyltriptycene-2,3,6,7,13,14-hexaol gave the corresponding dendrimers (**Scheme 3.8**).
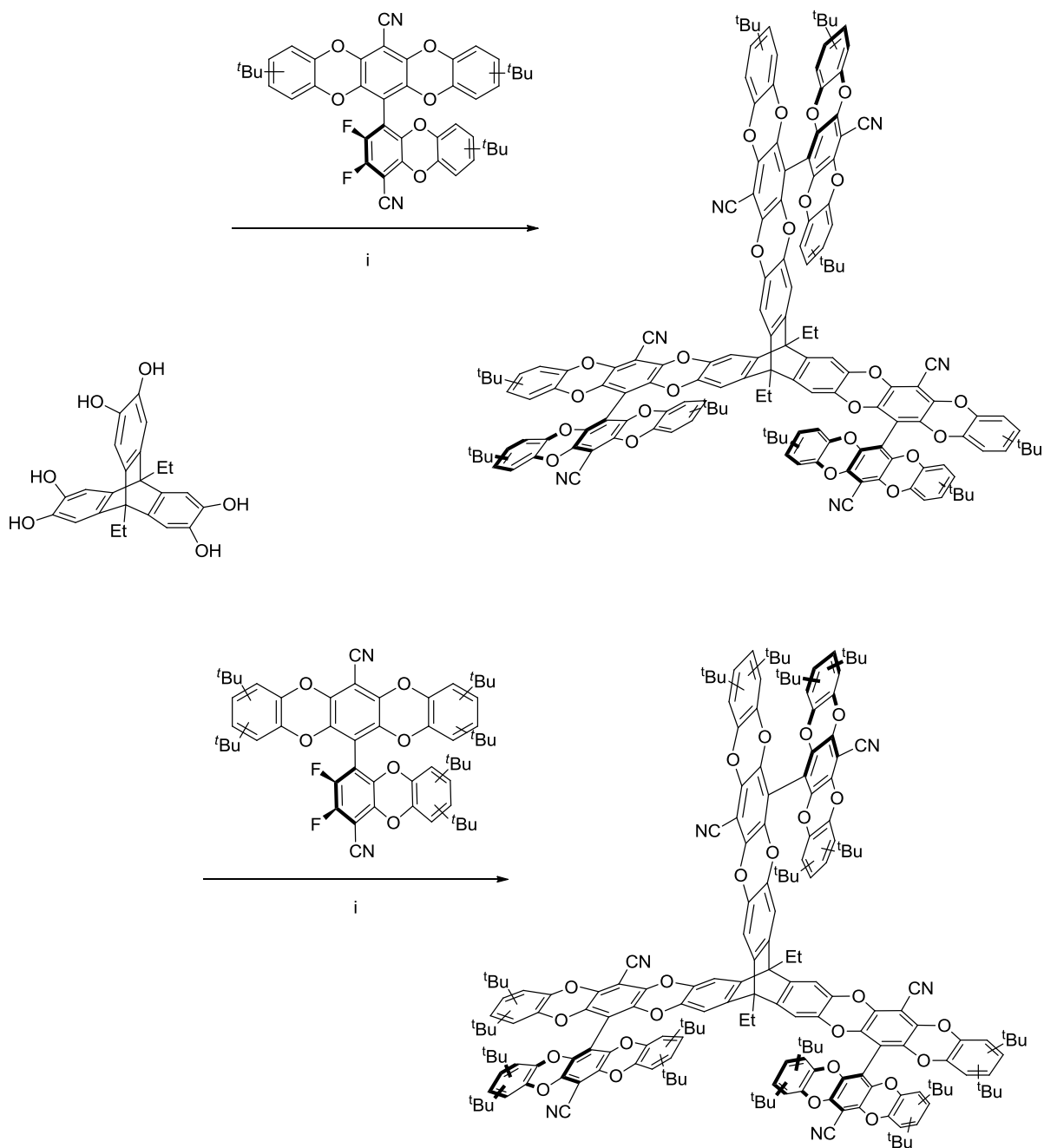
Scheme 3.8 Synthesis of the tri-[4-*tert*-butylcatechol]-9,10-diethyltriptycene and tri-[3,5-di-*tert*-butylcatechol]-9,10-diethyltriptycene dendrimers.
Reagents and conditions: i) K$_2$CO$_3$, DMF, 65 °C, 72 hrs.

Both reactions were carried out in just over three to one stoichiometry in favour of the branch units, to ensure complete substitution of the triptycene core. Analysis of the crude material for both reactions revealed the expected formation of dendrimer plus excess branch unit. Improved solubility of the products over the catechol analogue allowed for purification by column chromatography to isolate the desired dendrimers (as mixtures of

regioisomers), which were subsequently characterised by ^{1}H NMR, ^{13}C NMR, MALDI-MS and GPC. BET surface areas of the three catechol based dendrimers were measured using nitrogen sorption and are compared to those obtained for the corresponding tetra-[catechol] biphenyl adducts in **Figure 3.3** and **Table 3.1** below.
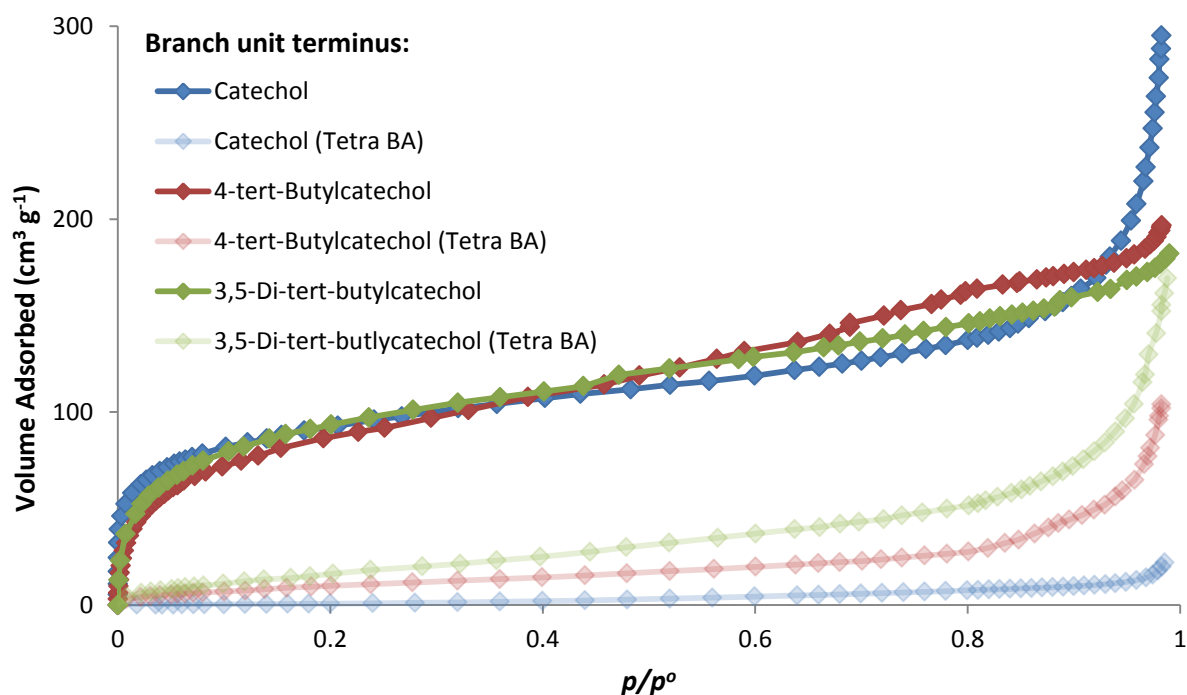
Figure 3.3 BET nitrogen adsorption isotherms for the three catechol based dendrimers (bold) and the corresponding tetra-[catechol] biphenyl adducts (Tetra BA) (faint). Desorption plots removed for clarity.

Branch unit terminus	BET surface area (m^2 g^{-1}) [Tetra biphenyl adduct]	Total pore volume (cm^3 g^{-1}) [Tetra biphenyl adduct]
Catechol	330 [7]	0.44 [0.03]
4-*tert*-Butylcatechol	320 [41]	0.30 [0.15]
3,5-Di-*tert*-butylcatechol	346 [67]	0.27 [0.23]

Table 3.1 BET nitrogen sorption data for the three catechol based dendrimers and the corresponding tetra-[catechol] biphenyl adducts in square brackets.

The results indicate that all three dendrimers have very similar surface areas, suggesting that the introduction of bulky substituents has little effect on the microporosity of dendrimers with catechol based termini. Given that the effects of bulky substituents on

tetra-[catechol] biphenyl adducts were quite small (**Table 3.1**), this is understandable, as the increased size of the dendrimer means that the addition of substituents has much less impact on the overall structure. One effect that can be observed is that the introduction of bulky groups diminishes adsorption seen at high relative pressure (**Figure 3.3**), which in turn decreases the total pore volume (**Table 3.1**). This late adsorption could be the result of some intrinsic mesoporosity due to *swelling,* movement of the constituent molecules to allow nitrogen to access originally inaccessible areas of the catechol DIM during adsorption.

3.4 Naphthalene-2,3-diol based DIMs

Continuing the trend of this thesis, a series of naphthalene-2,3-diol based branch units were prepared by reaction of the three naphthalene-2,3-diols discussed in Chapter 2.3.2 with octafluoro in three to one stoichiometry (**Scheme 3.9**).
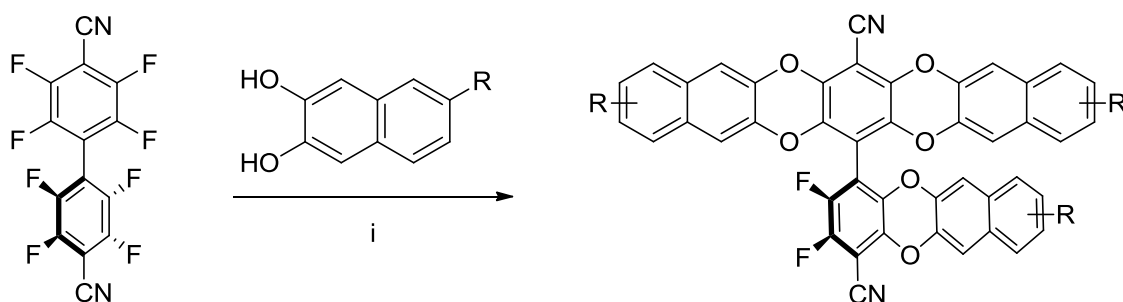
Scheme 3.9 Synthesis of the three tri-[naphthalene-2,3-diol] biphenyl adducts.
R = H, ^{t}Bu, Ad.
Reagents and conditions: i) K$_2$CO$_3$, DMF, 65 °C, 72 hrs.

All three tri-substituted adducts were isolated following column chromatography (as mixtures of regioisomers for the *tert*-butyl and adamantyl substituted adducts), and characterised by the usual techniques. Isolated yields were similarly poor to the tri-[catechol] biphenyl adducts due to either: poor solubility (R = H), or the presence of regioisomers (R = ^{t}Bu, Ad). Once isolated, each tri substituted adduct was reacted, in just over three to one stoichiometry, with freshly prepared 9,10-diethyltriptycene-2,3,6,7,13,14-hexaol to produce the corresponding dendrimer (**Scheme 3.10**).
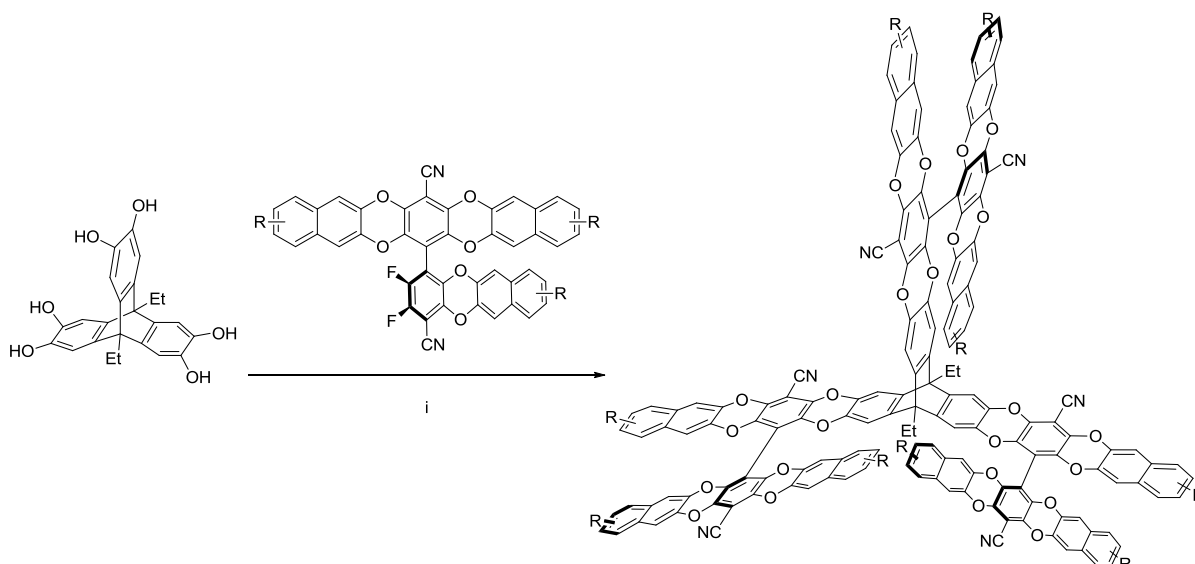
Scheme 3.10 Synthesis of the tri-[naphthalene-2,3-diol]-9,10-diethyltriptycene dendrimers.
R = H, *t*Bu, Ad.
Reagents and conditions: i) K$_2$CO$_3$, DMF, 65 °C, 72 hrs.

Again, GPC analysis of the crude products for each reaction revealed the expected presence of excess branch unit, which was subsequently removed *via* chloroform trituration (R = H) or column chromatography (R = *t*Bu, Ad) to yield the expected dendrimers (as a mixture of regioisomers). Full characterisation was achieved using ^{1}H NMR, ^{13}C NMR, GPC and MALDI-MS for dendrimers with R = *t*Bu or Ad substituents. However, the unsubstituted (R = H) dendrimer was almost completely insoluble in all common solvents and so only characterised by GPC (in very dilute solution) and MALDI-MS, both of which suggested purity. Once isolated, each dendrimer's porosity was evaluated by BET nitrogen sorption, the resultant isotherms and data are shown below in **Figure 3.4** and **Table 3.2**.
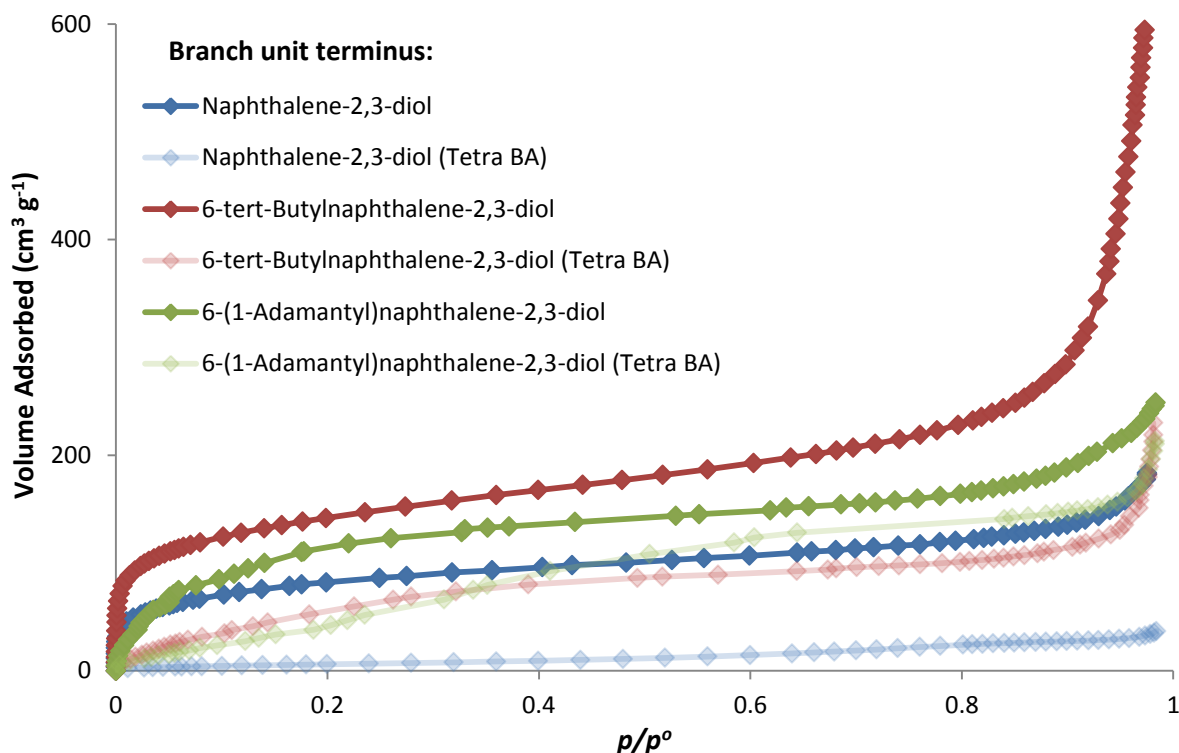
Figure 3.4 BET nitrogen adsorption plots for the three tri-[naphthalene-2,3-diol]-9,10-diethyltriptycene dendrimers (bold) and the corresponding tetra-[naphthalene-2,3-diol] biphenyl adducts (Tetra BA) (faint). Desorption plots removed for clarity.

Branch unit terminus	BET surface area ($m^2 g^{-1}$) [Tetra biphenyl adduct]	Total pore volume ($cm^3 g^{-1}$) [Tetra biphenyl adduct]
Naphthalene-2,3-diol	300 [25]	0.33 [0.05]
6-*tert*-Butylnaphthalene-2,3-diol	665 [260]	0.58 [0.33]
6-(1-Adamantyl)-naphthalene-2,3-diol	461 [132]	0.38 [0.25]

Table 3.2 BET nitrogen sorption data for the tri-[naphthalene-2,3-diol]-9,10-diethyltriptycene dendrimers and corresponding tetra-[naphthalene-2,3-diol] biphenyl adducts in square brackets.

Analysis of the data reveals a similar trend in porosity for the naphthalane-2,3-diol based dendrimers as was seen for the naphthalene-2,3-diol based biphenyl adducts: the addition of bulky *tert*-butyl groups improves the surface area, but addition of even bulkier adamantyl groups improves the surface area less (**Table 3.2**). This distinction may be due to the difference in sorption kinetics, rather than intrinsic porosity, as the isotherms in **Figure 3.7** clearly show good sorption kinetics for the *tert*-butyl substituted dendrimer and poor sorption kinetics for the adamantyl substituted dendrimer. This suggests that the bulkier

and less mobile adamantyl groups restrict the accessibility of the pores to probe gas molecules, resulting in possible underestimation of apparent surface area.

3.5 Triptycene-2,3-diol based DIMs

Prior to this work, the unsubstituted triptycene-2,3-diol based dendrimer ***DIM-1*** (R_1, R_2 = H, **Scheme 3.12**) was synthesised from the tri-[triptycene-2,3-diol] biphenyl branch unit (R_1, R_2 = H, **Scheme 3.11**) by Dr. Jonathan Walker and found to possess an apparent BET surface area of 600 m^2 g^{-1}. Given the impressive surface areas obtained for substituted triptycene-2,3-diol based OMIMs in Chapter 2.3.3.3 and the smaller substituted DIMs thus far, it seemed probable that substituted triptycene-2,3-diol based DIMs may lead to highly porous discrete molecules. Accordingly, a series of tri-[triptycene-2,3-diol] biphenyl branch units were prepared (**Scheme 3.11**).
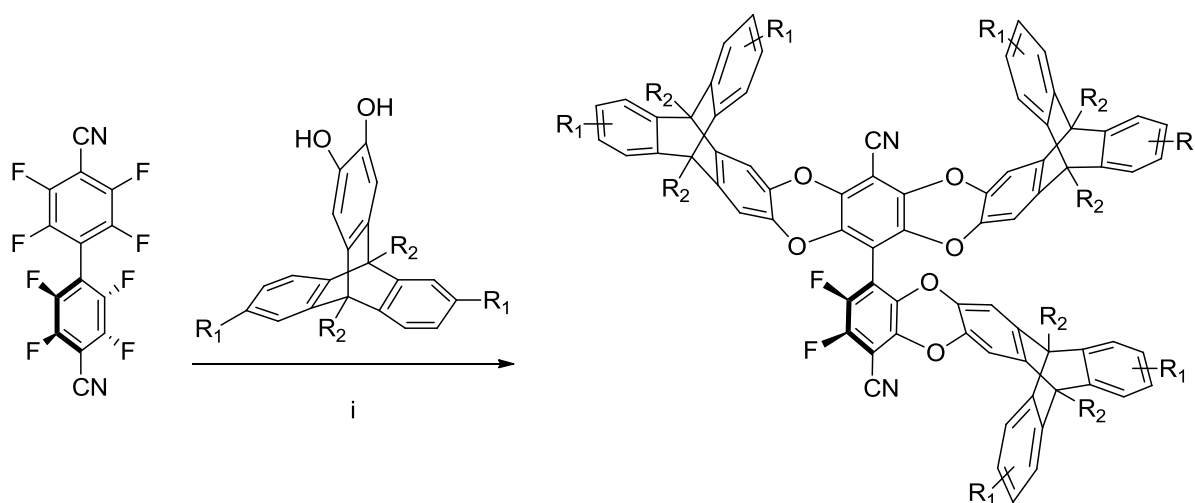
Scheme 3.11 Synthesis of tri-[triptycene-2,3-diol] biphenyl adducts.
R_1 = H, ^{t}Bu, R_2 = H, Me.
Reagents and conditions: i) K_2CO_3, DMF, 65 °C, 72 hrs.

Each tri-substituted adduct was synthesised by reacting octafluoro with three equivalents of a selected triptycene-2,3-diol, syntheses of which were described previously in Chapter 2.3.3.2, in analogous reaction conditions to those used previously. The crude reaction mixtures were purified *via* column chromatography and once isolated, each branch unit was characterised by ^{1}H, ^{13}C and ^{19}F NMR combined with MALDI-MS and GPC. Given the

somewhat large and awkward structure of the branch units, it was decided to analyse each *via* BET nitrogen sorption (prior to reaction with a core) to ascertain whether or not they were porous and if so, how their porosity compares with the tetra substituted biphenyl analogues. BET nitrogen sorption data is shown below in **Figure 3.5** and **Table 3.3**.
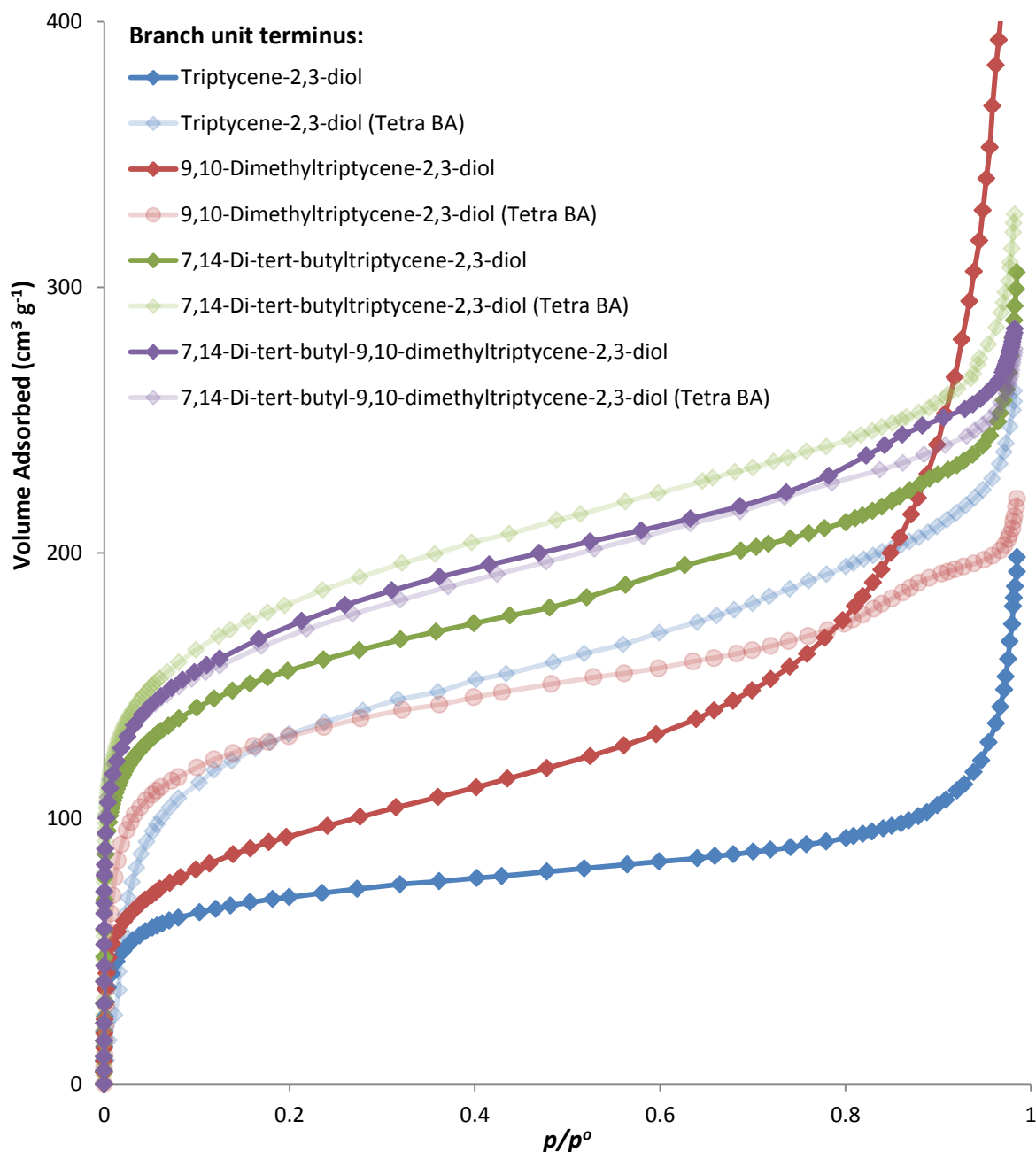
Figure 3.5 BET nitrogen adsorption isotherms for the four tri-[triptycene-2,3-diol] biphenyl adducts (bold) and the corresponding tetra-[triptycene-2,3-diol] biphenyl adducts (Tetra BA) (faint). Desorption plots removed for clarity.

Tri-[triptycene-2,3-diol] adduct	BET surface area ($m^2\,g^{-1}$) [Tetra biphenyl adduct]	Total pore volume ($cm^3\,g^{-1}$) [Tetra biphenyl adduct]
R_1 = H, R_2 = H	248 [485][a]	0.28 [0.40][a]
R_1 = H, R_2 = Me	337 [462]	0.75 [0.33]
R_1 = ^{t}Bu, R_2 = H	551 [654]	0.44 [0.54]
R_1 = ^{t}Bu, R_2 = Me	616 [599]	0.44 [0.42]

Table 3.3 BET nitrogen sorption data for the four tri-[triptycene-2,3-diol] biphenyl adducts and the corresponding tetra-[triptycene-2,3-diol] biphenyl adducts in square brackets.
a) Data supplied by Dr. Grazia Bezzu.

The results clearly demonstrate that even when not fully substituted, tri-[triptycene-2,3-diol] biphenyl adducts give rise to porous materials and in one case (R_1 = ^{t}Bu, R_2 = Me) gave rise to a material that is more porous than the fully (tetra) substituted adduct (**Table 3.3**). Little explanation can be offered for this seemingly anomalous result, other than that such a particular combination of substituents favours a more open structure, which can be more readily realised around a partially substituted core than around a more *crowded* fully substituted core. Alternatively, the difference in apparent surface area (17 $m^2\,g^{-1}$) could be accounted for by the degree of error in BET analysis. Each of the four triptycene-2,3-diol branch units was then reacted with freshly prepared 9,10-diethyltriptycene-2,3,6,7,13,14-hexaol in just over three to one stoichiometry to produce the corresponding dendrimers (**Scheme 3.12**).
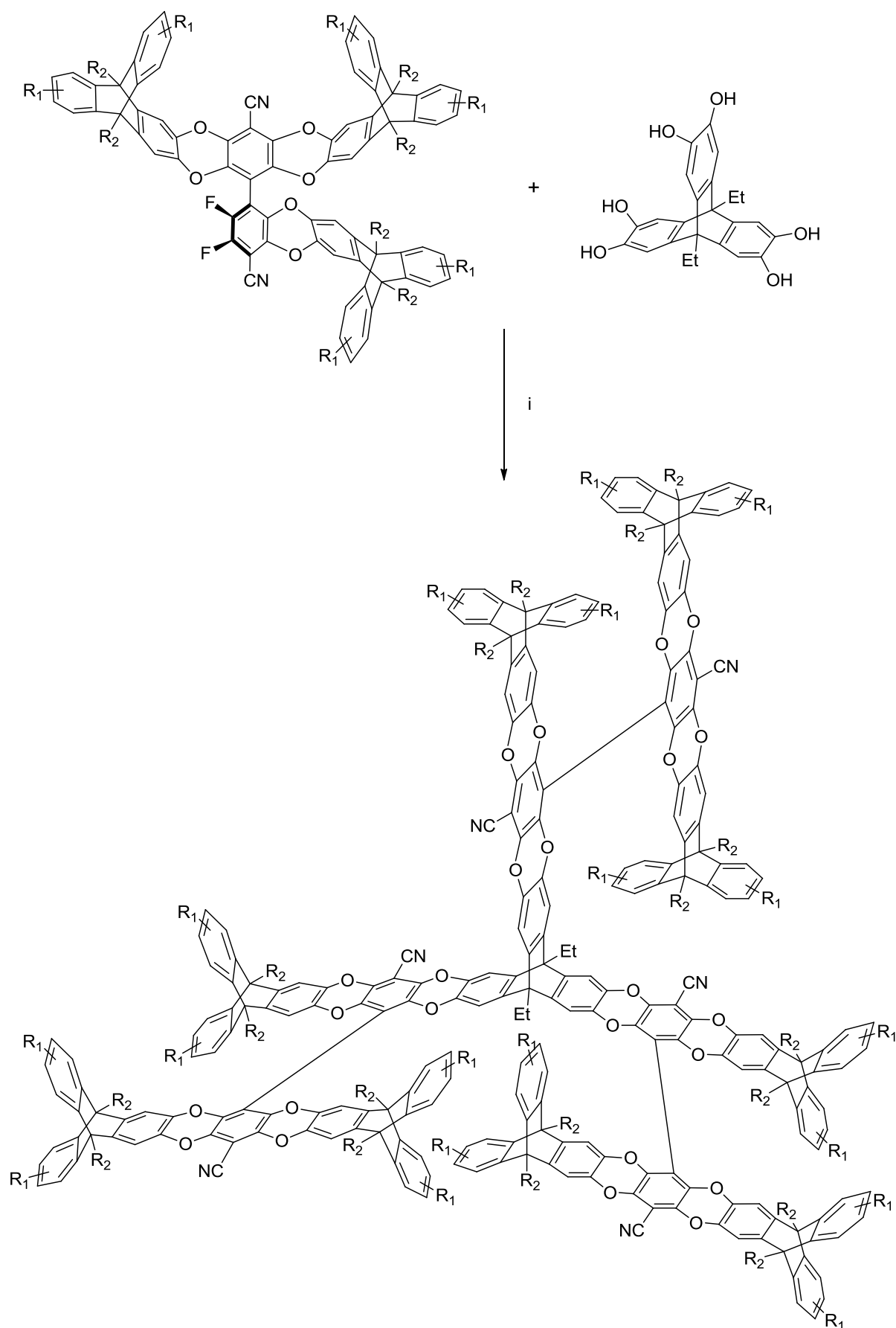
Scheme 3.12 Synthesis of tri-[triptycene-2,3-diol]-9,10-diethyltriptycene dendrimers.
$R_1 = H, {}^tBu$ $R_2 = H, Me.$
Reagents and conditions: i) K_2CO_3, DMF, 65 °C, 72 hrs.

As with all of the previously produced soluble DIMs, column chromatography was required to remove excess branch unit added to the reaction to ensure complete substitution of the core. Once isolated, as mixtures of regioisomers, the dendrimers were characterised by ^{1}H NMR, ^{13}C NMR, MALDI-MS and GPC, all of which confirmed complete substitution of the core and purity. BET nitrogen adsorption isotherms and corresponding data for the four triptycene-2,3-diol based dendrimers are shown below in **Figure 3.6** and **Table 3.4**.

Branch unit terminus:

- Triptycene-2,3-diol
- Triptycene-2,3-diol (Tetra BA)
- 9,10-Dimethyltriptycene-2,3-diol
- 9,10-Dimethyltriptycene-2,3-diol (Tetra BA)
- 7,14-Di-tert-butyltriptycene-2,3-diol
- 7,14-Di-tert-butyltriptycene-2,3-diol (Tetra BA)
- 7,14-Di-tert-butyl-9,10-dimethyltriptycene-2,3-diol
- 7,14-Di-tert-butyl-9,10-dimethyltriptycene-2,3-diol (Tetra BA)
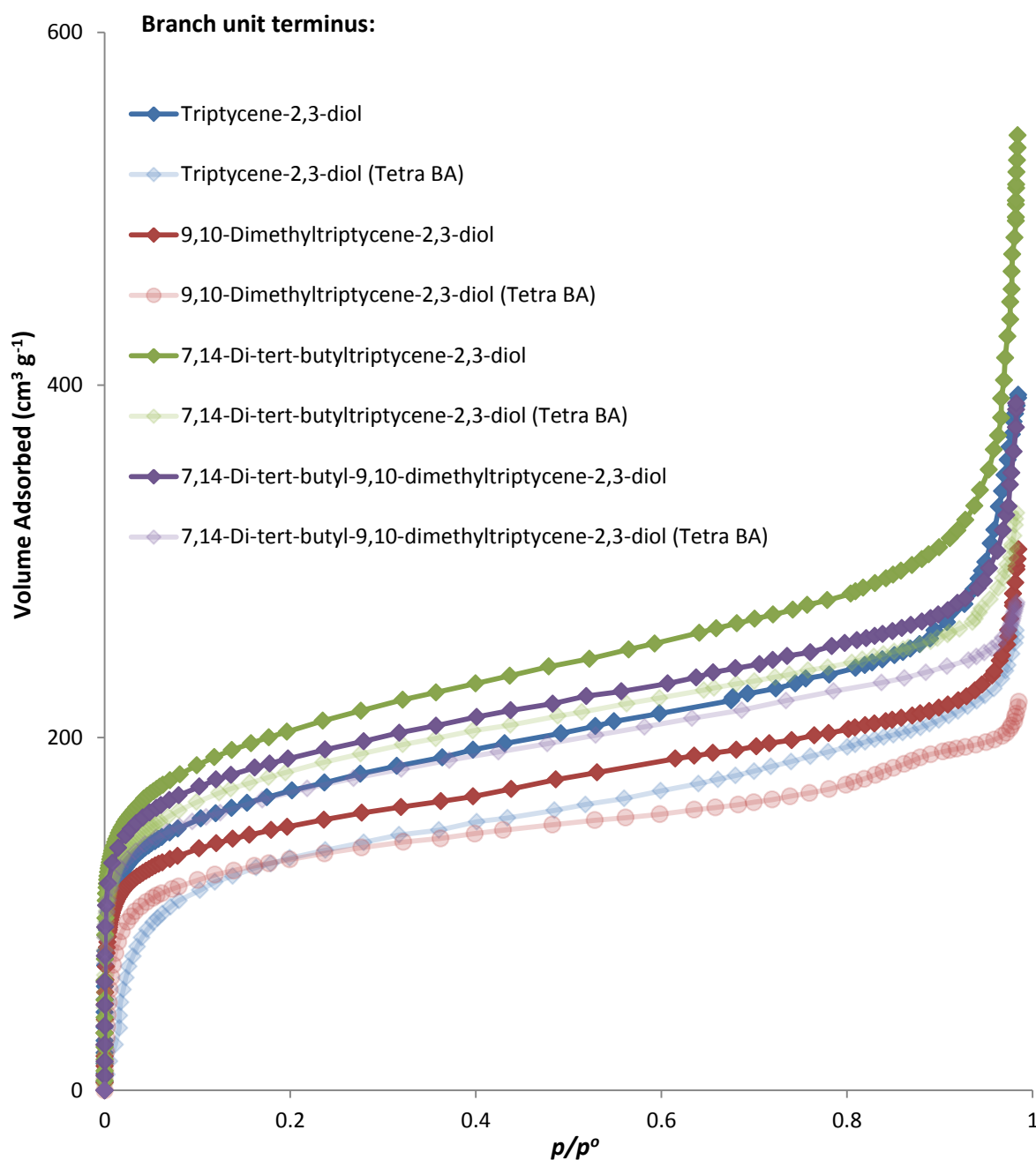
Figure 3.6 BET nitrogen adsorption isotherms for the four tri-[triptycene-2,3-diol]-9,10-diethyltriptycene dendrimers (bold) and the corresponding tetra-[triptycene-2,3-diol] biphenyl adducts (Tetra BA) (faint). Desorption plots removed for clarity.

Branch unit terminus	BET surface area (m^2 g^{-1}) [Tetra biphenyl adduct]	Total pore volume (cm^3 g^{-1}) [Tetra biphenyl adduct]
R$_1$ = H, R$_2$ = H	600^a [485]	0.59^a [0.40]
R$_1$ = H, R$_2$ = Me	528 [462]	0.45 [0.33]
R$_1$ = ^{t}Bu, R$_2$ = H	722 [654]	0.76 [0.54]
R$_1$ = ^{t}Bu, R$_2$ = Me	663 [599]	0.58 [0.42]

Table 3.4 BET nitrogen sorption data for the four tri-[triptycene-2,3-diol]-9,10-diethyltriptycene dendrimers and the corresponding tetra biphenyl adducts in square brackets.
a) Data supplied by Dr. Jonathan Walker.

The results in **Table 3.4** show universal improvement in surface area and total pore volumes for the DIMs in comparison with their corresponding tetra biphenyl adducts. The improvement is almost uniform for the three substituted triptycene-2,3-diols (ranging from 64 – 68 m^2 g^{-1}), however the improvement is much more (115 m^2 g^{-1}) for the unsubstituted (R$_1$, R$_2$ = H) triptycene-2,3-diol. This effect is likely due to the slow sorption kinetics associated with the unsubstituted tetra biphenyl adduct (**OMIM-1**) giving rise to an underestimation of surface area, which in turn gives rise to a larger improvement for the corresponding DIM (**DIM-1**). The results also show the same trend in surface area for each series (tetra biphenyl adducts and DIMs) with the R$_1$ = H, R$_2$ = Me substituted compounds both having the lowest surface area of their series, followed by the unsubstituted compounds (R$_1$, R$_2$ = H), then the highly substituted compounds (R$_1$ = ^{t}Bu, R$_2$ = Me) and finally the *tert*-butyl (R$_1$ = ^{t}Bu, R$_2$ = H) substituted compounds possessing the highest surface areas. The same trend was also seen with the penta-[triptycene-2.3-diol] terphenyl adducts discussed in Chapter 2.4.3, supporting the general observation that: *substitution at the R$_1$ position enhances surface area, whereas substitution at the R$_2$ position diminishes surface area*.

Unfortunately, an improved highest surface area for discrete molecules of this nature was not obtained in this series of triptycene-2,3-diol based DIMs, as the highest of this series (R$_1$ = ^{t}Bu, R$_2$ = H, BET surface area 722 m^2 g^{-1}) was just lower than that obtained for the penta-[7,14-di-*tert*-butyltriptycene-2,3-diol] terphenyl adduct (BET surface area 726 m^2 g^{-1}) discussed in Chapter 2.4.3. Though, such a difference in surface area is likely to be within

the experimental error for the measurement of such samples. However, given the encouraging results obtained for cy6-triptycene-2,3-diol based OMIMs in Chapters 2.3.3.3 and 2.4.3, it was decided to investigate the synthesis of the corresponding DIMs. As such, two branch units were prepared by reaction of three equivalents of each cy6-triptycene-2,3-diol (syntheses reported in Chapter 2.3.3.2) with octafluoro (**Scheme 3.13**).
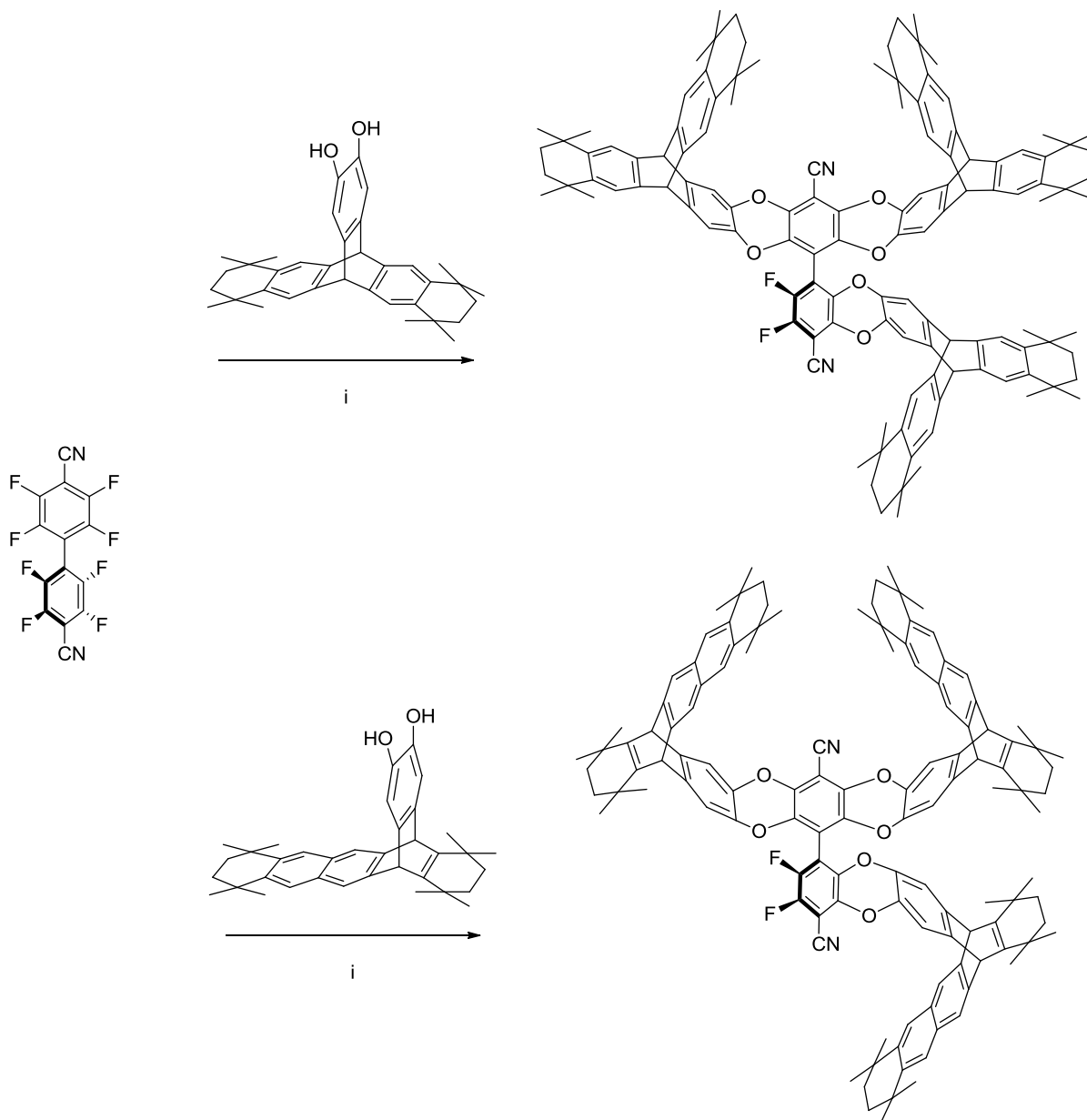
Scheme 3.13 Synthesis of the tri-[cy6-triptycene-2,3-diol] (upper) and tri-[ucy6-triptycene-2,3-diol] (lower, representation of one possible regioisomer) biphenyl adducts.
Reagents and conditions: i) K$_2$CO$_3$, DMF, 65 °C, 72 hrs.

Each branch unit was isolated following column chromatography of the crude reaction mixture to give the pure tri-[cy6-triptycene-2,3-diol] biphenyl adducts, which were subsequently characterised by ^{1}H, ^{13}C and ^{19}F NMR combined with MALDI-MS and GPC. As with the previous set of tri-[triptycene-2,3-diol] biphenyl adducts, BET nitrogen sorption studies were carried out on the branch units prior to reaction with a core. The resultant isotherms and relevant data are shown below in **Figure 3.7** and **Table 3.5**.
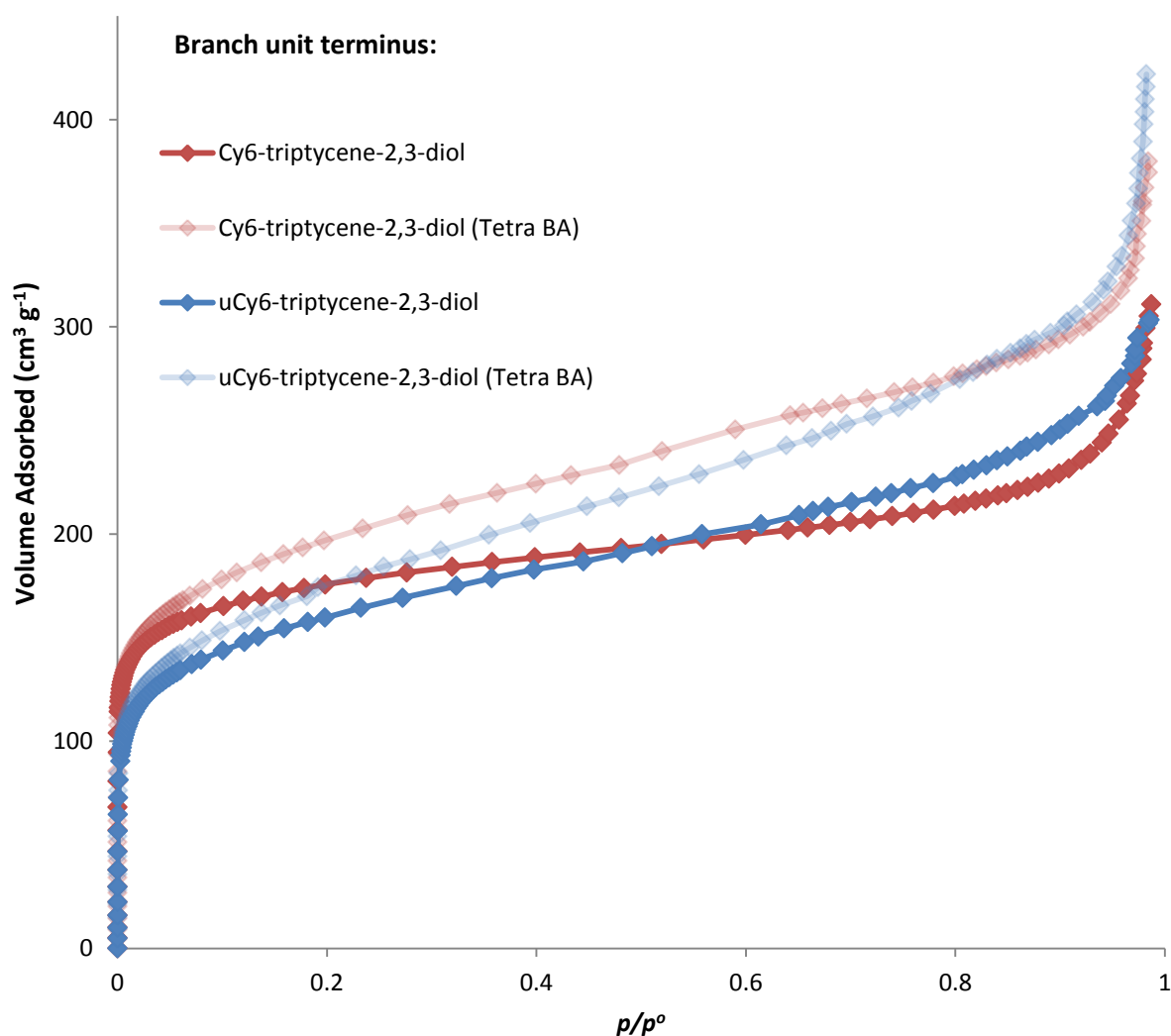
Figure 3.7 BET nitrogen adsorption isotherms for two tri-[cy6-triptycene-2,3-diol] biphenyl adducts (bold) and the corresponding tetra-[cy6-triptycene-2,3-diol] biphenyl adducts (Tetra BA) (faint). Desorption plots removed for clarity.

Tri-[cy6-triptycene-2,3-diol] adduct	BET surface area (m² g⁻¹) [Tetra biphenyl adduct]	Total pore volume (cm³ g⁻¹) [Tetra biphenyl adduct]
Symmetrical	612 [702]	0.46 [0.50]
Unsymmetrical	566 [622]	0.46 [0.64]

Table 3.5 BET nitrogen sorption data for the two tri-[cy6-triptycene-2,3-diol] biphenyl adducts and the corresponding tetra-[cy6-triptycene-2,3-diol] biphenyl adducts in square brackets.

As was observed for the majority of the previous tri-[triptycene-2,3-diol] biphenyl adducts (**Table 3.3**), both of the tri-[cy6-triptycene-2,3-diol] biphenyl adducts possess lower surface areas (and total pore volumes) than their tetra substituted counterparts, suggesting that addition of a fourth terminus to an biphenyl core is generally beneficial to the porosity of the material.

Both tri-[cy6-triptycene-2,3-diol] biphenyl adducts were then reacted with freshly prepared 9,10-diethyltriptycene-2,3,6,7,13,14-hexaol in efforts to isolate the corresponding dendrimers (**Schemes 3.14** and **3.15**).
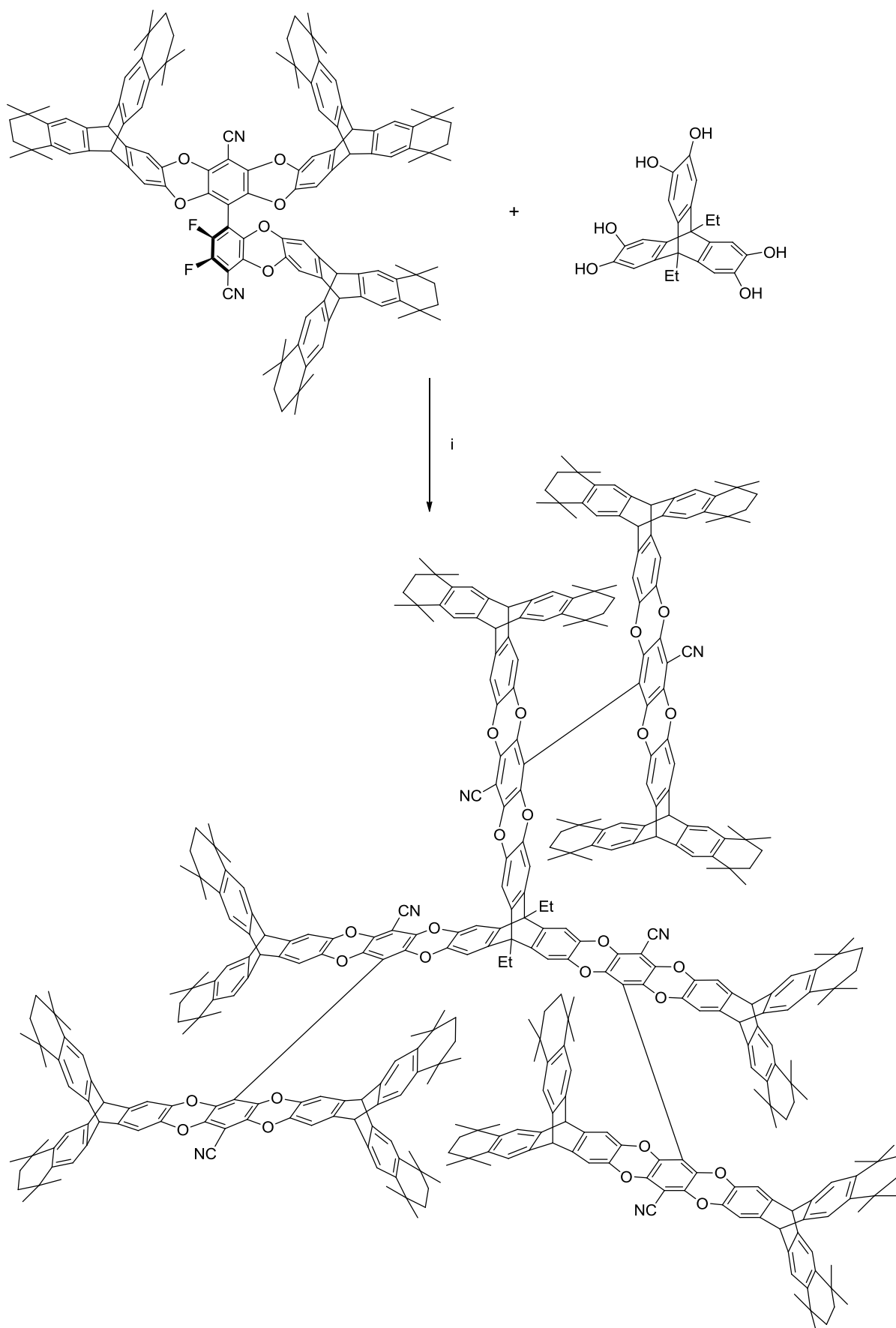
Scheme 3.14 Attempted **s**ynthesis of the tri-[cy6-triptycene-2,3-diol]-9,10-diethyltriptycene dendrimer.
Reagents and conditions: i) K$_2$CO$_3$, DMF, 65 °C, 72 hrs.

Unfortunately, when attempting to synthesise the tri-[cy6-triptycene-2,3-diol]-9,10-diethyltriptycene dendrimer under the typical reaction conditions employed throughout this thesis, it was found that the reaction did not proceed as efficiently as it had previously. TLC analysis showed little consumption of the tri-[cy6-triptycene-2,3-diol] branch unit after 72 hours at 65 °C, so it was decided to quench the reaction and recover the branch unit *via* column chromatography. Of the 213 mg used in the reaction, 94 % (200 mg) was recovered, indicating just how little reaction had occurred. GPC and MALDI-MS analysis of the remaining material showed evidence for dendrimer formation (**Figures 3.11** and **3.12**), but insufficient quantity of material meant that no further purification or characterisation was established.

Peak RV - (ml)	19.700	20.433
Mn - (Daltons)	3,193	1,441
Mw - (Daltons)	3,329	1,498
Mz - (Daltons)	3,491	1,547
Mp - (Daltons)	3,108	1,541
Mw / Mn	1.042	1.040
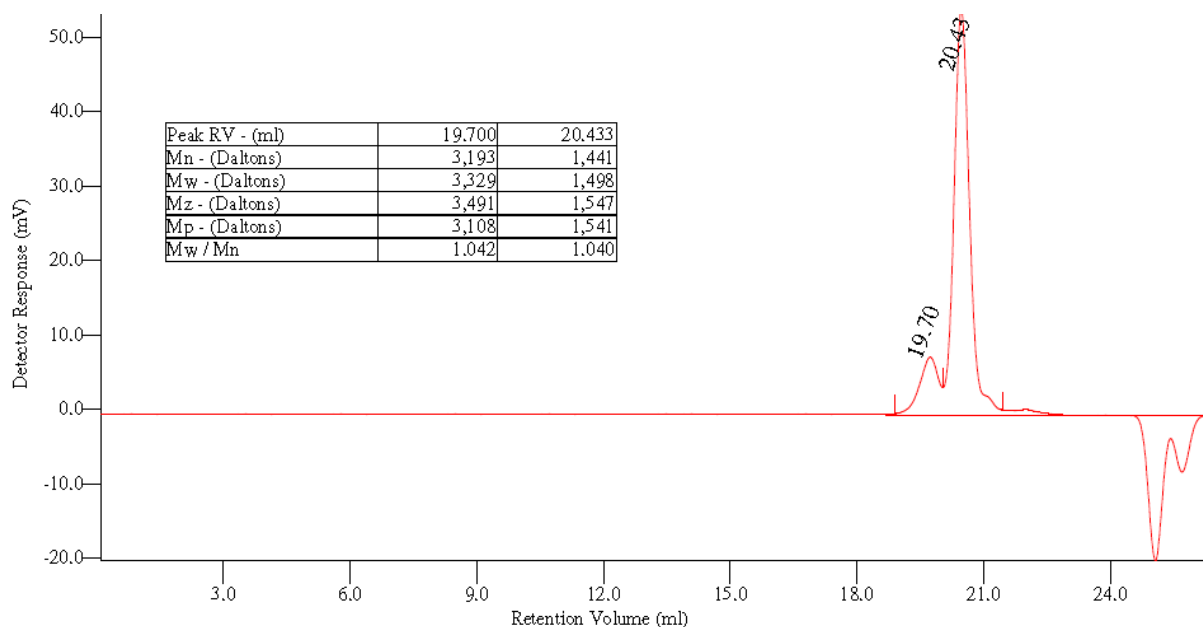
Figure 3.11 GPC trace and relevant data (inset) for the crude reaction products obtained from the attempted synthesis of the tri-[cy6-triptycene-2,3-diol]-9,10-diethyltriptycene DIM, showing DIM formation (left-hand peak) and residual branch unit (right-hand peak).
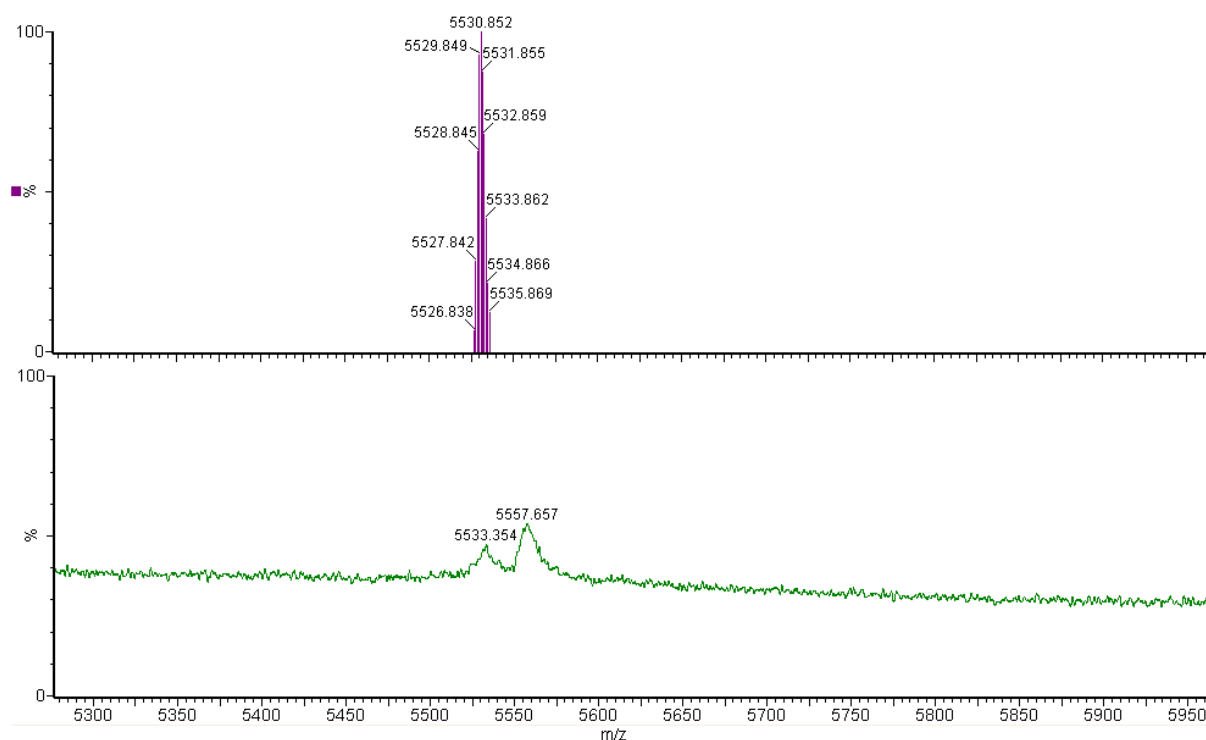
Figure 3.12 Expected isotope model (top) and MALDI mass spectrum (bottom) of the crude reaction products in the attempted synthesis of the tri-[cy6-triptycene-2,3-diol]-9,10-diethyltriptycene DIM, showing M$^+$ and [MNa]$^+$ peaks. Peaks are above the standard PEG 1000-3000 calibration range and so are slightly shifted.

Attempts were made to repeat the reaction using slightly modified reaction conditions (**Table 3.6**), but all were unsuccessful at producing any more than trace quantities of the desired dendrimer. It is possible that the highly reactive nature of the core combined with the sheer bulkiness of the branch unit, results in a statistical improbability that the branch unit will approach the core with the correct orientation to facilitate reaction before the core degrades. Given the complex, multi-step synthesis required to obtain the branch unit it was decided not to pursue the synthesis of the corresponding dendrimer any further.

Reaction Time (hours)	Temperature (°C)	K_2CO_3 (equivalents to branch unit)	Quantity of dendrimer produced	Branch unit recovered (%)
72	65	2.67	trace	94
72	90	2.67	trace	88
72	90	2	trace	85
72	90	0	0	98

Table 3.6 Reaction conditions and outcomes for the attempted syntheses of the tri-[cy6-triptycene-2,3-diol]-9,10-diethyltriptycene dendrimer.
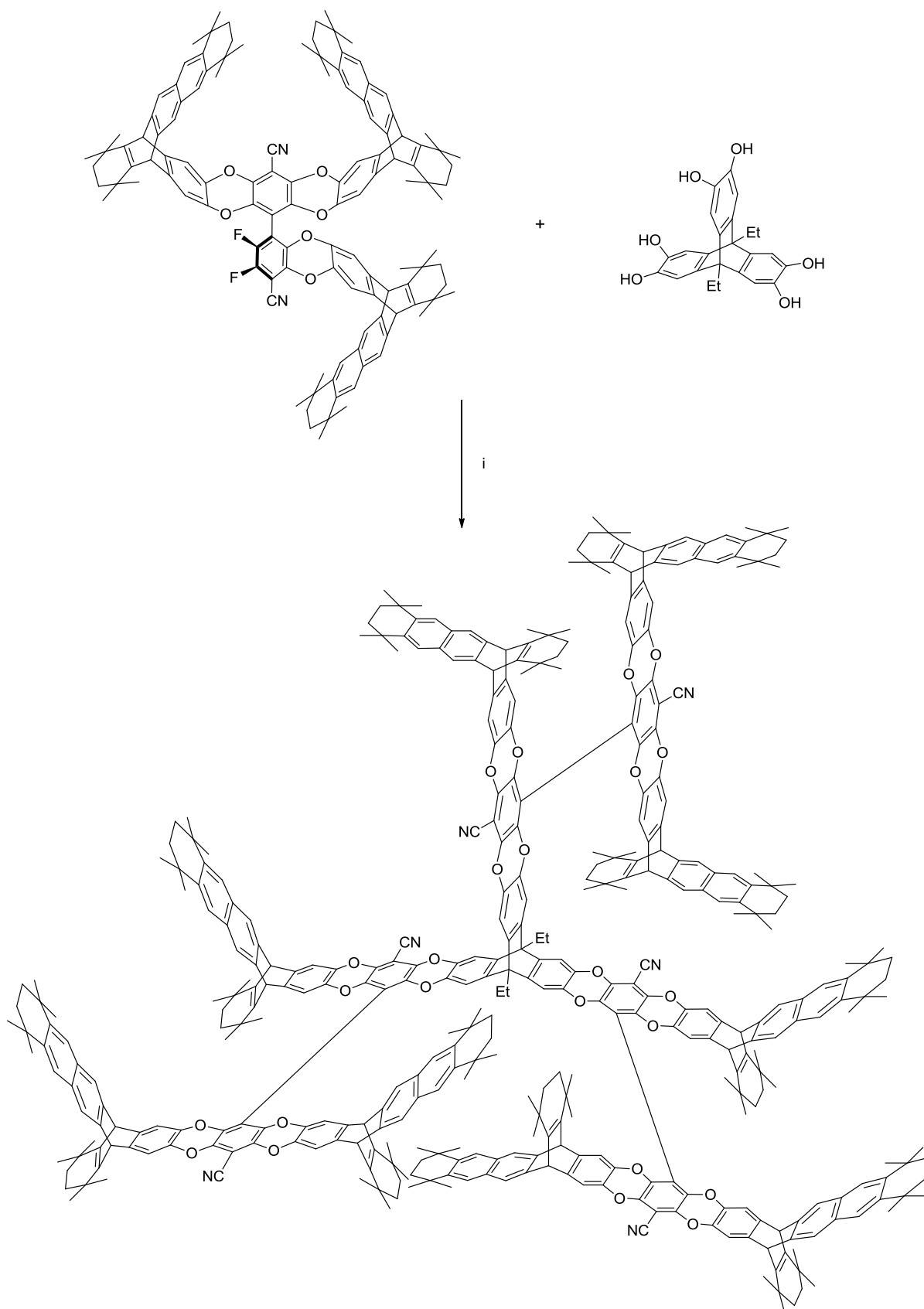
Scheme 3.15 Attempted synthesis of the tri-[ucy6-triptycene-2,3-diol]-9,10-diethyltriptycene dendrimer (structure shown is one possible regioisomer).
Reagents and conditions: i) K$_2$CO$_3$, DMF, 90 °C, 72 hrs.

Similar attempts were made to produce the dendrimer resulting from reaction of the tri-[ucy6-triptycene-2,3-diol] biphenyl adduct with freshly prepared 9,10-diethyltriptycene-2,3,6,7,13,14-hexaol (**Scheme 3.12**), however they proved equally unsuccessful, yielding only trace amounts of the desired dendrimer (observed by TLC, GPC and MALDI-MS). Again, given the complex synthesis required to obtain more branch unit, it was decided to not pursue the synthesis of this dendrimer further.

3.6 Summary and conclusions (DIMs)

A total of eleven novel branch units, in the form of tri-substituted biphenyls, were prepared and fully characterised by typical techniques. Five of these branch units were found to be microporous, with apparent BET surface areas ranging from 248 – 616 m^2 g^{-1} despite incomplete substitution. Nine branch units were successfully reacted with the 9,10-diethyltriptycene-2,3,6,7,13,14-hexaol core to generate microporous dendrimers with apparent BET surface areas ranging from 300 – 722 m^2 g^{-1}. Despite multiple attempts, the two remaining branch units were found to be incompatible with the reaction conditions employed to generate dendrimers in this research.

Universal improvement in apparent BET surface area was observed for all DIMs in comparison to their tri/tetra substituted biphenyl and penta substituted terphenyl adducts. This effect was most observable for small unsubstituted termini (catechol, naphthalene-2,3-diol), which generated dendrimers with apparent BET surface areas of 300 – 330 m^2 g^{-1}, compared with surface areas under 30 m^2 g^{-1} for all four corresponding OMIMs (biphenyl and terphenyl cores). This again advocates the use of triptycene in microporous materials, as it is clearly inducing porosity in an otherwise non-porous combination of precursors. Good improvement between OMIM and DIM apparent BET surface areas was also seen for substituted catechol and naphthalene-2,3-diols, although slow sorption kinetics remained an issue in the 6(1-adamantyl)naphthalene-2,3-diol DIM.

DIMs containing triptycene-2,3-diol based termini gave rise to some of the most microporous materials of this nature, possessing apparent BET surface areas ranging from 528 – 722 m^2 g^{-1}. The structure property relationships observed for OMIMs containing

triptycene-2,3-diol based termini in Chapter 2 were again observed: substitution of bridgehead protons with a methyl groups decreases the apparent BET surface area, whilst substitution with *tert*-butyl groups at the extremities leads to an increase in apparent BET surface area.

4. Sulfur-based Ladder Polymers of Intrinsic Microporosity

4.1 Background

Ladder *Polymers of Intrinsic Microporosity* (*PIMs*)[137] are typically produced through the reaction of tetra-hydroxy (bis-catechol) and tetra-halogenated (fluoro or chloro) monomers, to give long polymer chains linked by dibenzodioxin units (**Scheme 4.1**) (**Chapter 1.6.1**).
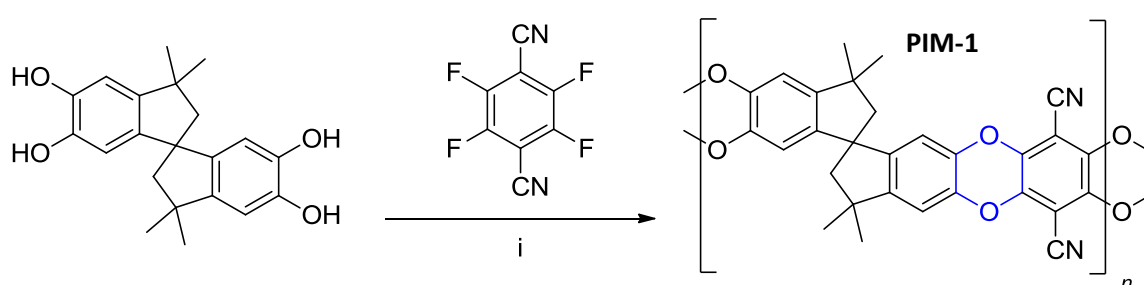
Scheme 4.1 Synthesis of the ladder *PIM-1* showing dibenzodioxane unit in blue.
Reagents and conditions: i) K$_2$CO$_3$, DMF, 65 °C, 3 days.

Whilst this structure leads to excellent porosity and gas separation properties,[15,172,173] it offers little scope for post-polymerisation modifications other than those involving the nitrile groups,[174-176] a trait that is often exploited in the synthesis of functional polymeric materials.[177,178] By utilising a tetra-thiol functionalised monomer, in the place of a tetra-hydroxy monomer, one can envisage the formation of *thianthrene* units along the polymer backbone (**Scheme 4.2**). These units may offer subtle changes to the polymer's properties due to their non-planar nature[179] and the increased polarisability of sulfur compared to oxygen. However, a more distinct difference is the fact that the thianthrene units could undergo post-polymerisation oxidation, to sulfones or sulfoxides (**Scheme 4.2**). These groups have shown to possess excellent gas separation properties when included in functional polymeric materials.[180,181]
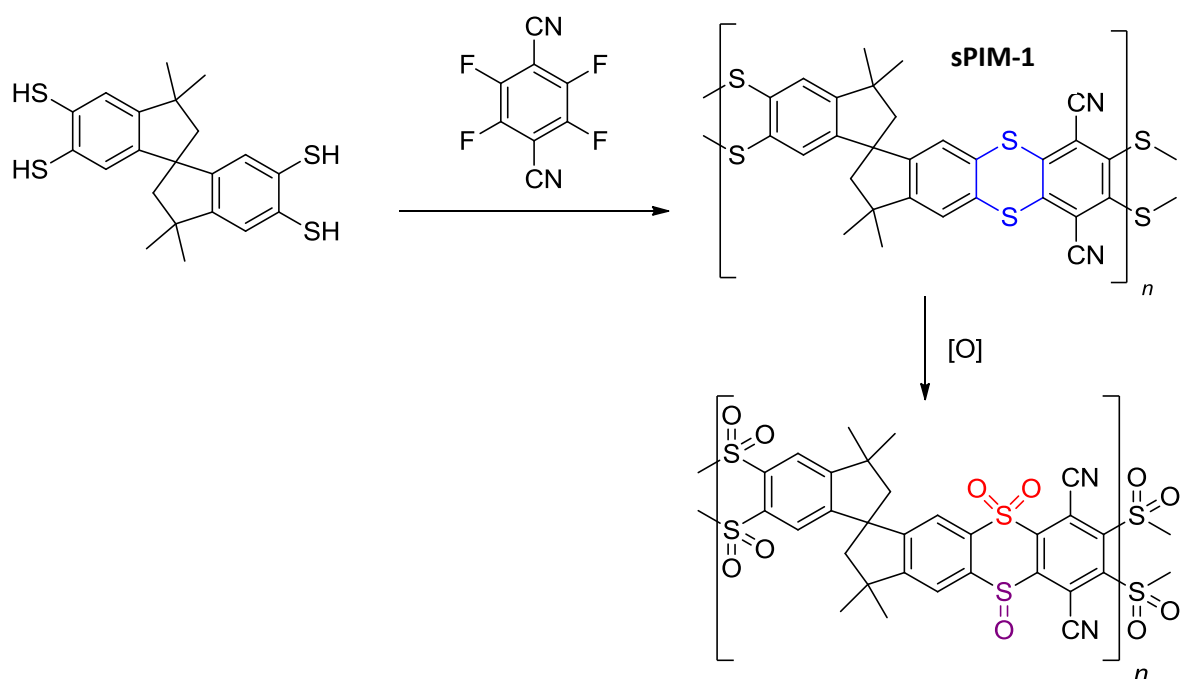
Scheme 4.2 Proposed synthesis of a sulfur analogue of PIM-1 (*sPIM-1*) showing thianthrene unit in blue, sulfone in red and sulfoxide in purple.

Du *et al.* have shown how sulfone containing PIMs can be synthesised by appending one[182] or two[183] sulfone containing groups to the halogenated monomer (**Scheme 4.3**). Both monomers were successfully incorporated into free-standing co-polymer membranes, consisting of various ratios of sulfonated to non-sulfonated monomers. It was found that the more sulfonated membranes showed increased selectivity for O_2/N_2 and CO_2/N_2 compared with the standard PIM-1.[182,183] However, a decrease in permeability was also noted and attributed to the space filling properties of the large sulfone containing side groups.
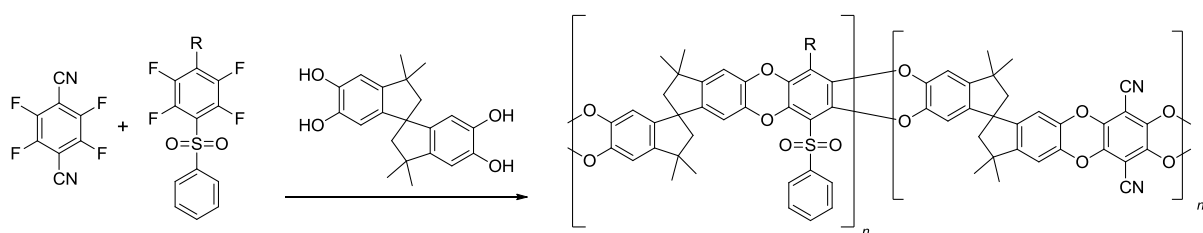
Scheme 4.3 Literature examples of sulfone containing co-PIMs.
R = CF_3, SO_2Et, SO_2Ph, SO_2Ph-*p*-OMe.

A more recent example of a sulfone containing PIM monomer was reported[184] in which the sulfone groups are formed by oxidation of thianthrene units within the backbone of the monomer (**Scheme 4.4**), presumably to try and limit their space filling effects. Again, good

selectivity for common gas pairs was observed, but a reduction in permeability was still apparent compared with PIM-1. This was attributed to the increased distance between spirocentres in the polymer chain, due to the increased size of the sulfone incorporating monomer, allowing for increased packing efficiency.
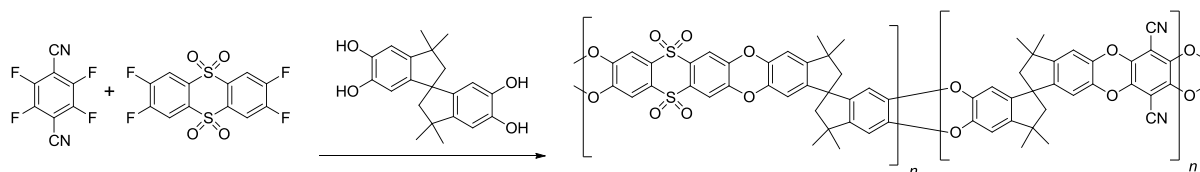
Scheme 4.4 Literature example of a sulfone containing PIM formed by pre-polymerisation oxidation of a thianthrene containing monomer.

At present, all known literature examples of sulfone containing PIMs[182-184] are produced from sulfone containing monomers, which are known to present polymerisation issues in cross-linking[184] due to the increased monomer activation. Furthermore, it has been noted that homo-polymers produced from a sulfone-containing fluorinated monomer and a catechol based monomer, are poorly soluble in common solvents.[184] By utilising dithiol containing monomers it is hypothesised that these issues can be avoided to aid the formation of highly soluble, thianthrene containing, ladder PIMs. Solution cast membranes of which could subsequently undergo post-polymerisation oxidation to produce sulfone containing PIMs that benefit from the enhanced selectivity associated with sulfone groups, without compromising the highly permeability associated with the PIM-1 structure.

This chapter will focus on the synthesis of thiol containing PIM monomers and their polymerisation into sulfur-based ladder PIMs (sPIMs).

4.2 Attempted syntheses of the sPIM-1 monomer – TTSBI

4.2.1 From THSBI

As shown in **Scheme 4.2**, the direct sulfur analogue of PIM-1 (*sPIM-1*), could be realised by the reaction of 5,5',6,6'-tetrathiol-3,3,3',3'-tetramethyl-1,1'-spirobisindane (TTSBI) with tetrafluoroterephthalonitrile (TFTPN), consequently the synthesis of TTSBI was investigated. Given that the catechol based PIM-1 monomer (5,5',6,6'-tetrahydroxy-3,3,3',3'-tetramethyl-1,1'-spirobisindane, THSBI) is commercially available, investigations were made into the conversion of THSBI to TTSBI (**Scheme 4.5**).
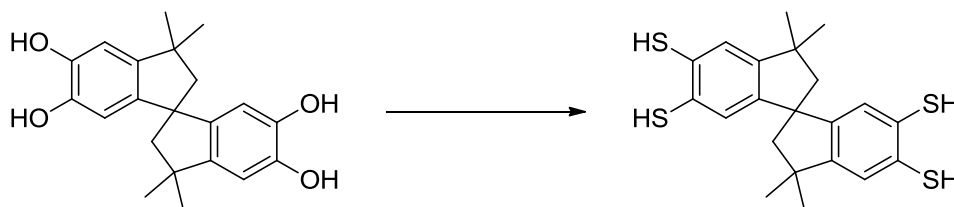
Scheme 4.5 Proposed conversion of THSBI to TTSBI.

The Newman-Kwart Rearrangement[185,186] offers a route for the transformation of phenols to thiophenols *via* an *O*-thiocarbamate, which, when subjected to high temperatures (> 200 °C) undergoes a thermal rearrangement to form the *S*-thiocarbamate that can subsequently be hydrolysed to yield the thiophenol (**Scheme 4.6**).
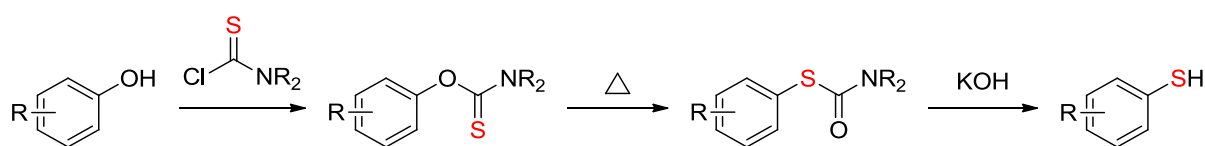
Scheme 4.6 Typical procedure for the conversion of a phenol to thiophenol utilising the Newman-Kwart Rearrangement. Sulfur atom shown in red for clarity.

Accordingly, THSBI was reacted with *N,N*-dimethylcarbamyl chloride to yield the corresponding tetra-*O*-thiocarbamate (**Scheme 4.7**). The isolated material was characterised by ^{1}H NMR, ^{13}C NMR, high resolution MS and X-ray crystallography, all of which confirmed the purity of the material.
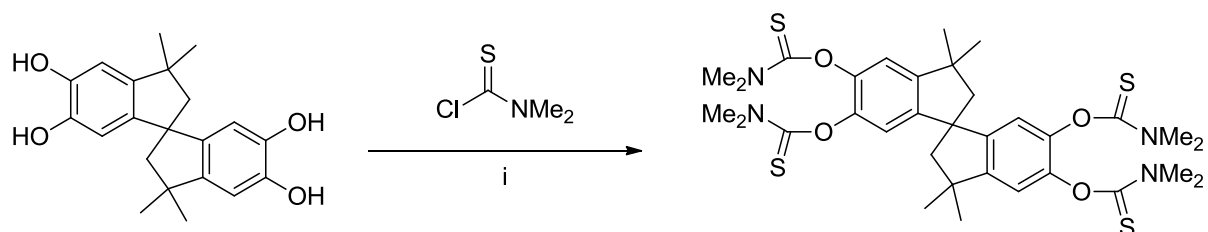
Scheme 4.7 Synthesis of the tetra-*O*-thiocarbamate from THSBI.
Reagents and conditions: i) KOH, MeOH, Reflux, 24 hrs.

Unfortunately, all attempts at converting the obtained tetra-*O*-thiocarbamate to the tetra-*S*-thiocarbamate (**Scheme 4.8**) were unsuccessful. A summary of the various attempts is given in **Table 4.1**.
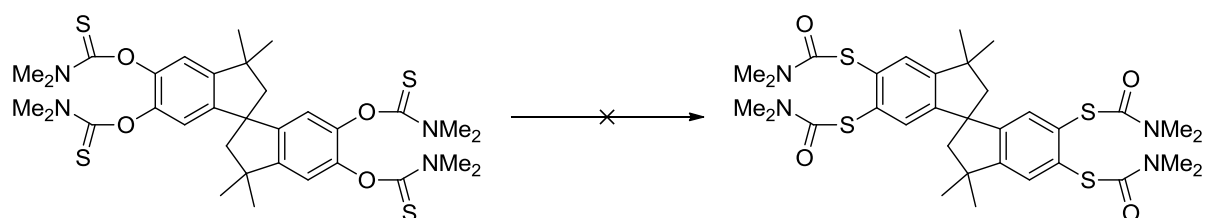
Scheme 4.8 Failed conversion of the tetra-*O*-thiocarbamate to the tetra-*S*-thiocarbamate.

Solvent	Concentration (mmol cm⁻³)	Reaction temp. (°C)	Reaction time (hours)	Heating method	Outcome	Isolated yield (%)
Ph_2O	3.1	260	3	Heating mantle	Total decomposition	0
Ph_2O	1.8	260	6	Heating mantle	Total decomposition	0
Ph_2O	1.8	205	12	Oil bath	Total decomposition	0
Ph_2O	0.6	205	12	Oil bath	Total decomposition	0
Ph_2O	0.5	260	12	Heating mantle	Total decomposition	0
Ph_2O	0.4	260	12	Heating mantle	Total decomposition	0
Ph_2O	0.8	260	0.5	Microwave	Total decomposition	0
Ph_2O	0.4	260	1	Microwave	Partially rearranged product and decomposition	0
Ph_2O	0.6	170	24	Oil bath	Trace amounts of partially rearranged product	0
Ph_2O	0.2	260	24	Heating mantle	Mixture of starting material, partially rearranged product and decomposition products	0
DCB	0.3	180	24	Oil bath	Mixture of starting material, partially rearranged product and decomposition products	0
Toluene	0.1	110	24	Oil bath	No reaction	0
Toluene[a]	0.1	110	24	Oil bath	Very little reaction	0
Ph_2O[a]	0.1	260	12	Heating mantle	Mixture of starting material, partially rearranged product and decomposition products	0

Table 4.1 Summary of attempted conversions of the tetra-*O*-thiocarbamate to the tetra-*S*-aryl thiocarbamate.
a) Reaction performed with 10 mol % Pd(^{t}Bu$_3$P)$_2$ catalyst, DCB = 1,2-dichlorobenzene.

The data shown in **Table 4.1** indicate that at high temperatures and concentrations, the reaction consumes all of the tetra-*O*-thiocarbamate and forms only decomposition products (none of the spirobisindane framework could be identified in the resultant ^{1}H NMRs). At lower temperature and concentrations, decomposition is avoided; however this is paired with incomplete/partial reaction of tetra-*O*-thiocarbamate. Attempts were made to catalyse the reaction according to literature procedures,[187] but these also proved unsuccessful.

It is well known and will be demonstrated later in this chapter, that the inclusion of a leaving group *ortho* to the *O*-thiocarbamate, greatly hinders the reaction by promoting an S_NAr attack of the sulfur atom at the *ortho* rather than *ipso* position.[188] This may explain why two *O*-thiocarbamate groups *ortho* to each other hinder the reaction, so much so that there is only one literature example of such a successful reaction.[189] Given that not even trace amounts of the fully rearranged *S*-thiocarbamate were detected during any reaction attempt, it was decided to pursue other synthetic pathways towards TTSBI.

4.2.2 From bisphenol A

Many literature procedures towards aromatic *ortho*-dithiol compounds utilise lithiation chemistry, in which the position *ortho* to a thiol group (as well as the thiol itself) is lithiated, and subsequently replaced by a second thiol group. A typical reaction involves the use of *n*-butyllithium as a base and elemental sulfur as the source of sulfur (**Scheme 4.9**).[190]
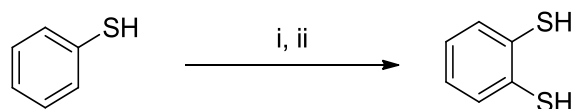
Scheme 4.9 Synthesis of benzene-1,2-thiol from thiophenol.
Reagents and conditions: i) *n*-BuLi, TMEDA, hexane, RT, 24 hrs, ii) S$_8$, 16 hrs, RT.

Combining this with two other literature procedures[191,192] provides a plausible synthetic pathway to TTSBI (**Scheme 4.10**). Bisphenol A is first converted to 6,6'-dihydroxy-3,3,3',3'-tetramethyl-1,1'-spirobisindane (DHSBI),[191] then to the corresponding di-*O*-thiocarbamate, which subsequently undergoes a Newman-Kwart rearrangement to give the di-*S*-thiocarbamate, followed by hydrolysis to give 6,6'-dithiol-3,3,3',3'-tetramethyl-1,1'-

spirobisindane (DTSBI).[192] DTSBI is then converted to the TTSBI by lithiation and subsequent *thiolation* of the least sterically hindered *ortho* positions to the thiols.
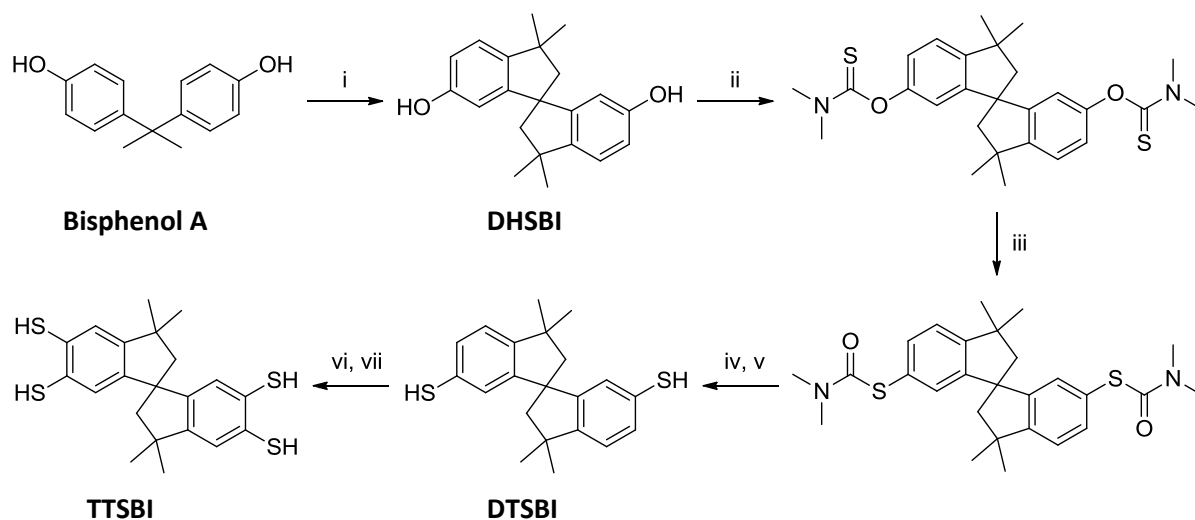
Scheme 4.10 Proposed synthetic pathway to TTSBI from bisphenol A
Reagents and conditions: i) MeSO$_3$H, 25 °C, 3 days, ii) *N,N*-dimethylcarbamyl chloride, KOH, MeOH, reflux, 24 hrs iii) Ph$_2$O, 260 °C, 4 hrs, iv) KOH, MeOH, Pyridine, reflux, 8 hrs, v) H$_3$O$^+$, vi) *n*-BuLi, TMEDA, hexane, vii) S$_8$.

Literature procedures[191,192] were followed, to give DTSBI in four steps, with an overall yield of 43 %. Each intermediate was characterised by ^{1}H NMR, ^{13}C NMR, IR and low resolution MS to confirm its structure and purity, particular care was taken in the dryness and purity of the di-*O*-thiocarbamate intermediate, so as to eliminate the chance of side reactions at high temperatures during the Newman-Kwart rearrangement.

Regrettably, all attempts at isolating any TTSBI from DTSBI (**Scheme 4.11**) were unsuccessful, despite the evidence of TTSBI forming in some cases (**Table 4.2**).
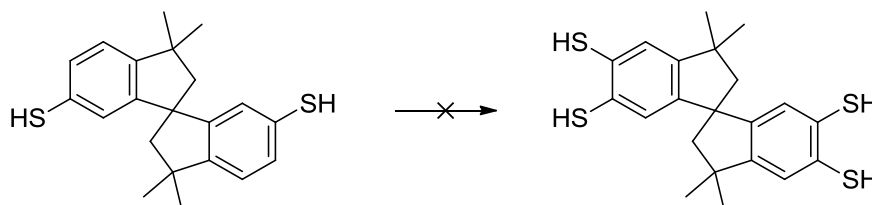
Scheme 4.11 Failed synthesis of TTSBI from DTSBI.

Solvent	Conditions	Outcome
Diethyl ether	4.2 eq. *n*-BuLi – RT, 24 hrs 2 eq. S_8 – RT, 20 hrs	Only DTSBI collected. Precipitates lack thiol peak in ^{1}H NMR
Cyclohexane	4.2 eq. *n*-BuLi – RT, 24 hrs 2 eq. S_8 – RT, 20 hrs	No evidence of TTSBI. Precipitates lack thiol peak in ^{1}H NMR
Cyclohexane	4.2 eq. *n*-BuLi – RT, 24 hrs 4 eq. S_8 – RT, 20 hrs 2.2 eq. LiAlH$_4$ – THF, reflux 20 hrs	^{1}H NMR evidence of TTSBI. Purification attempts failed
Cyclohexane	4.4 eq. *n*-BuLi – RT, 24 hrs 4.4 eq. S_8 – RT, 20 hrs 2.2 eq. LiAlH$_4$ – THF, reflux 20 hrs	^{1}H NMR evidence of TTSBI. Purification attempts failed
Hexane	4.4 eq. *n*-BuLi – RT, 24 hrs 6 eq. S_8 – RT, 20 hrs 3 eq. LiAlH$_4$ – THF, reflux 20 hrs	^{1}H NMR and LRMS evidence of TTSBI. Purification attempts failed

Table 4.2 Summary of attempted syntheses of TTSBI from DTSBI.

When attempting to follow a similar literature procedure[190] that only acidified the crude reaction mixture, evidence was seen for disulfide bond formation from the lack of peaks attributable to thiol groups observable in ^{1}H NMR spectra. Therefore, it was decided to adopt a different literature procedure[193] that utilised lithium aluminium hydride treatment to cleave any disulfide bonds formed during the reaction. This led to evidence for TTSBI formation, observed by ^{1}H NMR and low resolution MS, however any attempts to purify the crude reaction mixture were unsuccessful, possibly due to the reformation of disulfide bonds in solution yielding insoluble and impure polymeric materials.

4.2.3 From benzene-1,2-dithiol

The bis-catechol PIM-1 monomer, THSBI, can be synthesised in a simple one procedure pot from catechol and acetone under acidic conditions (**Scheme 4.12**).[194,195]
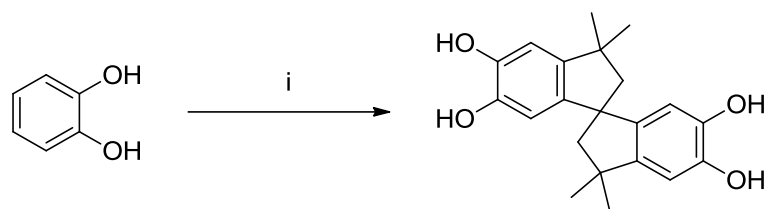
Scheme 4.12 Synthesis of THSBI from catechol.
Reagents and conditions: i) Acetone, HCl, Ac$_2$O, reflux, 12 hrs.

Consequently, benzene-1,2-dithiol, produced according to the literature procedure outlined in **Scheme 4.9**,[190] was subjected to the same conditions used in the synthesis of THSBI in an attempt to produce TTSBI (**Scheme 4.13**).
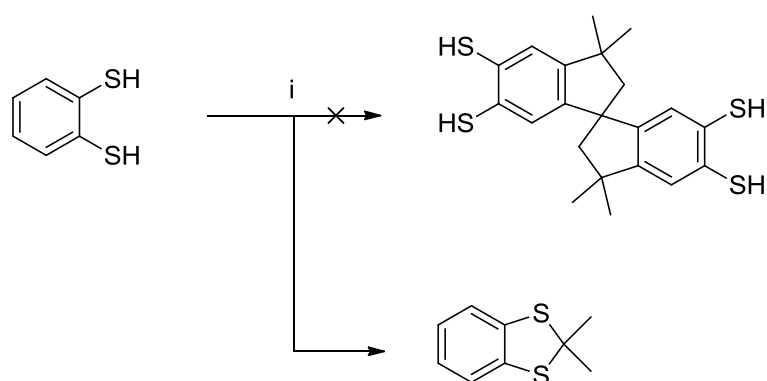
Scheme 4.13 Failed synthesis of TTSBI from the reaction benzene-1,2-dithiol with acetone, and the isolated product: *2,2-dimethyl-1,3-benzodithiole*.
Reagents and conditions: i) Acetone, HCl, Ac$_2$O, reflux, 12 hrs.

Unfortunately, the reaction served only to *protect* the dithiol, forming 2,2-dimethyl-1,3-benzodithiole (**Scheme 4.13**), with no evidence of any reaction occurring at the benzene ring. Further attempts using a large excess of acetone yielded the same protected dithiol as well as some evidence of reaction at the benzene ring, however, no evidence of TTSBI was seen by ^{1}H NMR or low resolution MS. It seems that the acidic conditions used in the literature[194,195] are sufficient to deprotect any dioxole formed during the formation of THSBI. However, when using a dithiol the protecting group is suitably stable to remain attached.

The reaction was repeated using *phorone* (**Scheme 4.14**), the self-condensation product of acetone, which has already undergone the necessary condensations to form the central aliphatic part of a spirobisindane framework. However, this again yielded predominantly

material formed by the reaction phorone with the thiol groups, and no evidence was seen for TTSBI formations by ^{1}H NMR or LRMS.
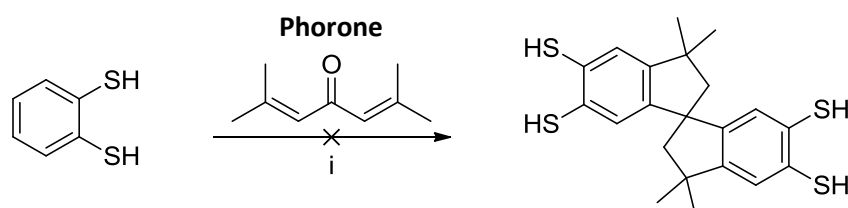
Scheme 4.14 Failed synthesis of TTSBI from the reaction benzene-1,2-dithiol and phorone.
Reagents and conditions: i) HCl, Ac$_2$O, reflux, 12 hrs.

4.2.4 From benzene

Given the limited success achieved with the previously proposed synthetic routes to TTSBI, it was decided to attempt the synthesis of the spirobisindane framework and endeavour to introduce tetra-functionality that would offer a more straightforward route to introducing the thiol groups. Literature procedures suggested that this could be achieved either by direct introduction of thiol groups to the hydrocarbon,[196] or by bromination[197] followed either by copper mediated introduction of a protected thiol[198] and subsequent deprotection,[199] or direct substitution of the bromine groups for thiol groups.[200]

Preparation of the spirobisindane hydrocarbon (**Scheme 4.15**) was performed according to the literature[110,201] and both the intermediate ketone and spirobisindane hydrocarbon were characterised by ^{1}H NMR, ^{13}C NMR, IR and low resolution MS to confirm their structure and purity.
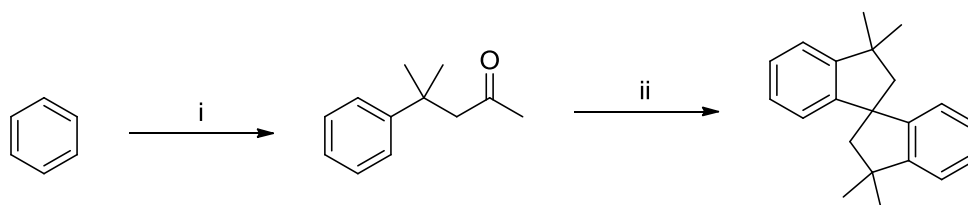
Scheme 4.15 Synthesis of the spirobisindane hydrocarbon from benzene.
Reagents and conditions: i) Mesityl oxide, AlCl$_3$, 4 hrs, RT ii) ZnCl$_2$, 180 °C, 5 mins.

Once isolated and thoroughly dried, investigations were made into the direct thiolation of the spirobisindane hydrocarbon, following a patented procedure by Shinichi *et al.*[196] for the direct *ortho*-thiolation of substituted benzenes (**Scheme 4.16**)
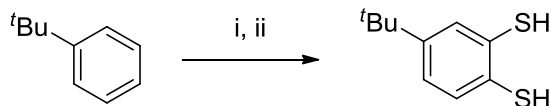
Scheme 4.16 Patented procedure for the *ortho*-thiolation of substituted benzenes.
Reagents and conditions: i) S$_2$Cl$_2$, ZnCl$_2$, DCE, 100 °C, 24 hrs, ii) Zn/HCl.

Unfortunately, all attempts at applying this procedure to the spirobisindane hydrocarbon (**Scheme 4.17**) yielded no trace of TTSBI, only un-reacted spirobisindane was recovered.
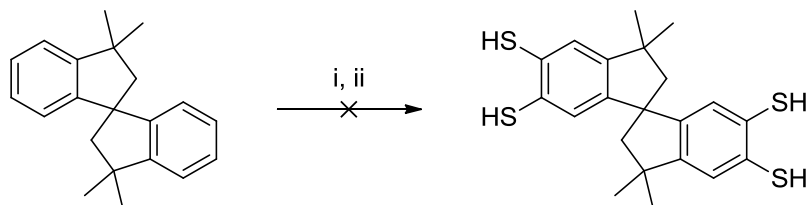
Scheme 4.17 Unsuccessful conversion of spirobisindane to TBSBI.
Reagents and conditions: i) S$_2$Cl$_2$, ZnCl$_2$, DCE, 100 °C, 24 hrs, ii) Zn/HCl.

Given that the direct thiolation of the spirobisindane hydrocarbon was unsuccessful, it was decided to pursue routes to TTSBI *via* 5,5',6,6'-tetrabromo-3,3,3',3'-tetramethyl-1,1'-spirobisindane (TBSBI). Details of the refinement for the tetra-bromination of spirobisindane are summarised below in **Scheme 4.18** and **Table 4.3**.
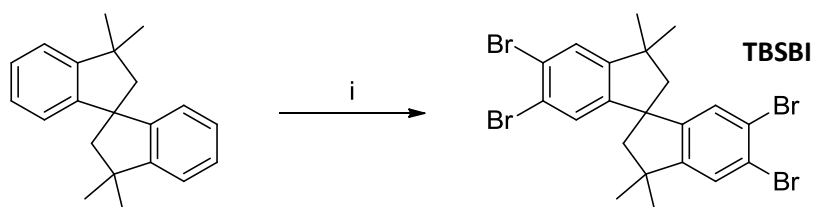
Scheme 4.18 Bromination of spirobisindane to give TBSBI.
Reagents and conditions: i) DCM, 4.23 eq. Br$_2$, Fe$_{(cat)}$, Reflux, 12 hrs.

Solvent	Brominating reagent	Equivalents	Catalyst	Temperature (°C)	Reaction time (hours)	Outcome	Crude purity (%)
Chloroform	PHBPB	4	-	61	48	No Reaction	-
Chloroform	NBS	4	-	61	48	No Reaction	-
Chloroform	Br_2	4	-	35	24	Under brominated material	-
Chloroform	Br_2	4	-	61	24	Under brominated material	-
Chloroform	Br_2	4	Fe powder	15	24	Under brominated material	-
Chloroform	Br_2	4	Fe powder	35	24	Under brominated material	-
Chloroform	Br_2	4	Fe powder	61	1	Under brominated material	-
Chloroform	Br_2	4	Fe powder	61	3.5	TBSBI and under brominated material	60[a]
Chloroform	Br_2	4.25	Fe powder	61	12	TBSBI and over brominated material[b]	84
DCM	Br_2	4	Fe powder	40	12	TBSBI and under brominated material	76
DCM	Br_2	4.1	Fe powder	40	12	TBSBI and under brominated material	82
DCM	Br_2	4.2	Fe powder	40	12	TBSBI and under brominated material	88
DCM	Br_2	4.3	Fe powder	40	12	TBSBI and over brominated material	95
DCM	Br_2	4.25	Fe powder	40	12	TBSBI and over brominated material	96.5
DCM	Br_2	4.23	Fe powder	40	12	TBSBI and over brominated material	97.5

Table 4.3 Summary of the reaction conditions and outcome for the bromination of spirobisindane.
a) Recrystallised to 78 % purity, b) up to hexabromospirobisindane detected by low resolution MS.
PHBPB = Pyridinium hydrobromide perbromide, NBS = N-bromosuccinimide.

Through the repeated trituration of the partially over-brominated samples in hexane, it was found possible to increase the purity of TBSBI to over 99 %, although in doing so yields dropped from approximately 85 to 65 %. Structure and purity of the hexane treated TBSBI were confirmed by ^{1}H NMR, ^{13}C NMR, high resolution MS and single crystal X-ray diffraction (**Figure 4.1**) studies.
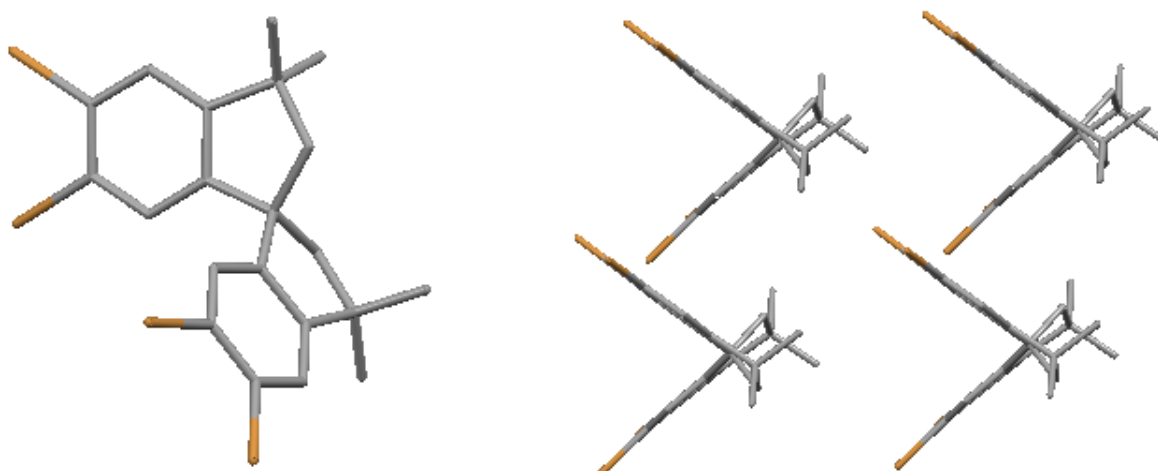
Figure 4.1 Crystal structure (left) and packing (right), showing spirocentre geometry, of TBSBI. Crystals obtained *via* slow diffusion of methanol into chloroform solution.
Protons and solvent molecules removed for clarity.

With a straightforward synthetic pathway to multi-gram quantities of TBSBI established, attempts were made to convert the four bromine groups to thiols. Literature procedures[202,203] demonstrate how hexabromotriphenylene can be converted to a hexa(alkylthio)triphenylene by reaction with sodium thiomethoxide followed by reaction of the consequent hexaanion with a suitable iodoalkane, to give the corresponding hexa(alkylthio)triphenylene in over 90 % yield (**Scheme 4.19**).
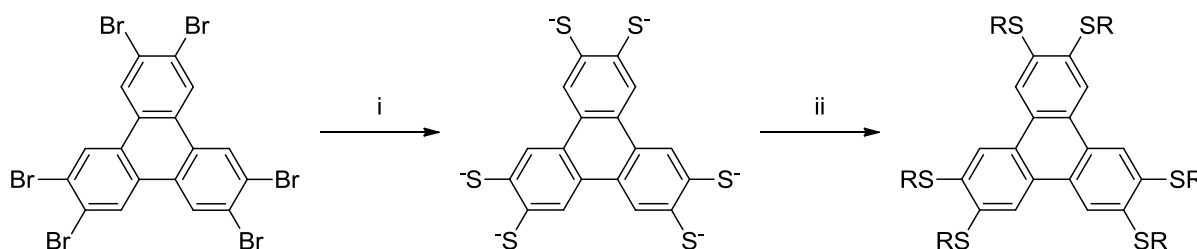
Scheme 4.19 Conversion of hexabromotriphenylene to hexa(alkylthio)triphenylene.
R = Me, Et, Pr.
Reagents and conditions: I) CH_3SNa, 1,3-dimethyl-2-imidazolidinone, 240 °C, ii) RI.

It was hypothesised that exposing the hexaanion, produced during the first part of the procedure, to acidic conditions would yield the hexathiol in equally impressive yields. Accordingly, attempts were made to convert TBSBI to TTSBI by adapting this procedure (**Scheme 4.20**).
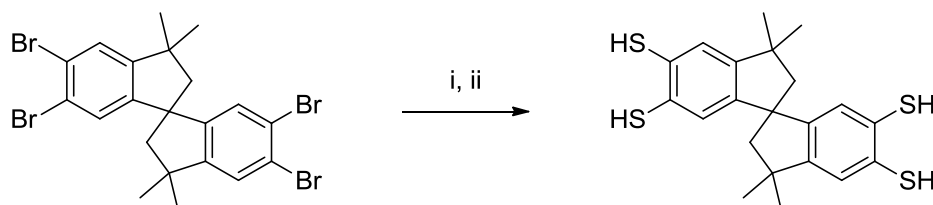
Scheme 4.20 Attempted conversion of TBSBI to TTSBI.
Reagents and conditions: I) CH$_3$SNa, 1,3-dimethyl-2-imidazolidinone, 240 °C, ii) H$_3$O$^+$.

Evidence could be seen by ^{1}H NMR and low resolution MS for partial substitution of the bromines for thiol groups, however only a trace amount of TTSBI was observed, even when the reaction was repeated using a large excess of sodium thiomethoxide and allowed to proceed for up to 48 hrs. Given the limited success, harsh reaction conditions and relative expense of the materials used in this procedure, it was decided to pursue other relevant literature procedures for the conversion of TBSBI to TTSBI.

Two literature procedures by Ferretti *et al.*[198,199] reveal how 1,2-dibromobenzene can be reacted with the copper salt of 1-butanethiol (cuprous *n*-butylmercaptide) to give 1,2-bis(*n*-butylthio)benzene, and subsequently *deprotected* by the addition of sodium metal to ammonia solution to give bezene-1,2-dithiol (**Scheme 4.21**).
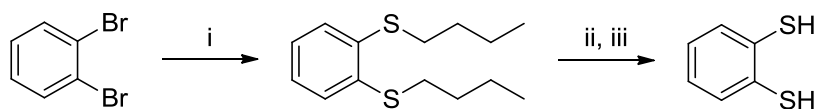
Scheme 4.21 Conversion of 1,2-dibromobenzene to benzene-1,2-dithiol.
Reagents and conditions: i) CuS(CH$_2$)$_3$CH$_3$, quinoline, pyridine, reflux, 4 hours, ii) Na, NH$_3$, -33 °C, iii) HCl.

The first procedure by Ferretti *et al.*[198] was adapted for the conversion of TBSBI into the corresponding tetra-(*n*-butylthio)spirobisindane, *TnBTSBI* (**Scheme 4.22**).
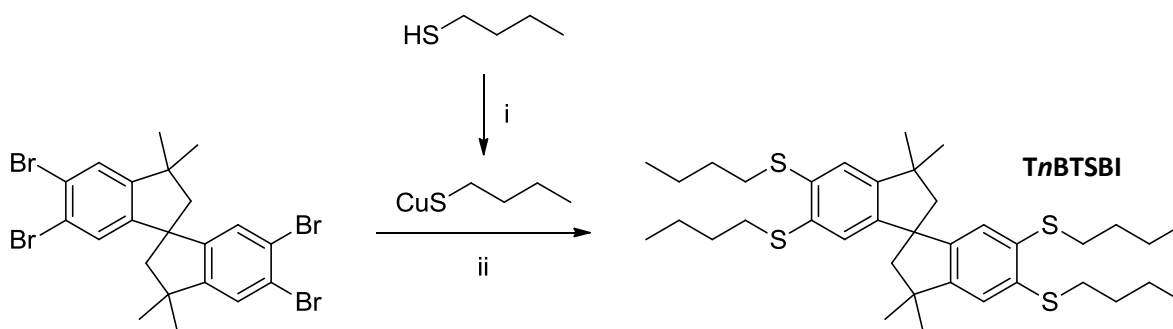
Scheme 4.22 Synthesis of T*n*BTSBI.
Reagents and conditions: i) Ethanol, Cu$_2$O, reflux, 72 hrs, ii) quinoline, pyridine, reflux, 12 hrs.

TBSBI was reacted with an excess (4.5 equivalents) of freshly prepared cuprous *n*-butylmercaptide in a mixture of quinoline and pyridine. The crude reaction products were found to contain T*n*BTSBI and a trace impurity, revealed by low resolution MS to be penta-(*n*-butylthio)spirobisindane (**Figure 4.2**), formed due to trace impurities of pentabromospirobisindane in the TBSBI starting material. Purification was achieved *via* column chromatography and tetra-(*n*-butylthio)spirobisindane, T*n*BTSBI was isolated in a 72 % yield. ^{1}H NMR, ^{13}C NMR and high resolution MS confirmed the structure and purity of the isolated material.
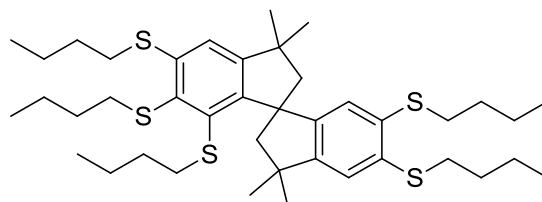
Figure 4.2 Penta-(*n*-butylthio)spirobisindane impurity removed *via* column chromatography.

By adapting literature procedures[199,204] for the deprotection of *n*-butylthiobenzenes (**Scheme 4.20**), T*n*BTSBI was deprotected by the portionwise addition of lithium metal to ammonia solution using THF as a co-solvent (**Scheme 4.23**).
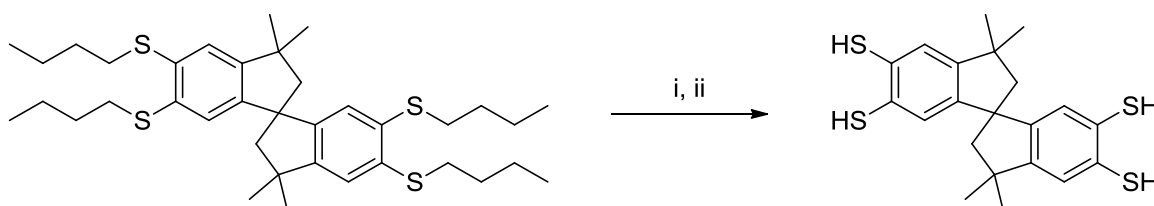
Scheme 4.23 Deprotection of T*n*BTSBI to give TTSBI.
Reagents and conditions: i) Li, THF, NH$_3$, -33 °C, ii) HCl.

Following an acidic work up, TTSBI was isolated in 82 % yield as a white powder and its structure confirmed by ^{1}H NMR, ^{13}C NMR, IR and high resolution MS without the need for any further purification. Once isolated, the powder was stored under nitrogen to eliminate disulfide bond formation through oxidation. **Scheme 4.24** shows the full synthesis of TTSBI from benzene.
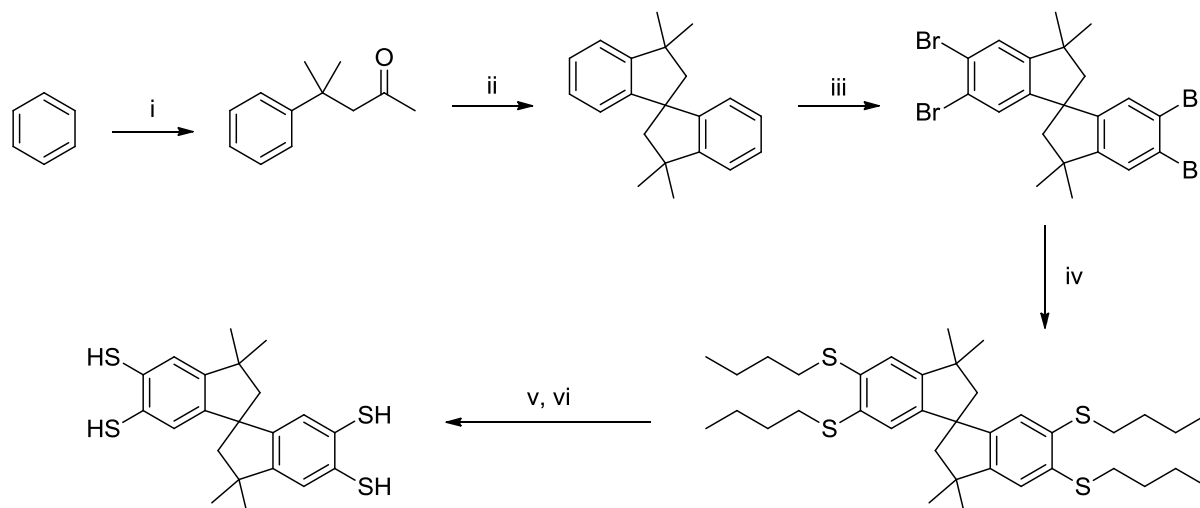
Scheme 4.24 Full synthesis of TTSBI.
Reagents and conditions: i) Mesityl oxide, AlCl$_3$, 4 hrs, RT ii) ZnCl$_2$, 180 °C, 5 mins, iii) DCM, 4.23 eq. Br$_2$, Fe$_{(cat)}$, Reflux, 12 hrs, iv) cuprous *n*-butylmercaptide, quinoline, pyridine, reflux, 12 hrs, v) Li, THF, NH$_3$, -33 °C, vi) HCl.

4.3 sPIM-1 synthesis

Once a suitable quantity of TTSBI had been synthesised, it was reacted with TFTPN under typical PIM forming conditions in an effort to produce a sample of sPIM-1 (**Scheme 4.25**).[103]
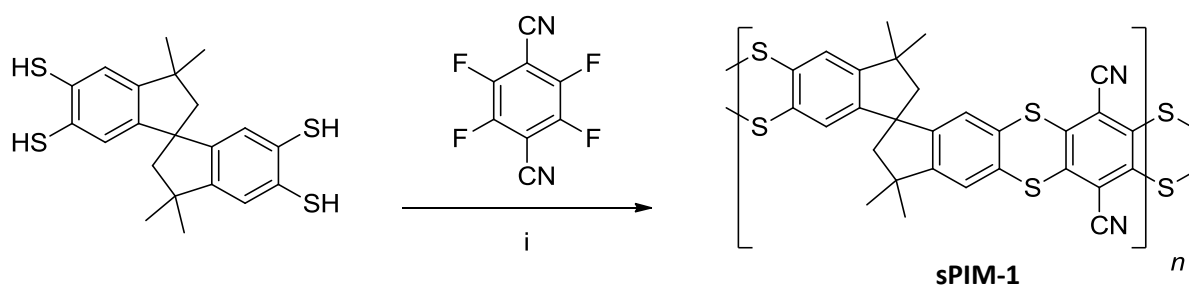
Scheme 4.25 Synthesis of sPIM-1 from TTSBI and TFTPN.
Reagents and conditions: i) K$_2$CO$_3$, DMF, 65 °C, 3 days.

In contrast to PIM-1 formation, sPIM-1 polymerisation yielded a yellow/orange precipitate almost immediately upon addition of the anhydrous solvent. Regardless, the reaction was allowed to continue for three days, during which time, little change to the reaction's colour or viscosity could be observed (typically PIM-1 polymerisations become more viscous over time).

Following an aqueous work up, the crude reaction products were found to be insoluble in all common organic solvents, including sulfuric acid. Accordingly, the material was assumed to be cross-linked (**Figure 4.3**), and so sequentially refluxed in THF, chloroform and methanol to remove any soluble material. After each reflux, trace amounts of soluble material were collected and analysed by ^{1}H NMR, revealing them to be non-polymeric material. Once dried, the insoluble material was collected in approximately 80 % yield (according to the sPIM-1 repeat unit, **Scheme 4.25**). BET analysis of this material revealed it to be porous, possessing a surface area of 353 m^{2}g^{-1} (**Figure 4.5**, **Table 4.4**), indicating that polymerisation had occurred.
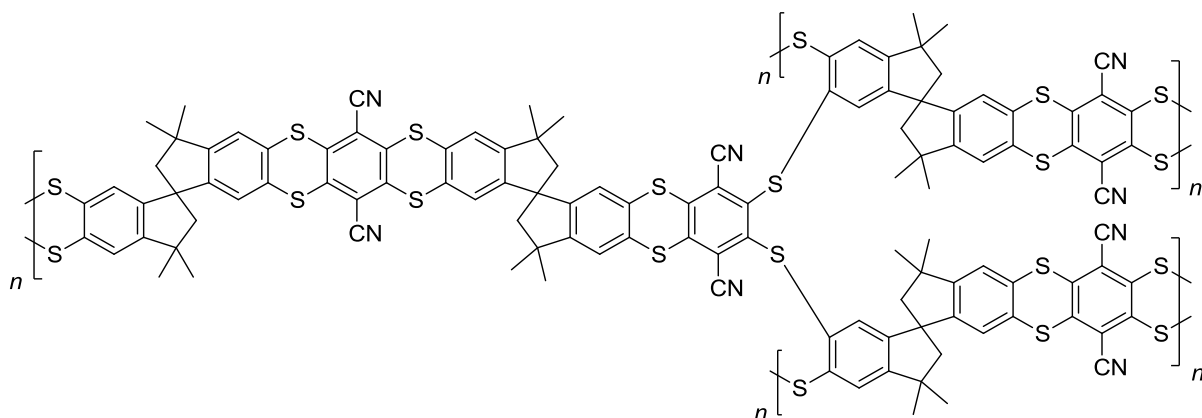
Figure 4.3 Cross-linked sPIM-1.

Given the confirmed high purity of both monomers prior to synthesis, it was hypothesised that the cross-linking was due to the highly reactive nature of the thiol groups of TTSBI (in comparison with the hydroxyl groups of THSBI). It was therefore decided to repeat the polymerisation without the addition of any base, in an effort to slow down the reaction and thus promote ladder polymer formation. This yielded similar crude reaction products to the previous attempt, crucially however, more material was found to be soluble in chloroform, approximately 15 % of the crude reaction products. GPC analysis of this soluble fraction (**Figure 4.4**) showed it to be polymeric, although relatively low molecular weight.
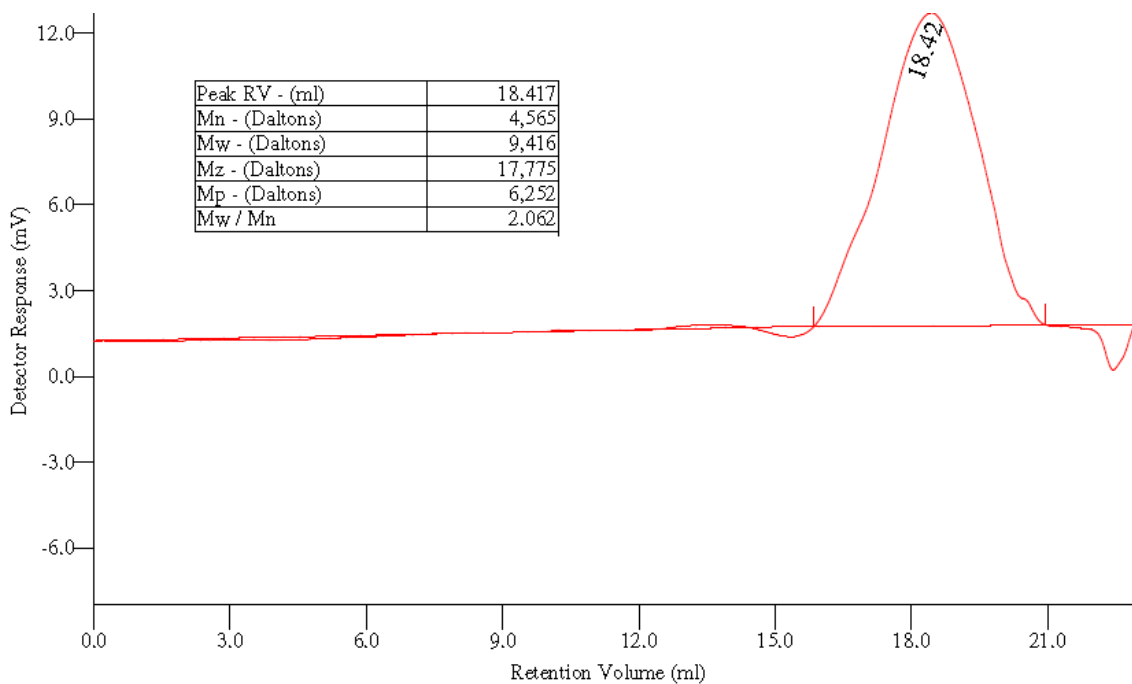
Figure 4.4 GPC trace of the chloroform soluble sPIM-1 and relevant data (inset).

Both the soluble and insoluble material isolated from the reaction were analysed by BET nitrogen sorption and the resultant adsorption isotherms and data are shown below, alongside PIM-1 for comparison (**Figure 4.5**, **Table 4.4**).
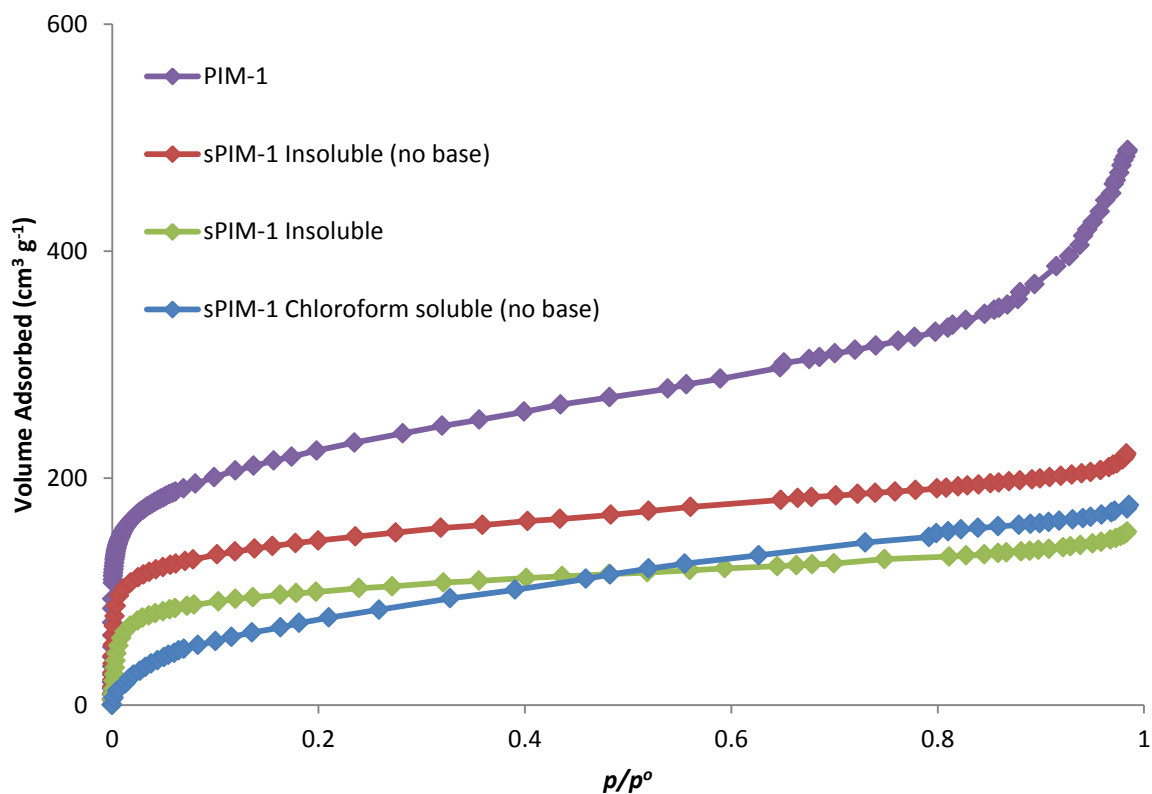
Figure 4.5 BET nitrogen adsorption isotherms for PIM-1 and sPIM-1 (soluble and insoluble). Desorption plots removed for clarity.

133

PIM	BET surface area $(m^2\,g^{-1})$	Total pore volume $(cm^3\,g^{-1})$
PIM-1	796[a]	0.75[a]
sPIM-1 Insoluble	353	0.25
sPIM-1 Insoluble (no base)	510	0.34
sPIM-1 Chloroform soluble (no base)	307	0.31

Table 4.4 BET nitrogen sorption data for PIM-1 and sPIM-1 (soluble and insoluble).
a) Data supplied by Dr. Kadhum Msayib.

These data suggest that sPIM-1 has a lower surface area than PIM-1, an observation that is supported by recent computational simulations.[205] It is likely that the polymer chains of sPIM-1 are more *kinked* than PIM-1, due to the presence of non-planar thianthrene units along the polymer backbone, allowing for increased packing efficiency and hence lower porosity. Furthermore, the data indicates that the chloroform soluble fraction of sPIM-1 is less porous than the insoluble fraction. This is likely due to the low molecular weight of the chloroform soluble material allowing for more efficient packing of the polymer chains. Attempts were made to observe the MALDI mass spectrum of any oligomers present in the chloroform soluble sample, however none could be observed.

Further attempts at polymerising TTSBI with a less activated monomer: 2,3,5,6-tetrachloroterephthalonitrile (TCTPN) (**Scheme 4.26**), proved equally unsuccessful. Typical PIM forming conditions led to largely insoluble materials, with the isolated soluble fraction consisting of very low molecular weight material ($M_w < 5000$ g mol^{-1}), as measured by GPC. Milder reaction conditions (lower/room temperature, no base) led to the formation of mostly soluble materials, but GPC analysis revealed them to be even lower molecular weight ($M_w < 3000$ g mol^{-1}).
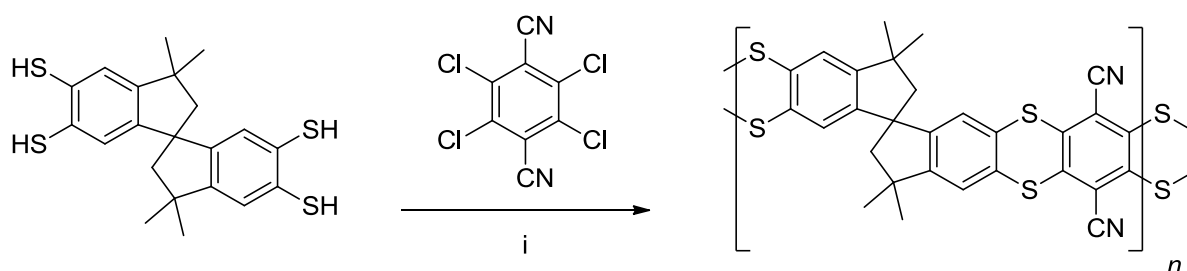
Scheme 4.25 Synthesis of sPIM-1 from TTSBI and TCTPN.
Reagents and conditions: i) K$_2$CO$_3$, DMF, 65 °C, 3 days.

The fact that no soluble sample of sPIM-1 had a molecular weight of over 10,000 g mol^{-1}, suggests that the insolubility of sPIM-1 is inherent to its structure and that regardless of cross-linking, a suitably high molecular weight sample of sPIM-1 would be insoluble in common solvents.

4.4 sPIM-0 concept and monomer synthesis

During the attempted synthesis of the sPIM-1 monomer (TTSBI) from bisphenol A (**Scheme 4.10**), it was realised that if halide groups could be introduced to the *ortho* positions of DTSBI (**Scheme 4.27**), a potential sPIM monomer would exist. Such a monomer could undergo a self-polymerisation (as both halide and chalcogen groups are present) to give a hypothetical polymer dubbed *sPIM-0* (due to its smaller repeat unit compared with sPIM-1).
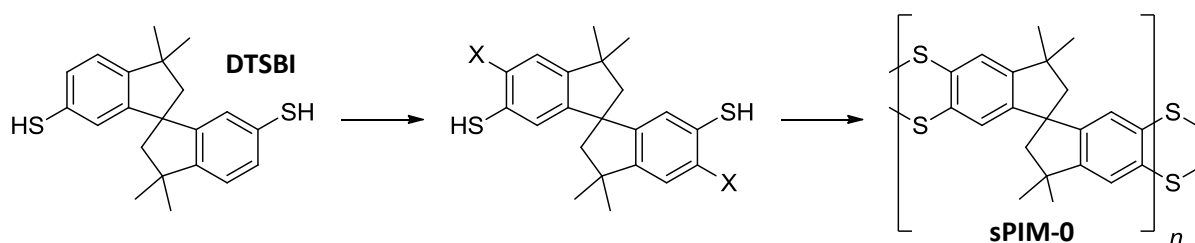
Scheme 4.27 Hypothetical synthesis of sPIM-0 *via* self-polymerisation of a halide and thiol containing monomer.

Given the ease of handling of brominating reagents, over chlorinating or fluorinating reagents, as well as the literature already established on carbon-sulfur bond formation from catalysed couplings of aryl thiol with aryl bromides,[206,207] it was decided to investigate the synthesis of 5,5'-dibromo-6,6'-dithio-3,3,3',3'-tetramethyl-1,1'-spirobisindane, *DBDTSBI*. Unfortunately, direct bromination of DTSBI was not possible (**Scheme 4.28**), as it is well known that exposure of thiols to brominating conditions causes disulfide bond formation.[208,209] Indeed attempts at doing so yielded material that showed no trace of a thiol peak in ^{1}H NMR spectra.
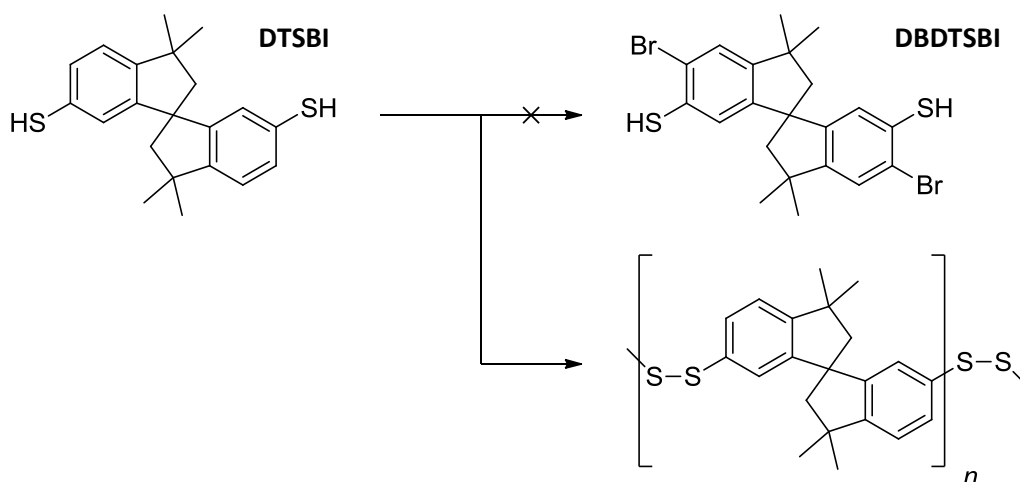
Scheme 4.28 Disulfide bond formation, resulting in polymers, when exposing DTSBI to brominating conditions.

Fortunately however, the introduction of bromine groups *ortho* to aromatic hydroxy groups is a straightforward procedure,[210,211] meaning that 5,5'-dibromo-6,6'-dihydroxy-3,3,3',3'-tetramethyl-1,1'-spirobisindane, *DBDHSBI*, could be easily synthesised from DHSBI (**Scheme 4.29**).
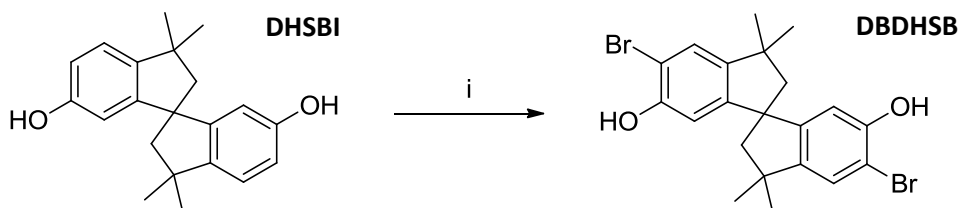
Scheme 4.29 Synthesis of DBDHSBI from DHSBI.
Reagents and conditions: i) Pyridinium hydrobromide perbromide, chloroform, RT, 12hrs.

The isolation of DBDHSBI was found to be straightforward when using pyridinium hydrobromide perbromide. Attempts in which two equivalents of the brominating reagent were used yielded the formation of some tri-brominated material, observed by low resolution MS. Separation of this impurity was possible, but difficult on a large scale. Separation of mono-brominated material however, was significantly simpler, prompting the use of a slightly reduced quantity of pyridinium hydrobromide perbromide. This discovery allowed for the isolation of DBDHSBI in near quantitative yields. Its structure and purity were confirmed by ^{1}H NMR, ^{13}C NMR, IR and high resolution MS.

The conversion of DBDHSBI to the corresponding sPIM-0 monomer required that the two hydroxy groups be converted to thiols. As discussed in Chapter 4.2.1, this is commonly achieved using the Newman-Kwart Rearrangement.[185,186] Thus, DBDHSBI was reacted with *N,N*-dimethylcarbamyl chloride under basic conditions to yield the di-*O*-thiocarbamate (**Scheme 4.30**).
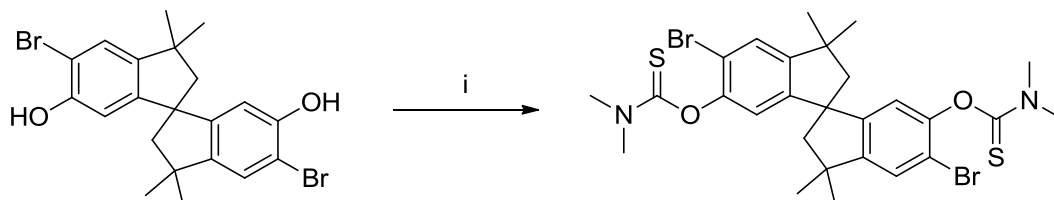
Scheme 4.30 Synthesis of the di-*O*-thiocarbamate from DBDHSBI.
Reagents and conditions: i) N,N-dimethylcarbamyl chloride, KOH, MeOH, reflux, 24 hrs.

Formation of the di-*O*-thiocarbamate was achieved through adapting the literature procedure by Sugioka and Hay.[192] Following purification *via* column chromatography, the purified di-*O*-thiocarbamate was fully characterised by ^{1}H NMR, ^{13}C NMR, IR, high resolution MS and X-ray crystallography.

The Newman-Kwart rearrangement of the di-*O*-thiocarbamate (**Scheme 4.31**) was not so simple. As mentioned previously, the high temperature rearrangement is hindered by the presence leaving groups *ortho* to the *O*-thiocarbamate, as they promote an *ortho*, rather than *ipso*, S$_N$Ar attack of the sulfur atom.[188] A summary of the reaction conditions attempted for this rearrangement is shown in **Table 4.5**.
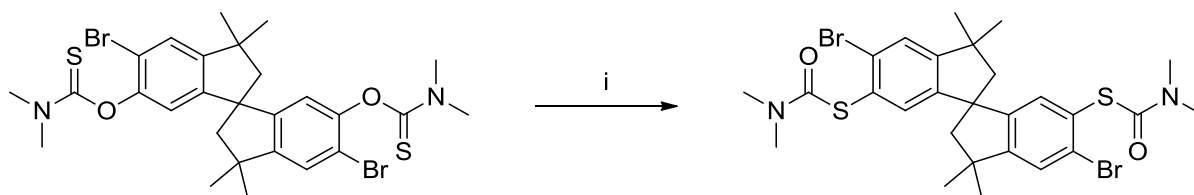
Scheme 4.31 Rearrangement of the di-*O*-thiocarbamate to the di-*S*-thiocarbamate.
Reagents and conditions: i) Ph$_2$O, reflux, 3 hrs.

Solvent	Concentration (mmol cm⁻³)	Reaction temp. (°C)	Reaction time (hours)	Heating method	Outcome	Isolated yield (%)
No solvent	-	110	0.33	Microwave	Decomposition	0
Toluene	2.0	110	48	Oil bath	No reaction (suspension)	0
Toluene	0.2	110	48	Oil bath	No reaction (solution)	0
N,N-DMA	0.3	194	48	Oil bath	Trace of product	0
N,N-DMA	0.4	275	4	Microwave	Trace of product	0
Ph_2O	3.4	260	12	Heating mantle	Decomposition	0
Ph_2O	3.4	260	1.5	Heating mantle	Product formation plus residual SM	10
Ph_2O	3.4	260	3	Heating mantle	Product formation with decomposition	0
Ph_2O	2.7	260	3.5	Heating mantle	Product formation plus residual SM	8
Ph_2O	2.0	260	2	Heating mantle	Product formation	26
Ph_2O	1.8	220	1	Oil bath	Trace of product	0
Ph_2O	1.7	260	3	Heating mantle	Product formation, with decomposition	0
Ph_2O	0.9	260	3	Heating mantle	Product formation	21
Ph_2O	0.5	260	3	Heating mantle	Product formation	34
Ph_2O	0.4	260	3	Heating mantle	Product formation	37
Ph_2O	0.35	260	3	Heating mantle	Product formation	55
Ph_2O	0.2	260	5	Heating mantle	Product formation	31
Ph_2O	0.06	200	18	Oil bath	Trace of product	0

Table 4.5 Summary of the reaction attempts for conversion of the di-*O*-thiocarbamate to the di-*S*-thiocarbamate. N,N-DMA = N,N'-Dimethylaniline, Ph_2O = Diphenyl ether.

As shown in **Table 4.5**, the Newman-Kwart rearrangement of the di-*O*-thiocarbamate (**Scheme 4.31**) is highly dependent on concentration; at high concentrations the elevated reaction temperatures can lead to decomposition of the reagent and product.[188] Optimal reaction conditions were found to be a *gentle* three hour reflux at a concentration of approximately 0.35 mmol cm^{-3}. These conditions allowed for total consumption of the di-*O*-thiocarbamate, whilst limiting decomposition and subsequent formation of any side products. This in turn allowed for simple isolation of the product (after removal of the bulk of the solvent *via* distillation) by trituration in diethyl ether. Once isolated, the di-*S*-thiocarbamate was fully characterised by ^{1}H NMR, ^{13}C NMR, IR and high resolution MS. Subsequent hydrolysis of the obtained di-*S*-thiocarbamate (**Scheme 4.32**) was straightforward, resulting in the isolation of DBDTSBI in near quantitative yields.
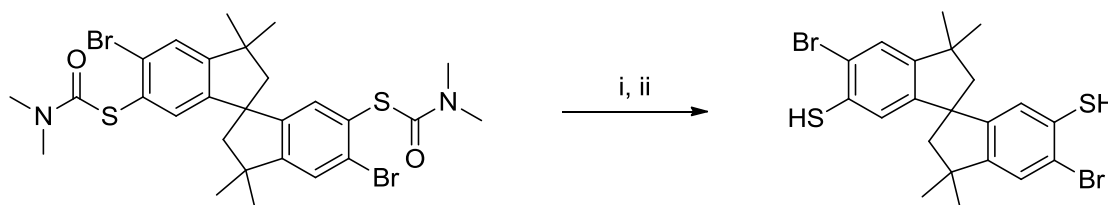
Scheme 4.32 Hydrolysis of the di-*S*-thiocarbamate to give DBDTSBI.
Reagents and conditions: i) KOH, MeOH, reflux, 24 hrs, ii) H$_3$O$^+$.

Once isolated, the sPIM-0 monomer, DBDTSBI, was fully characterised by ^{1}H NMR, ^{13}C NMR, IR, high resolution MS and X-ray crystallography (**Figure 4.6**), to confirm its purity and structure.
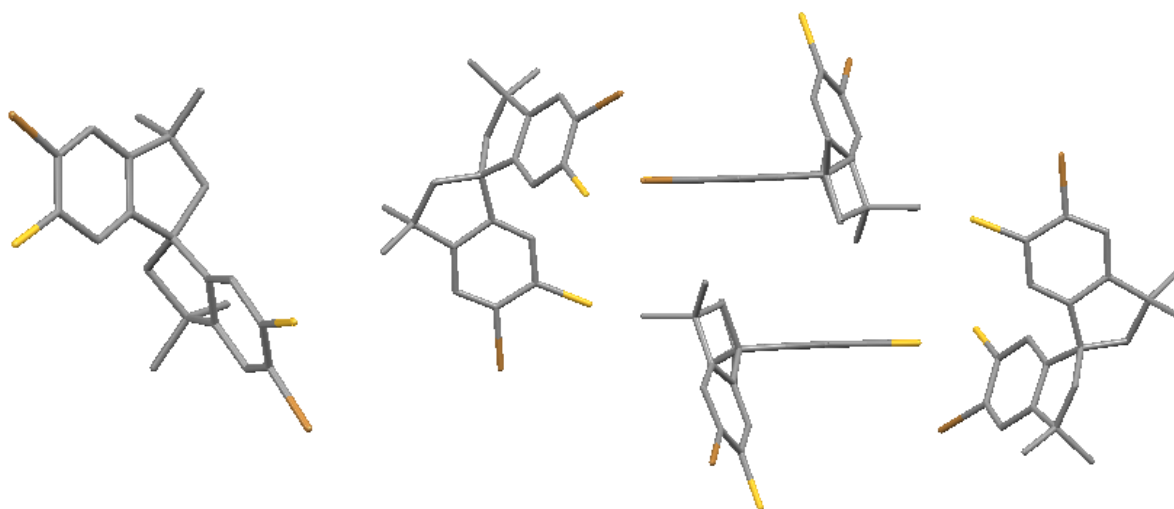
Figure 4.6 Crystal structure (left) and packing (right) of the sPIM-0 monomer, DBDTSBI. Crystals obtained *via* slow diffusion of methanol into chloroform solution. Protons and solvent molecules removed for clarity.

4.5 sPIM-0 synthesis

Once a suitable quantity of well dried sPIM-0 monomer (DBDTSBI) had been obtained, efforts were made to polymerise it according to **Scheme 4.33**.
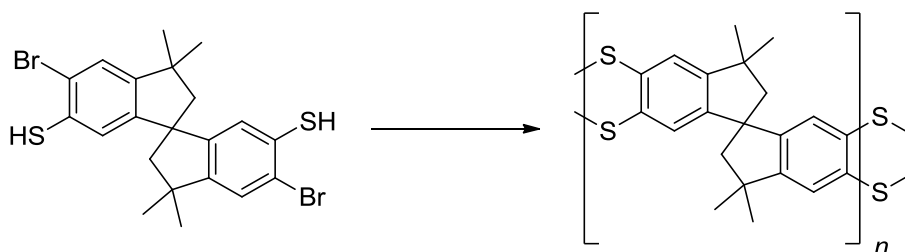
Scheme 4.33 Polymerisation of DBDTSBI to give sPIM-0.

Details of the various polymerisation attempts, many adapted from literature procedures for aryl thiol-halide coupling,[207,212-215] are given below in **Table 4.6**. Corresponding nitrogen adsorption isotherms and data for successful attempts are shown in **Figure 4.7**.

Entry	Solvent	Concentration (mmol cm^{-3})	Reaction temperature (°C)	Reaction time (hours)	Base (eq.)	Catalyst (eq.)	Outcome	BET surface area (m^2 g^{-1})	Pore volume (cm^3 g^{-1})
1	DMF	0.5	65	72	K$_2$CO$_3$ (2.2)	-	No reaction	-	-
2	DMF	0.5	130	72	K$_2$CO$_3$ (3.0)	-	No reaction	-	-
3	DMSO	0.3	130	72	KOH (3.6)	-	No reaction	-	-
4	DMSO	0.2	100	48	KO^{t}Bu (2.2)	CuBr (0.005)[a]	No reaction	-	-
5	DMSO	0.5	120	48	Cs$_2$CO$_3$ (2.2)	CuI (0.4)	Insoluble material	108	0.20
6	DMF	0.2	130	120	Cs$_2$CO$_3$ (2.2)	CuBr (0.4)	Insoluble material	30	0.13
7	DMSO	0.2	120	96	Cs$_2$CO$_3$ (2.2)	CuBr (0.4)	Insoluble material	438	0.38
8	DMSO	0.2	120	96	Cs$_2$CO$_3$ (2.2)	CuBr (2.0)	Insoluble material	416	0.53
9	DMSO	0.2	110	48	Cs$_2$CO$_3$ (2.2)	Cu$_2$O (0.4)	Insoluble material	349	0.50
10	DMSO	0.05	110	168	Cs$_2$CO$_3$ (2.2)	CuBr (0.4)	Partially soluble material[b]	21	0.06

Table 4.6 Summary of the sPIM-0 polymerisation attempts.
a) Reaction performed with 0.01 equivalents of benzenetriazole.
b) GPC (chloroform) of soluble fraction shows M_n = 3354, M_w = 4604, M_w/M_n = 1.373.

141
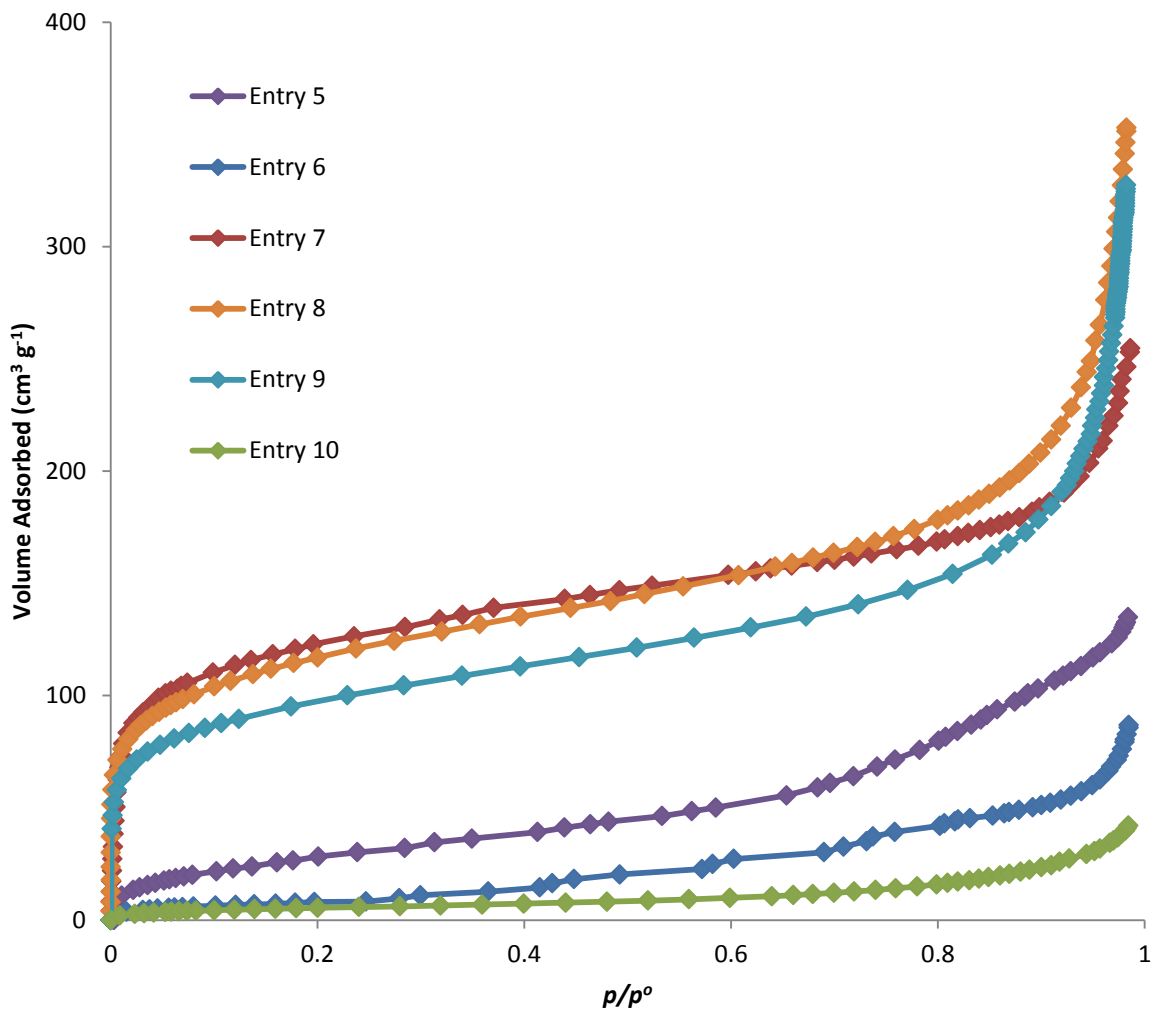
Figure 4.7 BET nitrogen adsorption isotherms for the various batches of sPIM-0 produced according to Table 4.6. Desorption plots removed for clarity.

As **Table 4.6** shows, almost all of the isolated batches of sPIM-0 were insoluble in all common solvents, possibly due to cross-linking occurring during polymerisation. In an effort to eliminate any cross-linking, polymerisations were performed in very dilute solution, in order to encourage the second reaction between a thiol and a bromide to occur intra-molecularly. Some success was seen, as soluble fractions were shown by GPC to be polymeric, though these were very low molecular weight (M_W < 5000 g mol^{-1}), and the bulk (> 95 %) of the material obtained was insoluble. This suggested that the insolubility was inherent to the structure of the polymer and not due solely due cross-linking, though some cross-linked material may still form during polymerisation.

4.6 sPIM-2 concept and monomer synthesis

Through the reaction of dithiol and di-halide containing monomers, one can envisage how an efficient polymerisation would yield a high molecular weight, single-stranded polymeric material (**Scheme 4.34**).
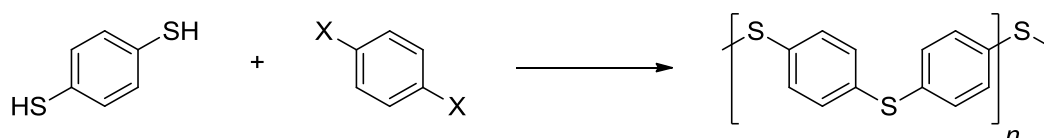
Figure 4.33 Formation of a single-stranded polymer from dithiol and di-halide containing monomers.

With just one bond between each monomer, the non-rigid polymer shown in **Scheme 4.34** can freely rotate, likely rendering it useless as a porous material. If however, one of the monomers were to contain a group that, after subsequent activation, can form new bonds between constituents units of the polymer, a porous, rigid, often cross-linked,[89,91] material can be formed. If these groups are *ortho* to the group employed in the initial polymerisation, then ladder polymers can be formed. Freund *et al.*[216] demonstrated this in their synthesis of ladder poly(phenylene sulfides). Through the reaction of dithiol and dihalide-diketone containing monomers, high molecular weight polymers were produced which, after reduction of the constituent ketone groups, could undergo a Lewis-acid mediated cyclisation to form ladder polymers (**Scheme 4.35**).
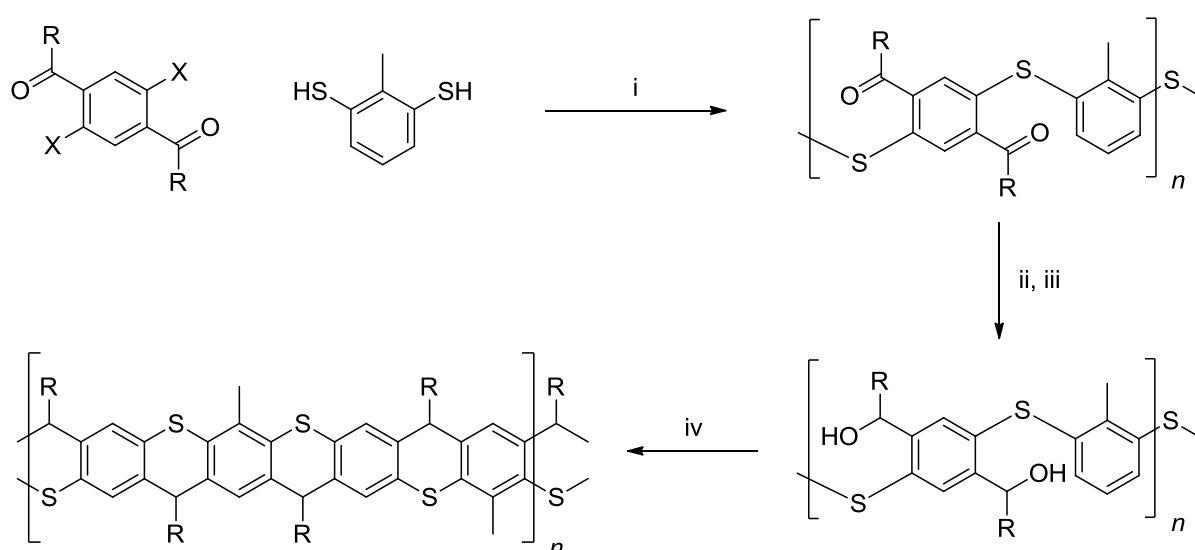
Scheme 4.35 Formation of a single-stranded polymer, and subsequent cyclisation to a ladder polymer.
Reagents and conditions: i) DMAC, K_2CO_3, 120 °C, 24 hrs, ii) THF, $LiAlH_4$, RT, 6 hrs, iii) H_3O^+, iv) $SnCl_4$, $CHCl_3$, 3 hrs, RT.
$R = C_6H_5$, X = Br, Cl, F.

These ladder polymers produced by Freund *et al.*[216] are unlikely to be porous (they were developed for their electrical rather than porosity related properties), due to their lack of any *site of contortion* or *awkward molecular geometry*. However, if one of the monomers were to be replaced by one that contained either of these typical porosity-inducing attributes, it seems highly probable that a new sulfur-containing ladder PIM could be formed. Fortuitously, one such monomer has already been prepared during the research programme (Chapter 4.2.2): 6,6'-dithiol-3,3,3',3'-tetramethyl-1,1'-spirobisindane,[192] DTSBI (**Figure 4.8**).
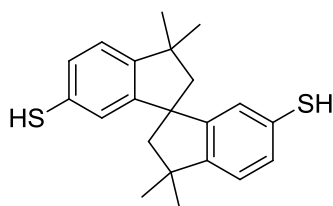
Figure 4.8 DTSBI, a potential ladder sPIM monomer.

Unfortunately, none of the halogenated monomers employed in **Scheme 4.33** are commercial, and the only relevant reference given in the paper by Freund *et al.*[216] is for the synthesis of the di-bromo monomer,[217] which is: '*not sufficiently reactive with respect to our nucleophilic aromatic substitutions*'.[216] At the time of writing, no published literature procedures for the di-chloro or di-fluoro monomers could be found, only di-bromo[217] or di-iodo.[218] Accordingly, a novel synthesis for a compatible di-chloro functionalised monomer, 1,4-dichloro-2,5-di(4'-methylbenzoyl)benzene, DCDMB, was designed (**Scheme 4.36**).
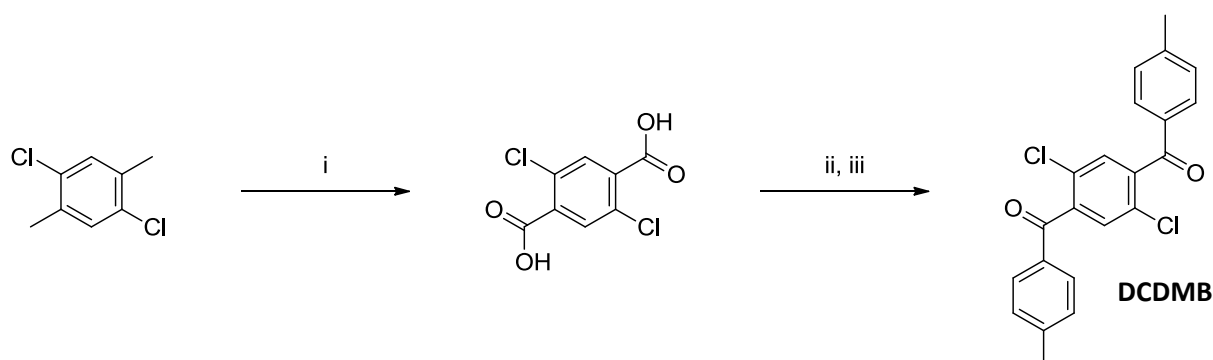
Scheme 4.36 Synthesis of 1,4-dichloro-2,5-di(4'-methylbenzoyl)benzene, DCDMB.
Reagents and conditions: I) KMnO$_4$, 18-crown-6, CHCl$_3$, pyridine, H$_2$O, reflux, 72 hrs, ii) SOCl$_2$, cyclohexane, DMF, iii) CHCl$_3$, Toluene, AlCl$_3$.

2,5-Dichloroterephthalic acid (**Scheme 4.36**) is commercially available, but is very expensive,[219] so it was therefore decided to begin the synthesis with the oxidation of 2,5-dichloro-*p*-xylene, a much cheaper precursor to 2,5-dichloroterephthalic acid. Many literature procedures[220-223] report complete conversion of the xylene to the di-acid utilising potassium permanganate in a refluxing mixture of pyridine and water. However, several attempts at repeating this proved unsuccessful, as large quantities of the mono-acid (**Figure 4.9)** remained, as determined by ^{1}H NMR and low resolution MS, even after several days refluxing employing multiple equivalents of potassium permanganate (**Table 4.7**).
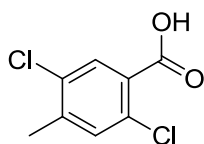
Figure 4.9 Mono-acid impurity found in large quantities when following literature procedures for the complete oxidation of 2,5-dichloro-*p*-xylene.

Though they could be separated through chloroform trituration, the mono-acid being more soluble than the di-acid, it was desirable to push the reaction further towards completion before attempting such purification. Thankfully, through the addition of chloroform and a *phase transfer catalyst*, 18-crown-6, which allowed for oxidation of the mono-acid to occur in the organic phase, this was found to be achievable (**Table 4.7**).

Solvent system	Concentration (mmol cm^{-3})	KMnO$_4$ (eq.)	Reaction time (hours)	Crude product	
				Mono-acid (%)	Di-acid (%)
Pyridine/H$_2$O: 4/1	0.3	5.5	24	62	38
Pyridine/H$_2$O: 4/1	0.3	7.5	48	61	39
Pyridine/H$_2$O: 4/1	0.3	10	72	61	39
Pyridine/H$_2$O/ CHCl$_3$: 4/1/2.5^a	0.2	10	24	3	97

Table 4.7 Summary of the oxidation of 2,5-dichloro-*p*-xylene to 2,5-dichlroterephthalic acid.
a) Reaction performed in the presence 18-crown-6 (10 mg).

Further purification of the 97 % pure di-acid could be achieved by repeated refluxing of the crude material in chloroform and discarding the soluble material, which contained a higher proportion of mono-acid compared to the insoluble material. Purities of approximately 99 % were achieved using this procedure.

Once a highly pure sample of the di-acid in **Scheme 4.36** was obtained, it was converted to DCDMB by *in-situ* generation of the di-acid chloride, *via* the DMF catalysed reaction with thionyl chloride, followed by subsequent Lewis acid-mediated Friedel-Crafts acylation with toluene (**Scheme 4.36**).[224] This step was found to proceed efficiently, although crude low resolution MS and ^{1}H NMR studies revealed the presence of a trace impurity in the form of the hydrolysed mono-substituted acid (**Figure 4.10**). However, this impurity was easily removed *via* methanol trituration to yield the monomer in near quantitative yield.
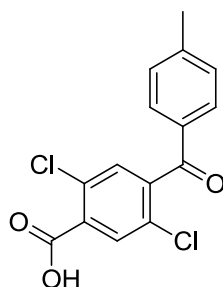
Figure 4.10 Hydrolysed mono-substituted acid – a trace impurity in the synthesis of DCDMB.

^{1}H NMR studies of methanol treated DCDMB revealed it to contain a mixture of regioisomers, in which the terminal methyl groups were either *ortho* or *para* to the ketone (**Figure 4.11**).
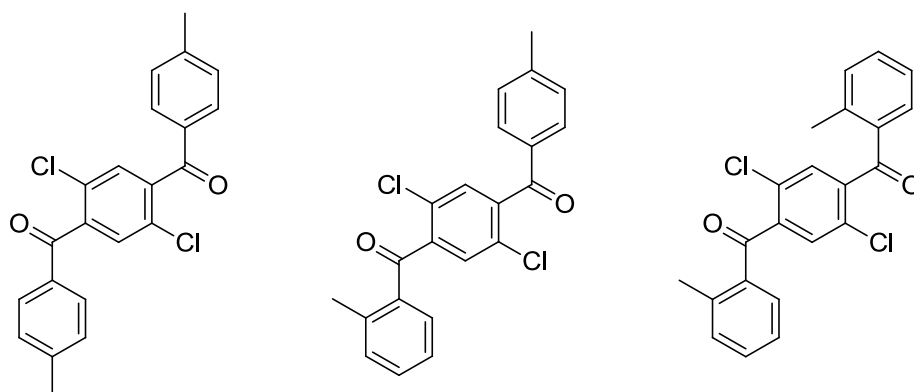
Figure 4.11 Three possible regioisomers of DCDMB; *para-para* (left), *ortho-para* (centre) and *ortho-ortho* (right).

Methanol treated reaction products contained approximately 83 % *para-para*, 16 % *ortho-para* and 1 % *ortho-ortho* products, as determined by comparison of the methyl integrals in ^{1}H NMR spectra. Recrystallisation of the methanol treated material from ethyl acetate yielded *para-para* material at approximately 97 % purity, this material was fully characterised by ^{1}H NMR, ^{13}C NMR, IR, high resolution MS and X-ray crystallography (**Figure 4.12**) to confirms its structure. Further purification was not required, as the presence of regioisomers was not anticipated to inhibit the subsequent polymerisation.
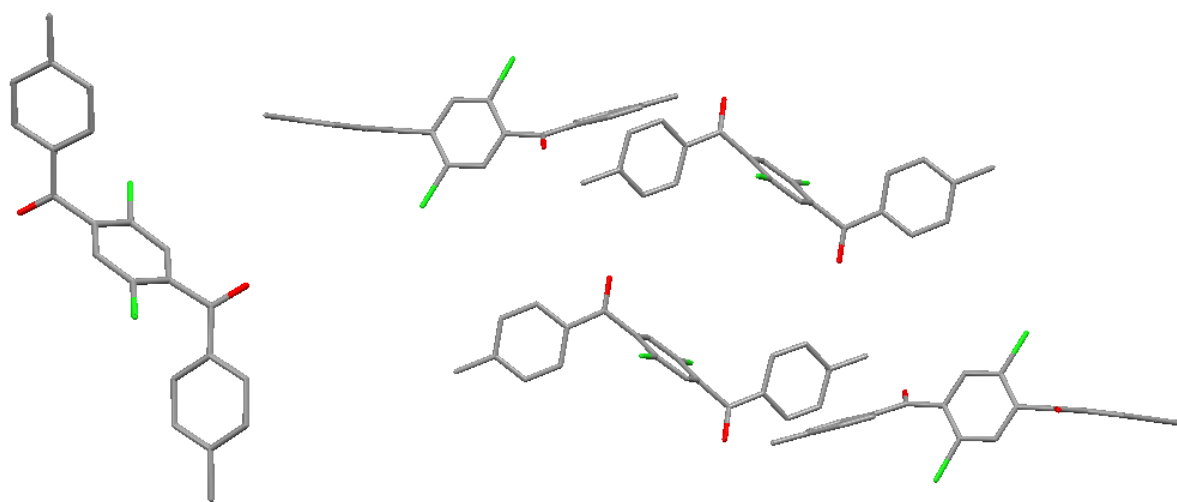
Figure 4.12 Crystal structure (left) and packing (right) of DCDMB showing *para-para* arrangement of the methyl groups. Crystals obtained *via* slow diffusion of methanol into chloroform solution. Protons and solvent molecules removed for clarity.

4.7 sPIM-2 synthesis

Based on the literature procedure by Freund *et al.*,[216] the polymerisation of DTSBI and DCDMB to give a polymer dubbed *sPIM-2-diketone* (**Scheme 4.37**) was investigated. A summary of the various reaction conditions employed and their outcomes is shown in **Table 4.8**.
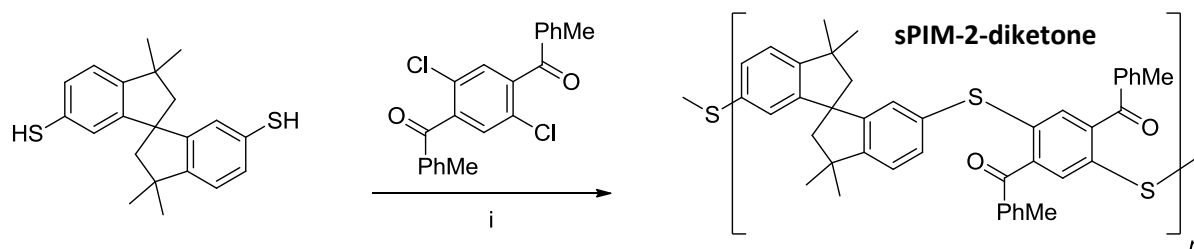
Scheme 4.37 Polymerisation of DTSBI and DCDMB to give sPIM-2-diketone.
Reagents and conditions: i) DMAC, K_2CO_3, 96 hrs, 115 °C.

Solvent	Concentration (mmol cm^{-3})	Scale (g)	Base (eq.)	Reaction temperature (°C)	Reaction time (hours)	Acetone treated M_W	Acetone treated PDI	Acetone treated Yield (%)
DMF	0.26	1.12	K$_2$CO$_3$ (3)	110	48	11212	1.273	14
DMSO	0.33	0.89	K$_2$CO$_3$ (4)	160	48	10315	1.922	48
DMAC	0.34	1.00	K$_2$CO$_3$ (2)	115	72	18198	1.321	34
DMAC	0.34	0.92	Cs$_2$CO$_3$ (2)	120	72	16587	1.411	31
DMAC[a]	0.35	1.90	K$_2$CO$_3$ (2)	150	72	11301	1.487	42
DMAC	0.89	0.95	K$_2$CO$_3$ (2)	180[b]	3	8707	1.616	19
DMAC	0.92	1.26	K$_2$CO$_3$ (2)	120	96	19545	1.561	35
DMAC	0.95	1.19	Cs$_2$CO$_3$ (2)	120	96	17653	1.782	33
DMSO	1.35	1.36	K$_2$CO$_3$ (2)	160	72	15416	1.896	41
DMSO[c]	0.96	1.11	K$_2$CO$_3$ (1.5)	95	72	10717	2.49	46
DMAC	1.18	1.13	K$_2$CO$_3$ (1)	110	96	15574	1.681	47
DMAC	1.67	1.51	K$_2$CO$_3$ (1)	120	48	18186	1.791	58
DMAC	1.74	2.26	K$_2$CO$_3$ (1)	120	48	23512	1.534	21
DMAC	1.62	4.10	K$_2$CO$_3$ (1)	115	96	24997	1.335	27

Table 4.8 Summary of the sPIM-2-diketone polymerisation attempts.
a) Reaction performed with 2 equivalents of KF, b) Microwave assisted c) Toluene co-solvent.

Following a typical aqueous work up, the first sPIM-2-diketone polymerisation attempt yielded crude reaction products in near quantitative yield. However, GPC analysis revealed a bimodal distribution (**Figure 4.13**) indicating the presence of some low molecular weight impurities, likely to be *cyclics,*[216] in which short polymer chains *loop round* and react with themselves.

Peak RV - (ml)	18.167	20.133
Mn - (Daltons)	5,986	1,194
Mw - (Daltons)	11,113	1,227
Mz - (Daltons)	19,424	1,259
Mp - (Daltons)	7,813	1,239
Mw / Mn	1.857	1.028
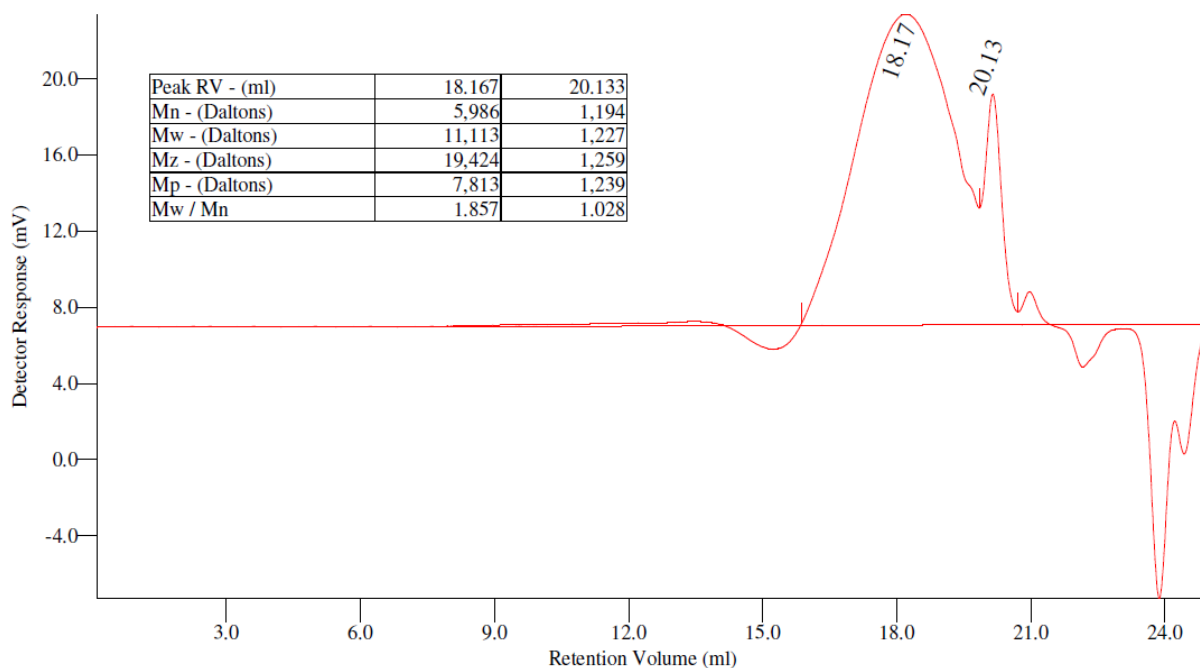
Figure 4.13 GPC trace and relevant data (inset) for the crude reaction products from the polymerisation of sPIM-2-diketone showing bimodal distribution.

Treatment of the crude reaction products with acetone was found to remove the low molecular weight material, leading to a unimodal GPC trace. Each subsequent sPIM-2 polymerisation attempt was accordingly treated with acetone as part of the work up, leading to significantly less than quantitative yields (**Table 4.8**). MALDI-MS analysis of the acetone soluble material confirmed the presence of cyclics (**Figure 4.14**).
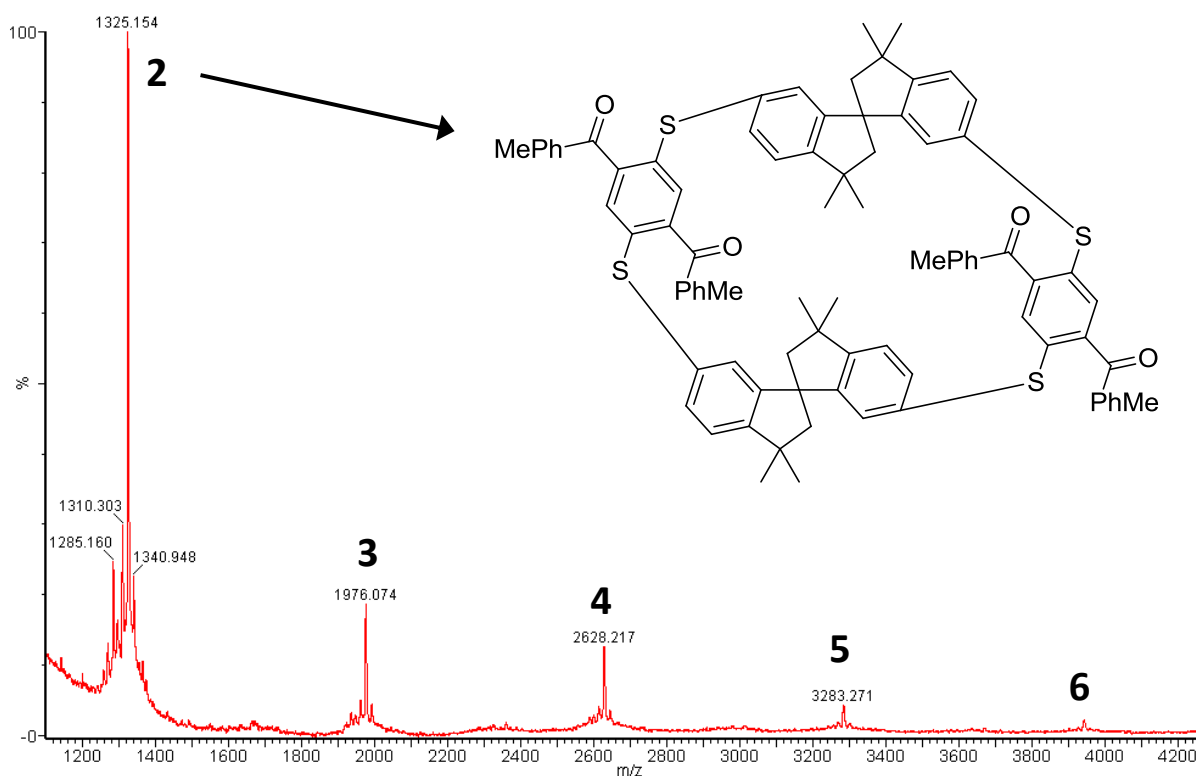
Figure 4.14 MALDI mass spectrum of the acetone soluble material produced during sPIM-2-diketone formation, showing cyclic dimer (inset structure) to hexamer mono-sodium adducts.

Unfortunately, none of the attempted polymerisations yielded equally high molecular weight material compared with the results obtained by Freund *et al.* (M_w up to 380,000).[216] However, given the geometric structure of the dithiol monomer (DTSBI), and the flexibility of the short polymer chains in solution, it is hypothesised that the low molecular weights obtained in **Table 4.8** are due to inevitable cyclic formation during the reaction. Evidence for this can be seen in the fact that at least 50 % of the crude reaction products are small cyclics removed by acetone treatment, indicating that cyclic formation is extensive, regardless of concentration. Re-precipitation of acetone treated sPIM-2-diketone, *via* the dropwise addition of a concentrated chloroform solution into acetone, allowed for some improvement, M_W up to 35,000 (**Figure 4.15**), but this came with the unavoidable side-effect of further diminishing the yield. BET analysis of the high molecular weight material revealed it to be non-porous (**Figure 4.16**), as expected due to the non-rigid, single-stranded nature of the polymer.
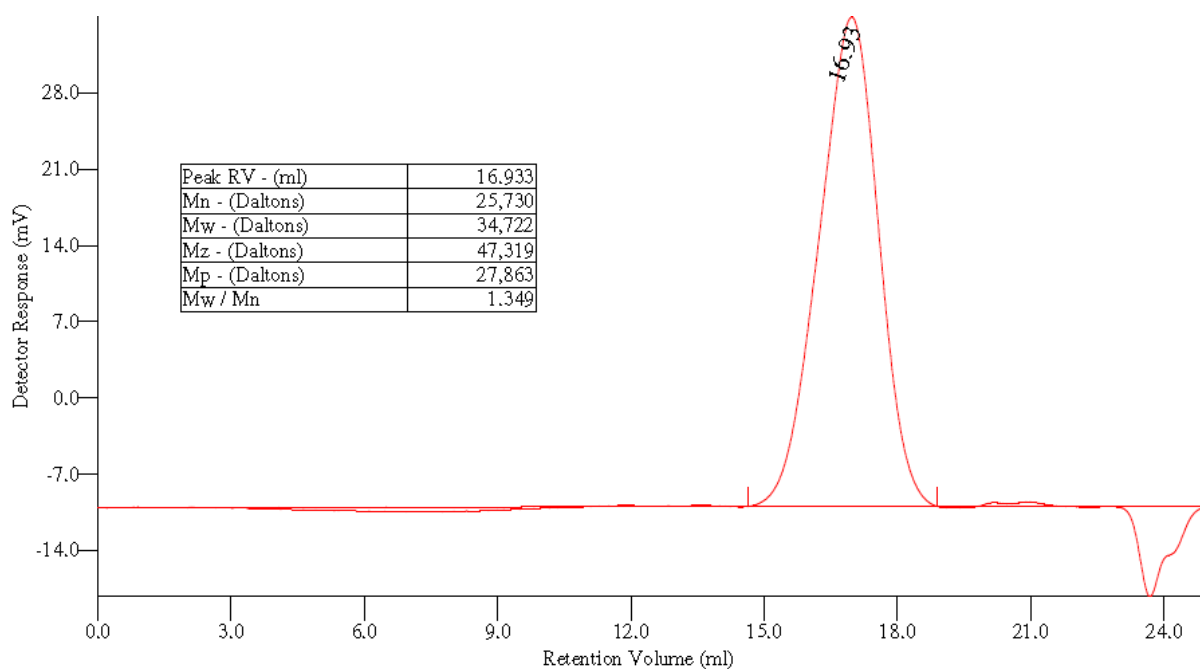
Figure 4.15 GPC trace and relevant data (inset) of re-precipitated sPIM-2-diketone.

Reduction and subsequent cyclisation of sPIM-2-diketone to sPIM-2, *via* sPIM-2-diol (**Scheme 4.38**), was achieved according to the similar procedure by Freund *et al.*.[216]
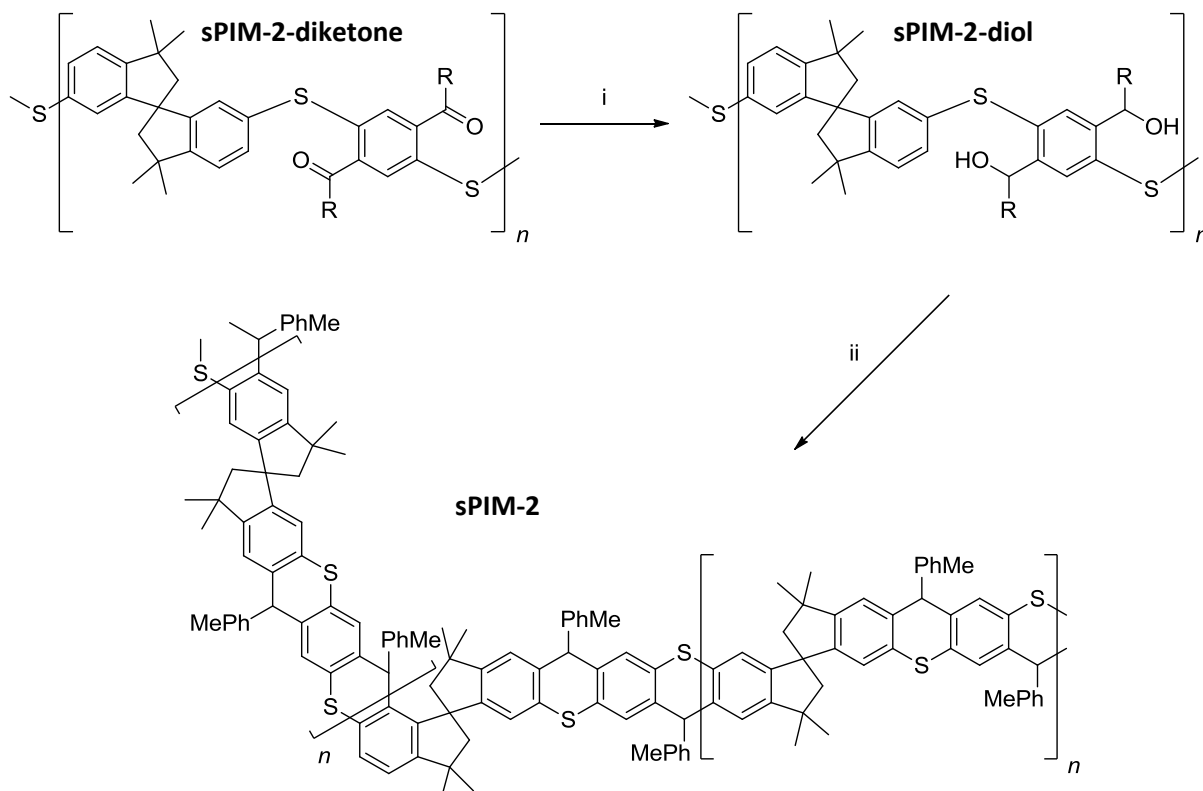
Scheme 4.38 sPIM-2-diketone reduction to give sPIM-2-diol and subsequent cyclisation to give sPIM-2. Due to two possible sites of cyclisation, the structure of sPIM-2 is likely to contain *kinks*.
Reagents and conditions: i) LiAlH$_4$, THF, RT, 6 hrs, ii) SnCl$_4$, CHCl$_3$, 3 hrs, RT.

151

Both the intermediate sPIM-2-diol and fully cyclised sPIM-2 were isolated in near quantitative yields and fully characterised by ^{1}H NMR, ^{13}C NMR, IR and GPC, all of which indicated complete conversion without loss of molecular weight. BET nitrogen sorption data of sPIM-2 and its polymeric precursors are shown below in **Figure 4.16** and **Table 4.9** alongside PIM-1 and other sPIMs produced in this chapter for comparison.
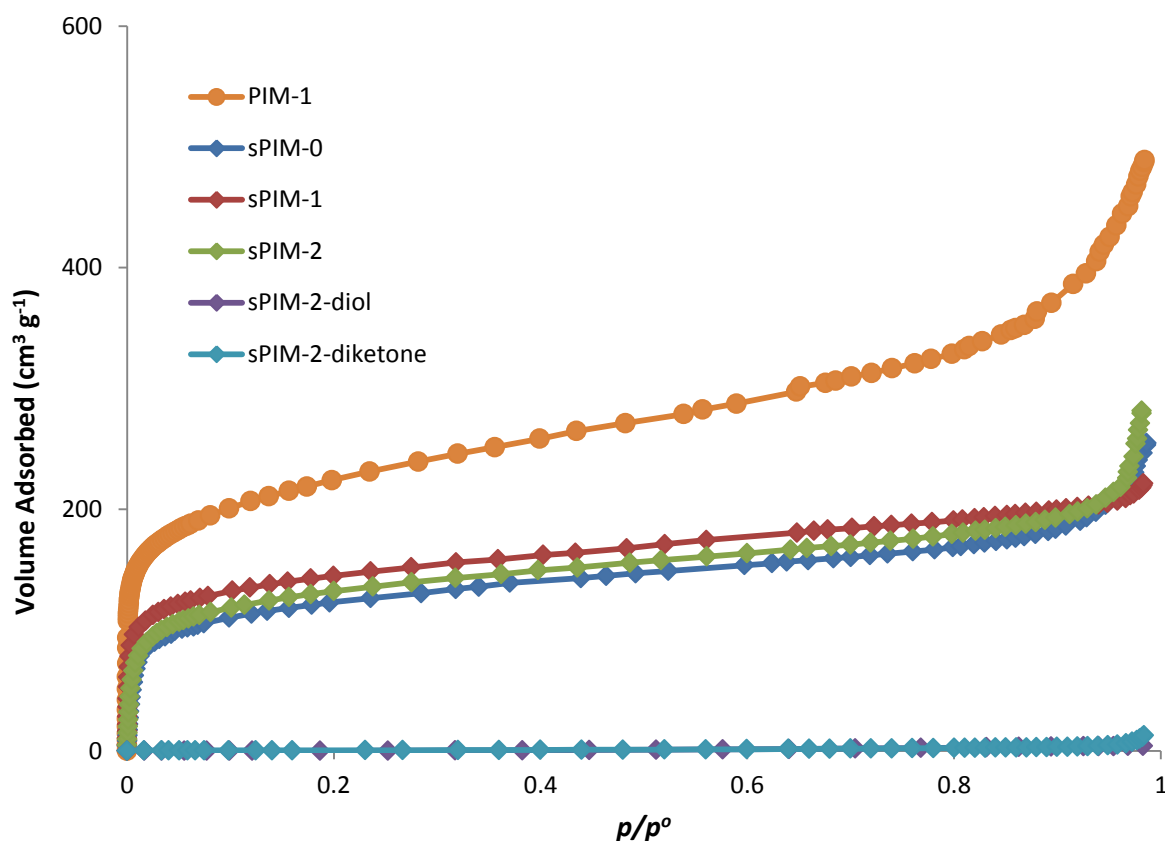
Figure 4.16 BET nitrogen adsorption isotherms for all sulfur based PIMs and PIM-1 for comparison. Desorption plots removed for clarity.

PIM	BET surface area (m^2 g^{-1})	Total Pore Volume (cm^3 g^{-1})
PIM-1	796[a]	0.50[a]
sPIM-0	438	0.38
sPIM-1	510	0.34
sPIM-2	470	0.43
sPIM-2-diol	0	0.01
sPIM-2-diketone	2	0.02

Table 4.9 BET nitrogen sorption data for all sulfur based PIMs and PIM-1 for comparison.
a) Data supplied by Dr. Kadhum Msayib.

The results for sPIM-2 and its two precursors offer an excellent demonstration of how essential rigidity is in the formation of microporous polymers. Single-stranded polymers, those with just a single bond between each monomer (sPIM-2-diketone and sPIM-2-diol), are able to organise themselves in a manner equivalent to efficient packing, whilst the corresponding ladder polymer, sPIM-2, is unable to do so, hence inefficient packing and consequent porosity.

4.8 Summary and conclusions (sPIMs)

Four novel monomers were synthesised and subsequently polymerised to give three novel sulfur containing polymers of intrinsic microporosity (sPIMs). All three were found to be microporous, possessing apparent BET surface areas in the range 438 – 510 m^2 g^{-1}. Solubilities of sPIM-0 and sPIM-1 were found to be poor, even when polymerisations were performed at high dilutions (in an attempt to limit cross-linking), so no further studies on post-polymerisation oxidation were carried out. sPIM-2 was found to be highly soluble in common organic solvents (DCM, chloroform) however, due to the shape and single-stranded nature of the initial (sPIM-2-diketone) polymer, cyclic formation was highly prevalent. This limited the molecular weight of the resultant sPIM-2 polymer (M_w: 34,700, PDI: 1.35) meaning that a free standing membrane was not be formed.

As demonstrated in **Figure 4.16**, all three sPIMs give rise to very similar isotherms and consequently similar degrees of microporosity, suggesting that the bulk structures of the polymers are similar. This is unsurprising considering each contains a spirobisindane unit adjacent to a six membered ring comprising of one or two sulfur atoms. However, each is significantly less microporous than the archetypical PIM-1, a trait that recent simulations suggest is likely due to the non-planar nature of the thianthrene units, leading to more efficient packing of the polymer chains.[205]

5. Experimental

5.1 Experimental techniques

General remarks

Commercially available reagents were used without further purification, with the exception of TCTPN (Sigma-Aldrich) which was recrystallised from acetone prior to use. Unless otherwise stated all reactions were carried out under an inert atmosphere of dry nitrogen gas (passed over anhydrous copper sulfate crystals). Oven-dried glassware was left in a 100 °C oven for at least 2 hrs and cooled under dry nitrogen flow prior to use. Anhydrous solvents were obtained *via* distillation over calcium hydride (DCM), drying over well activated molecular sieves (THF), purchased from Sigma-Aldrich (DMF) or from a solvent purification system (diethyl ether, toluene).

Column chromatography was performed over a silica gel (pore size 60 Å, particle size 40 – 63 μm) stationary phase. *Reducing* refers to the process of removing solvent(s) on a rotary evaporator connected to a diaphragm pump, *drying under vacuum* refers to the thorough drying of reduced samples in a vacuum oven.

Melting points (mp)

Melting points were recorded using a *Gallenkamp Melting Point* apparatus and are uncorrected.

Infrared spectra (IR)

Infrared adsorption spectra were recorded in the range 4000 – 400 cm^{-1} using a Perkin-Elmer 660 plus FTIR instrument, either as a thin film or nujol mull between sodium chloride plates.

Nuclear Magnetic Resonance (NMR)

^{1}H NMR spectra were recorded in a suitable deuterated solvent using an Avance Bruker DPX 400 instrument (400 MHz) or an Avance Bruker DPX 500 instrument (500 MHz). ^{13}C NMR spectra were recorded on the same machines at 100 MHz or 125 MHz respectively. ^{13}C-^{19}F

coupling was observed in fluorinated compounds, but not assigned, due to the large coupling constants leading to ambiguity between coupled and discrete peaks. ^{19}F NMR spectra were recorded on a Jeol JNM-ECP 300 instrument (300 MHz) at 282 MHz. Chemical shifts (δ) were recorded in parts per million (ppm) and corrected according to solvent peaks listed in **Table 5.1**.

Solvent	Formula	[1]H Corrected δ	[13]C Corrected δ
Acetone-d_6	$(CD_3)_2CO$	2.05	29.90, 206.68
Chloroform-d	$CDCl_3$	7.24	77.23
Deuterium oxide	D_2O	4.80	-
DMSO-d_6	$(CD_3)_2SO$	2.50	39.51
Methanol-d_4	CD_3OD	3.31	49.15
THF-d_8	$(CD_2)_4O$	1.72, 3.58	25.37, 67.57

Table 5.1 Corrected ^{1}H and ^{13}C chemical shifts of employed deuterated solvents.

Multiplicity is reported as singlet (*s*), doublet (*d*), doubled-doublet (*dd*), doubled-triplet (*dt*), triplet (*t*), quartet (*q*), pentet (*p*) or multiplet (*m*). Broad or complex peaks are further labelled *br* or *complex* respectively. Coupling constants (*J*) are quoted in Hz.

Mass spectrometry

Small molecule (MW < 1000 g mol^{-1}) low-resolution mass spectrometric (LRMS) and high resolution mass spectrometric (HRMS) data were obtained using a Waters GCT Premier E1 instrument, utilising either electron impact (EI) or electrospray (ES) ionisation. Large molecule (MW ≥ 1000 g mol^{-1}) low-resolution mass spectrometric data were obtained using a Waters Micromass Q-Tof micro mass spectrometer, utilising matrix assisted laser desorption ionisation (MALDI) and calibrated to poly-ethylene glycol standards (MW 1000 – 3000 g mol^{-1}).

BET surface areas

Low-temperature (77 K) nitrogen adsorption/desorption isotherms were obtained using a Coulter SA3100 surface area analyser. Accurately weighed samples of roughly 0.10 g were degassed for 15 hrs at 135 °C under high vacuum prior to analysis.

Thermo-Gravimetric Analysis (TGA)

Thermo-gravimetric analyses were performed on a Thermal Analysis SDT Q600 system, heating samples at a rate of 10 °C/min from room temperature (RT) to 1000 °C.

Elemental analysis (EA)

Elemental analyses were performed by MEDAC Ltd.

X-Ray crystal structure determination

Single crystal X-ray structures were recorded either at Cardiff University using a Bruker-Nonius Kappa CCD area-detector diffractometer equipped with an Oxford Cryostream low temperature cooling device operating at 150(2) K (λ = 0.71073 Å), or at station I19 of the Diamond Light Source using synchrotron radiation and a Rigaku Satum 724 CCD diffractometer (graphite monochromated radiation). All structures were solved by direct methods and all calculations were carried out using the SHELX-97 package.

Gel permeation chromatography (GPC)

Gel permeation chromatography (GPC) analyses were performed on chloroform solutions (1 mg ml^{-1}) using a GPC MAX variable loop equipped with two KF-805L SHODEX columns and a RI(VE3580) detector, operating at a flow rate of 1 ml min^{-1}. Calibration was achieved using Viscotek polystyrene standards (M_w 1000 – 1,000,000 g mol^{-1}).

Due to the linear nature of the calibration standards, analysis of large, non-linear materials often results in an underestimation of molecular weight.[225] As such, M_w and M_n values reported for large OMIMs and DIMs are often substantially lower than the expected values.

5.2 Experimental procedures

5.2.1 Precursors

4,4'-Dicyano-2,2',3,3',5,5',6,6'-octafluorobiphenyl and **4,4',4''-tricyano-2,2',2'',3,3'',5,5',5'',6,6',6''-undecafluoro-[1,1':3',1''-terphenyl]**
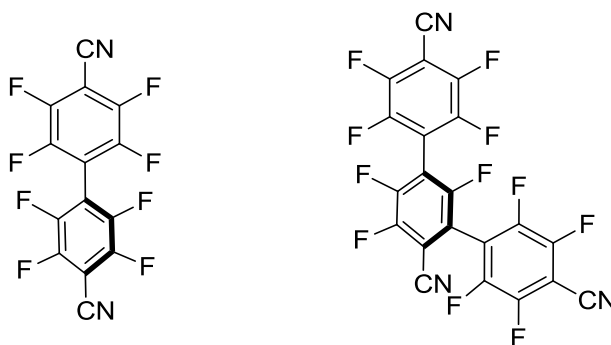
According to the literature procedure by Kaneko,[143] hexaethylphosphorous triamide (6.40 g, 25.9 mmol) was added dropwise to a solution of pentafluorobenzonitrile (10.0 g, 51.8 mmol) in anhydrous diethyl ether (30 ml). The reaction mixture was stirred for 3 hrs at RT and the resultant deep-red solution concentrated under reduced pressure. The crude reaction products were purified by column chromatography (hexane/DCM 3/2) to give the following:

4,4'-Dicyano-2,2',3,3',5,5',6,6'-octafluorobiphenyl: (R_f = 0.5, 3.05 g, 34 %) as a white powder (mp 108 – 110 °C, literature mp 129 – 131 °C[226]); IR (DCM film) 2251, 1490, 1291, 1266, 1001 cm^{-1}; ^{19}F NMR (282 MHz, CDCl$_3$) δ -129.4 – -129.6 (4F, m, ArF), -133.3 – -133.4 (4F, m, ArF) [literature ^{19}F NMR (CDCl$_3$) δ -129.8 (4F), -133.7 (4F)[227]]; ^{13}C NMR (125 MHz, CDCl$_3$) δ 149.0 – 148.7 (m), 146.3 – 146.1 (m), 145.5 – 145.3 (m), 143.0 – 142.9 (m) 112.0 – 111.8 (m), 106.7, 97.6 – 97.3 (m) (^{19}F-^{13}C coupling not assigned); HRMS (EI$^+$, *m/z*) calc. for C$_{14}$F$_8$N$_2$: 347.9934 (M$^+$), found 347.9932. Crystallography data (methanol): Monoclinic, space group: P2$_1$/n, *a* = 10.2692(9) Å, *b* = 11.2116(15) Å, *c* = 22.236(3) Å, β = 93.097(7), *V* = 2556.38 Å^3, *Z* = 8, R_1 = 9.64.

4,4',4''-Tricyano-2,2',2'',3,3'',5,5',5'',6,6',6''-undecafluoro-[1,1':3',1''-terphenyl]: (R_f = 0.4, 0.56 g, 6 %) as a white powder (mp 194 – 196 °C); IR (DCM film) 2247, 1494, 1470, 1312, 1263, 1032 cm^{-1}; ^{19}F NMR (282 MHz, CDCl$_3$) δ -109.3 – -109.4 (1F, m, ArF), -124.9 – -125.1

(1F, m, Ar*F*), -131.3 – -131.5 (1F, m, Ar*F*), -133.4 – -133.5 (2F, m, Ar*F*), -133.6 – -133.7 (2F, m, Ar*F*), -136.2 – -136.3 (2F, m, Ar*F*), -136.8 – -136.9 (2F, m, Ar*F*); ^{13}C NMR (125 MHz, CDCl$_3$) δ 153.9 – 153.8 (m), 151.9 – 151.8 (m), 148.8 – 148.6 (m), 146.7 – 146.5 (m), 145.4 – 145.2 (m), 143.4 – 143.2 (m), 115.0 – 114.7 (m), 114.2 – 114.0 (m), 112.0 – 111.6 (m), 109.5 – 109.4 (m), 107.7 – 107.6 (m), 106.7 – 106.6 (m), 97.9 – 97.6 (m) (^{19}F-^{13}C coupling not assigned); HRMS (EI$^+$, *m/z*), calc. for C$_{21}$F$_{11}$N$_3$: 502.9917 (M$^+$), found 502.9925. Crystallography data (propan-2-ol): Monoclinic, space group: P2$_1$/c, *a* = 14.1204(16) Å, *b* = 9.0370(11) Å, *c* = 15.4785(16) Å, β = 107.275(7), *V* = 1886.05 Å^3, *Z* = 4, *R$_1$* = 7.74.

6-*tert*-Butylnaphthalene-2,3-diol
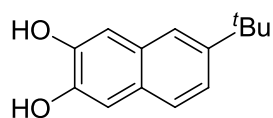
tert-Butanol (1.00 ml, 17.3 mmol) was added dropwise to a suspension of naphthalene-2,3-diol (2.77 g, 17.3 mmol) in trifluoroacetic acid (50 ml) and stirred for 72 hrs at RT. After quenching with water (250 ml), the precipitate was filtered, washed with water (500 ml) and dried under vacuum to give 6-*tert*-butylnaphthalene-2,3-diol (3.11 g, 84 %) as a white powder (mp 160 – 162 °C, literature mp 159 – 160 °C[228]); IR (DCM film) 3434, 2961, 2867, 1523, 1429, 1267, 1165, 1114 cm^{-1}; ^{1}H NMR (400 MHz, (CD$_3$)$_2$SO) δ 9.42 (1H, s, O*H*), 9.39 (1H, s, O*H*), 7.50 – 7.46 (2H, m, Ar*H*), 7.27 (1H, dd, *J* = 8.6, 1.8 Hz, Ar*H*), 7.05 (2H, d, *J* = 13.1 Hz, Ar*H*), 1.32 (9H, s, ^{t}Bu*H*); ^{13}C NMR (125 MHz, (CD$_3$)$_2$SO) δ 146.7, 146.2, 144.9, 128.6, 126.7, 125.2, 121.5, 120.5, 109.7, 109.1, 34.1, 31.1; HRMS (EI$^+$, *m/z*) calc. for C$_{14}$H$_{16}$O$_2$: 216.1150 (M$^+$), found 216.1152.

6-(1-Adamantyl)naphthalene-2,3-diol
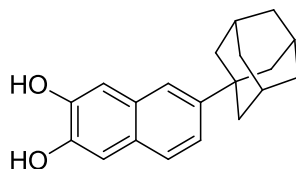
According to the literature procedure by Stepakov *et al.*,[146] adamantan-1-ol (1.13 g, 7.43 mmol) was added portionwise to a suspension of naphthalene-2,3-diol (1.19 g, 7.43 mmol) in trifluoroacetic acid (30 ml) and stirred for 12 hrs at RT. After quenching with water (200

ml), the precipitate was filtered, washed with water (300 ml) and dried under vacuum to give 6-(1-adamantyl)naphthalene-2,3-diol (1.98 g, 91 %) as a white powder (mp 208 – 210 °C, literature mp 210 – 212 °C[146]); IR (DCM film) 3417, 2900, 2847, 1522, 1429, 1269, 1246 cm^{-1}; ^{1}H NMR (400 MHz, (CD$_3$)$_2$SO) δ 9.39 (2H, br s, O*H*), 7.48 (1H, d, *J* = 8.6 Hz, Ar*H*), 7.41 (1H, s, Ar*H*), 7.26 (1H, d, *J* = 8.6 Hz, Ar*H*), 7.07 (1H, s, Ar*H*), 7.03 (1H, s, Ar*H*), 2.08 – 2.06 (3H, m, Ad*H*), 1.91 – 1.90 (6H, m, Ad*H*), 1.75 (6H, s, Ad*H*); ^{13}C NMR (100 MHz, (CD$_3$)$_2$SO) δ 146.8, 146.4, 145.3, 128.7, 126.9, 125.3, 120.9, 120.5, 109.8, 109.1, 42.7, 36.3, 35.6, 28.4; LRMS (EI$^+$, *m/z*) calc. for C$_{20}$H$_{22}$O$_2$: 294.16 (M$^+$), found 294.16.

2,3,6,7-Tetramethoxy-9,10-diethylanthracene
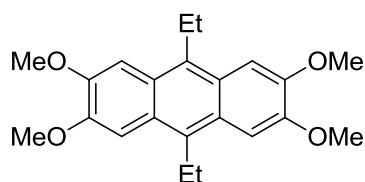
Based on the literature procedure by Shklyaev,[170] a solution of veratrole (27.6 g, 200 mmol) and propanal (29.0 g, 500 mmol) was added dropwise to 36N H$_2$SO$_4$ (200 ml) whilst maintaining a reaction temperature of 0 – 5 °C. The reaction mixture was then stirred for 3 hrs at RT, quenched with water (500 ml) and neutralised with 35 % aqueous ammonia solution. After cooling, the product was extracted into DCM (3 x 200 ml), washed with water (3 x 200 ml) and brine (100 ml), concentrated under reduced pressure and treated with boiling ethanol (250 ml) for 2 hrs to give 2,3,6,7-tetramethoxy-9,10-diethylanthracene (15.7 g, 44 %) as a yellow powder (mp 238 – 240 °C, literature mp 232 – 234 °C[73]); IR (DCM film) 2950, 2863, 2831, 1635, 1535, 1497, 1435, 1241, 1202, 1168 cm^{-1}; ^{1}H NMR (400 MHz, CDCl$_3$) δ 7.39 (4H, s, Ar*H*), 4.06 (12H, s, OC*H*$_3$), 3.45 (4H, q, *J* = 7.6 Hz, C*H*$_2$), 1.43 (6H, t, *J* = 7.6 Hz, C*H*$_3$); ^{13}C NMR (400 MHz, CDCl$_3$) δ 149.3, 131.0, 125.4, 102.7, 56.1, 22.3, 14.9; LRMS (EI$^+$, *m/z*) calc. for C$_{22}$H$_{26}$O$_4$: 354.18 (M$^+$), found 354.16.

4,5-Dimethoxybenzenediazonium-2-carboxylate chloride
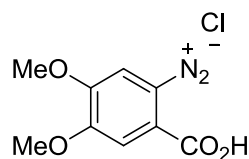
According to the literature procedure by Klanderman *et al.*,[148] 12N HCl (5 ml) was added to a suspension of 4,5-dimethoxyanthranilic acid (7.37 g, 37.4 mmol) in ethanol (250 ml) at 0 °C, followed by isoamyl nitrite (9.00 ml, 67.0 mmol). After stirring for 15 mins at RT, diethyl ether (250 ml) was added and the suspension stirred for a further 15 mins, filtered, washed with diethyl ether (300 ml) and dried under suction/nitrogen flow to give 4,5-dimethoxybenzenediazonium-2-carboxylate chloride (9.69 g, 97 %) as a light brown solid; ^{1}H NMR (400 MHz, D$_2$O) δ 8.04 (1H, s, Ar*H*), 7.79 (1H, s, Ar*H*), 4.10 (3H, s OC*H*$_3$), 3.98 (3H, s, OC*H*$_3$); ^{13}C NMR (400 MHz, D$_2$O) δ 163.6, 159.4, 152.2, 131.6, 115.2, 114.6, 102.8, 57.9, 57.5.

2,3,6,7,13,14-Hexamethoxy-9,10-diethyltriptycene
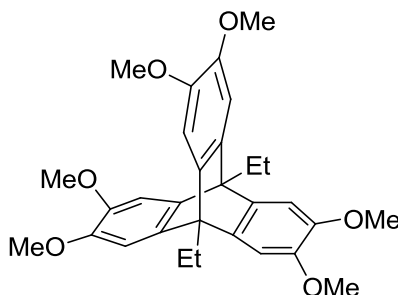
Based on the procedure by Ghanem *et al.*,[73] 1,2-epoxypropane (20 ml, 286 mmol) and freshly prepared 4,5-dimethoxybenzenediazonium-2-carboxylate chloride (14.9 g, 60.9 mmol) were added to a solution of 2,3,6,7-tetramethoxy-9,10-diethylanthracene (7.25 g, 20.7 mmol) in DCE (200 ml). The reaction mixture was refluxed for 24 hrs, cooled to RT and reduced. The resulting crude oil was purified by column chromatography (hexane/ethyl acetate 1/1, R_f = 0.3) and treated with methanol (50 ml) to give 2,3,6,7,13,14-hexamethoxy-9,10-diethyltriptycene (3.23 g, 32 %) as a white powder (mp 188 – 190 ° C, literature mp 274 – 276 °C[73]); IR (DCM film) 2936, 2851, 1582, 1486, 1404, 1274, 1154, 1046 cm^{-1}; ^{1}H NMR (500 MHz, CDCl$_3$) δ 6.98 (6H, s, Ar*H*), 3.83 (18H, s, OC*H*$_3$), 2.96 (4H, q, *J* = 7.1 Hz, C*H*$_2$), 1.66 (6H, t, *J* = 7.1 Hz, C*H*$_3$); ^{13}C NMR (500 MHz, CDCl$_3$) δ 145.5, 142.1, 107.8, 56.5, 52.9, 20.4, 11.3; LRMS (EI$^+$, *m/z*) calc. for C$_{30}$H$_{34}$O$_6$: 490.24 (M$^+$) found 490.25.

9,10-Diethyltriptycene-2,3,6,7,13,14-hexaol
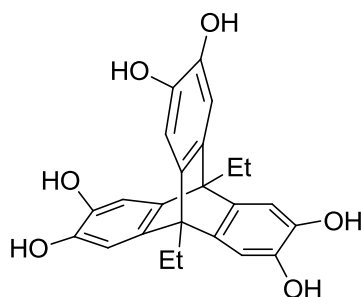
Based on the procedure of Ghanem *et al.*,[73] boron tribromide (0.64 ml, 6.63 mmol) was added dropwise to a solution of 2,3,6,7,13,14-hexamethoxy-9,10-diethyltriptycene (0.65 g, 1.32 mmol) in anhydrous DCM (15 ml) at 0 °C. After stirring for 4 hrs at RT, the resultant suspension was re-cooled to 0 °C, carefully quenched with ice water (20 ml) and then stirred vigorously under heavy nitrogen flow for 20 mins to remove the DCM. The crude product was then extracted into ethyl acetate (3 x 20 ml), washed with water (3 x 50 ml) and brine (50 ml), reduced to ~ 10 ml and re-precipitated by dropwise addition of hexane. The precipitate was filtered, washed with hexane (50 ml) and dried under suction/nitrogen flow to give 9,10-diethyltriptycene-2,3,6,7,13,14-hexaol (0.42 g, 77 %) as a white powder (mp decomposes over 210 °C, literature mp > 300 °C[73]); IR (DCM film) 3412, 1640, 1483, 1446, 1296, 1227 cm^{-1}; ^{1}H NMR (400 MHz, CD$_3$OD) δ 6.79 (6H, s, ArH), 2.72 (4H, q, J = 7.0 Hz, CH_2) 1.61 (6H, t, J = 7.0 Hz, CH_3); ^{13}C NMR (500 MHz, CD$_3$OD) δ 141.6, 111.5, 53.1, 21.5, 11.6 (one carbon missing); LRMS (EI$^+$, *m/z*) calc. for C$_{24}$H$_{22}$O$_6$: 406.14 (M$^+$), found 406.13.

2,3-Dimethoxytriptycene
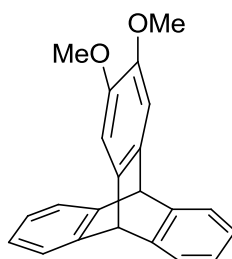
Based on the literature procedure by Peng *et al.*,[147] 1,2-epoxypropane (30 ml, 429 mmol) and freshly prepared 2-carboxy-4,5-dimethoxybenzenediazonium chloride (12.5 g, 51.1 mmol) were added to a solution of anthracene (3.43 g, 19.2 mol) in DCE (250 ml). The reaction mixture was heated to reflux for 24 hrs and cooled to RT. The crude product was

then purified by column chromatography (DCM/hexane 1/1, R_f = 0.3) and triturated in methanol (50 ml) for 2 hrs to give 2,3-dimethoxytriptycene (2.11 g, 35 %) as a white powder (mp 183 – 185 °C, literature mp 181 – 183 °C[229]); IR (DCM film) 3064, 3002, 2955, 2830, 1501, 1460, 1294, 1265, 1190, 1154, 1082 cm^{-1}; ^{1}H NMR (400 MHz, CDCl$_3$) δ 7.36 (4H, dd, J = 5.3, 3.2 Hz, ArH), 7.01 (2H, s ArH), 6.97 (4H, dd, J = 5.3, 3.2 Hz, ArH), 5.34 (2H, s, ArH), 3.82 (6H, s, OCH_3); ^{13}C NMR (125 MHz, CDCl$_3$) δ 146.3, 145.9, 138.3, 125.2, 123.5, 108.9, 56.4, 54.0; LRMS (EI$^+$, m/z) calc. For C$_{22}$H$_{18}$O$_2$: 314.13 (M$^+$), found 314.12.

Triptycene-2,3-diol
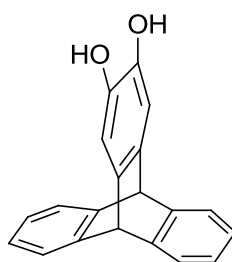
Based on the literature procedure by Peng *et al.*,[147] boron tribromide (0.47 ml, 4.88 mmol) was added dropwise to a solution of 2,3-dimethoxytriptycene (1.02 g, 3.24 mmol) in anhydrous DCM (10 ml) at 0 °C. After stirring for 10 mins at 0 °C and 3 hrs at RT, the reaction was re-cooled to 0 °C and quenched by dropwise addition of ice water (20 ml). After stirring for 15 mins, the organic phase was collected, washed with water (3 x 20 ml) and brine (20 ml) and dried over anhydrous magnesium sulfate. The product was then afforded as a precipitate by dropwise addition of hexane, filtered and dried under suction/nitrogen flow to give triptycene-2,3-diol (0.76 g, 82 %) as a white powder (mp 242 – 248 °C with decomposition, literature mp decomposed over 80 °C[147]); IR (DCM film) 3237, 2957, 1687, 1502, 1458, 1306 cm^{-1}; ^{1}H NMR (400 MHz, (CD$_3$)$_2$CO) δ 7.56 (2H, br s, OH), 7.37 (4H, dd, J = 5.3, 3.2, ArH), 6.97 (2H, s, ArH), 6.94 (4H, dd, J = 5.3, 3.2, ArH), 5.41 (2H, s, CH); ^{13}C NMR (125 MHz, (CD$_3$)$_2$CO) δ 147.4, 142.3, 138.4, 125.6, 124.1, 112.8, 54.2; LRMS (EI$^+$, m/z) calc. for C$_{20}$H$_{14}$O$_2$: 286.10 (M$^+$), found 286.10.

2,6-Di-*tert*-butylanthracene
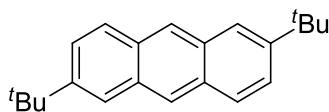
According to the literature procedure by Herron *et al.*,[149] *tert*-butanol (10.8 g, 146 mmol) was added dropwise to a suspension of anthracene (7.13 g, 40.0 mmol) in trifluoroacetic acid (40 ml). After refluxing for 24 hrs the resulting precipitate was filtered, washed with water (400 ml) and dried under suction. The crude solid was then triturated in methanol (50 ml) for 3 hrs to give 2,6-di-*tert*-butylanthracene (3.60 g, 31 %) as a white solid (mp 250 – 252 °C, literature mp 250.2 °C[230]); IR (DCM film) 3055, 2967, 2867, 1365, 1265 cm^{-1}; ^{1}H NMR (400 MHz, CDCl$_3$) δ 8.31 (2H, s, Ar*H*), 7.92 (2H, d, *J* = 8.9 Hz, Ar*H*), 7.85 (2H, d, *J* = 1.9 Hz, Ar*H*), 7.53 (2H, dd, *J* = 8.9, 1.9 Hz, Ar*H*), 1.44 (18H, s, ^{t}Bu*H*); ^{13}C NMR (125 MHz, CDCl$_3$) δ 147.5, 131.8, 130.7, 128.0, 125.6, 125.0, 122.5, 36.1, 31.2; LRMS (EI$^+$, *m/z*) calc. for C$_{22}$H$_{26}$: 290.20 (M$^+$), found 290.20.

2,3-Dimethoxy-7,14-di-*tert*-butyltriptycene
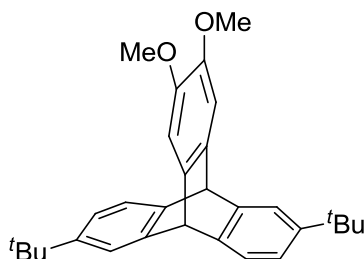
1,2-epoxypropane (35 ml, 500 mmol) and freshly prepared 4,5-dimethoxybenzenediazonium-2-carboxylate chloride (13.0 g, 50.9 mol) were added to a solution of 2,6-di-*tert*-butylanthracene (2.91 g, 10.0 mmol) in DCE (250 ml). The reaction mixture was refluxed for 24 hrs, cooled to RT and reduced. The crude product was then purified by column chromatography (DCM/hexane 1/1, R_f = 0.35) and triturated in methanol (50 ml) for 2 hrs to give 2,3-dimethoxy-7,14-di-*tert*-butyltriptycene (0.67 g, 16 %) as a white solid (mp 257 – 259 °C); IR (DCM film) 2959, 2867, 2830, 1482, 1290, 1221, 1089 cm^{-1}; ^{1}H NMR (400 MHz, CDCl$_3$) δ 7.39 (2H, s, Ar*H*), 7.27 (2H, d, *J* = 7.6 Hz, Ar*H*), 7.00 (2H, s, Ar*H*), 6.97 (2H, d, *J* = 7.6 Hz, Ar*H*), 5.27 (2H, s, C*H*), 3.82 (6H, s, OC*H$_3$*), 1.25 (18H, s, ^{t}Bu*H*); ^{13}C NMR (100 MHz, CDCl$_3$) δ 148.0, 146.0, 145.9, 143.1, 138.7, 122.8, 121.7, 120.9, 56.4, 34.7, 31.7; HRMS

(EI⁺, *m/z*) calc. for $C_{30}H_{34}O_2$: 426.2559 (M⁺), found 426.2559. Crystallography data (chloroform/methanol): Monoclinic, space group P2₁/c, *a* = 8.1081(2) Å, *b* = 14.6715(3) Å, *c* = 21.1715(4) Å, *β* = 94.368(2), *V* = 2511.2 Å³, *Z* = 4, R_1 = 4.30.

7,14-Di-*tert*-butyltriptycene-2,3-diol
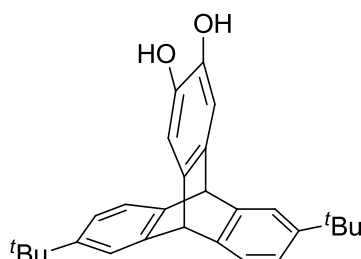
Boron tribromide (0.35 ml, 3.63 mmol) was added dropwise to a solution of 2,3-dimethoxy-7,14-di-*tert*-butyltriptycene (0.51 g, 1.20 mmol) in anhydrous DCM (10 ml) at 0 °C. After stirring for 10 mins at 0 °C and 3 hrs at RT, the reaction was re-cooled to 0 °C and quenched with the dropwise addition of ice water (20 ml). The organic layer was collected, washed with water (3 x 20 ml) and brine (20 ml), dried over anhydrous magnesium sulfate, reduced and dried under nitrogen flow to give 7,14-di-*tert*-butyltriptycene-2,3-diol (0.41 g, 86 %) as a white solid (mp > 300 °C); IR (DCM film) 3408, 2961, 2904, 2868, 1691, 1481, 1459, 1306, 1262 cm⁻¹; ¹H NMR (400 MHz, (CD₃)₂CO) *δ* 7.53 (2H, s, O*H*), 7.45 (2H, d, *J* = 1.9 Hz, Ar*H*), 7.27 (2H, d, *J* = 7.7 Hz, Ar*H*), 6.97 (2H, dd, *J* = 7.7, 1.9 Hz, Ar*H*), 5.35 (2H, s, C*H*), 1.23 (18H, s, ᵗBu*H*); ¹³C NMR (125 MHz, (CD₃)₂CO) *δ* 148.5, 147.4, 144.7, 142.4, 138.9, 123.6, 122.1, 121.3, 112.8, 54.1, 35.2, 31.9; HRMS (EI⁺, *m/z*) calc. for $C_{28}H_{30}O_2$: 398.2246 (M⁺), found 398.2257.

9,10-Dimethylanthracene
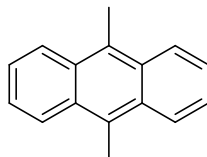
According to the literature procedure by Yagodkin *et al.*,[150] 3M methylmagnesium bromide in diethyl ether (60.7 ml, 182 mmol) was added dropwise over the course of 1 hr to a solution of 9,10-dichloroanthracene (7.50 g, 30.3 mmol) and PEPPSI™-IPr catalyst (1.34 g, 1.97 mmol) in 1,4-dioxane (600 ml). Once addition was complete, the reaction was allowed to stir for 24 hrs at RT, quenched with water (600 ml) and extracted into ethyl acetate (3 x

200 ml). The combined organic extracts were washed with water (3 x 200 ml), reduced to ~ 150 ml, filtered (to remove traces of catalyst), washed with brine (200 ml), dried over anhydrous magnesium sulfate and triturated in acetone for 3 hrs to give 9,10-dimethylanthracene (6.12 g, 98 %) as a yellow solid (mp 177 – 179 °C, literature mp 181 – 183 °C[150]); IR (DCM film) 3050, 2987, 2937, 1617, 1443, 1364, 1265 cm^{-1}; ^{1}H NMR (400 MHz, CDCl$_3$) δ 8.33 (4H, dd, J = 6.8, 3.3 Hz, ArH), 7.52 (4H, dd, J = 6.8, 3.3 Hz, ArH), 3.10 (6H, s, CH_3); ^{13}C NMR (125 MHz, CDCl$_3$) δ 130.1, 128.6, 125.5, 124.9, 14.3; LRMS (EI$^+$, m/z) calc. for C$_{16}$H$_{14}$: 206.11 (M$^+$), found 206.11.

2,3-Dimethoxy-9,10-dimethyltriptycene
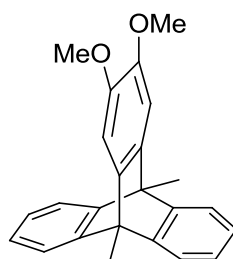
1,2-Epoxypropane (25.0 ml, 357 mmol) and freshly prepared 2-carboxy-4,5-dimethoxybenzenediazonium chloride (12.5 g, 51.1 mmol) were added to a solution of 9,10-dimethylanthracene (3.08 g, 14.9 mmol) in DCE (250 ml). The mixture was heated to reflux for 24 hrs, cooled to RT and reduced. The crude product was then purified by column chromatography (DCM/hexane 4/1, R_f = 0.4) and triturated in methanol (50 ml) for 2 hrs to give 2,3-dimethoxy-9,10-dimethyltriptycene (3.17 g, 62 %) as a white powder (mp 186 – 188 °C); IR (DCM film) 3063, 2969, 2827, 1597, 1506, 1447, 1289, 1200, 1040 cm^{-1}; ^{1}H NMR (400 MHz, CDCl$_3$) δ 7.39 (4H, dd, J = 5.4, 3.2 Hz, ArH), 7.06 (4H, dd, J = 5.4, 3.2 Hz, ArH), 7.01 (2H, s, ArH), 3.88 (6H, s, OCH_3), 2.45 (6H, s, CCH_3); ^{13}C NMR (125 MHz, CDCl$_3$) δ 148.8, 146.1, 141.5, 124.8, 120.3, 106.5, 56.6, 48.4, 13.8; HRMS (EI$^+$, m/z) calc. for C$_{24}$H$_{22}$O$_2$: 342.1620 (M$^+$), found 342.1626. Crystallography data (chloroform/methanol): Monoclinic, space group P2$_1$/a, a = 8.8226(3) Å, b = 12.9360(4) Å, c = 15.4299(5) Å, β = 92.364(2), V = 1759.5 Å^3, Z = 4, R_1 = 5.00.

9,10-Dimethyltriptycene-2,3-diol
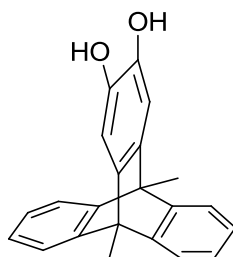
Boron tribromide (0.60 ml, 6.33 mmol) was added dropwise to a solution of 2,3-dimethoxy-9,10-dimethyltriptycene (1.01 g, 2.95 mmol) in anhydrous DCM (10 ml) at 0 °C. After stirring for 10 mins at 0 °C and 3 hrs at RT, the reaction was re-cooled to 0 °C and quenched with the dropwise addition of ice water (20 ml). The organic layer was collected, washed with water (3 x 20 ml) and brine (20 ml) and dried over anhydrous magnesium sulfate. The product was then precipitated by dropwise addition of hexane (~ 10 ml), filtered, washed with hexane and dried under suction/nitrogen flow to give 9,10-dimethyltriptycene-2,3-diol (0.90 g, 97 %) as a white solid (mp > 300 °C). IR (DCM film) 3372, 3063, 2970, 1695, 1446, 1304 cm^{-1}; ^{1}H NMR (400 MHz, (CD$_3$)$_2$CO) δ 7.55 (2H, s, OH), 7.34 (4H, dd, J = 8.8, 5.2 Hz, ArH), 6.99 (4H, dd, J = 8.8, 5.2 Hz, ArH), 6.91 (2H, s, ArH), 2.32 (6H, s CH_3); ^{13}C NMR (125 MHz, (CD$_3$)$_2$CO) δ 150.1, 142.1, 141.3, 125.3, 120.9, 110.1, 48.7, 14.1; HRMS (EI^{+}, *m/z*) calc. for C$_{22}$H$_{18}$O$_2$: 314.1307 (M^{+}), found 314.1304.

2,6-Di-*tert*-butyl-9,10-dimethylanthracene
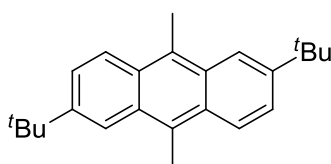
According to the literature procedure by Fu and Harvey,[151] *tert*-butanol (12.2 g, 165 mmol) was added dropwise to a suspension of 9,10-dimethylanthracene (8.46 g, 41.0 mmol) in trifluoroacetic acid (60 ml). After refluxing for 24 hrs the crude reaction mixture was cooled to RT, poured into ice water (400 ml), stirred for 30 mins and extracted with DCM (3 x 75 ml). The combined organic extracts were washed with water (2 x 150 ml) and brine (100 ml), reduced, triturated in acetone (50 ml) for 2 hrs, filtered, washed with cold acetone (20 ml) and dried under suction to give 2,6-di-*tert*-butyl-9,10-dimethylanthracene (5.22 g, 40 %) as a

white powder (mp 235 – 237 °C, literature mp 245 – 247 °C[151]); IR (DCM film) 2955, 2865, 1630, 1457, 1378, 1357 cm^{-1}; ^{1}H NMR (400 MHz, CDCl$_3$) δ 8.27 (2H, d, J = 9.3 Hz, ArH), 8.20 (2H, d, J = 1.5 Hz, ArH), 7.61 (2H, dd, J = 9.3, 1.8, ArH), 3.09 (6H, s, CH_3), 1.50 (18H, s, ^{t}BuH); ^{13}C NMR (125 MHz, CDCl$_3$) δ 146.5, 129.7, 128.8, 127.7, 125.2, 124.2, 119.6, 36.3, 31.3, 14.2; LRMS (EI^{+}, m/z) calc. for C$_{24}$H$_{30}$: 318.23 (M^{+}), found 318.23.

2,3-Dimethoxy-7,14-di-*tert*-butyl-9,10-dimethyltriptycene
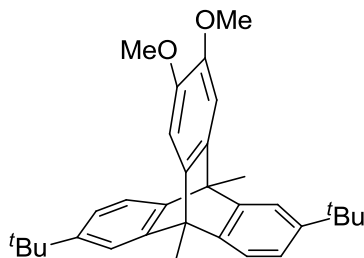
1,2-Epoxypropane (25.0 ml, 357 mmol) and freshly prepared 2-carboxy-4,5-dimethoxybenzenediazonium chloride (11.9 g, 48.6 mmol) were added to a solution of 2,6-di-*tert*-butyl-9,10-dimethylanthracene (3.03 g, 9.51 mmol) in DCE (200 ml). The mixture was heated to reflux for 24 hrs, cooled to RT and reduced. The crude product was then purified by column chromatography (DCM/hexane 1/1, R_f = 0.4) and triturated in methanol (50 ml) for 2 hrs to give 2,3-dimethoxy-7,14-di-*tert*-butyl-9,10-dimethyltriptycene (1.94 g, 45 %) as a white powder (mp 222 – 224 °C); IR (DCM film) 2964, 2903, 2867, 1481, 1458, 1291, 1241, 1200, 1044 cm^{-1}; ^{1}H NMR (400 MHz, CDCl$_3$) δ 7.35 (2H, d, J = 2.9 Hz, ArH), 7.24 (2H, d, J = 12.6 Hz, ArH), 7.01 (2H, dd, J = 12.6, 2.9 Hz, ArH), 6.94 (2H, s, ArH), 3.83 (6H, s, OCH_3), 2.39 (6H, s, CCH_3), 1.25 (18H, s, ^{t}BuH); ^{13}C NMR (125 MHz, CDCl$_3$) δ 148.6, 147.5, 146.1, 145.9, 141.9, 121.3, 119.8, 117.6, 106.2, 56.5, 48.3, 34.8, 31.8, 13.9; HRMS (EI^{+}, m/z) calc. for C$_{32}$H$_{38}$O$_2$: 454.2872 (M^{+}), found 484.2874.

7,14-Di-*tert*-butyl-9,10-dimethyltriptycene-2,3-diol
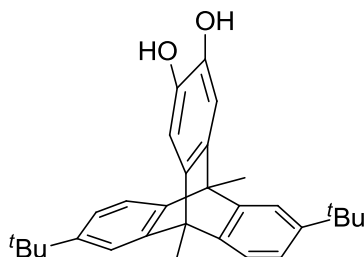
Boron tribromide (0.62 ml, 6.43 mmol) was added dropwise to a solution of 2,3-dimethoxy-7,14-di-*tert*-butyl-9,10-dimethyltriptycene (1.46 g, 2.20 mmol) in anhydrous DCM (10 ml) at 0 °C. After stirring for 10 mins at 0 °C and 3 hrs at RT, the reaction was re-cooled to 0 °C and quenched with the dropwise addition of ice water (20 ml). The organic layer was collected, washed with water (3 x 20 ml) and brine (20 ml), dried over anhydrous magnesium sulfate, reduced and dried under nitrogen flow to give 7,14-di-*tert*-butyl-9,10-dimethyltriptycene-2,3-diol (1.30 g, 95 %) as a pale brown solid (mp > 300 °C). IR (DCM film) 3390, 2965, 2903, 2868, 1616, 1480, 1455, 1362, 1302 cm^{-1}; ^{1}H NMR (400 MHz, (CD$_3$)$_2$CO) δ 7.53 (2H, s, O*H*), 7.40 (2H, d, *J* = 1.8 Hz, Ar*H*), 7.23 (2H, d, *J* = 7.9 Hz, Ar*H*), 7.01 (2H, dd, *J* = 7.8, 1.9 Hz, Ar*H*), 6.89 (2H, s, Ar*H*), 2.32 (6H, s, C*H$_3$*), 1.24 (18H, s, ^{t}Bu*H*); ^{13}C NMR (125 MHz, (CD$_3$)$_2$CO) δ 149.8, 147.9, 147.3, 142.0, 141.6, 121.6, 120.4, 118.0, 110.1, 48.5, 36.2, 31.9, 14.2; HRMS (EI$^+$, *m/z*) calc. for C$_{30}$H$_{34}$O$_2$: 426.2559 (M$^+$), found 426.2562.

2,5-Dichloro-2,5-dimethylhexane

According to the literature procedure by Wagner *et al.*,[153] a suspension of 2,5-dimethyl-2,5-hexanediol (20.0 g, 137 mmol) in 12N HCl (150 ml) was stirred vigorously for 24 hrs at RT, filtered, washed with water (1000 ml) and partially dried under suction. The resultant white solid was dissolved in diethyl ether (100 ml), washed with water (3 x 100 ml) and brine (100 ml), dried over anhydrous magnesium sulfate and reduced to give 2,5-dichloro-2,5-dimethylhexane (23.4 g, 93 %) as a white powder (mp 64 – 66 °C, literature mp 63 – 65.8 °C[153]); IR (DCM film) 2995, 2966, 2922, 1371, 1250, 1209, 1145, 1084 cm^{-1}; ^{1}H NMR (400

MHz, CDCl$_3$) δ 1.91 (4H, s, CH_2), 1.56 (12H, s, CH_3); ^{13}C NMR (100 MHz, CDCl$_3$) δ 70.5, 41.3, 32.7; LRMS (EI$^+$, *m/z*) calc. for C$_8$H$_{16}$Cl$_2$: 182.06 (M$^+$), found 146.09 (M-HCl)$^+$.

1,1,4,4,8,8,11,11-Octamethyl-1,2,3,4,8,9,10,11-octahydropentacene
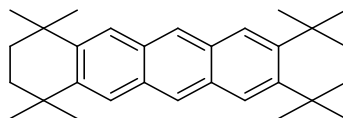
Based on the literature procedure by Bouffard *et al.*,[154] a solution of 9,10-dihydroanthracene (7.62 g, 42.3 mmol) and 2,5-dichloro-2,5-dimethylhexane (23.3 g 127 mmol) in anhydrous DCM (200 ml) was cooled to -78 °C (dry-ice/acetone bath). Titanium (IV) chloride (14.0 ml, 127 mmol) was added dropwise over the course of 30 mins and the resulting orange solution left to slowly warm to RT. After 16 hrs stirring at RT, the crude reaction mixture was poured over crushed ice (500 ml) and allowed to stir for 2 hrs. The product was then extracted into DCM (3 x 100 ml) and the combined organic extracts washed with water (3 x 200 ml) and saturated aqueous sodium hydrogen carbonate solution (100 ml), reduced and treated with boiling methanol (100 ml) for 2 hrs to give 1,1,4,4,8,8,11,11-octamethyl-1,2,3,4,8,9,10,11-octahydropentacene (10.1 g, 60 %) as a pale yellow solid (mp 255 – 257 °C, literature mp 255 – 256 °C[154]); IR (DCM film) 2958, 2926, 2867, 1672, 1605, 1461, 1364, 1265 cm^{-1}; ^{1}H NMR (400 MHz, CDCl$_3$) δ 8.18 (2H, s, ArH), 7.87 (4H, s, ArH), 1.78 (8H, s, CH_2), 1.42 (24H, s, CH_3); ^{13}C NMR (125 MHz, CDCl$_3$) δ 143.8, 130.7, 124.7, 123.9, 35.4, 34.9, 32.9; HRMS (EI$^+$, *m/z*) calc. for C$_{30}$H$_{38}$: 398.2974 (M$^+$), found 398.2976.

2,3-Dimethoxy-ucy6-triptycene and 2,3-dimethoxy-cy6-triptycene
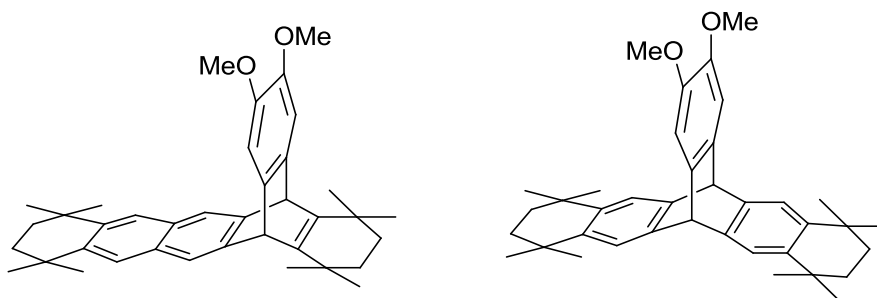
1,2-Epoxypropane (15 ml, 214 mmol) and freshly prepared 2-carboxy-4,5-dimethoxybenzenediazonium chloride (6.00 g, 24.5 mmol) were added to a solution of

1,1,4,4,8,8,11,11-octamethyl-1,2,3,4,8,9,10,11-octahydropentacene (2.00 g, 5.02 mmol) in DCE (150 ml). The mixture was heated to reflux for 24 hrs, cooled to RT and the crude reaction products were then purified *via* column chromatography (hexane/ethyl acetate 19/1), to give the following:

2,3-Dimethoxy-ucy6-triptycene: (R_f = 0.25, 0.90 g, 34 %) as a white powder (mp 274 – 276 °C); IR (DCM film) 2955, 2926, 2861, 1491, 1462, 1295, 1285, 1220, 1096 cm^{-1}; ^{1}H NMR (400 MHz, CDCl$_3$) δ 7.59 (2H, s, Ar*H*), 7.44 (2H, s, Ar*H*), 6.86 (2H, s, Ar*H*), 4.97 (2H, s, C*H*), 3.80 (6H, s, OC*H$_3$*), 1.69 (4H, s, C*H$_2$*), 1.34 – 1.28 (16H, m, C*H$_2$*/CC*H$_3$*), 1.05 (6H, s, CC*H$_3$*), 1.00 (6H, s, CC*H$_3$*); ^{13}C NMR (125 MHz, CDCl$_3$) δ 146.9, 146.1, 144.2, 143.5, 139.4, 130.0, 124.7, 118.8, 108.0, 56.6, 50.4, 36.6, 36.4, 34.6, 34.1, 32.7, 32.6, 27.3, 27.0; HRMS (EI$^+$, *m/z*) calc. for C$_{38}$H$_{46}$O$_2$: 543.3498 (M$^+$), found 534.3481. Crystallography data (chloroform/methanol): Monoclinic, space group P2$_1$/n, *a* = 19.538(5) Å, *b* = 8.798(5) Å, *c* = 20.033(5) Å, β = 114.939(5), *V* = 3122.49 Å^3, *Z* = 4, R_1 = 8.10.

2,3-Dimethoxy-cy6-triptycene: (R_f = 0.20, 0.39 g, 15 %) as a white solid (mp > 300 °C); IR (DCM film) 2957, 2859, 1479, 1362, 1293, 1222, 1086 cm^{-1}; ^{1}H NMR (500 MHz, CDCl$_3$) δ 7.26 (4H, s, Ar*H*), 6.98 (2H, s, Ar*H*), 5.19 (2H, s, C*H*), 3.80 (6H, s, OC*H$_3$*), 1.61 (8H, s, C*H$_2$*), 1.22 (24H, s, CC*H$_3$*); ^{13}C NMR (125 MHz, CDCl$_3$) δ 146.1, 143.0, 141.1, 139.1, 121.4, 109.0, 56.4, 53.6, 35.5, 34.4, 32.2, 31.1; HRMS (EI$^+$, *m/z*) calc. for C$_{38}$H$_{46}$O$_2$: 543.3498 (M$^+$), found 534.3490. Crystallography data (chloroform/methanol): Monoclinic, space group P2$_1$/c, *a* = 13.8840(12) Å, *b* = 8.9553(8) Å, *c* = 24.8969(15) Å, β = 104.109(4), *V* = 3002.18 Å^3, *Z* = 4, R_1 = 10.66.

Cy6-triptycene-2,3-diol
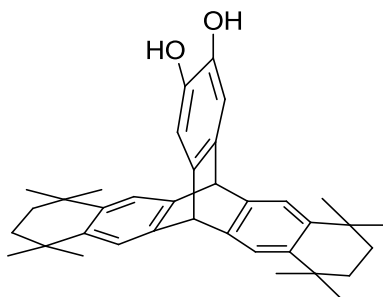
Boron tribromide (0.42 ml, 4.43 mmol) was added dropwise to a solution of 2,3-dimethoxy-cy6-triptycene (1.16 g, 2.17 mmol) in anhydrous DCM (15 ml) at 0 °C. After stirring for 10

mins at 0 °C and 3 hrs at RT, the reaction was re-cooled to 0 °C and quenched with the dropwise addition of ice water (20 ml). The organic layer was collected, washed with water (3 x 20 ml) and brine (20 ml), dried over anhydrous magnesium sulfate, reduced and dried under suction/nitrogen flow to give cy6-triptycene-2,3-diol (1.08 g, 98 %) as a white solid (mp > 300 °C); IR (DCM film) 3376, 2957, 2924, 2859, 1473, 1457, 1303 cm^{-1}; ^{1}H NMR (400 MHz, (CD$_3$)$_2$CO) δ 7.50 (2H, s, O*H*), 7.32 (4H, s, Ar*H*), 6.93 (2H, s, Ar*H*), 5.26 (2H, s, C*H*), 1.60 (8H, s, C*H*$_2$), 1.19 (24H, s, C*H*$_3$); ^{13}C NMR (125 MHz, (CD$_3$)$_2$CO) δ 144.4, 142.2, 141.5, 138.9, 121.8, 112.6, 53.6, 36.1, 34.9, 32.32, 32.28; HRMS (EI$^+$, *m/z*) calc. for C$_{36}$H$_{42}$O$_2$: 506.3185 (M$^+$), found 506.3174.

uCy6-triptycene-2,3-diol
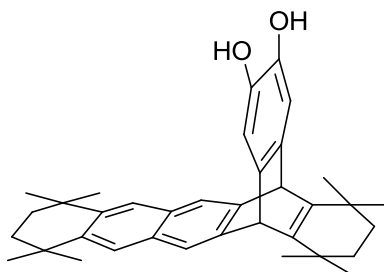
Boron tribromide (0.32 ml, 3.38 mmol) was added dropwise to a solution of 2,3-dimethoxy-ucy6-triptycene (0.90 g, 1.68 mmol) in anhydrous DCM (10 ml) at 0 °C. After stirring for 10 mins at 0 °C and 3 hrs at RT, the reaction was re-cooled to 0 °C and quenched with the dropwise addition of ice water (20 ml). The organic layer was collected, washed with water (3 x 20 ml) and brine (20 ml), dried over anhydrous magnesium sulfate, reduced and dried under suction/nitrogen flow to give ucy6-triptycene-2,3-diol (0.79 g, 93 %) as a white solid (mp > 300 °C); IR (DCM film) 3368, 2956, 2925, 2862, 1460, 1362, 1304 cm^{-1}; ^{1}H NMR (400 MHz, (CD$_3$)$_2$CO) δ 7.67 (2H, s, O*H*), 7.51 (2H, s, Ar*H*), 7.38 (2H, s, Ar*H*), 6.87 (2H, s, Ar*H*), 5.06 (2H, s, C*H*), 1.73 (4H, s, C*H*$_2$), 1.35 – 1.32 (16H, m, C*H*$_2$/C*H*$_3$), 1.07 (6H, s, C*H*$_3$), 1.04 (6H, s, C*H*$_3$); ^{13}C NMR (125 MHz, (CD$_3$)$_2$CO) δ 147.9, 145.5, 143.8, 142.2, 139.4, 131.2, 125.3, 119.3, 111.7, 50.6, 36.3, 36.0, 35.1, 34.6, 32.86, 32.85, 27.4, 27.2; HRMS (EI$^+$, *m/z*) calc. for C$_{36}$H$_{42}$O$_2$: 506.3185 (M$^+$), found 506.3169.

6,6'-Dihydroxy-3,3,3',3'-tetramethyl-1,1'-spirobisindane
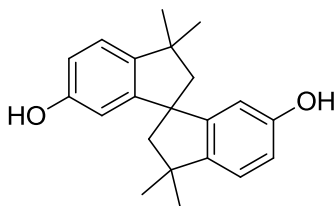
Based on the literature procedure by Chen *et al.*,[191] a solution of bisphenol A (58.0 g, 262 mmol) in methanesulfonic acid (320 g) was stirred for 96 hrs at 25 °C. The resulting deep red solution was poured into ice water (1250 ml), stirred for 3 hrs, filtered, washed with water (1000 ml) and partially dried under suction. The resultant wet pink solid was recrystallised from 60 % aqueous ethanol and dried under vacuum to give 6,6'-dihydroxy-3,3,3',3'-tetramethyl-1,1'-spirobisindane (20.4 g, 78 %) as a white fluffy solid (mp 210 – 212 °C, literature mp 218 °C[191]); IR (DCM film) 3184, 2950, 2861, 1604, 1490, 1468, 1361, 1286, cm^{-1}; ^{1}H NMR (400 MHz, (CD$_3$)$_2$SO) δ 9.00 (2H, s, O*H*), 6.99 (2H, d, *J* = 8.2 Hz, Ar*H*), 6.59 (2H, dd, *J* = 8.2, 2.3 Hz, Ar*H*), 6.10 (2H, d, *J* = 2.3 Hz, Ar*H*), 2.25 (2H, d, *J* = 13.0 Hz, CH*H*), 2.10 (2H, d, *J* = 13.0 Hz, C*H*H), 1.31 (6H, s, C*H$_3$*), 1.25 (6H, s, C*H$_3$*); ^{13}C NMR (400 MHz, (CD$_3$)$_2$SO) δ 156.8, 151.5, 142.2, 122.4, 114.4, 110.0, 59.4, 57.0, 42.4, 31.7, 30.5; LRMS (EI$^+$, *m/z*) calc. for C$_{21}$H$_{24}$O$_2$: 308.18 (M$^+$), found 308.18.

6,6'-Bis(N,N-dimethyl-*O*-thiocarbamate)-3,3,3',3'-tetramethyl-1,1'-spirobisindane
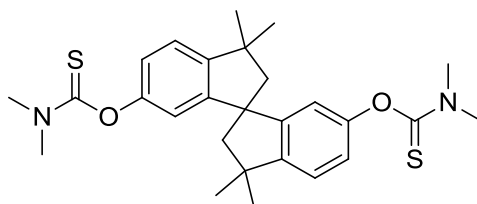
Based on the literature procedure by Sugioka and Hay,[192] N,N-dimethylthiocarbamoyl chloride (8.89 g, 71.9 mmol) was added to a solution of 6,6'-dihydroxy-3,3,3',3'-tetramethyl-1,1'-spirobisindane (10.1 g, 32.7 mmol) and potassium hydroxide (4.04 g, 72.0 mmol) in methanol (150 ml) at 0 °C. After 10 mins, the ice bath was removed, the reaction allowed to stir for 10 mins at RT and then heated to reflux for 12 hrs. The crude reaction mixture was cooled to RT, filtered, washed with water (200 ml) and methanol (200 ml) and then recrystallised from toluene to give 6,6'-bis(N,N-dimethyl-*O*-thiocarbamate)-3,3,3',3'-tetramethyl-1,1'-spirobisindane (10.8 g, 68 %) as pale yellow crystals (mp 246 – 248 °C,

literature mp 278 °C[192]); IR (DCM film) 2945, 2862, 1533, 1483, 1394, 1291, 1254, 1191, 1145 cm⁻¹; ¹H NMR (400 MHz, CDCl₃) δ 7.13 (2H, d, J = 8.2 Hz, Ar*H*), 6.90 (2H, dd, J = 8.2, 2.2, Ar*H*), 6.50 (2H, d, J = 2.2 Hz, Ar*H*), 3.37 (6H, s, NC*H₃*), 3.23 (6H, s, NC*H₃*), 2.36 (2H, d, J = 13.2 Hz, CH*H*), 2.27 (2H, d, J = 13.2 Hz, C*H*H), 1.36 (6H, s, CC*H₃*), 1.34 (6H, s, CC*H₃*); ¹³C NMR (400 MHz, CDCl₃) δ 187.9, 153.6, 151.5, 149.6, 122.3, 121.4, 118.6, 59.5, 57.5, 43.4, 43.3, 38.8, 31.8, 30.4; LRMS (EI⁺, *m/z*) calc. for C₂₇H₃₄N₂O₂S₂: 482.21 (M⁺), found 482.20.

6,6'-Bis(N,N-dimethyl-*S*-thiocarbamate)-3,3,3',3'-tetramethyl-1,1'-spirobisindane
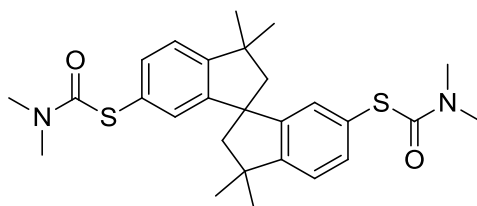
Based on the literature procedure by Sugioka and Hay,[192] a solution of 6,6'-bis(N,N-dimethyl-*O*-thiocarbamate)-3,3,3',3'-tetramethy-1,1'-spirobisindane (2.00 g, 4.14 mmol) in diphenyl ether (1.00 g) was refluxed for 5 hrs then cooled to RT. The crude reaction products were triturated in diethyl ether (50 ml) for 3 hrs, filtered, washed with diethyl ether (20 ml) and dried under suction to give 6,6'-bis(N,N-dimethyl-*S*-thiocarbamate)-3,3,3',3'-tetramethyl-1,1'-spirobisindane (1.72 g, 86 %) as a white powder (mp 238 – 240 °C, literature mp 244 °C[192]); IR (DCM film) 2954, 2925, 2856, 1669, 1472, 1362, 1260, 1092 cm⁻¹; ¹H NMR (400 MHz, CDCl₃) δ 7.34 (2H, dd, J = 7.9, 1.6 Hz, Ar*H*), 7.17 (2H, d, J = 7.9 Hz, Ar*H*), 6.88 (2H, d, J = 1.6 Hz, Ar*H*), 2.99 (12H, br s, NC*H₃*), 2.32 (2H, d, J = 13.2 Hz, CH*H*), 2.25 (2H, d, J = 13.2 Hz, C*H*H), 1.36 (6H, s, CC*H₃*), 1.31 (6H, s, CC*H₃*); ¹³C NMR (400 MHz, CDCl₃) δ 167.4, 153.6, 151.1, 135.0, 131.5, 127.1, 122.7, 59.4, 57.7, 43.6, 37.0, 31.7, 30.2; LRMS (EI⁺, *m/z*) calc. for C₂₇H₃₄N₂O₂S₂: 482.21 (M⁺), found 482.17.

6,6'-Dithiol-3,3,3',3'-tetramethyl-1,1'-spirobisindane
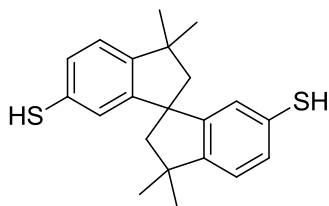
Based on the literature procedure by Sugioka and Hay,[192] a suspension of 6,6'-bis(N,N-dimethyl-*S*-thiocarbamate)-3,3,3',3'-tetramethyl-1,1'-spirobisindane (3.43 g, 7.11 mmol) and potassium hydroxide (3.99 g, 71.1 mmol) in methanol (15 ml) and pyridine (15 ml) was heated to reflux. The resulting solution was refluxed for 24 hrs, cooled to RT and reduced. The residual solid was taken up into water (50 ml), washed with chloroform (3 x 50 ml) and acidified with 2N HCl (50 ml). The resulting precipitate was stirred for 1 hr, filtered, washed with water (100 ml) and dried under vacuum to give 6,6'-dithiol-3,3,3',3'-tetramethyl-1,1'-spirobisindane (2.27 g, 94 %) as an off-white powder (mp 144 – 146 °C, literature mp 157 °C[192]); IR (DCM film) 2955, 2923, 2861, 2564, 1473, 1102 cm^{-1}; ^{1}H NMR (400 MHz, CDCl$_3$) δ 7.15 (2H, d, J = 7.8 Hz, Ar*H*), 7.06 (2H, d, J = 7.8 Hz, Ar*H*), 6.73 (2H, s, Ar*H*) 3.32 (2H, s, S*H*), 2.33 (2H, d, J = 13.1 Hz, CH*H*), 2.20 (2H, d, J = 13.1 Hz, C*H*H), 1.38 (6H, s, C*H$_3$*), 1.32 (6H, s, C*H$_3$*); ^{13}C NMR (400 MHz, CDCl$_3$) δ 151.6, 150.4, 128.9, 128.8, 125.8, 122.8, 59.4, 57.7, 43.4, 31.8, 30.3; LRMS (EI$^+$, *m/z*) calc. for C$_{21}$H$_{24}$S$_2$: 340.13 (M$^+$), found 340.13.

5,5'-Dibromo-6,6'-dihydroxy-3,3,3',3'-tetramethyl-1,1'-spirobisindane
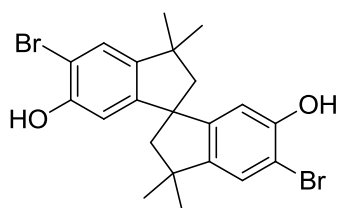
90 % Pyridinium hydrobromide perbromide (20.2 g, 63.3 mmol) was added portionwise to a partial solution of 6,6'-dihydroxy-3,3,3',3'-tetramethyl-1,1'-spirobisindane (9.29 g, 30.1 mmol) in chloroform (200 ml) at 0 °C contained in a flask fitted with an outlet leading to a saturated sodium bisulfite aqueous solution. Once addition was complete, the reaction mixture was allowed to warm to RT, stirred for 12 hrs, then warmed to 50 °C and heated until HBr evolution ceased. After cooling to RT, the reaction was quenched with water (200 ml) and extracted with chloroform (3 x 100 ml). The combined organic extracts were

washed with water (3 x 200 ml) and brine (200 ml), dried over anhydrous magnesium sulfate and purified *via* column chromatography (DCM, R_f = 0.3) to give 5,5'-dibromo-6,6'-dihydroxy-3,3,3',3'-tetramethyl-1,1'-spirobisindane (13.0 g, 93 %) as a white powder (mp 205 – 207 °C); IR (DCM film) 3492, 2957, 2923, 2862, 1478, 1322, 1189 cm^{-1}; ^{1}H NMR (400 MHz, CDCl$_3$) δ 7.20 (2H, s, Ar*H*), 6.42 (2H, s, Ar*H*), 5.32 (2H, s, O*H*), 2.30 (2H, d, *J* = 13.1 Hz, CH*H*), 2.18 (2H, d, *J* = 13.1 Hz, C*H*H), 1.33 (6H, s, C*H*$_3$), 1.28 (6H, s, C*H*$_3$); ^{13}C NMR (500 MHz, CDCl$_3$) δ 151.9, 151.7, 146.3, 125.4, 111.7, 109.5, 59.6, 57.6, 43.4, 32.0, 30.5; HRMS (EI$^+$, *m/z*) calc. for C$_{21}$H$_{22}$Br$_2$O$_2$: 463.9987 (M$^+$), found 463.9990.

5,5'-Dibromo-6,6'-bis(N,N-dimethyl-*O*-thiocarbamate)-3,3,3',3'-tetramethyl-1,1'-spirobisindane
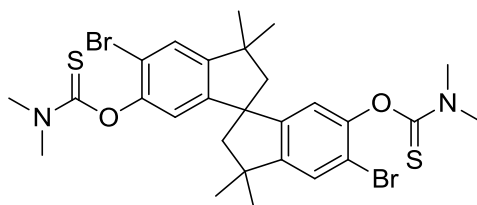
N,N-dimethylcarbamoyl chloride (7.60 g, 61.5 mmol) was added to a solution of 5,5'-dibromo-6,6'-dihydroxy-3,3,3',3'-tetramethyl-1,1'-spirobisindane (13.0 g, 27.9 mmol) and potassium hydroxide (3.45 g, 61.5 mmol) in methanol (250 ml) at 0 °C. The reaction was then warmed to RT and heated to reflux for 12 hrs. After cooling to RT the reaction mixture was filtered, washed with water (200 ml) and methanol (200 ml) and the crude product purified by column chromatography (DCM/hexane 7/3, R_f = 0.3) to give 5,5'-dibromo-6,6'-bis(N,N-dimethyl-*O*-thiocarbamate)-3,3,3',3'-tetramethyl-1,1'-spirobisindane (11.9 g, 66 %) as a white powder (mp 259 – 261 °C); IR (DCM film) 2955, 2864, 1538, 1475, 1389, 1281, 1195, 1123 cm^{-1}; ^{1}H NMR (400 MHz, CDCl$_3$) δ 7.32 (2H, s, Ar*H*), 6.58 (2H, s, Ar*H*), 3.39 (6H, s, NC*H*$_3$), 3.29 (6H, s, NC*H*$_3$), 2.35 (2H, d, *J* = 13.2 Hz, CH*H*), 2.26 (2H, d, *J* = 13.2 Hz, C*H*H), 1.35 (6H, s, CC*H*$_3$), 1.33 (6H, s, CC*H*$_3$); ^{13}C NMR (500 MHz, CDCl$_3$) δ 186.6, 151.4, 150.4, 126.4, 121.2, 115.6, 59.3, 57.2, 43.6, 43.5, 38.9, 31.7, 30.3; HRMS (ES$^+$, *m/z*) calc. for C$_{27}$H$_{32}$Br$_2$O$_2$N$_2$S$_2$: 639.0350 (MH$^+$), found 639.0362. Crystallography data (chloroform/methanol): Monoclinic, space group: P2$_1$/n, *a* = 10.8224(2) Å, *b* = 21.0818(6) Å, *c* = 13.1502(3) Å, β = 111.9810(10), *V* = 2782.20 Å^3, *Z* = 4, R_1 = 4.49.

5,5'-Dibromo-6,6'-bis(N,N-dimethyl-*S*-thiocarbamate)-3,3,3',3'-tetramethyl-1,1'-spirobisindane
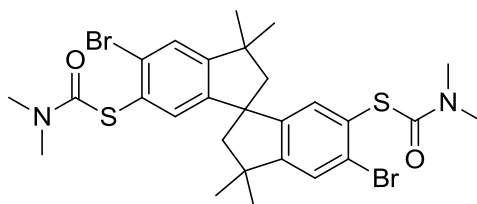
A solution of 3,3,3',3'-tetramethyl-5,5'-dibromo-6,6'-bis(N,N-dimethyl-*O*-thiocarbamate)-1,1'-spirobisindane (0.75 g, 1.17 mmol) in diphenyl ether (3.75 g) was gently refluxed for 3 hrs. After cooling to RT, the pale yellow solution was triturated in hexane (30 ml) for 12 hrs and filtered to give 5,5'-dibromo-6,6'-bis(N,N-dimethyl-*S*-thiocarbamate)-3,3,3',3'-tetramethyl-1,1'-spirobisindane (0.41 g, 55 %) as a white powder (mp 226 − 228 °C); IR (DCM film) 2955, 2863, 1674, 1467, 1363, 1260, 1094 cm^{-1}; ^{1}H NMR (400 MHz, CDCl$_3$) δ 7.45 (2H, s, Ar*H*), 7.01 (2H, s, Ar*H*), 3.04 − 2.98 (12H, m, NC*H*$_3$), 2.31 (2H, d, *J* = 13.2 Hz, CH*H*), 2.24 (2H, d, *J* = 13.2 Hz, C*H*H), 1.35 (6H, s, CC*H*$_3$), 1.31 (6H, s, CC*H*$_3$); ^{13}C NMR (500 MHz, CDCl$_3$) δ 165.6, 156.0, 150.0, 134.2, 129.7, 129.0, 127.4, 59.3, 57.3, 43.9, 37.2, 31.6, 30.1; HRMS (ES$^+$, *m/z*) calc. for C$_{27}$H$_{32}$Br$_2$O$_2$N$_2$S$_2$: 639.0350 (MH$^+$), found 639.0382.

5,5'-Dibromo-6,6'-dithiol-3,3,3',3'-tetramethyl-1,1'-spirobisindane
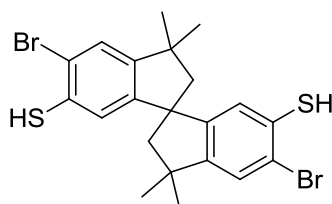
A solution of 5,5'-dibromo-6,6'-bis(N,N-dimethyl-*S*-thiocarbamate)-3,3,3',3'-tetramethyl-1,1'-spirobisindane (0.94 g, 1.47 mmol) and potassium hydroxide (0.84 g, 15.0 mmol) in methanol (30 ml) was refluxed for 24 hrs. After cooling to RT, the methanol was removed under reduced pressure and the residual solid taken up into water (50 ml). After washing with chloroform (3 x 50 ml), the aqueous phase was acidified with 2N HCl (50 ml) and stirred for 30 mins. The resultant precipitate was filtered, washed with water (200 ml) and dried under vacuum to give 5,5'-dibromo-6,6'-dithiol-3,3,3',3'-tetramethyl-1,1'-spirobisindane (0.66 g, 90 %) as a white powder (mp 233 − 235 °C); IR (DCM film) 2954, 2923, 2862, 2565, 1466, 1362, 1282, 1111 cm^{-1}; ^{1}H NMR (400 MHz, CDCl$_3$) δ 7.31 (2H, s, Ar*H*), 6.75 (2H, s, Ar*H*),

3.85 (2H, s, S*H*), 2.29 (2H, d, *J* = 13.2 Hz, CH*H*), 2.14 (2H, d, *J* = 13.2 Hz, C*H*H), 1.34 (6H, s, C*H*$_3$), 1.29 (6H, s, C*H*$_3$); ^{13}C NMR (500 MHz, CDCl$_3$) δ 152.0, 150.4, 132.4, 127.0, 125.5, 121.3, 59.4, 57.4, 43.7, 31.7, 30.2; HRMS (EI$^+$, *m/z*) calc. for C$_{21}$H$_{22}$Br$_2$S$_2$: 495.9530 (M$^+$), found 495.9541. Crystallography data (chloroform/methanol): Triclinic, space group P$\overline{1}$, *a* = 11.0034(8) Å, *b* = 11.0193(11) Å, *c* = 17.8535(12) Å, α = 80.162(7), β = 80.985(6), γ = 89.995(7) *V* = 2105.76 Å^3, *Z* = 4, *R$_1$* = 11.87.

5,5',6,6'-Tetrakis(N,N-dimethyl-*O*-thiocarbamate)-3,3,3',3'-tetramethyl-1,1'-spirobisindane
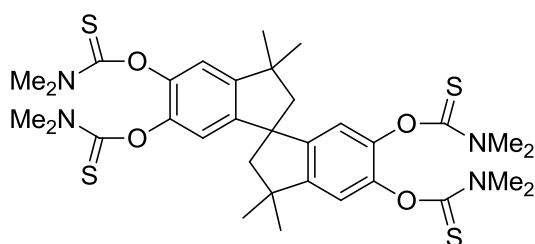
N,N-dimethylcarbamoyl chloride (1.54 g, 12.5 mmol) was added to a solution of 5,5',6,6'-tetrahydroxy-3,3,3',3'-tetramethyl-1,1'-spirobisindane (1.00 g, 2.94 mmol) and potassium hydroxide (0.86 g, 15.3 mmol) in methanol (25 ml) at 0 °C. The reaction mixture was refluxed for 12 hrs and cooled to RT. The resultant precipitate was filtered, washed with water (200 ml) and methanol (200 ml), dried under suction and recrystallised from toluene to give 5,5',6,6'-tetrakis(N,N-dimethyl-*O*-thiocarbamate)-3,3,3',3'-tetramethyl-1,1'-spirobisindane (1.05 g, 52 %) as large off-white crystals (mp 240 – 242 °C); IR (DCM film) 3036, 2955, 2864, 1538, 1487, 1394, 1323, 1285, 1133 cm^{-1}; ^{1}H NMR (400 MHz, CDCl$_3$) δ 6.91 (2H, s, Ar*H*), 6.65 (2H, s, Ar*H*), 3.41 (6H, s, NC*H*$_3$), 3.35 (6H, s, NC*H*$_3$), 3.26 (6H, s, NC*H*$_3$), 3.21 (6H, s, NC*H*$_3$), 2.37 (2H, d, *J* = 13.1 Hz, CH*H*), 2.30 (2H, d, *J* = 13.1 Hz, C*H*H), 1.36 (6H, s, CC*H*$_3$), 1.34 (6H, s, CC*H*$_3$); ^{13}C NMR (125 MHz, CDCl$_3$) δ 187.3, 187.2, 150.3, 148.0, 145.0, 144.9, 120.0, 117.5, 59.4, 57.6, 48.6, 43.44, 43.39, 38.9, 31.7, 30.4; HRMS (EI$^+$, *m/z*) calc. for C$_{33}$H$_{44}$N$_4$O$_4$S$_4$: 688.2255 (M$^+$), found 688.2245. Crystallography data (chloroform/methanol): Monoclinic, space group P2$_1$/n, *a* = 17.0636(9) Å, *b* = 6.9355(4) Å, *c* = 29.9278(13) Å, β = 94.196(3), *V* = 3532.3 Å^3, *Z* = 4, *R$_1$* = 9.23.

Benzene-1,2-dithiol
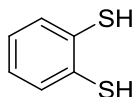
Based on the literature procedure by Giolando and Kirschbaum,[190] an oven dried 2-neck flask, fitted with a solid addition side arm containing sublimed sulfur (2.33 g, 72.7 mmol), was charged with TMEDA (12.0 ml, 80.0 mmol), 2.5M *n*-BuLi in hexanes (64.0 ml, 160.0 mmol) and freshly distilled hexane (40 ml). A solution of thiophenol (8.00 g, 72.6 mmol) in freshly distilled hexane (20 ml) was added dropwise to the resultant solution at 0 °C. Once addition was complete, the reaction mixture was allowed to warm to RT, stirred for 24 hrs, re-cooled to -10 °C (ice/ethanol bath) and the sublimed sulfur (2.33 g, 72.7 mmol) added from the side arm. After stirring at -10 °C for 2 hrs and at RT for 16 hrs, the reaction was re-cooled to -10 °C, quenched with ice water (100 ml) and neutralised with 2N HCl. The aqueous layer was then extracted with diethyl ether (3 x 100 ml), the organic extracts combined, washed with water (150 ml), dried over anhydrous magnesium sulfate and reduced. The crude oil was then purified by distillation collecting the distillate boiling between 90 – 100 °C at 10.7 mbar (literature bp 95 °C at 6.7 mbar)[231] to give benzene-1,2-dithiol (3.68 g, 36 %) as a colourless oil; IR (DCM film) 3055, 2956, 2926, 2538, 1570, 1452, 1429, 1266, 1041 cm^{-1}; ^{1}H NMR (400 MHz, CDCl$_3$) δ 7.35 – 7.32 (2H, m, ArH), 7.06 – 7.04 (2H, m, ArH), 3.73 (2H, s, SH); ^{13}C NMR (125 MHz, CDCl$_3$) δ 131.3, 131.2, 126.8; LRMS (EI^{+}, *m/z*) calc. for C$_6$H$_6$S$_2$: 141.98 (M^{+}), found 141.98.

4-Methyl-4-phenylpentan-2-one
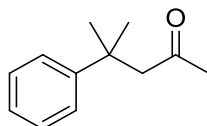
Based on the literature procedure by Tsang *et al.*,[232] mesityl oxide (40.0 ml, 350 mmol) was added dropwise over the course of 30 mins to a suspension of aluminium (III) chloride (60.0 g, 450 mmol) in anhydrous benzene (140 ml, 1570 mmol) at 0 °C. After warming slowly to RT and stirring for 4 hrs, the reaction was poured over ice water (600 ml), left to stir for 2 hrs and extracted into diethyl ether (3 x 100 ml). The combined organic extracts were washed with water (3 x 100 ml) and brine (100 ml), dried over anhydrous magnesium sulfate,

reduced and purified by distillation, collecting the fraction that boiled between 120 – 125 °C at 10.8 mbar (literature bp 100 – 101 °C at 5.3 mbar[233]) to give 4-methyl-4-phenylpentan-2-one (52.7 g, 86 %) as a colourless oil; IR (DCM film) 3059, 2955, 2878, 1705, 1496, 1444, 1358 cm^{-1}; ^{1}H NMR (500 MHz, CDCl$_3$) δ 7.38 – 7.30 (3H, m, Ar*H*), 7.19 (2H, t, *J* = 7.0 Hz, Ar*H*), 2.74 (2H, s, C*H*$_2$), 1.78 (3H, s, OCC*H*$_3$), 1.44 (6H, s, C(C*H*$_3$)$_2$); ^{13}C NMR (125 MHz, CDCl$_3$) δ 207.6, 148.2, 128.3, 126.0, 125.5, 56.9, 37.3, 31.7, 28.9; LRMS (EI$^+$, *m/z*) calc. for C$_{12}$H$_{16}$O: 176.12 (M$^+$), found 176.12.

3,3,3',3'-Tetramethyl-1,1'-spirobisindane
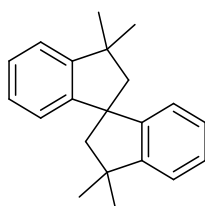
Based on the literature procedure by Hoffman,[234] a suspension of zinc (II) chloride (40.7 g, 299 mmol) in 4-methyl-4-phenylpentan-2-one (52.7 g, 299 mmol) was cautiously heated to 180 °C. After the resultant violent reaction had subsided, the reaction was cooled to RT and washed with hexane (5 x 100 ml). The combined organic washings were washed with water (3 x 100 ml) and brine (100 ml), reduced and triturated in methanol (300 ml) for 6 hrs. The resultant white precipitate was recrystallised from hexane to give 3,3,3',3'-tetramethyl-1,1'-spirobisindane (19.1 g, 46 %) as white crystals (mp 127 – 129 °C, literature mp 130.5 – 131 °C[234]); IR (DCM film) 3063, 3018, 2956, 2922, 2861, 1479, 1447, 1360 cm^{-1}; ^{1}H NMR (500 MHz, CDCl$_3$) δ 7.28 – 7.22 (4H, m, Ar*H*), 7.20 – 7.17 (2H, m, Ar*H*), 6.85 (2H, d, *J* = 7.6 Hz, Ar*H*), 2.40 (2H, d, *J* = 13.0 Hz, CH*H*), 2.30 (2H, d, *J* = 13.0 Hz, C*H*H) 1.45 (6H, s, C*H*$_3$), 1.41 (6H, s, C*H*$_3$); ^{13}C NMR (125 MHz, CDCl$_3$) δ 152.4, 150.9, 127.3, 127.1, 124.5, 122.0, 59.7, 58.0, 43.7, 32.0, 30.5; LRMS (EI$^+$, *m/z*) calc. for C$_{21}$H$_{24}$: 276.12 (M$^+$), found 276.12.

5,5',6,6'-Tetrabromo-3,3,3',3'-tetramethyl-1,1'-spirobisindane
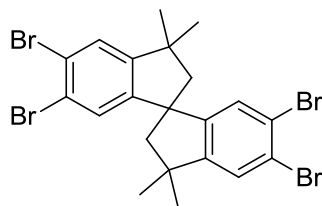
Bromine (15.72 g, 98.37 mmol) was added dropwise to a mixture of 3,3,3',3'-tetramethyl-1,1'-spirobisindane (6.470 g, 23.43 mmol) and iron powder (0.010 g, 0.179 mmol) in anhydrous DCM (50 ml) at 0 °C. The reaction was allowed to warm to RT, heated to reflux for 5 hrs, cooled to RT, washed with water (2 x 50 ml) and aqueous sodium metabisulfite solution and dried over anhydrous magnesium sulfate. The crude reaction products were treated with boiling hexane (50 ml) for 12 hrs, filtered and dried under suction to give 5,5',6,6'-tetrabromo-3,3,3',3'-tetramethyl-1,1'-spirobisindane (10.8 g, 78 %) as a white powder (mp 222 – 224 °C); IR (DCM film) 2956, 2923, 2863, 1464, 1363, 1349, 1282, 1263, 1108, 1095 cm^{-1}; ^{1}H NMR (500 MHz, CDCl$_3$) δ 7.40 (2H, s, Ar*H*), 7.00 (2H, s, Ar*H*), 2.32 (2H, d, *J* = 12.4 Hz, CH*H*), 2.17 (2H, d, *J* = 12.4 Hz, C*H*H), 1.36 (6H, s, C*H*$_3$), 1.30 (6H, s, C*H*$_3$); ^{13}C NMR (125 MHz, CDCl$_3$) δ 153.6, 150.9, 129.5, 127.8, 123.8, 123.4, 59.3, 57.2, 48.8, 31.6, 30.1; HRMS (EI$^+$, *m/z*) calc. for C$_{21}$H$_{20}$Br$_4$: 589.8278 (M$^+$), found 589.8282. Crystallography data (chloroform/methanol): Triclinic, space group P$\overline{1}$, *a* = 8.5011(3) Å, *b* = 10.4578(3) Å, *c* = 13.2028(3) Å, *α* = 68.7140(10), *β* = 87.4160(10), *γ* = 70.797(2), *V* = 1029.15 Å^3, *Z* = 2, *R$_1$* = 3.82.

Copper(I) *n*-butylmercaptide
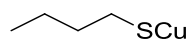
Based on the literature procedure by Adams *et al*.,[235] 1-butanethiol (2.10 ml, 19.5 mmol) was added to a suspension of copper(I) oxide (1.22 g, 8.53 mmol) in ethanol (25 ml). The red suspension was refluxed under nitrogen for 72 hrs, cooled to RT and the resulting white precipitate filtered, washed with ethanol (200 ml) and dried under vacuum to give copper(I) *n*-butylmercaptide (2.40 g, 92 %) as white powder.

5,5',6,6'-Tetrakis(*n*-butylsulfane)-3,3,3',3'-tetramethyl-1,1'-spirobisindane
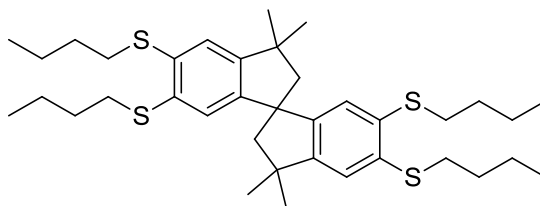
A solution of 5,5',6,6'-tetrabromo-3,3,3',3'-tetramethyl-1,1'-spirobisindane (1.85 g, 3.12 mmol) and freshly prepared copper(I) *n*-butylmercaptide (2.10 g, 13.7 mmol) in a mixture of anhydrous pyridine (10 ml) and anhydrous quinoline (30 ml) was heated to 170 °C for 24 hrs then cooled to RT. The resulting dark solution was poured over a mixture of 12N HCl (30 ml) and crushed ice (100 ml), stirred for 2 hrs and extracted into diethyl ether (3 x 50 ml). The combined organic extracts were washed with water (150 ml), 35 % aqueous ammonia solution (2 x 100 ml), water (100 ml) and brine (100 ml), dried over anhydrous magnesium sulfate and reduced. The crude brown oil was then purified *via* column chromatography (hexane/DCM 4/1, R_f = 0.25) to give 5,5',6,6'-tetrakis(*n*-butylsulfane)-3,3,3',3'-tetramethyl-1,1'-spirobisindane (1.42 g, 72 %) as a colourless oil; IR (DCM film) 2955, 2927, 2861, 1465, 1361, 1266 cm^{-1}; ^{1}H NMR (500 MHz, CDCl$_3$) δ 7.05 (2H, s, Ar*H*), 6.67 (2H, s, Ar*H*), 2.92 (4H, t, *J* = 7.4 Hz, SC*H*$_2$), 2.72 (4H, t, *J* = 7.4 Hz, SC*H*$_2$), 2.30 (2H, d, *J* = 13.1 Hz, Me$_2$CC*H*H), 2.18 (2H, d, *J* = 13.1 Hz, Me$_2$CCH*H*), 1.67 (4H, p, *J* = 7.4 Hz, SCH$_2$C*H*$_2$), 1.54 – 1.45 (8H, m, SCH$_2$C*H*$_2$CH$_2$), 1.36 (6H, s, CC*H*$_3$), 1.36 – 1.32 (4H, m, SCH$_2$C*H*$_2$CH$_2$), 1.31 (6H, s, CC*H*$_3$), 0.93 (6H, t, *J* = 7.4 Hz, S(CH$_2$)$_3$C*H*$_3$), 0.81 (6H, t, *J* = 7.4 Hz, S(CH$_2$)$_3$C*H*$_3$); ^{13}C NMR (125 MHz, CDCl$_3$) δ 151.0, 148.7, 136.6, 135.8, 125.6, 122.7, 59.7, 57.5, 48.6, 33.54, 33.46, 31.7, 31.19, 31.15, 30.4, 22.3, 22.2, 13.9, 13.8; HRMS (EI$^+$, *m/z*) calc. for C$_{37}$H$_{56}$S$_4$: 628.3265 (M$^+$), found 628.3256.

5,5',6,6'-Tetrathiol-3,3,3',3'-tetramethyl-1,1'-spirobisindane
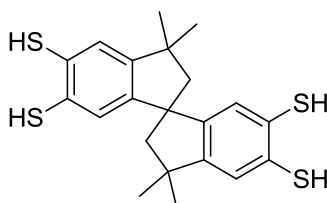
A solution of 5,5',6,6'-tetrakis(*n*-butylsulfane)-3,3,3',3'-tetramethyl-1,1'-spirobisindane (1.10 g, 1.75 mmol) in anhydrous THF (10 ml) was placed in an oven dry, 2-neck flask fitted with a dry nitrogen line and a dry ice/acetone condenser. The system was thoroughly purged with

nitrogen before replacing the nitrogen line with a steady flow of gaseous ammonia. Once liquid ammonia (~ 15 ml) had collected in the flask, the gaseous ammonia was disconnected, and lithium metal (0.200 g, 28.1 mmol) added portionwise, allowing for the blue colour to subside between additions. Once the blue colour persisted for 30 mins, ammonium chloride (0.600 g, 11.2 mmol) was added and the dry ice condenser removed. The crude white suspension was left to dry under nitrogen flow for 12 hrs then taken up into water (30 ml), washed with diethyl ether (30 ml) and acidified with 2N HCl (100 ml). After stirring for 30 mins, the resultant precipitate was filtered, washed with 2N HCl (50 ml) and water (200 ml) and dried under vacuum to give 5,5',6,6'-tetrathiol-3,3,3',3'-tetramethyl-1,1'-spirobisindane (0.58 g, 82 %) as a white powder (mp 140 – 142 °C); IR (DCM film) 2954, 2922, 2861, 2538, 1467, 1362, 1264 cm^{-1}; ^{1}H NMR (500 MHz, CDCl$_3$) δ 7.17 (2H, s, Ar*H*), 6.77 (2H, s, Ar*H*), 3.72 (2H, s, S*H*), 3.60 (2H, s, S*H*), 2.27 (2H, d, *J* = 13.1 Hz, CH*H*), 2.13 (2H, d, *J* = 13.1 Hz, C*H*H), 1.33 (6H, s, C*H$_3$*), 1.28 (6H, s, C*H$_3$*); ^{13}C NMR (125 MHz, CDCl$_3$) δ 152.0, 149.8, 129.9, 129.8, 127.2, 125.1, 59.5, 57.3, 43.6, 31.7, 30.2; HRMS (EI^{+}, *m/z*) calc. for C$_{21}$H$_{24}$S$_4$: 404.0761 (M^{+}), found 404.0766.

2,5-Dichloro-4-methylbenzoic acid
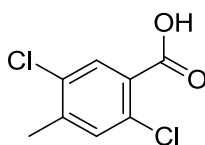
A mixture of 2,5-dichloro-*p*-xylene (5.00 g, 28.6 mmol), potassium permanganate (26.0 g, 165 mmol), pyridine (80 ml) and water (30 ml) was refluxed for 24 hrs, cooled briefly, filtered and washed with hot water (100 ml). The combined aqueous filtrates were reduced, acidified with 2N HCl (150 ml), stirred for 30 mins, the resultant precipitate filtered, washed with water (500 ml) and dried under vacuum. The crude products were then refluxed in chloroform (200 ml) for 2 hrs, filtered, and washed with chloroform (50 ml). The combined organic filtrates were reduced under vacuum and dried to give 2,5-dichloro-4-methylbenzoic acid (2.59 g, 44 %) as a white solid (mp > 300 °C, literature mp > 300 °C[236]); IR (DCM film) 2924, 2629, 2537, 1714, 1680, 1597, 1300, 1256, 1085 cm^{-1}; ^{1}H NMR (400 MHz, (CD$_3$)$_2$CO) δ 7.91 (1H, s, Ar*H*), 7.54 (1H, s, Ar*H*), 2.42 (3H, s, C*H$_3$*); ^{13}C NMR (125 MHz, (CD$_3$)$_2$CO) δ 165.4,

142.5, 134.2, 133.4, 132.5, 130.2, 19.9; LRMS (EI$^+$, *m/z*) calc. for C$_8$H$_6$Cl$_2$O$_2$: 203.97 (M$^+$), found 203.97.

2,5-Dichloroterephthalic acid
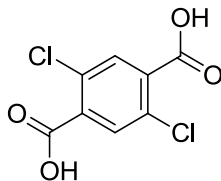
A mixture of 2,5-dichloro-*p*-xylene (17.5 g, 100 mmol), potassium permanganate (158 g, 1000 mmol), 18-crown-6 (0.015 g, 0.057 mmol), pyridine (270 ml), water (70 ml) and chloroform (150 ml) was refluxed for 72 hrs, cooled briefly, filtered and washed with hot water (300 ml). The combined aqueous filtrates were reduced under vacuum, acidified with 2N HCl (300 ml) and stirred for 30 mins. The resultant precipitate was then filtered, washed with water (800 ml) and dried under vacuum. The crude product was refluxed in chloroform (300 ml) for 2 hrs, filtered hot, washed with chloroform (100 ml) and dried to give 2,5-dichloroterephthalic acid (11.4 g, 49 %) as a white solid (mp > 300 °C, literature mp 305 °C[237]); IR (DCM film) 2991, 1685, 1249, 1084 cm^{-1}; ^{1}H NMR (400 MHz, (CD$_3$)$_2$CO) δ 7.99 (2H, s, Ar*H*); ^{13}C NMR (125 MHz, (CD$_3$)$_2$CO) δ 165.1, 135.3, 134.1, 132.2 LRMS (EI$^+$, *m/z*) calc. for C$_8$H$_4$Cl$_2$O$_4$: 233.95 (M$^+$), found 233.95.

1,4-Dichloro-2,5-di(4'-methylbenzoyl)benzene
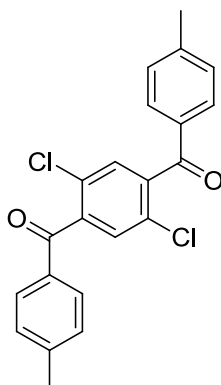
Thionyl chloride (15.0 ml, 207 mmol) and anhydrous DMF (0.5 ml) were added to a suspension of 2,5-dichloroterephthalic acid (2.35 g, 10.0 mmol) in anhydrous cyclohexane (5 ml) and refluxed for 24 hrs. The resultant solution was cooled to RT before excess thionyl

chloride and cyclohexane were removed *via* distillation. The residual white powder was dissolved in anhydrous chloroform and cooled to -10 °C (ice/ethanol bath). Anhydrous toluene (2.65 ml, 25.0 mmol) was added followed by the portionwise addition of aluminium (III) chloride (3.33 g, 25.0 mmol), and the reaction slowly warmed to RT. After stirring for a further 12 hrs at RT, the reaction products were poured over crushed ice (150 ml), stirred for 2 hrs and extracted into chloroform (3 x 100 ml). The combined organic extracts were washed with 2N HCl (100 ml), water (3 x 100 ml) and brine (100 ml), dried over anhydrous magnesium sulfate and reduced. The crude pale yellow solid was then triturated in methanol (150 ml) for 2 hrs, filtered, dried and recrystallised from ethyl acetate to give 1,4-dichloro-2,5-di(4'-methylbenzoyl)benzene (2.75 g, 72 %) as a fluffy white solid (mp 169 – 171 °C); IR (DCM film) 3060, 1666, 1605, 1350, 1249, 1183, 1082 cm^{-1}; ^{1}H NMR (400 MHz, CDCl$_3$) δ 7.73 (4H, d, J = 8.0 Hz, ArH), 7.43 (2H, s, ArH), 7.30 (4H, d, J = 8.0 Hz, ArH), 2.44 (6H, s, CH_3); ^{13}C NMR (125 MHz, CDCl$_3$) δ 192.9, 146.8, 141.4, 133.3, 130.5, 130.3, 130.1, 129.8, 22.1; HRMS (EI$^+$, *m/z*) calc. for C$_{22}$H$_{16}$Cl$_2$O$_2$: 382.0527, found 382.0526. Crystallography data (chloroform/methanol): Monoclinic, space group: P2$_1$/c, a = 16.1281(4) Å, b = 4.92160(10) Å, c = 23.2810(6) Å, β = 98.565(2), V = 1827.34 Å^3, Z = 4, R_1 = 3.93.

5.2.2 Organic Molecules of Intrinsic Microporosity (OMIMs)

General Procedure 1

Anhydrous fluorinated and catechol/dithiol compounds were added to an oven-dried, single-necked flask equipped with a magnetic stirrer bar. After flushing with dry nitrogen for 5 mins, anhydrous DMF was added *via* syringe and the reaction mixture heated to form a solution. At which point, oven dried potassium carbonate was added, the reaction sealed under dry nitrogen flow, heated to 65 °C and left to stir for 72 hrs. After cooling to RT, the reaction mixture was poured into water (20 times DMF volume), acidified with 2N HCl (5 times DMF volume) and allowed to stir as a suspension for 2 hrs. The crude product was then collected *via* filtration, washed with water (20 times DMF volume), methanol (20 times DMF volume) and dried under suction. Following any required purification, the product was further dried in a 100 °C vacuum oven.

5.2.2.1 Di-substituted adducts

Di-[benzene-1,2-dithiol] phenyl adduct
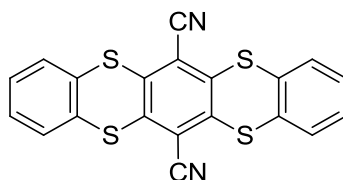
Benzene-1,2-dithiol (0.648 g, 4.56 mmol), 2,3,5,6-tetrafluoroterephthalonitrile (0.414 g, 2.07 mmol) and potassium carbonate (1.80 g, 13.0 mmol) were reacted together in anhydrous DMF (10 ml) in accordance with general procedure 1 to give the di-[benzene-1,2-dithiol] phenyl adduct (0.78 g, 94 %) as a yellow powder (mp > 300 °C); IR (DCM film) 2921, 2224, 1447, 1425, 1319, 1248 cm^{-1}; ^{13}C NMR (101 MHz, solid state) δ 141.1, 130.3 (br), 113.0 (some carbons missing); HRMS (EI$^+$, *m/z*) calc. for $C_{22}H_8N_2S_4$: 403.9570, found 403.9552; elemental analysis calc. C: 59.38, H: 1.99, N: 6.92, S: 31.71, found C: 58.46, H: 2.04, N: 6.91, S: 29.78.

Di-[catechol] biphenyl adduct
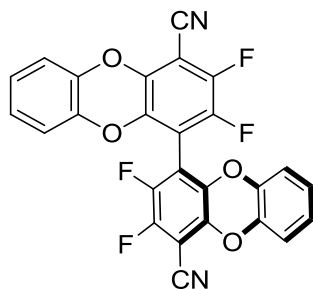
4,4'-Dicyano-2,2',3,3',5,5',6,6'-octafluorobiphenyl (0.795 g, 2.28 mmol), catechol (0.754 g, 6.85 mmol) and potassium carbonate (2.50 g, 18.1 mmol) were reacted together in anhydrous DMF (15 ml) in accordance with general procedure 1. Purification was achieved using column chromatography (5/4/1 hexane/DCM/toluene, R_f = 0.3) to give the di-[catechol] biphenyl adduct (trace) as a yellow powder; ^{19}F NMR (282 MHz, CDCl$_3$) δ -136.0 (2F, d, *J* = 22.1 Ar*F*), -138.9 (2F, d, *J* = 22.1, Ar*F*); LRMS (EI[+], *m/z*) calc. for C$_{26}$H$_8$F$_4$N$_2$O$_4$: 488.04 (M[+]), found 488.02.

Di-[triptycene-2,3-diol] biphenyl adduct
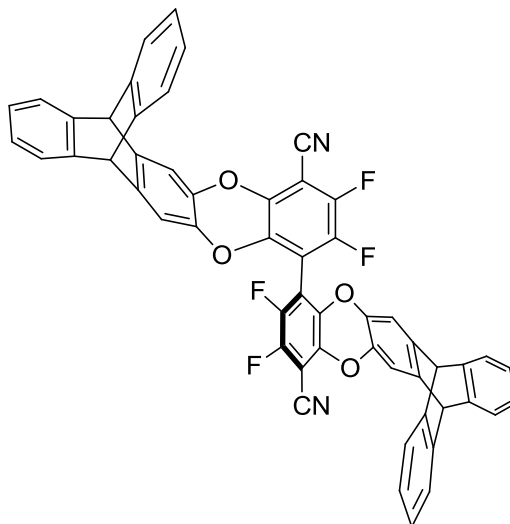
4,4'-Dicyano-2,2',3,3',5,5',6,6'-octafluorobiphenyl (0.233 g, 0.669 mmol), triptycene-2,3-diol (0.576 g, 2.01 mmol) and potassium carbonate (0.740 g, 5.35 mmol) were reacted together in anhydrous DMF (10 ml) in accordance with general procedure 1. Purification was achieved using column chromatography (hexane/DCM 3/2, R_f = 0.3) to give the di-[triptycene-2,3-diol] biphenyl adduct (0.115 g, 20 %) as a yellow powder (mp > 300 °C); IR (DCM film) 3066, 2963, 2924, 2243, 1456, 1384, 1280, 1140 cm^{-1}; ^{1}H NMR (500 MHz, CDCl$_3$)

δ 7.37 – 7.34 (4H, m, Ar*H*), 7.30 – 7.28 (2H, m, Ar*H*), 7.24 – 7.23 (2H, m, Ar*H*), 7.06 (2H, s, Ar*H*), 7.03 – 6.96 (8H, m, Ar*H*), 6.79 (2H, s, Ar*H*), 5.34 (2H, s, C*H*), 5.21 (2H, s, C*H*); ^{13}C NMR (125 MHz, CDCl$_3$) *δ* 144.6, 144.5, 144.5, 144.4, 143.4, 143.2, 141.2, 141.2, 141.2, 137.2, 137.0, 136.8, 125.8, 125.8, 125.8, 125.7, 123.9, 123.9, 123.8, 113.0, 112.9, 111.2, 111.1, 108.8, 108.8, 93.9, 93.8, 77.6, 77.5, 77.4, 77.2, 77.0, 53.5, 53.4 (^{19}F-^{13}C coupling not assigned); ^{19}F NMR (282 MHz, CDCl$_3$) *δ* -136.3 (2F, d, *J* = 21.3 Hz, Ar*F*), -139.2 (2F, d, *J* = 21.3 Hz, Ar*F*); HRMS (EI$^+$, *m/z*) calc. for C$_{54}$H$_{24}$F$_4$N$_2$O$_4$: 840.1672 (M$^+$), found 840.1699; GPC analysis (CHCl$_3$) M_n = 813, M_w = 829 g mol^{-1} relative to polystyrene, M_w/M_n = 1.020; BET surface area = 9 m^2 g^{-1}; total pore volume = 0.02 cm^3 g^{-1} at *p/p^o* = 0.98.
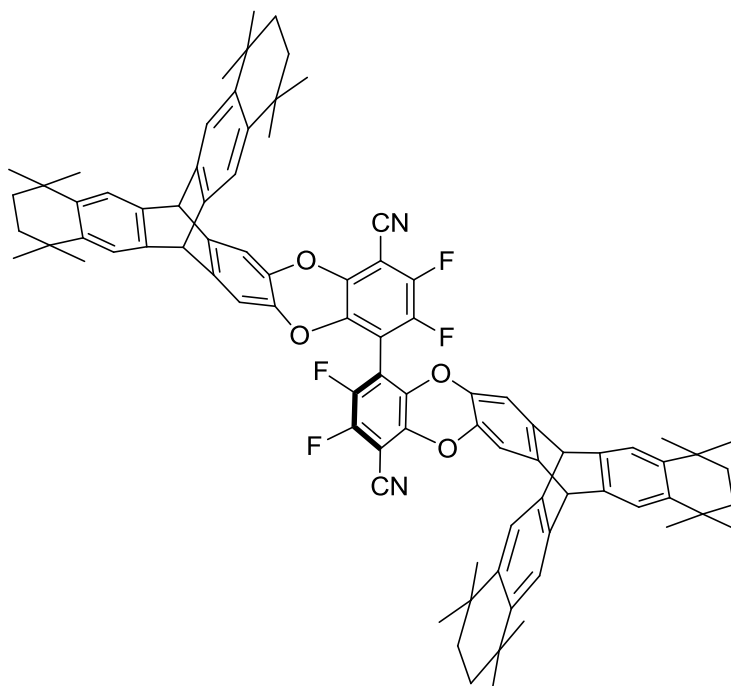
Di-[cy6-triptycene-2,3-diol] biphenyl adduct

4,4'-Dicyano-2,2',3,3',5,5',6,6'-octafluorobiphenyl (0.116 g, 0.333 mmol), cy6-triptycene-2,3-diol (0.505 g, 1.00 mmol) and potassium carbonate (0.367 g, 2.66 mmol) were reacted together in anhydrous DMF (10 ml) in accordance with general procedure 1. Purification was achieved using column chromatography (hexane/toluene 13/7, R_f = 0.25) to give the di-[cy6-triptycene-2,3-diol] biphenyl adduct (0.169 g, 40 %) as a yellow powder (mp > 300 °C); IR (DCM film) 2962, 2865, 2245, 1458, 1362, 1280, 1140, 1015 cm^{-1}; ^{1}H NMR (400 MHz, CDCl$_3$) *δ* 7.22 (4H, s, Ar*H*), 7.18 (2H, s, Ar*H*), 7.12 (2H, s, Ar*H*), 7.03 (2H, s, Ar*H*), 6.77 (2H, s, Ar*H*), 5.16 (2H, s, C*H*), 5.06 (2H, s, C*H*), 1.56 – 1.53 (16H, m, C*H$_2$*), 1.24 – 1.08 (48H, m, C*H$_3$*); ^{13}C

NMR (125 MHz, CDCl$_3$) δ 144.2, 144.1, 141.9, 141.9, 141.8, 141.8, 141.5, 141.5, 141.4, 141.3, 136.7, 136.5, 121.8, 121.7, 121.6, 112.8, 112.7, 108.8, 53.1, 35.4, 34.5, 34.4, 32.3, 32.2, 32.2, 32.0, 29.9 (^{19}F-^{13}C coupling not assigned); ^{19}F NMR (282 MHz, CDCl$_3$) δ -136.5 (2F, d, J = 21.7 Hz, ArF), -139.6 (2F, d, J = 21.7 Hz, ArF); LRMS (MALDI, m/z) calc. for C$_{66}$H$_{80}$F$_4$N$_2$O$_4$: 1280.61 (M$^+$), found 1280.57; GPC analysis (CHCl$_3$) M_n = 1189, M_w = 1218 g mol^{-1} relative to polystyrene, M_w/M_n = 1.025.

5.2.2.2 Tri-substituted adducts (Branch Units)

Tri-[R-catechol] biphenyl adducts
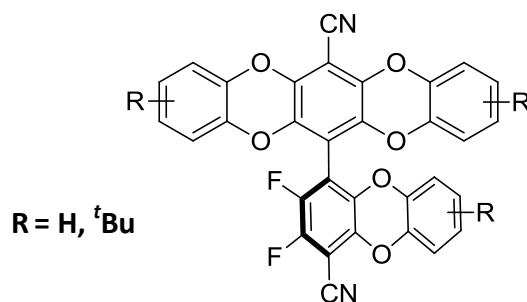
[R = H]: Tri-[catechol] biphenyl adduct

4,4'-Dicyano-2,2',3,3',5,5',6,6'-octafluorobiphenyl (0.795 g, 2.28 mmol), catechol (0.754 g, 6.85 mmol) and potassium carbonate (2.50 g, 18.1 mmol) were reacted together in anhydrous DMF (15 ml) in accordance with general procedure 1. Purification was achieved using column chromatography (5/4/1 hexane/DCM/toluene, R_f = 0.25) to give the tri-[catechol] biphenyl adduct (0.370 g, 29 %) as a yellow powder (mp > 300 °C); IR (DCM film) 2239, 1497, 1454, 1268, 1101, 1036 cm^{-1}; ^{1}H NMR (400 MHz, CDCl$_3$) δ 7.04 − 6.89 (9H, m, ArH), 6.69 (3H, dd, J = 8.0, 1.6 Hz, ArH); ^{13}C NMR (125 MHz, CDCl$_3$) δ 140.8, 140.6, 140.4, 140.0, 136.0, 125.9, 125.7, 125.5, 125.4, 117.1, 116.9 (^{19}F-^{13}C coupling not assigned, some carbons missing); ^{19}F NMR (282 MHz, CDCl$_3$) δ -136.6 (1F, d, J = 22.0, ArF), -138.8 (1F, d, J = 22.0, ArF); HRMS (EI$^+$, m/z) calc. for C$_{32}$H$_{12}$F$_2$N$_2$O$_6$: 558.0663 (M$^+$), found 558.0657; GPC analysis (CHCl$_3$) M_n = 522, M_w = 534 g mol^{-1} relative to polystyrene, M_w/M_n = 1.025.

[R = ^{t}Bu]: Tri-[4-*tert*-butylcatechol] biphenyl adduct

4,4'-Dicyano-2,2',3,3',5,5',6,6'-octafluorobiphenyl (0.312 g, 0.896 mmol), 4-*tert*-butylcatechol (0.447 g, 2.69 mmol) and potassium carbonate (0.990 g, 7.16 mmol) were reacted together in anhydrous DMF (10 ml) in accordance with general procedure 1. Purification was achieved using column chromatography (hexane/toluene/DCM 3/1/1, R_f = 0.25) to give the tri-[4-*tert*-butylcatechol] biphenyl adduct (mixture of regioisomers) (0.371 g, 57 %) as a yellow powder (mp > 300 °C); IR (DCM film) 2962, 2926, 2855, 2241, 1725, 1513, 1447, 1285, 1014 cm^{-1}; ^{1}H NMR (400 MHz, CDCl$_3$) δ 7.06 – 6.84 (6H, m, Ar*H*), 6.76 – 6.56 (3H, m, Ar*H*), 1.26 – 1.13 (27H, m, ^{t}Bu*H*); ^{13}C NMR (125 MHz, CDCl$_3$) δ 149.7 – 149.1 (m), 141.3 – 141.2 (m), 140.2 – 139.6 (m), 138.4 – 137.9 (m), 137.4 – 137.3 (m), 136.1 – 135.8 (m), 122.4 – 121.9 (m), 116.4 – 116.1 (m), 114.4 – 114.0 (m), 110.7 – 110.6 (m), 109.5 – 109.4 (m), 93.2 – 93.1 (m), 92.0, 91.9, 34.8 – 34.7 (m), 31.4 – 31.3 (m), 29.9 (^{19}F-^{13}C coupling not assigned, extra carbons due to regioisomeric nature); ^{19}F NMR (282 MHz, CDCl$_3$) δ -136.7 – -136.9 (1F, cluster of doublets, Ar*F*), -139.0 – -139.3 (1F, cluster of doublets, Ar*F*); LRMS (EI$^+$, *m/z*) calc. for C$_{44}$H$_{36}$F$_2$N$_2$O$_6$: 726.25 (M$^+$), found 726.25; GPC analysis (CHCl$_3$) M_n = 771, M_w = 813 g mol^{-1} relative to polystyrene, M_w/M_n = 1.055.

Tri-[3,5-di-*tert*-butylcatechol] biphenyl adduct
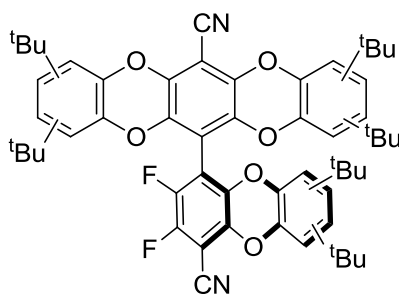
4,4'-Dicyano-2,2',3,3',5,5',6,6'-octafluorobiphenyl (0.510 g, 1.46 mmol), 3,5-di-*tert*-butylcatechol (0.977 g, 4.39 mmol) and potassium carbonate (1.62 g, 11.7 mmol) were reacted together in anhydrous DMF (15 ml) in accordance with general procedure 1. Purification was achieved using column chromatography (hexane/toluene/DCM 7/2/1, R_f = 0.25) to give the tri-[3,5-di-*tert*-butylcatechol] biphenyl adduct (mixture of regioisomers) (0.453 g, 39 %) as a yellow powder (mp > 300 °C); IR (DCM film) 2964, 2908, 2871, 2239, 1454, 1414, 1304, 1276, 1038, 1018 cm^{-1}; ^{1}H NMR (400 MHz, CDCl$_3$) δ 6.97 – 6.84 (5H, m,

Ar*H*), 6.65 − 6.58 (1H, m, Ar*H*), 1.47 − 1.04 (54H, m, ^{t}Bu*H*); ^{13}C NMR (125 MHz, CDCl$_3$) δ 148.3, 148.0, 147.7 − 147.6 (m), 140.7 − 139.7 (m), 138.2 − 138.1 (m), 137.8, 137.4, 137.2, 136.9 − 136.8 (m), 136.4, 136.0 − 135.8 (m), 120.3 − 120.2 (m), 120.1 − 120.0 (m), 119.8 − 119.7 (m), 112.6 − 112.4 (m), 35.5 − 35.4 (m), 34.9 − 34.8 (m), 31.43 − 31.39 (m), 30.12 − 30.05 (m), 29.5 − 29.4 (m) (^{19}F-^{13}C coupling not assigned, extra carbons due to regioisomeric nature); ^{19}F NMR (282 MHz, CDCl$_3$) δ -137.3 − -137.9 (1F, cluster of doublets, Ar*F*), -139.4 − -140.1 (1F, cluster of doublets, Ar*F*); LRMS (MALDI, *m/z*) calc. for C$_{56}$H$_{60}$F$_2$N$_2$O$_6$: 894.44 (M$^+$), found 894.43; GPC analysis (CHCl$_3$) M_n = 904, M_w = 949 g mol^{-1} relative to polystyrene, M_w/M_n = 1.050.

Tri-[R-naphthalene-2,3-diol] biphenyl adducts

R = H, ^{t}Bu, Ad
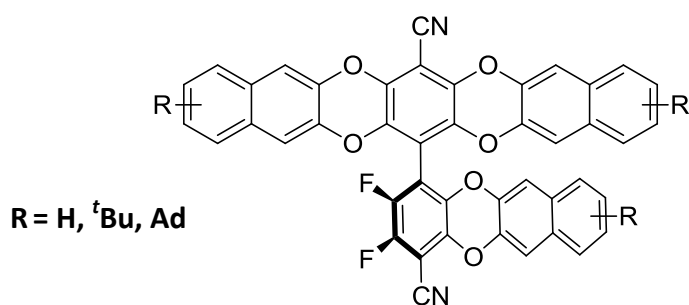
[R = H]: Tri-[naphthalene-2,3-diol] biphenyl adduct

4,4'-Dicyano-2,2',3,3',5,5',6,6'-octafluorobiphenyl (0.505 g, 1.45 mmol), naphthalene-2,3-diol (0.697 g, 4.35 mmol) and potassium carbonate (1.60 g, 11.6 mmol) were reacted together in anhydrous DMF (10 ml) in accordance with general procedure 1. Purification was achieved using column chromatography (hexane/DCM/toluene 2/2/1, R_f = 0.23) to give the tri-[naphthalene-2,3-diol] biphenyl adduct (0.334 g, 33 %) as a yellow powder (mp > 300 °C); IR (DCM film) 3062, 2237, 1516, 1431, 1261, 1167, 1017 cm^{-1}; ^{1}H NMR (400 MHz, CDCl$_3$) δ 7.70 − 7.68 (3H, m, Ar*H*), 7.52 − 7.27 (12H, m, Ar*H*), 7.14 (2H, s, Ar*H*), 7.11 (1H, s, Ar*H*); ^{13}C NMR (125 MHz, CDCl$_3$) δ 139.9 − 139.8 (m), 139.8, 139.7, 139.5 − 139.4 (m), 135.5, 131.3 − 131.2 (m), 127.4 − 127.3 (m), 126.6 − 126.4 (m), 113.62 − 113.60 (m), 113.5, 113.3, 110.2, 93.7, 93.6 (^{19}F-^{13}C coupling not assigned); ^{19}F NMR (282 MHz, CDCl$_3$) δ -136.2 (1F, d, *J* = 21.9 Hz, Ar*F*), -138.5 (1F, d, *J* = 21.9 Hz, Ar*F*); LRMS (EI$^+$, *m/z*) calc. for C$_{44}$H$_{18}$F$_2$N$_2$O$_6$: 708.11 (M$^+$), found 708.12; GPC analysis (CHCl$_3$) M_n = 571, M_w = 603 g mol^{-1} relative to polystyrene, M_w/M_n = 1.056.

[R = *t*Bu]: Tri-[6-*tert*-butylnaphthalene-2,3-diol] biphenyl adduct

4,4'-Dicyano-2,2',3,3',5,5',6,6'-octafluorobiphenyl (0.630 g, 1.81 mmol), 6-*tert*-butylnaphthalene-2,3-diol (1.163 g, 5.43 mmol) and potassium carbonate (2.00 g, 14.5 mmol) were reacted together in anhydrous DMF (15 ml) in accordance with general procedure 1. Purification was achieved using column chromatography (hexane/toluene/DCM 3/1/1, R_f = 0.25) to give the tri-[6-*tert*-butylnaphthalene-2,3-diol] biphenyl adduct (mixture of regioisomers) (0.429 g, 27 %) as a yellow powder (mp > 300 °C); IR (DCM film) 2959, 2925, 2855, 2240, 1515, 1441, 1249, 1017 cm^{-1}; ^{1}H NMR (400 MHz, CDCl$_3$) δ 7.64 – 7.60 (3H, m, Ar*H*), 7.47 – 7.32 (9H, m, Ar*H*), 7.14 – 7.02 (3H, m, Ar*H*), 1.36 – 1.25 (27H, m, *t*Bu*H*); ^{13}C NMR (125 MHz, CDCl$_3$) δ 149.5 – 149.3 (m), 140.0 – 139.1 (m), 135.6, 131.3 – 131.2 (m), 129.4 – 129.3 (m), 128.2 – 127.8 (m), 127.1, 127.0, 125.5, 125.3, 122.5, 122.4, 113.7 – 112.7 (m), 110.5, 109.6, 109.2, 104.4, 92.31 – 92.30 (m), 35.04 – 34.99 (m), 31.4 – 31.2 (m) (^{19}F-^{13}C coupling not assigned, extra carbons due to regioisomeric nature); ^{19}F NMR (282 MHz, CDCl$_3$) δ -136.5 – -136.7 (1F, cluster of doublets, Ar*F*), -138.5 – -138.9 (1F, cluster of doublets, Ar*F*); LRMS (EI$^+$, *m/z*) calc. for C$_{56}$H$_{42}$F$_2$N$_2$O$_6$: 876.30 (M$^+$), found 876.30; GPC analysis (CHCl$_3$) M_n = 1037, M_w = 1075 g mol^{-1} relative to polystyrene, M_w/M_n = 1.037.

[R = Ad]: Tri-[6-(1-adamantyl)naphthalene-2,3-diol] biphenyl adduct

4,4'-Dicyano-2,2',3,3',5,5',6,6'-octafluorobiphenyl (0.320 g, 0.919 mmol), 6-(1-adamantyl)naphthalene-2,3-diol (0.812 g, 2.73 mmol) and potassium carbonate (1.02 g, 7.38 mmol) were reacted together in anhydrous DMF (10 ml) in accordance with general procedure 1. Purification was achieved using column chromatography (hexane/toluene/DCM 3/1/1, R_f = 0.2) to give the tri-[6-(1-adamantyl)naphthalene-2,3-diol] biphenyl adduct (mixture of regioisomers) (0.120 g, 12 %) as a yellow powder (mp > 300 °C); IR (DCM film) 2904, 2849, 2240, 1515, 1441, 1266, 1244, 1017 cm^{-1}; ^{1}H NMR (400 MHz, CDCl$_3$) δ 7.65 – 7.55 (3H, m, Ar*H*), 7.46 – 7.29 (9H, m, Ar*H*), 7.14 – 7.01 (3H, m, Ar*H*), 2.11 – 1.70 (45H, m, Ad*H*); ^{13}C NMR (500 MHz, CDCl$_3$) δ 149.7 – 149.5 (m), 139.9 – 139.0 (m), 131.4 – 131.3 (m), 130.5, 129.42 – 129.38 (m), 127.1 – 126.9 (m), 124.9 – 124.7 (m), 122.6 – 122.4 (m), 113.7 – 112.7 (m), 110.5, 110.2, 109.6 – 109.5 (m), 109.2, 92.3, 43.2 – 43.1 (m), 37.0 – 36.6 (m), 29.9, 29.14 – 29.05 (m) (^{19}F-^{13}C coupling not assigned, extra carbons due to

regioisomeric nature); ^{19}F NMR (282 MHz, CDCl$_3$) δ -136.6 – -136.8 (1F, cluster of doublets, Ar*F*), -138.5 – -138.9 (1F, cluster of doublets, Ar*F*); LRMS (MALDI, *m/z*) calc. for C$_{74}$H$_{60}$F$_2$N$_2$O$_6$: 1110.44 (M$^+$), found 1110.23; GPC analysis (CHCl$_3$) M_n = 1065, M_w = 1090 g mol^{-1} relative to polystyrene, M_w/M_n = 1.023.

Tri-[R$_1$,R$_2$-triptycene-2,3-diol] biphenyl adducts
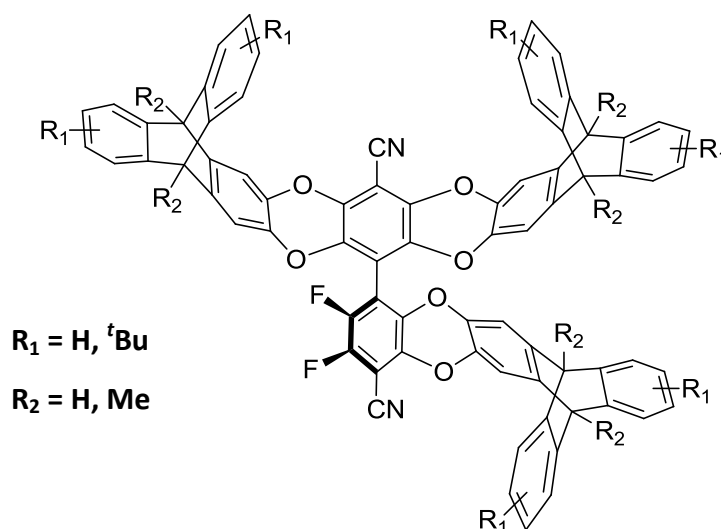
R$_1$ = H, ^{t}Bu

R$_2$ = H, Me

[R$_1$ = H, R$_2$ = H]: Tri-[triptycene-2,3-diol] biphenyl adduct

4,4'-Dicyano-2,2',3,3',5,5',6,6'-octafluorobiphenyl (0.233 g, 0.669 mmol), triptycene-2,3-diol (0.576 g, 2.01 mmol) and potassium carbonate (0.740 g, 5.35 mmol) were reacted together in anhydrous DMF (10 ml) in accordance with general procedure 1. Purification was achieved using column chromatography (hexane/DCM 3/2, R_f = 0.25) to give the tri-[triptycene-2,3-diol] biphenyl adduct (0.185 g, 21 %) as a yellow powder (mp > 300 °C); IR (DCM film) 2959, 2923, 2241, 1446, 1285, 1140, 1013 cm^{-1}; ^{1}H NMR (500 MHz, CDCl$_3$) δ 7.34 – 7.31 (6H, m, Ar*H*), 7.27 – 7.24 (2H, m, Ar*H*), 7.21 – 7.17 (4H, m, Ar*H*), 7.04 (1H, s, Ar*H*), 7.01 (2H, s, Ar*H*), 6.99 – 6.93 (12H, m, Ar*H*), 6.72 (3H, s, Ar*H*), 5.31 (1H, s, C*H*), 5.29 (2H, s, C*H*), 5.17 (2H, s, C*H*), 5.13 (1H, s, C*H*); ^{13}C NMR (125 MHz, CDCl$_3$) δ 144.8, 144.7, 144.7, 144.60 – 144.59 (m), 144.5, 143.1, 142.9, 142.7, 142.6, 139.7, 137.4, 137.2, 137.1, 136.8, 135.8, 125.7 – 125.6 (m), 123.8 – 123.7 (m), 113.1, 112.9, 112.8, 91.8, 53.5, 53.4, 53.3 (^{19}F-^{13}C coupling not assigned); ^{19}F NMR (282 MHz, CDCl$_3$) δ -137.0 (1F, d, *J* = 20.8 Hz, Ar*F*), -139.5 (1F, d, *J* = 20.8 Hz, Ar*F*); LRMS (MALDI, *m/z*) calc. for C$_{74}$H$_{36}$F$_2$N$_2$O$_6$: 1086.25 (M$^+$), found 1086.39; GPC

analysis (CHCl$_3$) M_n = 955, M_w = 975 g mol^{-1} relative to polystyrene, M_w/M_n = 1.020; BET surface area = 248 m^2 g^{-1}; total pore volume = 0.28 cm^3 g^{-1} at p/p^o = 0.98.

[R$_1$ = ^{t}Bu, R$_2$ = H]: Tri-[7,14-di-*tert*-butyltriptycene-2,3-diol] biphenyl adduct

4,4'-Dicyano-2,2',3,3',5,5',6,6'-octafluorobiphenyl (0.140 g, 0.420 mmol), 7,14-di-*tert*-butyltriptycene-2,3-diol (0.481 g, 1.21 mmol) and potassium carbonate (0.500 g, 3.62 mmol) were reacted together in anhydrous DMF (10 ml) in accordance with general procedure 1. Purification was achieved using column chromatography (hexane/toluene/DCM 3/1/1, R_f = 0.15) to give the tri-[7,14-di-*tert*-butyltriptycene-2,3-diol] biphenyl adduct (mixture of regioisomers) (0.210 g, 37 %) as a yellow powder (mp > 300 °C); IR (DCM film) 2961, 2869, 2241, 1444, 1284, 1140, 1014 cm^{-1}; ^{1}H NMR (500 MHz, CDCl$_3$) δ 7.36 − 7.35 (3H, m, Ar*H*), 7.28 − 6.87 (18H, m, Ar*H*), 6.76 − 6.70 (3H, m, Ar*H*), 5.26 − 5.23 (3H, m, C*H*), 5.12 − 5.08 (3H, m, C*H*), 1.24 − 1.14 (54H, m, ^{t}Bu*H*); ^{13}C NMR (125 MHz, CDCl$_3$) δ 148.7, 144.7 − 144.5 (m), 143.74 − 143.68 (m), 143.3 − 143.1 (m), 142.0 − 141.8 (m), 139.7, 139.6, 139.4, 137.3 − 137.0 (m), 135.8, 123.3 − 123.1 (m), 122.2 − 122.1 (m), 121.2 − 120.9 (m), 112.8 − 112.7 (m), 109.1, 93.0, 53.44 − 53.36 (m), 34.8, 34.7, 31.7 (^{19}F-^{13}C coupling not assigned, extra carbons due to regioisomeric nature); ^{19}F NMR (282 MHz, CDCl$_3$) δ -136.9 − -137.2 (1F, cluster of doublets, Ar*F*), -139.6 − -139.8 (1F, cluster of doublets, Ar*F*); LRMS (MALDI, *m/z*) calc. for C$_{98}$H$_{84}$F$_2$N$_2$O$_6$: 1423.63 (M$^+$), found 1423.66; GPC analysis (CHCl$_3$) M_n = 1488, M_w = 1518 g mol^{-1} relative to polystyrene, M_w/M_n = 1.021; BET surface area = 551 m^2 g^{-1}; total pore volume = 0.44 cm^3 g^{-1} at p/p^o = 0.98.

[R$_1$ = H, R$_2$ = Me]: Tri-[9,10-dimethyltriptycene-2,3-diol] biphenyl adduct

4,4'-Dicyano-2,2',3,3',5,5',6,6'-octafluorobiphenyl (0.155 g, 0.445 mmol), 9,10-dimethyltriptycene-2,3-diol (0.598 g, 1.90 mmol) and potassium carbonate (0.615 g, 4.45 mmol) were reacted together in anhydrous DMF (10 ml) in accordance with general procedure 1. Purification was achieved using column chromatography (hexane/toluene/DCM 9/7/4, R_f = 0.20) to give the tri-[9,10-dimethyltriptycene-2,3-diol] biphenyl adduct (0.110 g, 21 %) as a yellow powder (mp > 300 °C); IR (DCM film) 3064, 2972, 2919, 2241, 1442, 1289, 1168, 1013 cm^{-1}; ^{1}H NMR (500 MHz, CDCl$_3$) δ 7.32 − 7.30 (6H, m, Ar*H*), 7.26 − 7.24 (2H, m, Ar*H*), 7.21 − 7.18 (4H, m, Ar*H*), 7.03 − 6.95 (15H, m, Ar*H*), 6.65 (1H, s, Ar*H*), 6.63 (2H, s, Ar*H*), 2.34 − 2.32 (9H, m, C*H$_3$*), 2.21 − 2.17 (9H, m, C*H$_3$*); ^{13}C NMR (125

MHz, CDCl$_3$) δ 147.70, 147.66, 147.6, 147.53, 147.50, 146.5, 146.2, 146.0, 145.9, 142.4, 142.3, 141.1 – 140.9 (m), 139.7, 137.2, 136.9, 136.6, 135.8, 125.3 – 125.2 (m), 120.7, 120.66 – 120.63 (m), 113.3, 113.2, 110.6, 110.4, 110.29, 110.25, 109.30 – 109.27 (m), 109.1, 93.1, 93.0, 91.8, 48.5 – 48.4 (m), 13.7, 13.6, 13.5 (^{19}F-^{13}C coupling not assigned); ^{19}F NMR (282 MHz, CDCl$_3$) δ -136.7 (1F, d, J = 20.8 Hz, ArF), -139.6 (1F, d, J = 20.8 Hz, ArF); LRMS (MALDI, m/z) calc. for C$_{80}$H$_{48}$F$_2$N$_2$O$_6$: 1170.35 (M$^+$), found 1171.33 (MH$^+$); GPC analysis (CHCl$_3$) M_n = 1064, M_w = 1086 g mol^{-1} relative to polystyrene, M_w/M_n = 1.020; BET surface area = 337 m^2 g^{-1}; total pore volume = 0.75 cm^3 g^{-1} at p/p^o = 0.98.

[R$_1$ = ^{t}Bu, R$_2$ = Me]: Tri-[7,14-di-*tert*-butyl-9,10-dimethyltriptycene-2,3-diol] biphenyl adduct

4,4'-Dicyano-2,2',3,3',5,5',6,6'-octafluorobiphenyl (0.0885 g, 0.254 mmol), 7,14-di-*tert*-butyl-9,10-dimethyltriptycene-2,3-diol (0.336 g, 0.788 mmol) and potassium carbonate (0.280 g, 2.03 mmol) were reacted together in anhydrous DMF (10 ml) in accordance with general procedure 1. Purification was achieved using column chromatography (7/2/1 hexane/toluene/DCM, R_f = 0.20) to give the tri-[7,14-di-*tert*-butyl-9,10-dimethyltriptycene-2,3-diol] biphenyl adduct (mixture of regioisomers) (0.146 g, 38 %) as a yellow powder (mp > 300 °C); IR (DCM film) 3063, 2966, 2869, 2241, 1612, 1443, 1290, 1013 cm^{-1}; ^{1}H NMR (500 MHz, CDCl$_3$) δ 7.30 – 6.92 (21H, m, ArH), 6.63 – 6.60 (3H, m, ArH), 2.30 – 2.17 (18H, m, CH_3), 1.22 – 1.13 (54H, m, ^{t}BuH); ^{13}C NMR (125 MHz, CDCl$_3$) δ 148.1 – 148.0 (m), 147.4 – 147.2 (m), 147.0 – 146.9 (m), 146.63 – 146.57 (m), 146.5 – 146.4 (m), 146.3, 144.9 – 144.7 (m), 141.0 – 140.9 (m), 139.73 – 139.66 (m), 137.1, 136.8 – 136.7 (m), 136.40, 136.38, 135.8, 135.7, 121.7 – 121.6 (m), 120.3 – 120.1 (m), 117.8, 113.3 – 113.1 (m), 110.7 – 110.1 (m), 109.4, 109.1, 92.8, 91.7, 48.3, 48.2, 34.82, 34.76, 31.7, 13.8, 13.7, 13.6 (^{19}F-^{13}C coupling not assigned, extra carbons due to regioisomeric nature); ^{19}F NMR (282 MHz, CDCl$_3$) δ -136.8 – -137.1 (1F, cluster of doublets, ArF), -139.9 – -140.0 (1F, cluster of doublets, ArF); LRMS (MALDI, m/z) calc. for C$_{104}$H$_{96}$F$_2$N$_2$O$_6$: 1507.73 (M$^+$), found 1507.64; GPC analysis (CHCl$_3$) M_n = 1398, M_w = 1436 g mol^{-1} relative to polystyrene, M_w/M_n = 1.027; BET surface area = 616 m^2 g^{-1}; total pore volume 0.44 = cm^3 g^{-1} at p/p^o = 0.98.

Tri-[cy6-triptycene-2,3-diol] biphenyl adduct

4,4'-Dicyano-2,2',3,3',5,5',6,6'-octafluorobiphenyl (0.116 g, 0.333 mmol), cy6-triptycene-2,3-diol (0.505 g, 1.00 mmol) and potassium carbonate (0.367 g, 2.66 mmol) were reacted together in anhydrous DMF (10 ml) in accordance with general procedure 1. Purification was achieved using column chromatography (13/7 hexane/toluene, R_f = 0.20) to give the tri-[cy6-triptycene-2,3-diol] biphenyl adduct (0.273 g, 47 %) as a yellow powder (mp > 300 °C); IR (DCM film) 3018, 2960, 2927, 2864, 2245, 1444, 1280, 1140, 1015 cm^{-1}; ^{1}H NMR (400 MHz, CDCl$_3$) δ 7.19 (6H, s, Ar*H*), 7.13 (2H, s, Ar*H*), 7.08 (2H, s, Ar*H*), 7.06 (2H, s, Ar*H*), 7.00 (1H, s, Ar*H*), 6.96 (2H, s, Ar*H*), 6.70 (1H, s, Ar*H*), 6.67 (2H, s, Ar*H*), 5.12 (1H, s, C*H*), 5.11 (2H, s, C*H*), 5.00 (2H, s, C*H*), 4.98 (1H, s, C*H*), 1.54 (24H, s, C*H$_2$*), 1.18 – 1.04 (72H, m, C*H$_3$*); ^{13}C NMR (125 MHz, CDCl$_3$) δ 144.00, 143.98, 143.81 – 143.77 (m), 143.5, 143.4, 141.7 – 141.5 (m), 139.6, 137.1, 136.88, 136.85, 136.5, 135.7, 121.7, 121.6, 121.5, 112.9, 112.7, 112.6, 109.00, 108.99, 91.6, 53.04, 52.97, 35.4, 34.43, 34.36, 32.7 – 32.0 (m) (^{19}F-^{13}C coupling not assigned); ^{19}F NMR (282 MHz, CDCl$_3$) δ -137.1 (1F, d, *J* = 20.8 Hz, Ar*F*), -140.2 (1F, d, *J* = 20.8 Hz, Ar*F*); LRMS (m/z, MALDI) calc. for C$_{122}$H$_{120}$F$_2$N$_2$O$_6$: 1747.92 (M$^+$), found 1747.73; GPC analysis (CHCl$_3$) M_n = 1515, M_w = 1549 g mol^{-1} relative to polystyrene, M_w/M_n = 1.022; BET surface area = 612 m^2 g^{-1}; total pore volume = 0.46 cm^3 g^{-1} at *p/p^o* = 0.98.

Tri-[ucy6-triptycene-2,3-diol] biphenyl adduct
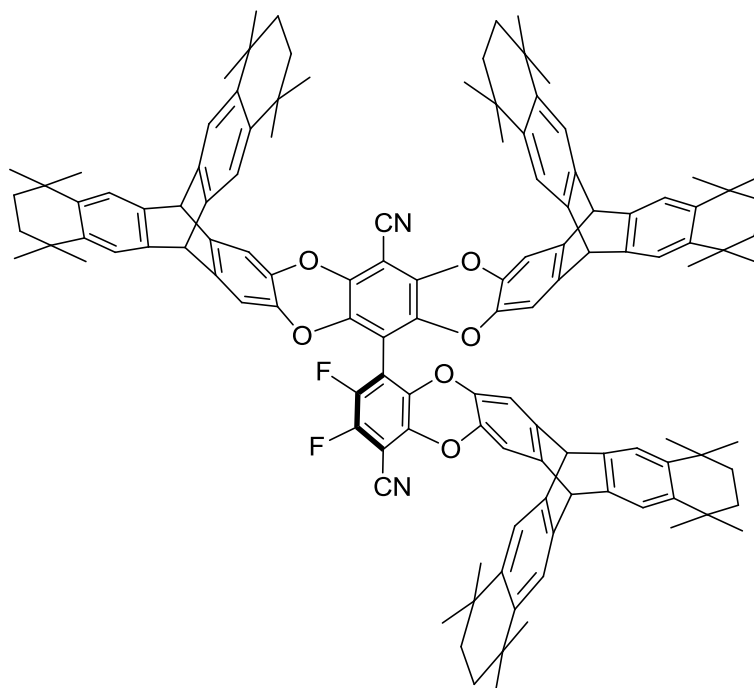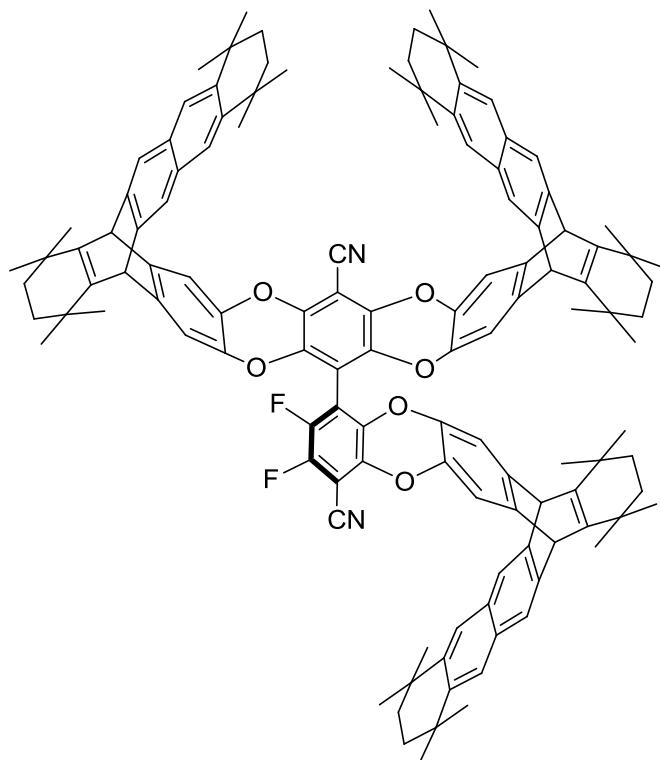

4,4'-Dicyano-2,2',3,3',5,5',6,6'-octafluorobiphenyl (0.133 g, 0.382 mmol), ucy6-triptycene-2,3-diol (0.579 g, 1.14 mmol) and potassium carbonate (0.330 g, 2.39 mmol) were reacted together in anhydrous DMF (10 ml) in accordance with general procedure 1. Purification was achieved using column chromatography (13/7 hexane/toluene, R_f = 0.20) to give the tri-[ucy6-triptycene-2,3-diol] biphenyl adduct (mixture of regioisomers) (0.168 g, 25 %) as a yellow powder (mp > 300 °C); IR (DCM film) 2957, 2925, 2863, 2241, 1609, 1447, 1283, 1185, 1011 cm^{-1}; ^{1}H NMR (500 MHz, CDCl$_3$) δ 7.68 – 7.58 (6H, m, Ar*H*), 7.48 – 7.37 (6H, m, Ar*H*), 6.96 – 6.88 (3H, m, Ar*H*), 6.59 – 6.42 (3H, m, Ar*H*), 4.99 – 4.68 (6H, m, C*H*), 1.72 – 1.70 (12H, m, C*H$_2$*), 1.37 – 1.21 (48H, m, C*H$_2$*/C*H$_3$*), 0.99 – 0.67 (36H, m, C*H$_3$*); ^{13}C NMR (125 MHz, CDCl$_3$) δ 146.7 – 146.4 (m), 144.2, 143.9 – 143.5 (m), 142.7 – 142.4 (m), 141.2 – 141.0 (m), 139.9 – 139.7 (m), 137.5 – 137.4, 137.2, 137.0 – 136.9 (m), 136.0 – 135.9 (m), 130.1, 124.77, 124.74, 124.6, 119.5 – 119.4 (m), 113.5 – 113.4 (m), 111.6 – 111.3 (m), 110.63 – 110.57 (m), 109.4 – 109.2 (m), 92.9, 91.7, 50.0 – 49.7 (m), 35.4, 34.6, 34.0 – 33.9 (m), 32.9 – 32.7 (m) 27.2 – 26.7 (m) (^{19}F-^{13}C coupling not assigned, extra carbons due to regioisomeric nature); ^{19}F NMR (282 MHz, CDCl$_3$) δ -137.3 – -137.6 (1F, cluster of doublets, Ar*F*), -139.6 – -139.8 (1F, cluster of doublets, Ar*F*); LRMS (MALDI, *m/z*) calc. for C$_{122}$H$_{120}$F$_2$N$_2$O$_6$: 1747.92 (M$^+$),

found 1748.45; GPC analysis (CHCl$_3$) M_n = 1722, M_w = 1782 g mol^{-1} relative to polystyrene, M_w/M_n = 1.034; BET surface area = 566 m^2 g^{-1}; total pore volume = 0.46 cm^3 g^{-1} at p/p^o = 0.98.

Di-[cy6-triptycene-2,3-diol]-mono-[triptycene-2,3-diol] biphenyl adduct
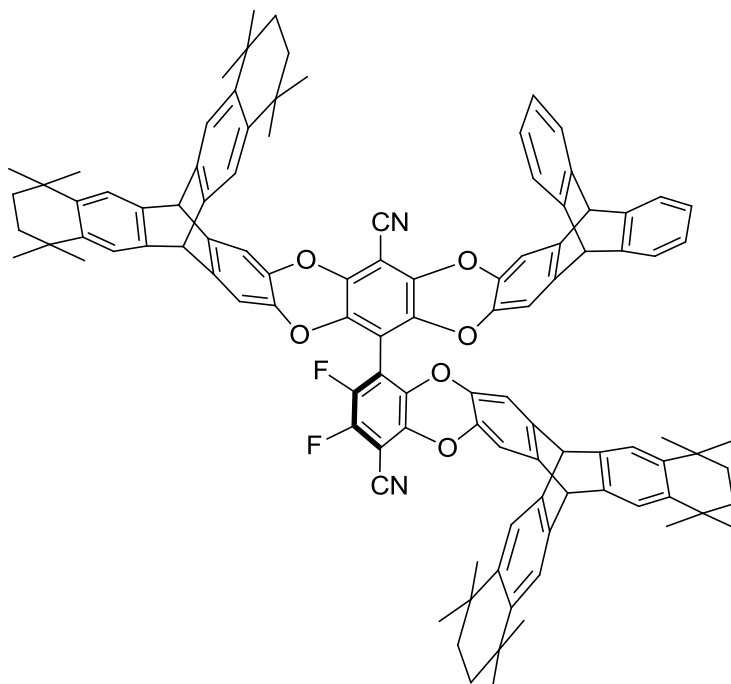
Di-[cy6-triptycene-2,3-diol] biphenyl adduct (0.135 g, 0.105 mmol), triptycene-2,3-diol (0.075 g, 0.262 mmol) and potassium carbonate (0.110 g, 0.796 mmol) were reacted together in anhydrous DMF (10 ml) in accordance with general procedure 1. Purification was achieved using column chromatography (6/3/1 hexane/DCM/toluene, R_f = 0.2) to give the di-[cy6-triptycene-2,3-diol]-mono-[triptycene-2,3-diol] biphenyl adduct (0.023 g, 14 %) as a yellow powder (mp > 300 °C); IR (DCM film) 3053, 2960, 2926, 2855, 1447, 1287, 1265, 1142, 1013 cm^{-1}; ^{1}H NMR (500 MHz, CDCl$_3$) δ 7.33 – 7.31 (2H, m, Ar*H*), 7.28 – 6.93 (17H, m, Ar*H*), 6.72 (2H, d, *J* = 2.6 Hz, Ar*H*), 6.68 (1H, s, Ar*H*), 5.28 (1H, s, C*H*), 5.16 (1H, s, C*H*), 5.14 (1H, s, C*H*), 5.12, (1H, s, C*H*), 5.01 (1H, s, C*H*), 4.98 (1H, s, C*H*), 1.57 – 1.53 (16H, m, C*H$_2$*). 1.27 – 1.05 (48H, m, C*H$_3$*); ^{13}C NMR (125 MHz, CDCl$_3$) δ 144.7 – 144.5 (m), 141.6 – 141.4 (m), 125.6, 123.7, 121.7 – 121.5 (m), 120.5, 112.7, 112.6, 53.0, 36.5, 34.5, 34.42, 34.36, 32.4 – 31.9 (m), 29.93, 29.85. 29.6, 22.9, 14.4 (multiple carbons missing, ^{19}F-^{13}C coupling not assigned); ^{19}F NMR (282 MHz, CDCl$_3$) δ -137.2 (1F, d, *J* = 22.0 Hz, Ar*F*), -139.9 (1F, d, *J* = 22.0

Hz, Ar*F*); LRMS (MALDI, *m/z*) calc. for $C_{106}H_{92}F_2N_2O_6$: 1527.70 (M$^+$), found 1527.39; GPC analysis (CHCl$_3$) M_n = 1421, M_w = 1520 g mol^{-1} relative to polystyrene, M_w/M_n = 1.070.

5.2.2.3 Tetra-substituted adducts

Tetra-[benzene-1,2-dithiol] biphenyl adduct
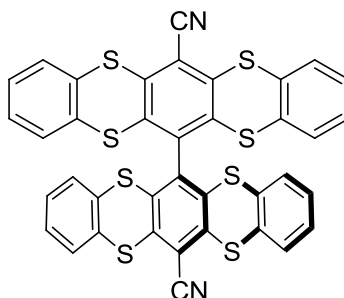
4,4'-Dicyano-2,2',3,3',5,5',6,6'-octafluorobiphenyl (0.299 g, 0.859 mmol), benzene-1,2-dithiol (0.513 g, 3.61 mmol) and potassium carbonate (1.19 g, 8.61 mmol) were reacted together in anhydrous DMF (10 ml) in accordance with general procedure 1. Purification was achieved using column chromatography (3/2 DCM/hexane, R$_f$ = 0.4) to give the tetra-[benzene-1,2-dithiol] biphenyl adduct (0.626 g, 96 %) as a yellow powder (mp > 300 °C); IR (DCM film) 2924, 2224, 1674, 1564, 1451, 1428, 1310, 1249 cm^{-1}; ^{1}H NMR (500 MHz, CDCl$_3$) *δ* 7.59 (4H, d, *J* = 7.5 Hz, Ar*H*), 7.31 – 7.28 (4H, m, Ar*H*), 7.17 – 7.14 (4H, m, Ar*H*), 6.99 (4H, d, *J* = 7.5 Hz, Ar*H*); ^{13}C NMR (125 MHz, CDCl$_3$) *δ* 141.0, 138.5, 137.5, 134.0, 133.8, 129.6, 129.5, 129.0, 128.9, 114.6, 113.4; HRMS (EI$^+$, *m/z*) calc. for $C_{38}H_{16}N_2S_8$: 755.9079 (M$^+$), found 755.9090; GPC analysis (CHCl$_3$) M_n = 578, M_w = 628 g mol^{-1} relative to polystyrene, M_w/M_n = 1.087; BET surface area = 10 m^2 g^{-1}; total pore volume = 0.03 cm^3 g^{-1} at *p/p^o* = 0.98.

Tetra-[R-catechol] biphenyl adducts

R = H, ^{t}Bu
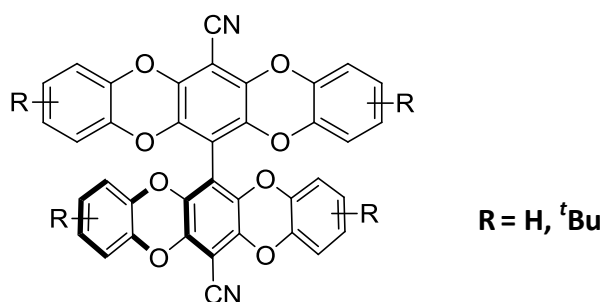
[R = H]: Tetra-[catechol] biphenyl adduct

4,4'-Dicyano-2,2',3,3',5,5',6,6'-octafluorobiphenyl (0.230 g, 0.661 mmol), catechol (0.306 g, 2.78 mmol) and potassium carbonate (0.913 g, 6.61 mmol) were reacted together in anhydrous DMF (10 ml) in accordance with general procedure 1. Purification was achieved using column chromatography (1/1 DCM/hexane, R_f = 0.4) to give the tetra-[catechol] biphenyl adduct (0.307 g, 74 %) as a yellow powder (mp > 300 °C); IR (DCM film) 2234, 1495, 1440, 1309, 1272, 1253 cm^{-1}; ^{1}H NMR (500 MHz, CDCl$_3$) δ 7.00 (4H, d, J = 8.0 Hz, ArH), 6.96 – 6.93 (4H, m, ArH), 6.88 – 6.85 (4H, m, ArH), 6.66 (4H, d, J = 8.0 Hz, ArH); ^{13}C NMR (125 MHz, CDCl$_3$) δ 141.1, 140.8, 140.0, 136.2, 125.3, 125.2, 117.0, 114.4, 110.6, 91.7 (one carbon missing); HRMS (EI$^+$, m/z) calc. for C$_{38}$H$_{16}$N$_2$O$_8$: 628.0907 (M$^+$), found 628.0903; GPC analysis (CHCl$_3$) M_n = 548, M_w = 578 g mol^{-1} relative to polystyrene, M_w/M_n = 1.055; BET surface area = 7 m^2 g^{-1}; total pore volume = 0.03 cm^3 g^{-1} at p/p^o = 0.98. Crystallography data (CHCl$_3$/MeOH): Triclinic, space group = P$\overline{1}$, a = 11.0410(6) Å, b = 11.3324(7) Å, c = 14.2766(7) Å, α = 113.045(5), β = 90.659(4), γ = 106.663(5), V = 1559.14 Å^3, Z = 2, R_1 = 4.01.

[R = ^{t}Bu]: Tetra-[4-*tert*-butylcatechol] biphenyl adduct

4,4'-Dicyano-2,2',3,3',5,5',6,6'-octafluorobiphenyl (0.184 g, 0.529 mmol), 4-*tert*-butylcatechol (0.359 g, 2.11 mmol) and potassium carbonate (0.729 g, 5.27 mmol) were reacted together in anhydrous DMF (10 ml) in accordance with general procedure 1. Purification was achieved using column chromatography (hexane/DCM 7/3, R_f = 0.3) to give the tetra-[4-*tert*-butylcatechol] biphenyl adduct (mixture of regioisomers) (0.360 g, 80 %) as a yellow powder (mp > 300 °C); IR (DCM film) 2964, 2907, 2871, 2238, 1512, 1436, 1287, 1122 cm^{-1}; ^{1}H NMR (400 MHz, CDCl$_3$) δ 7.04 – 6.52 (12H, m, ArH), 1.24 – 1.13 (36H, m, ^{t}BuH); ^{13}C NMR (125 MHz, CDCl$_3$) δ 149.11, 149.10, 149.05, 149.03, 148.97 148.93, 148.91, 148.8,

140.5, 140.43, 140.38, 140.3, 140.24, 140.20, 140.1, 140.0, 139.9 139.8, 138.82, 137.77, 138.7, 138.6, 138.5, 138.4, 138.3, 138.21, 138.16, 136.4, 136.2, 136.0, 135.9, 133.5, 133.1, 121.93, 121.88, 121.7, 116.3, 116.2, 114.30, 114.26, 114.2, 111.62, 111.59, 110.2, 91.4, 91.3, 34.74, 34.70, 34.67, 31.41, 31.39, 31.35 (extra carbons due to regioisomeric nature); LRMS (EI$^+$, *m/z*) calc. for $C_{54}H_{48}N_2O_8$: 852.33 (M$^+$), found 852.31; GPC analysis (CHCl$_3$) M_n = 881, M_w = 922 g mol^{-1} relative to polystyrene, M_w/M_n = 1.047; BET surface area = 41 m^2 g^{-1}; total pore volume = 0.15 cm^3 g^{-1} at *p/p^o* = 0.98.

Tetra-[3,5-di-*tert*-butylcatechol] biphenyl adduct
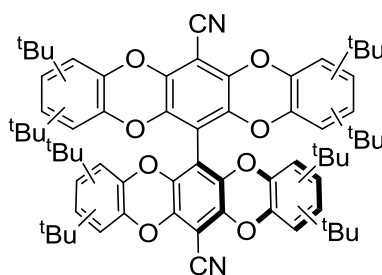
4,4'-Dicyano-2,2',3,3',5,5',6,6'-octafluorobiphenyl (0.269 g, 0.773 mmol), 3,5-di-*tert*-butylcatechol (0.722 g, 3.25 mmol) and potassium carbonate (1.07 g, 7.75 mmol) were reacted together in anhydrous DMF (10 ml) in accordance with general procedure 1. Purification was achieved column chromatography (DCM/hexane 1/1, R_f = 0.3) to give the tetra-[3,5-di-*tert*-butylcatechol] biphenyl adduct (mixture of regioisomers) (0.580 g, 70 %) as a yellow powder (mp > 300 °C); IR (DCM film) 2963, 2907, 2871, 2237, 1451, 1413, 1304, 1276, 1231, 1037, 1018 cm^{-1}; ^{1}H NMR (400 MHz, CDCl$_3$) *δ* 6.97 – 6.81 (5H, m, Ar*H*), 6.67 – 6.60 (3H, m, Ar*H*), 1.51 – 1.07 (72H, m, ^{t}Bu*H*); ^{13}C NMR (125 MHz, CDCl$_3$) *δ* 147.50, 147.48, 147.4, 147.28, 147.26, 147.24, 147.21, 141.0, 140.8, 140.6, 140.6, 140.4, 140.1, 139.91, 139.89, 139.8, 139.7, 139.6, 137.9, 137.8, 137.6, 137.53, 137.49, 137.46, 137.2, 137.1, 136.91, 136.86, 136.8, 136.21, 136.16, 136.1, 136.0, 135.91, 135.86, 119.6, 119.4, 112.6, 112.5, 112.4, 112.3, 111.8, 111.4, 90.5, 35.42, 35.36, 35.34, 35.33, 34.9, 31.4, 30.2, 30.08, 30.05, 30.0, 29.5, 29.43, 29.38, 29.35, 29.3 (extra carbons due to regioisomeric nature); LRMS (MALDI, *m/z*) calc. for $C_{70}H_{80}N_2O_8$: 1076.59 (M$^+$), found 1076.71; GPC analysis (CHCl$_3$) M_n = 1011 M_w = 1062 g mol^{-1} relative to polystyrene, M_w/M_n = 1.089; BET surface area = 67 m^2 g^{-1}; total pore volume = 0.231 cm^3 g^{-1} at *p/p^o* = 0.98.

Tetra-[R-naphthalene-2,3-diol] biphenyl adducts

R = H, ^{t}Bu, Ad
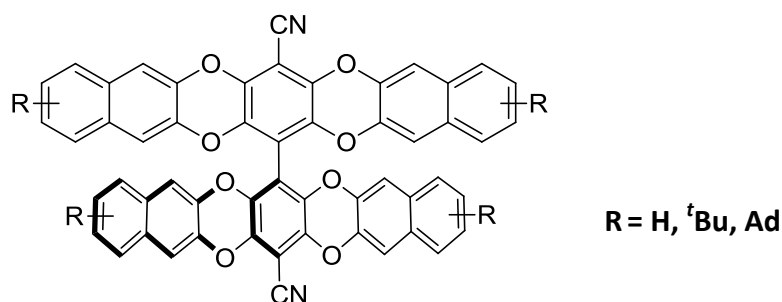
[R = H]: Tetra-[naphthalene-2,3-diol] biphenyl adduct

4,4'-Dicyano-2,2',3,3',5,5',6,6'-octafluorobiphenyl (0.208 g, 0.597 mmol), naphthalene-2,3-diol (0.402 g, 2.51 mmol) and potassium carbonate (0.825 g, 5.97 mmol) were reacted together in anhydrous DMF (10 ml) in accordance with general procedure 1. Purification was achieved using column chromatography (3/2 DCM/hexane, R_f = 0.4) to give the tetra-[naphthalene-2,3-diol] biphenyl adduct (0.219 g, 44 %) as a yellow powder (mp > 300 °C); IR (DCM film) 3056, 2921, 2850, 2236, 1516, 1475, 1447, 1430, 1396, 1362, 1264, 1169 cm^{-1}; ^{1}H NMR (400 MHz, (C$_4$D$_8$)O) δ 7.73 (4H, d, J = 8.1 Hz, ArH), 7.62 (4H, s, ArH), 7.49 (4H, d, J = 8.1 Hz, ArH), 7.35 – 7.31 (4H, m, ArH), 7.27 – 7.24 (8H, m, ArH), ^{13}C NMR (125 MHz, (C$_4$D$_8$)O) δ 132.5, 132.3, 128.1, 128.0, 126.9, 117.0, 114.0, 113.9, 111.2 (multiple carbons missing); ^{13}C NMR (101 MHz, Solid State) 139.8, 138.1, 134.9, 130.4, 125.9, 115.3, 113.5, 111.2 (multiple carbons missing); LRMS (MALDI, m/z) calc. for C$_{54}$H$_{24}$N$_2$O$_8$: 828.15 (M$^+$), found 828.36. GPC analysis (CHCl$_3$) M_n = 876, M_w = 955 g mol^{-1} relative to polystyrene, M_w/M_n = 1.029; BET surface area = 25 m^2 g^{-1}; total pore volume = 0.054 cm^3 g^{-1} at p/p^o = 0.98; Crystallography data (THF): Triclinic, space group = P$\overline{1}$, a = 14.554(8) Å, b = 14.969(7) Å, c = 24.018(12) Å, α = 76.716(16), β = 80.534(13), γ = 85.658(16), V = 5019.26 Å^3, Z = 4, R_1 = 14.07.

[R = ^{t}Bu]: Tetra-[6-*tert*-butylnaphthalene-2,3-diol] biphenyl adduct

4,4'-Dicyano-2,2',3,3',5,5',6,6'-octafluorobiphenyl (0.179 g, 0.514 mmol), 6-*tert*-butylnaphthalene-2,3-diol (0.462 g, 2.14 mmol) and potassium carbonate (0.709 g, 5.13 mmol) were reacted together in anhydrous DMF (10 ml) in accordance with general procedure 1. Purification was achieved using column chromatography (3/2 hexane/DCM, R_f = 0.4) to give the tetra-[6-*tert*-butylnaphthalene-2,3-diol] biphenyl adduct (mixture of

regioisomers) (0.346 g, 64 %) as a yellow powder (mp > 300 °C); IR (DCM film) 2961, 2907, 2869, 2238, 1514, 1434, 1250, 1002 cm^{-1}; ^{1}H NMR (400 MHz, CDCl$_3$) δ 7.65 – 7.61 (4H, m, Ar*H*), 7.46 – 7.24 (12H, m, Ar*H*), 7.13 – 6.98 (4H, m, Ar*H*), 1.381 – 1.378 (18H, m, ^{t}Bu*H*), 1.28 – 1.26 (18H, m, ^{t}Bu*H*); ^{13}C NMR (125 MHz, CDCl$_3$) δ 149.08, 149.06, 149.01, 148.99, 148.95, 140.32, 140.29, 140.23, 140.21, 140.18, 140.17, 140.12, 140.08, 140.05, 140.0, 139.93, 139.87, 139.82, 139.80, 139.76, 139.74, 139.67, 139.64, 139.60, 139.55, 139.50, 139.49, 139.46, 139.4, 139.34, 139.28, 135.9, 135.84, 135.80, 135.76, 135.74, 135.69, 135.67, 135.6, 131.3, 131.20, 131.17, 131.1, 129.29, 129.26, 129.2, 127.0, 126.9, 125.1, 122.5, 122.4, 113.50, 113.47, 113.39, 113.37, 113.3, 113.0, 112.9, 112.84, 112.79, 112.77, 112.75, 112.7, 111.6, 110.7, 91.74, 91.70, 35.0, 34.9, 31.4, 31.2 (extra carbons due to regioisomeric nature); LRMS (EI$^+$, *m/z*) calc. for C$_{70}$H$_{56}$N$_2$O$_8$: 1052.40 (M$^+$), found 1052.44; GPC analysis (CHCl$_3$) M_n = 1063, M_w = 1112 g mol^{-1} relative to polystyrene, M_w/M_n = 1.046; BET surface area = 260 m^2 g^{-1}; total pore volume = 0.334 cm^3 g^{-1} at p/p^o = 0.98.

[R = Ad]: Tetra-[6-(1-adamantyl)naphthalene-2,3-diol] biphenyl adduct

4,4'-Dicyano-2,2',3,3',5,5',6,6'-octafluorobiphenyl (0.161 g, 0.462 mmol), 6-(1-adamantyl)naphthalene-2,3-diol (0.573 g, 1.94 mmol) and potassium carbonate (0.640 g, 4.63 mmol) were reacted together in anhydrous DMF (10 ml) in accordance with general procedure 1. Purification was achieved using column chromatography (3/2 hexane/DCM, R_f = 0.4) to give the tetra-[6-(1-adamantyl)naphthalene-2,3-diol] biphenyl adduct (mixture of regioisomers) (0.245 g, 39 %) as a yellow powder (mp > 300 °C); IR (DCM film) 2903, 2848, 2238, 1514, 1434, 1266, 1244, 1002 cm^{-1}; ^{1}H NMR (500 MHz, CDCl$_3$) δ 7.63 – 7.55 (4H, m, Ar*H*), 7.45 – 7.22 (12H, m, Ar*H*), 7.10 – 7.00 (4H, m, Ar*H*), 2.12 – 1.59 (60H, m, Ad*H*); ^{13}C NMR (125 MHz, CDCl$_3$) δ 149.09, 149.08, 149.02, 149.00, 139.93, 139.89, 139.87, 139.81, 139.80, 139.77, 139.7, 139.63, 139.62, 139.59, 139.56, 139.52, 139.47, 139.43, 139.40, 139.36, 139.31, 139.28, 139.26, 139.21, 139.18, 139.1, 139.0, 135.7, 135.6, 135.51, 135.46, 135.4, 131.2, 131.12, 131.10, 131.06, 131.01, 131.00, 129.2, 129.1, 126.8, 124.32, 124.25, 122.2, 113.2, 113.13, 113.05, 112.7, 112.6, 112.4, 111.33, 111.30, 110.6, 91.5, 43.0, 42.9, 36.8, 36.7, 36.34, 36.26, 28.9, 28.8 (extra carbons due to regioisomeric nature); LRMS (MALDI, *m/z*) calc. for C$_{94}$H$_{80}$N$_2$O$_8$: 1365.59 (M$^+$), found 1365.59; GPC analysis (CHCl$_3$) M_n = 1134, M_w = 1195 g mol^{-1} relative to polystyrene, M_w/M_n = 1.050; BET surface area = 132 m^2 g^{-1}; total pore volume = 0.247 cm^3 g^{-1} at p/p^o = 0.98.

Tetra-[R$_1$,R$_2$-triptycene-2,3-diol] biphenyl adducts

R$_1$ = H, ^{t}Bu

R$_2$ = H, Me

[R$_1$ = ^{t}Bu, R$_2$ = H]: Tetra-[7,14-di-*tert*-butyltriptycene-2,3-diol] biphenyl adduct

4,4'-Dicyano-2,2',3,3',5,5',6,6'-octafluorobiphenyl (0.057 g, 0.164 mmol), 7,14-di-*tert*-butyltriptycene-2,3-diol (0.294 g, 0.738 mmol) and potassium carbonate (0.230 g, 1.66 mmol) were reacted together in anhydrous DMF (10 ml) in accordance with general procedure 1. Purification was achieved using column chromatography (3/1/1 hexane/toluene/DCM, R_f = 0.25) to give the tetra-[7,14-di-*tert*-butyltriptycene-2,3-diol] biphenyl adduct (mixture of regioisomers) (0.202 g, 69 %) as a yellow powder (mp > 300 °C); IR (DCM film) 2962, 2905, 2869, 2238, 1608, 1447, 1330, 1285, 1264, 1141, 1014 cm^{-1}; ^{1}H NMR (500 MHz, CDCl$_3$) δ 7.35 – 7.34 (4H, m, Ar*H*), 7.25 – 7.18 (8H, m, Ar*H*), 7.09 – 7.05 (4H, m, Ar*H*), 6.98 – 6.85 (12H, m, Ar*H*), 6.68 – 6.67 (4H, m, Ar*H*), 5.22 – 5.20 (4H, m, Ar*H*), 5.05 – 5.04 (4H, m, Ar*H*), 1.26 – 1.14 (72H, m, ^{t}Bu*H*); ^{13}C NMR (125 MHz, CDCl$_3$) δ 148.4, 148.33, 148.32, 144.5, 144.4, 142.8, 142.64, 142.58, 142.56, 141.8, 141.73, 141.67, 139.31, 139.29, 139.26, 137.24, 137.20, 137.18, 136.9, 136.84, 136.83, 136.78, 135.7, 135.63, 135.61, 135.56, 135.5, 123.0, 122.9, 121.92, 121.86, 121.8, 120.83, 120.75, 120.7, 112.8, 112.7, 112.4, 111.0, 110.4, 90.7, 53.2, 53.1, 34.6, 34.53, 34.51, 34.46, 31.49, 31.47, 31.4 (extra carbons due to regioisomeric nature); LRMS (MALDI, *m/z*) calc. for C$_{126}$H$_{112}$N$_2$O$_8$: 1781.84 (M$^+$), found 1781.87; GPC analysis (CHCl$_3$) M_n = 1628, M_w = 1667 g mol^{-1} relative to polystyrene, M_w/M_n = 1.024; BET surface area = 654 m^2 g^{-1}; total pore volume = 0.54 cm^3 g^{-1} at p/p^o = 0.98; elemental analysis calc. C: 84.91, H: 6.33, N: 1.57, found C: 82.87, H: 6.39, N: 1.52; TGA (nitrogen): Initial weight loss due to thermal degradation commences at ~ 483 °C.

[R₁ = H, R₂ = Me]: Tetra-[9,10-dimethyltriptycene-2,3-diol] biphenyl adduct

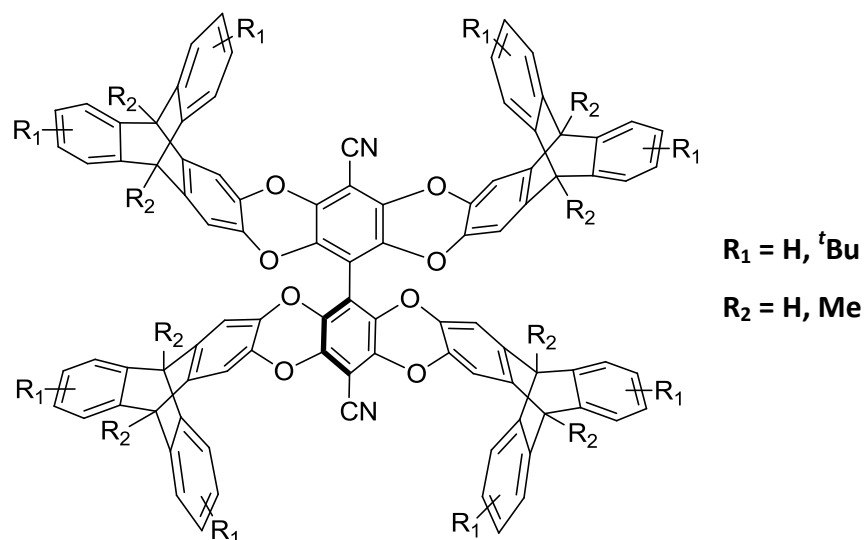4,4'-Dicyano-2,2',3,3',5,5',6,6'-octafluorobiphenyl (0.153 g, 0.439 mmol), 9,10-dimethyltriptycene-2,3-diol (0.622 g, 1.98 mmol) and potassium carbonate (0.610 g, 4.41 mmol) were reacted together in anhydrous DMF (10 ml) in accordance with general procedure 1. Purification was achieved using column chromatography (2/1/1 DCM/hexane/toluene, R_f = 0.2) to give the tetra-[9,10-dimethyltriptycene-2,3-diol] biphenyl adduct (0.322 g, 51 %) as a yellow powder (mp > 300 °C); IR (DCM film) 3062, 2974, 2238, 1612, 1446, 1290, 1169, 1006 cm⁻¹; ¹H NMR (500 MHz, CDCl₃) δ 7.33 (8H, d, *J* = 7.2 Hz, Ar*H*), 7.20 (8H, d, *J* = 7.2 Hz, Ar*H*), 7.05 − 6.98 (20H, m, Ar*H*), 6.63 (4H, s, Ar*H*), 2.35 (12H, s, C*H₃*), 2.18 (12H, s, C*H₃*); ¹³C NMR (125 MHz, CDCl₃) δ 147.68, 147.66, 145.8, 145.6, 139.5, 137.4, 137.0, 135.7, 125.1, 120.7, 120.6, 111.2, 110.9, 110.5, 110.2, 91.0, 48.36, 48.35, 13.7, 13.5; LRMS (MALDI, *m/z*) calc. for $C_{102}H_{64}N_2O_8$: 1445.47 (M⁺), found 1445.81; GPC analysis (CHCl₃) M_n = 1216, M_w = 1245 g mol⁻¹ relative to polystyrene, M_w/M_n = 1.023; BET surface area = 462 m² g⁻¹; total pore volume = 0.33 cm³ g⁻¹ at p/p^o = 0.98; Crystallography data (chloroform/methanol): Monoclinic, space group: P2₁/n, *a* = 20.0299(3) Å, *b* = 24.0548(5) Å, *c* = 21.1645(3) Å, *β* = 91.2530(10), *V* = 10194.9 Å³, *Z* = 4, R_1 = 11.98;

[R₁ = ᵗBu, R₂ = Me]: Tetra-[7,14-di-*tert*-butyl-9,10-dimethyltriptycene-2,3-diol] biphenyl adduct

4,4'-Dicyano-2,2',3,3',5,5',6,6'-octafluorobiphenyl (0.0571 g, 0.164 mmol), 7,14-di-*tert*-butyl-9,10-dimethyltriptycene-2,3-diol (0.294 g, 0.689 mmol) and potassium carbonate (0.227 g, 1.64 mmol) were reacted together in anhydrous DMF (10 ml) in accordance with general procedure 1. Purification was achieved using column chromatography (3/1/1 hexane/toluene/DCM, R_f = 0.25) to give the tetra-[7,14-di-*tert*-butyl-9,10-dimethyltriptycene-2,3-diol] biphenyl adduct (0.146 g, 47 %) as a yellow powder (mp > 300 °C); IR (DCM film) 2966, 2869, 2239, 1612, 1443, 1290, 1001 cm⁻¹; ¹H NMR (500 MHz, CDCl₃) δ 7.31 (4H, s, Ar*H*), 7.24 − 7.19 (8H, m, Ar*H*), 7.09 − 7.06 (4H, m, Ar*H*), 7.03 − 6.99 (4H, m, Ar*H*), 6.97 − 6.89 (8H, m, Ar*H*), 2.33 (12H, s, C*H₃*), 2.18 (12H, s, C*H₃*), 1.25 − 1.15 (72H, m, ᵗBu*H*); ¹³C NMR (125 MHz, CDCl₃) δ 147.9, 147.43, 147.36, 146.2, 146.0, 145.9, 144.9, 144.82, 144.79, 139.53, 139.47, 137.32, 137.27, 137.25, 137.2, 136.9, 136.84, 136.78, 136.7, 135.8, 135.7, 135.6, 121.63, 121.58, 120.1, 120.0, 117.9, 117.73, 117.67, 111.21, 111.16,

111.0, 110.52, 110.45, 110.4, 110.3, 110.0, 90.9, 48.23, 48.19, 34.82, 34.80, 34.77, 34.7, 31.71, 31.69, 31.67, 13.8, 13.5 (extra carbons due to regioisomeric nature); LRMS (MALDI, *m/z*) calc. for $C_{134}H_{128}N_2O_8$: 1893.97 (M$^+$), found 1893.63; GPC analysis (CHCl$_3$) M_n = 1645, M_w = 1688 g mol^{-1} relative to polystyrene, M_w/M_n = 1.026; BET surface area = 599 m^2 g^{-1}; total pore volume = 0.42 cm^3 g^{-1} at *p/p^o* = 0.98.

Tetra-[cy6-triptycene-2,3-diol] biphenyl adduct

4,4'-Dicyano-2,2',3,3',5,5',6,6'-octafluorobiphenyl (0.035 g, 0.101 mmol), cy6-triptycene-2,3-diol (0.230 g, 0.454 mmol) and potassium carbonate (0.180 g, 1.30 mmol) were reacted together in anhydrous DMF (10 ml) in accordance with general procedure 1. Purification was achieved using column chromatography (3/1/1 hexane/toluene/DCM, R_f = 0.25) to give the tetra-[cy6-triptycene-2,3-diol] biphenyl adduct (0.184 g, 83 %) as a yellow powder (mp > 300 °); IR (DCM film) 2922, 2853, 2238, 1608, 1447, 1287, 1185, 1141, 1004 cm^{-1}; ^{1}H NMR (500 MHz, CDCl$_3$) *δ* 7.18 (8H, s, Ar*H*), 7.05 (8H, s, Ar*H*), 6.95 (4H, s, Ar*H*), 6.62 (4H, s, Ar*H*), 5.10 (4H, s, C*H*), 4.95 (4H, s, C*H*), 1.54 (32H, s, C*H*$_2$), 1.18 – 1.04 (96H, m, C*H*$_3$); ^{13}C NMR (125 MHz, CDCl$_3$) *δ* 143.2, 143.0, 141.72, 141.67, 141.5, 139.3, 137.1, 136.8, 135.4, 121.6, 121.5, 112.8, 112.5, 111.2, 110.7, 90.6, 53.0, 52.9, 35.4, 34.4, 34.3, 32.3, 32.2, 32.0; LRMS (MALDI, *m/z*) calc. for $C_{158}H_{160}N_2O_8$: 2214.22 (M$^+$), found 2214.55; GPC analysis (CHCl$_3$) M_n = 1776, M_w = 1822 g mol^{-1} relative to polystyrene, M_w/M_n = 1.026; BET surface area = 702 m^2 g^{-1}; total

pore volume = 0.60 cm^3 g^{-1} at *p/p^o* = 0.98. Crystallography data (chloroform/methanol): Monoclinic, space group: P2$_1$/n, *a* = 22.33(3) Å, *b* = 25.38(3) Å, *c* = 30.52(4) Å, *β* = 110.8400(10), *V* = 16165.2 Å^3, *Z* = 4, *R$_1$* = 16.75.
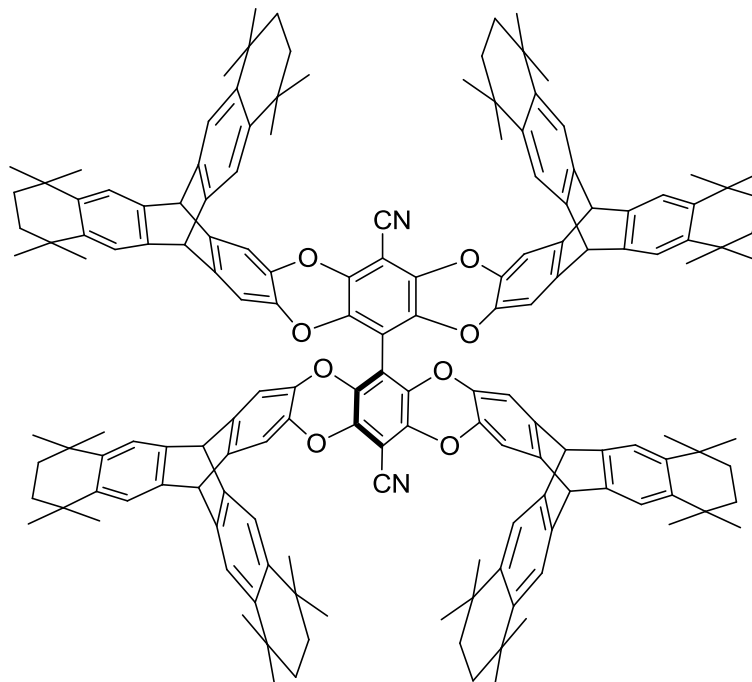
Tetra-[ucy6-triptycene-2,3-diol] biphenyl adduct
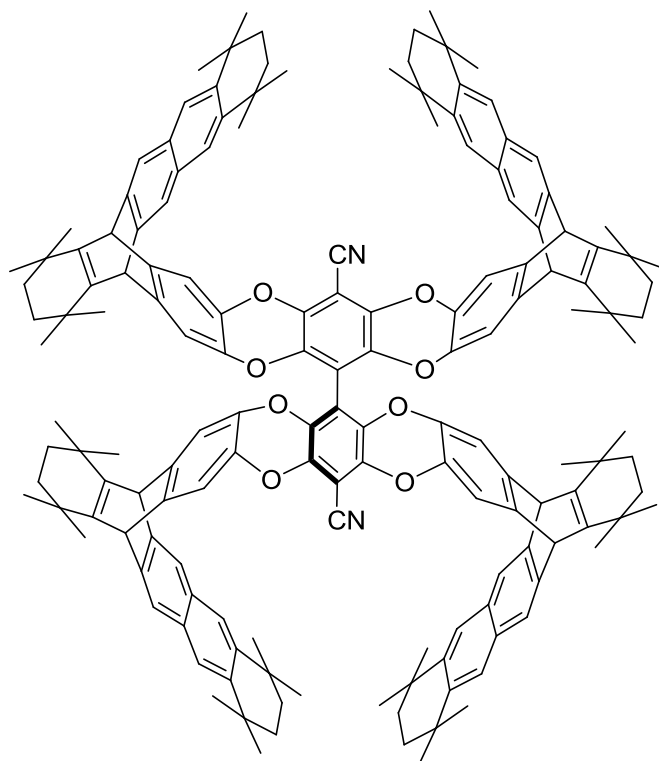
4,4'-Dicyano-2,2',3,3',5,5',6,6'-octafluorobiphenyl (0.078 g, 0.224 mmol), ucy6-triptycene-2,3-diol (0.480 g, 0.947 mmol) and potassium carbonate (0.350 g, 2.53 mmol) were reacted together in anhydrous DMF (10 ml) in accordance with general procedure 1. Purification was achieved using column chromatography (3/1/1 hexane/toluene/DCM, *R$_f$* = 0.25) to give the tetra-[ucy6-triptycene-2,3-diol] biphenyl adduct (mixture of regioisomers) (0.426 g, 86 %) as a yellow powder (mp > 300 °C); IR (DCM film) 2956, 2925, 2861, 2238, 1437, 1283, 1141, 1002 cm^{-1}; ^{1}H NMR (400 MHz, CDCl$_3$) *δ* 7.65 − 7.24 (16H, m, Ar*H*), 6.92 − 6.85 (4H, m, Ar*H*), 6.67 − 6.49 (4H, m, Ar*H*), 4.97 − 4.67 (8H, m, C*H*), 1.76 − 1.70 (16H, m, C*H$_2$*), 1.36 − 1.14 (64H, m, C*H$_2$*/C*H$_3$*), 1.03 − 0.59 (48H, m, C*H$_3$*); ^{13}C NMR (101 MHz, CDCl$_3$) *δ* 146.6, 146.5, 146.4, 146.1, 143.7, 143.6, 143.4, 143.1, 142.7, 142.6, 139.5, 139.4, 138.4, 136.8, 135.9, 135.5, 130.00, 129.98, 124.7, 124.6, 119.3, 119.2, 111.3, 90.7, 49.9, 35.1, 34.6, 34.04, 33.99, 33.95, 32.7, 32.6, 31.2, 26.84, 26.82 (some carbons missing, extra carbons due to

regioisomeric nature); LRMS (MALDI, *m/z*) calc. for $C_{158}H_{160}N_2O_8$: 2214.22 (M$^+$), found 2215.59 (MH$^+$); BET surface area = 622 m^2 g^{-1}; total pore volume = 0.64 cm^3 g^{-1} at *p/p^o* = 0.98.

Di-[triptycene-2,3-diol]-di-[propellane-2,3-diol] biphenyl adduct
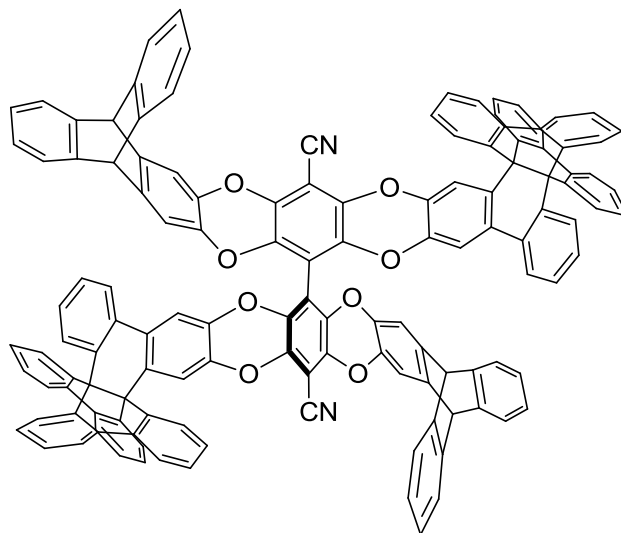
Di-[triptycene-2,3-diol] biphenyl adduct (0.102 g, 0.121 mmol), propellane-2,3-diol (0.150 g, 0.293 mmol) and potassium carbonate (0.100 g, 0.724 mmol) were reacted together in anhydrous DMF (10 ml) in accordance with general procedure 1 and purified by column chromatography (6/3/1 DCM/hexane/toluene, *R$_f$* = 0.2) to give the di-[triptycene-2,3-diol]-di-[propellane-2,3-diol] biphenyl adduct (mixture of regioisomers) (0.181 g, 84 %) as a yellow powder (mp > 300°); IR (DCM film) 3065, 2960, 2923, 2238, 1441, 1321, 1281, 1012 cm^{-1}; ^{1}H NMR (500 MHz, CDCl$_3$) *δ* 7.70 – 5.87 (64H, m, Ar*H*), 5.31 – 5.25 (2H, m, C*H*), 5.14 – 5.11 (2H, m, C*H*); ^{13}C NMR (125 MHz, CDCl$_3$) *δ* 144.7, 144.6, 142.4, 139.1, 134.9, 129.2, 127.82, 127.77, 127.7, 127.54, 127.50, 127.48, 125.7, 125.61, 125.56, 124.1, 124.04, 124.00, 123.9, 123.74, 123.65, 106.9, 53.53, 53.49, 53.46, 53.40, 53.37 (some carbons missing, extra carbons due to regioisomeric nature); LRMS (MALDI, *m/z*) calc. for $C_{130}H_{68}N_2O_8$: 1785.50 (M$^+$), found 1786.73 (MH$^+$); GPC analysis (CHCl$_3$) *M$_n$* = 1248, *M$_w$* = 1279 g mol^{-1} relative to polystyrene, *M$_w$/M$_n$* = 1.025; BET surface area = 481 m^2 g^{-1}; total pore volume = 0.38 cm^3 g^{-1} at *p/p^o* = 0.98.

Di-[triptycene-2,3-diol]-di-[cy6-triptycene-2,3-diol] biphenyl adduct
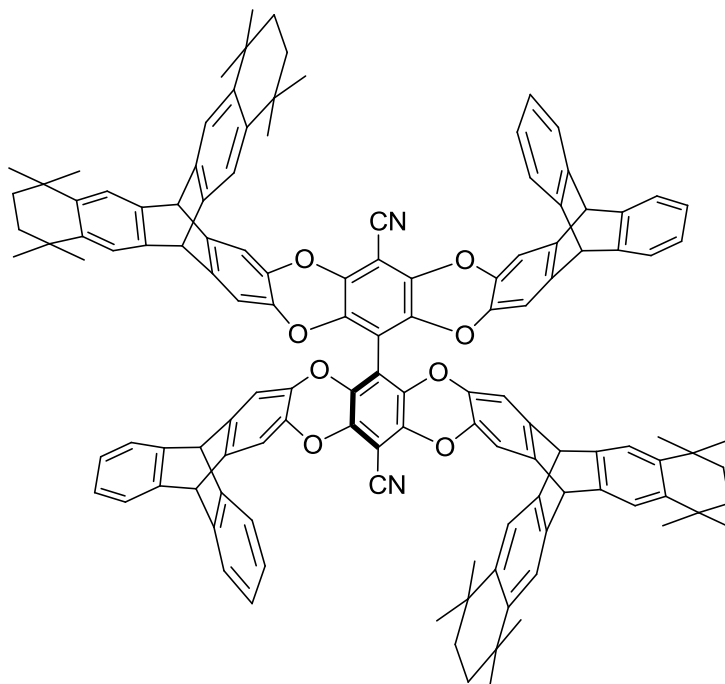
Di-[cy6-triptycene-2,3-diol] biphenyl adduct (0.135 g, 0.105 mmol), triptycene-2,3-diol (0.075 g, 0.262 mmol) and potassium carbonate (0.110 g, 0.796 mmol) were reacted together in anhydrous DMF (10 ml) in accordance with general procedure 1. Purification was achieved using column chromatography (6/3/1 hexane/DCM/toluene, R_f = 0.2) to give the di-[triptycene-2,3-diol]-di-[cy6-triptycene-2,3-diol] biphenyl adduct (0.093 g, 50 %) as a yellow powder (mp > 300 °C); IR (DCM film) 2958, 2923, 2238, 1443, 1286, 1139, 1001 cm^{-1}; ^{1}H NMR (500 MHz, CDCl$_3$) δ 7.30 – 7.27 (4H, m, Ar*H*), 7.21 – 7.16 (8H, m, Ar*H*), 7.05 (4H, s, Ar*H*), 6.98 – 6.89 (10H, m, Ar*H*), 6.86 – 6.83 (2H, m, Ar*H*), 6.64 (4H, s, Ar*H*), 5.25 (2H, s, C*H*), 5.11 – 5.10 (4H, m, C*H*), 4.94 (2H, s, C*H*), 1.56 – 1.52 (16H, m, C*H$_2$*), 1.21 – 1.04 (48H, m, C*H$_3$*); ^{13}C NMR (125 MHz, CDCl$_3$) δ 144.7, 144.6, 143.2, 143.0, 142.4, 142.1, 141.7, 141.64, 141.59, 141.55, 141.53, 141.49, 139.5, 139.3, 137.5, 137.2, 136.9, 135.7, 135.6, 125.53, 125.50, 123.9, 123.8, 123.7, 123.6, 121.6, 121.5, 113.1, 112.9, 112.7, 112.5, 111.1, 110.7, 110.2, 90.8, 53.4, 53.3, 53.0, 52.8, 35.41, 35.35, 35.3, 34.42, 34.39, 34.36, 34.3, 32.3, 32.24, 32.19, 32.17, 32.13, 32.05, 32.0, 31.9; LRMS (MALDI, *m/z*) calc. for C$_{126}$H$_{104}$N$_2$O$_8$: 1773.78 (M$^+$), found 1773.73; GPC analysis (CHCl$_3$) M_n = 1455, M_w = 1494 g mol^{-1} relative to polystyrene, M_w/M_n = 1.026; BET surface area = 179 m^{2}g^{-1}; total pore volume = 0.14 cm^{3}g^{-1} at *p/p^o* = 0.98.

5.2.2.4 Penta-substituted adducts

Penta-[R-catechol] terphenyl adducts

R = H, ^tBu
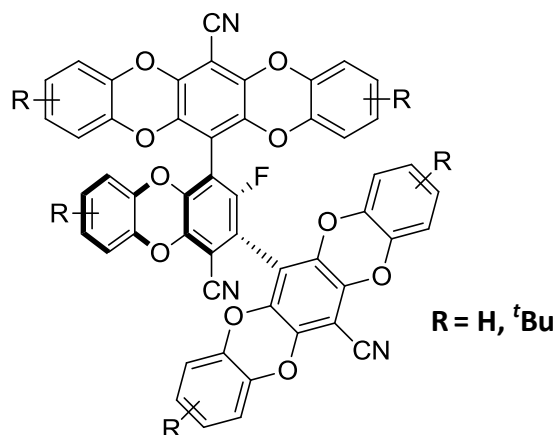
[R = H]: Penta-[catechol] terphenyl adduct

4,4′,4′′-Tricyano-2,2′,2′′,3,3′′,5,5′,5′′,6,6′,6′′-undecafluoro-[1,1′:3′,1′′-terphenyl] (0.146 g, 0.290 mmol), catechol (0.176 g, 1.60 mmol) and potassium carbonate (0.500 g, 3.62 mmol) were reacted together in anhydrous DMF (10 ml) in accordance with general procedure 1. Purification was achieved using column chromatography (9/1 DCM/hexane, R_f = 0.35) to give the penta-[catechol] terphenyl adduct (0.215 g, 87 %) as a yellow powder (mp > 300 °C); IR (DCM film) 2237, 1607, 1495, 1450, 1274, 1254, 1033 cm^{-1}; ^{1}H NMR (400 MHz, CDCl$_3$) δ 7.07 – 6.86 (15H, m, Ar*H*), 6.79 – 6.76 (3H, m, Ar*H*), 6.72 (2H, dd *J* = 8.1, 1.3 Hz, Ar*H*); ^{13}C NMR (125 MHz, CDCl$_3$) δ 142.53, 142.48, 140.9, 140.81, 140.76, 140.7, 140.6, 140.1, 140.0, 136.2, 136.1, 125.8, 125.6, 125.40, 125.38, 117.2, 117.1, 117.1, 116.9, 112.5, 112.4, 110.37, 110.35, 110.3, 103.5, 103.4, 92.3, 92.1 (^{19}F-^{13}C coupling not assigned); ^{19}F NMR (282 MHz, CDCl$_3$) δ -112.2 (1F, s, Ar*F*); LRMS (EI$^+$, *m/z*) calc. for C$_{51}$H$_{20}$FN$_3$O$_{10}$: 853.11 (M$^+$), found 853.15; GPC analysis (CHCl$_3$) M_n = 822, M_w = 862 g mol^{-1} relative to polystyrene, M_w/M_n = 1.048; BET surface area = 13 m^2 g^{-1}; total pore volume = 0.05 cm^3 g^{-1} at p/p^o = 0.98.

[R = ^tBu]: Penta-[4-*tert*-butylcatechol] terphenyl adduct

4,4′,4′′-Tricyano-2,2′,2′′,3,3′′,5,5′,5′′,6,6′,6′′-undecafluoro-[1,1′:3′,1′′-terphenyl] (0.124 g, 0.246 mmol), 4-*tert*-butylcatechol (0.245 g, 1.47 mmol) and potassium carbonate (0.410 g, 2.97 mmol) were reacted together in anhydrous DMF (10 ml) in accordance with general procedure 1. Purification was achieved using column chromatography (1/1 DCM/hexane, R_f

= 0.45) to give the penta-[4-*tert*-butylcatechol] terphenyl adduct (mixture of regioisomers) (0.180 g, 64 %) as a yellow powder (mp > 300 °C); IR (DCM film) 2964, 2906, 2870, 2237, 1604, 1515, 1456, 1273, 1122, 1010 cm^{-1}; ^{1}H NMR (500 MHz, CDCl$_3$) δ 7.13 – 6.62 (15H, m, Ar*H*), 1.27 – 1.10 (45H, m, ^{t}Bu*H*); ^{13}C NMR (125 MHz, CDCl$_3$) δ 149.2, 149.11, 149.10, 149.05, 141.2, 140.4, 140.3, 140.24, 140.19, 140.14, 140.10, 140.05, 140.0, 138.52, 138.45, 138.41, 138.36, 138.3, 138.23, 138.19, 136.3, 136.2, 136.1, 122.3, 122.1, 121.93, 121.87, 116.5, 116.43, 116.37, 116.2, 116.0, 114.4, 114.0, 113.09, 113.85, 111.9, 110.6, 92.0, 91.8, 34.9, 34.8, 34.69, 34.68, 34.65, 31.41, 31.36, 31.3 (^{19}F-^{13}C coupling not assigned, extra carbons due to regioisomeric nature); ^{19}F NMR (282 MHz, CDCl$_3$) δ -111.8 – -112.6 (1F, cluster of singlets, Ar*F*); LRMS (MALDI, *m/z*) calc. for C$_{71}$H$_{60}$FN$_3$O$_{10}$: 1133.43 (M$^+$), found 1133.20; GPC analysis (CHCl$_3$) M_n = 1106, M_w = 1131 g mol^{-1} relative to polystyrene, M_w/M_n = 1.023; BET surface area = 7 m^2 g^{-1}; total pore volume = 0.01 cm^3 g^{-1} at *p/p^o* = 0.98.

Penta-[3,5-di-*tert*-butylcatechol] terphenyl adduct
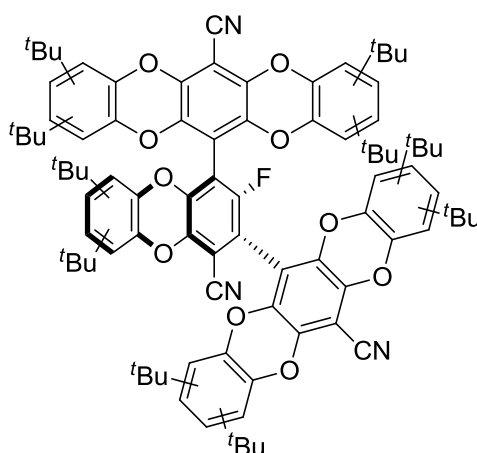
4,4',4''-Tricyano-2,2',2'',3,3'',5,5',5'',6,6',6''-undecafluoro-[1,1':3',1''-terphenyl]   (0.106   g, 0.211 mmol), 3,5-di-*tert*-butylcatechol (0.280 g, 1.26 mmol) and potassium carbonate (0.350 g, 2.53 mmol) were reacted together in anhydrous DMF (10 ml) in accordance with general procedure 1. Purification was achieved using column chromatography (3/1/1 hexane/DCM/toluene, R_f = 0.4) to give the penta-[3,5-di-*tert*-butylcatechol] terphenyl adduct (mixture of regioisomers) (0.263 g, 88 %) as a yellow powder (mp > 300 °C); IR (DCM film) 2962, 2871, 2237, 1446, 1412, 1305, 1261, 1230, 1037, 1019 cm^{-1}; ^{1}H NMR (400 MHz, CDCl$_3$) δ 7.00 – 6.22 (10H, m, Ar*H*), 1.54 – 0.88 (90H, m, ^{t}Bu*H*); ^{13}C NMR (125 MHz, CDCl$_3$) δ 148.0, 147.7 – 147.4 (m), 140.5 – 139.6 (m), 138.1 – 137.8 (m), 137.5 – 137.1 (m), 120.3 –

119.4 (m), 113.0 − 111.9 (m), 111.2, 110.6, 91.6, 91.4, 35.4 − 35.3 (m), 35.0 − 34.7 (m), 34.41, 34.36, 31.4 − 31.2 (m), 31.02, 30.98, 30.9, 30.4, 30.2, 30.1 − 29.5 (m) (^{19}F-^{13}C coupling not assigned, extra carbons due to regioisomeric nature); ^{19}F NMR (282 MHz, CDCl$_3$) δ -106.2 − -110.8 (1F, cluster of singlets, Ar*F*); LRMS (MALDI, *m/z*) calc. for C$_{91}$H$_{100}$FN$_3$O$_{10}$: 1414.74 (M$^+$), found 1414.99; GPC analysis (CHCl$_3$) M_n = 1378, M_w = 1421 g mol^{-1} relative to polystyrene, M_w/M_n = 1.031; BET surface area = 102 m^2 g^{-1}; total pore volume = 0.37 cm^3 g^{-1} at p/p^o = 0.98.

Penta-[R-naphthalene-2,3-diol] terphenyl adducts
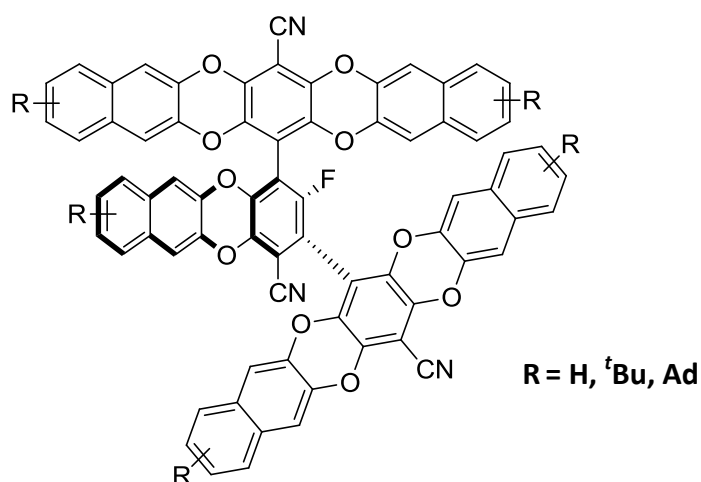
[R = H]: Penta-[naphthalene-2,3-diol] terphenyl adduct

4,4′,4′′-Tricyano-2,2′,2′′,3,3′′,5,5′,5′′,6,6′,6′′-undecafluoro-[1,1′:3′,1′′-terphenyl] (0.178 g, 0.354 mmol), naphthalene-2,3-diol (0.310 g, 1.94 mmol) and potassium carbonate (0.585 g, 4.23 mmol) were reacted together in anhydrous DMF (10 ml) in accordance with general procedure 1. Purification was achieved using column chromatography (7/2/1 DCM/hexane/toluene, R_f = 0.3) to give the penta-[naphthalene-2,3-diol] terphenyl adduct (0.049 g, 13 %) as a yellow powder (mp > 300 °C); IR (DCM film) 2920, 2850, 2236, 1520, 1451, 1263, 1170, 1013 cm^{-1}; ^{1}H NMR (400 MHz, (CD$_2$)$_4$O) δ 7.80 − 7.72 (6H, m, Ar*H*), 7.63 − 7.56 (5H, m, Ar*H*), 7.46 − 7.21 (19H, m, Ar*H*); ^{19}F NMR (282 MHz, CDCl$_3$) δ -111.72 (1F, s, Ar*F*); LRMS (MALDI, *m/z*) calc. for C$_{71}$H$_{30}$FN$_3$O$_{10}$: 1103.19 (M$^+$), found 1103.30; GPC analysis (CHCl$_3$) M_n = 871, M_w = 889 g mol^{-1} relative to polystyrene, M_w/M_n = 1.021; BET surface area = 29 m^2 g^{-1}; total pore volume = 0.11 cm^3 g^{-1} at p/p^o = 0.98. Crystallography data

(CHCl$_3$/MeOH): Triclinic, space group = P$\overline{1}$, a = 14.680(7) Å, b = 15.072(7) Å, c = 23.438(12) Å, α = 101.876(9), β = 102.840(5), γ = 94.462(4), V = 4906.28 Å^3, Z = 2, R_1 = 19.77.

[R = ^{t}Bu]: Penta-[6-*tert*-butylnaphthalene-2,3-diol] terphenyl adduct

4,4′,4′′-Tricyano-2,2′,2′′,3,3′′,5,5′,5′′,6,6′,6′′-undecafluoro-[1,1′:3′,1′′-terphenyl] (0.136 g, 0.270 mmol), 6-*tert*-butylnaphthalene-2,3-diol (0.320 g, 1.49 mmol) and potassium carbonate (0.747 g, 5.41 mmol) were reacted together in anhydrous DMF (10 ml) in accordance with general procedure 1. Purification was achieved using column chromatography (4/5/1 DCM/hexane/toluene, R_f = 0.3) to give the penta-[6-*tert*-butylnaphthalene-2,3-diol] terphenyl adduct (mixture of regioisomers) (0.162 g, 43 %) as a yellow powder (mp > 300 °C); IR (DCM film) 2961, 2869, 2237, 1514, 1443, 1248, 1012 cm^{-1}; ^{1}H NMR (500 MHz, CDCl$_3$) δ 7.69 – 7.09 (25H, m, ArH), 1.38 – 1.11 (45H, m, ^{t}BuH); ^{13}C NMR (125 MHz, CDCl$_3$) δ 149.6, 149.3 – 149.2 (m), 140.1 – 140.0 (m), 139.9 – 139.5 (m), 135.9 – 135.7 (m), 132.8, 132.5, 131.4 – 131.2 (m), 129.4 – 129.2 (m), 127.2 – 126.9 (m), 126.2, 125.6 – 125.5 (m), 122.7 – 122.5 (m), 122.3, 113.6 – 112.6 (m), 110.6 – 110.5 (m), 110.2, 92.3, 92.2, 35.1, 35.0, 34.68, 34.84, 31.34, 31.26, 31.22, 31.16 (^{19}F-^{13}C coupling not assigned, extra carbons due to regioisomeric nature); ^{19}F NMR (282 MHz, CDCl$_3$) δ -111.4 – -111.8 (1F, cluster of singlets, ArF); LRMS (MALDI, *m/z*) calc. for C$_{91}$H$_{70}$FN$_3$O$_{10}$: 1384.51 (M$^+$), found 1384.41; GPC analysis (CHCl$_3$) M_n = 1453, M_w = 1485 g mol^{-1} relative to polystyrene, M_w/M_n = 1.022; BET surface area = 259 m^2 g^{-1}; total pore volume = 0.35 cm^3 g^{-1} at *p/p^o* = 0.98.

[R = Ad]: Penta-[6-(1-adamantyl)naphthalene-2,3-diol] terphenyl adduct

4,4′,4′′-Tricyano-2,2′,2′′,3,3′′,5,5′,5′′,6,6′,6′′-undecafluoro-[1,1′:3′,1′′-terphenyl] (0.156 g, 0.310 mmol), 6-(1-adamantyl)naphthalene-2,3-diol (0.480 g, 1.63 mmol) and potassium carbonate (0.700 g, 5.07 mmol) were reacted together in anhydrous DMF (10 ml) in accordance with general procedure 1. Purification was achieved using column chromatography (7/2/1 DCM/hexane/toluene, R_f = 0.3) to give the penta-[6-(1-adamantyl)naphthalene-2,3-diol] terphenyl adduct (mixture of regioisomers) (0.531 g, 97 %) as a yellow powder (mp > 300 °C); IR (DCM film) 2903, 2848, 2351, 1514, 1446, 1265, 1243, 1012 cm^{-1}; ^{1}H NMR (500 MHz, CDCl$_3$) δ 7.68 – 7.10 (25H, m, ArH), 2.10 – 1.68 (75H, m, AdH); ^{13}C NMR (125 MHz, CDCl$_3$) δ 149.6, 149.5 – 149.3 (m), 142.4 – 142.1 (m), 140.1 – 140.0 (m), 139.8 – 139.3 (m), 135.9 – 135.6 (m), 131.5 – 131.3 (m), 129.6 – 129.4 (m), 127.1 – 126.9

(m), 125.0 – 124.6 (m), 122.6 – 122.3 (m), 113.6 – 113.4 (m), 113.0 – 112.6 (m), 110.6 – 110.4 (m), 92.3 – 92.1 (m), 42.2 – 43.0 (m), 37.0, 36.9, 36.6 – 36.4 (m), 29.13 – 29.06 (m) (^{19}F-^{13}C coupling not assigned, extra carbons due to regioisomeric nature); ^{19}F NMR (282 MHz, CDCl$_3$) δ -111.1 – -111.5 (1F, cluster of singlets, Ar*F*); LRMS (MALDI, *m/z*) calc. for C$_{121}$H$_{100}$FN$_3$O$_{10}$: 1775.10 (M$^+$), found 1777.57; GPC analysis (CHCl$_3$) M_n = 1403, M_w = 1543 g mol^{-1} relative to polystyrene, M_w/M_n = 1.100; BET surface area = 347 m^2 g^{-1}; total pore volume = 0.41 cm^3 g^{-1} at *p/p^o* = 0.98.

Penta-[R$_1$,R$_2$-triptycene-2,3-diol] terphenyl adducts

R$_1$ = H, ^{t}Bu

R$_2$ = H, Me

[R$_1$ = H, R$_2$ = H]: Penta-[triptycene-2,3-diol] terphenyl adduct

4,4′,4′′-Tricyano-2,2′,2′′,3,3′′,5,5′,5′′,6,6′,6′′-undecafluoro-[1,1′:3′,1′′-terphenyl] (0.060 g, 0.119 mmol), triptycene-2,3-diol (0.200 g, 0.698 mmol) and potassium carbonate (0.200 g, 1.45 mmol) were reacted together in anhydrous DMF (10 ml) in accordance with general procedure 1. Purification was achieved using column chromatography (3/1/1 DCM/hexane/toluene, R_f = 0.35) to give the penta-[triptycene-2,3-diol] terphenyl adduct (0.062 g, 30 %) as a yellow powder (mp > 300 °C); IR (DCM film) 3065, 2956, 2236, 1489, 1445, 1285, 1139, 1009 cm^{-1}; ^{1}H NMR (400 MHz, CDCl$_3$) δ 7.41 (2H, d, *J* = 7.0 Hz, Ar*H*), 7.37 – 7.34 (8H, m, Ar*H*), 7.26 – 7.14 (10H, m, Ar*H*), 7.07 – 6.91 (25H, m, Ar*H*), 6.84 (1H, s, Ar*H*),

6.78 (2H, s, ArH), 6.72 (2H, s, ArH), 5.38 (1H, s, CH), 5.32 (2H, s, CH), 5.31 (2H, s, CH), 5.18 (5H, s, CH); ^{13}C NMR (125 MHz, CDCl$_3$) δ 144.9, 144.8 – 144.6 (m), 143.02, 142.96, 142.7, 142.6 – 142.5 (m), 140.0, 139.8, 138.8, 137.7, 137.6, 137.5, 137.40, 137.36, 136.0, 135.9, 125.8 – 125.6 (m), 123.9 – 123.7 (m), 113.2, 113.04, 112.99, 112.8, 112.0, 110.0, 91.9, 91.7, 53.6, 53.5, 53.4 – 53.2 (m) (^{19}F-^{13}C coupling not assigned); ^{19}F NMR (282 MHz, CDCl$_3$) δ -111.7 (1F, s, ArF); LRMS (MALDI, m/z) calc. for C$_{121}$H$_{60}$FN$_3$O$_{10}$: 1734.43 (M$^+$), found 1734.99; GPC analysis (CHCl$_3$) M_n = 1493, M_w = 1533 g mol^{-1} relative to polystyrene, M_w/M_n = 1.027; BET surface area = 423 m^2 g^{-1}; total pore volume = 0.44 cm^3 g^{-1} at p/p^o = 0.98.

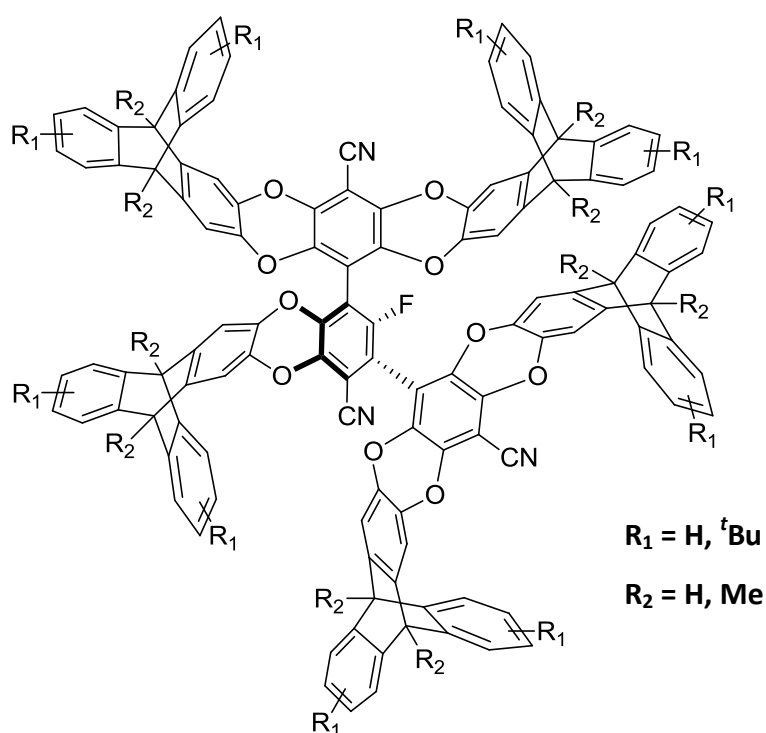### [R$_1$ = H, R$_2$ = Me]: Penta-[9,10-dimethyltriptycene-2,3-diol] terphenyl adduct

4,4',4''-Tricyano-2,2',2'',3,3'',5,5',5'',6,6',6''-undecafluoro-[1,1':3',1''-terphenyl] (0.101 g, 0.201 mmol), 9,10-dimethyltriptycene-2,3-diol (0.348 g, 1.11 mmol) and potassium carbonate (0.306 g, 2.21 mmol) were reacted together in anhydrous DMF (10 ml) in accordance with general procedure 1. Purification was achieved using column chromatography (2/2/1 DCM/hexane/toluene, R_f = 0.3) to give the penta-[9,10-dimethyltriptycene-2,3-diol] terphenyl adduct (0.296 g, 79 %) as a yellow powder (mp > 300 °C); IR (DCM film) 3054, 2977, 2920, 2237, 1612, 1446, 1291, 1264, 1169, 1011 cm^{-1}; ^{1}H NMR (400 MHz, CDCl$_3$) δ 7.36 (2H, d, J = 7.3 Hz, ArH), 7.32 – 7.28 (8H, m, ArH), 7.24 – 7.23 (4H, m, ArH), 7.19 – 7.14 (4H, m, ArH), 7.08 (4H, d, J = 8.6 Hz, ArH), 7.05 – 6.97 (24H, m, ArH), 6.75 (1H, s, ArH), 6.64 (4H, s, ArH), 2.39 – 2.32 (15H, m, CH_3), 2.22 (3H, s, CH_3), 1.99 (6H, s, CH_3), 1.91 (6H, s, CH_3); ^{13}C NMR (125 MHz, CDCl$_3$) δ 147.9, 147.8, 147.7 – 147.5 (m), 146.5, 146.4, 146.1, 146.0, 145.9, 142.4, 140.1, 139.9, 137.5, 137.4 – 137.2 (m), 136.0, 125.3 – 125.1 (m), 120.8 – 120.5 (m), 110.6 – 110.0 (m), 91.8, 91.6, 48.5 – 48.3 (m), 13.9 – 13.8 (m), 13.4, 13.3; (^{19}F-^{13}C coupling not assigned); ^{19}F NMR (282 MHz, CDCl$_3$) δ -111.7 (1F, s, ArH); LRMS (MALDI, m/z) calc. for C$_{131}$H$_{80}$FN$_3$O$_{10}$: 1874.59 (M$^+$), found 1875.91 (MH$^+$); GPC analysis (CHCl$_3$) M_n = 1571, M_w = 1611 g mol^{-1} relative to polystyrene, M_w/M_n = 1.025; BET surface area = 351 m^2 g^{-1}; total pore volume = 0.30 cm^3 g^{-1} at p/p^o = 0.98.

[R$_1$ = ^{t}Bu, R$_2$ = H]: Penta-[7,14-di-*tert*-butyltriptycene-2,3-diol] terphenyl adduct

4,4',4''-Tricyano-2,2',2'',3,3'',5,5',5'',6,6',6''-undecafluoro-[1,1':3',1''-terphenyl] (0.097 g, 0.193 mmol), 7,14-di-*tert*-butyltriptycene-2,3-diol (0.410 g, 1.03 mmol) and potassium carbonate (0.320 g, 2.32 mmol) were reacted together in anhydrous DMF (10 ml) in accordance with general procedure 1. Purification was achieved using column chromatography (2/1/1 DCM/hexane/toluene, R_f = 0.25) to give the penta-[7,14-di-*tert*-butyltriptycene-2,3-diol] terphenyl adduct (mixture of regioisomers) (0.360 g, 81 %) as a yellow powder (mp > 300 °C); IR (DCM film) 2962, 2905, 2869, 2237, 1446, 1285, 1264, 1140, 1010 cm^{-1}; ^{1}H NMR (500 MHz, CDCl$_3$) δ 7.46 – 6.61 (40H, m, Ar*H*), 5.34 – 5.13 (10H, m, C*H*), 1.32 – 1.14 (90H, m, ^{t}Bu*H*); ^{13}C NMR (125 MHz, CDCl$_3$) δ 148.8 – 148.5 (m), 144.8 – 144.6 (m), 143.2, 143.0, 142.1 – 141.8 (m), 137.4 – 137.1 (m), 135.92, 135.86, 123.3 – 123.0 (m), 122.3 – 122.0 (m), 121.2 – 121.1 (m), 112.9 – 112.7 (m), 91.8, 53.5 – 53.2 (m), 34.9 – 34.7 (m), 31.8 – 31.7 (m) (^{19}F-^{13}C coupling not assigned, extra carbons due to regioisomeric nature); ^{19}F NMR (282 MHz, CDCl$_3$) δ -111.5 – -112.1 (1F, cluster of singlets, Ar*F*); LRMS (MALDI, *m/z*) calc. for C$_{161}$H$_{140}$FN$_3$O$_{10}$: 2295.05 (M$^+$), found 2295.19; GPC analysis (CHCl$_3$) M_n = 2227, M_w = 2304 g mol^{-1} relative to polystyrene, M_w/M_n = 1.035; BET surface area = 726 m^2 g^{-1}; total pore volume = 0.72 cm^3 g^{-1} at *p/p^o* = 0.98.

[R$_1$ = ^{t}Bu, R$_2$ = Me]: Penta-[7,14-di-*tert*-butyl-9,10-dimethyltriptycene-2,3-diol] terphenyl adduct

4,4',4''-Tricyano-2,2',2'',3,3'',5,5',5'',6,6',6''-undecafluoro-[1,1':3',1''-terphenyl] (0.0639 g, 0.127 mmol), 7,14-di-*tert*-butyl-9,10-dimethyltriptycene-2,3-diol (0.298 g, 0.699 mmol) and potassium carbonate (0.210 g, 1.52 mmol) were reacted together in anhydrous DMF (10 ml) in accordance with general procedure 1. Purification was achieved using column chromatography (5/3/1 hexane/DCM/toluene, R_f = 0.25) to give the penta-[7,14-di-*tert*-butyl-9,10-dimethyltriptycene-2,3-diol] terphenyl adduct (mixture of regioisomers) (0.202 g, 65%) as a yellow powder (mp > 300 °C); IR (DCM film) 2966, 2869, 2237, 1612, 1446, 1291, 1265, 1011 cm^{-1}; ^{1}H NMR (400 MHz, CDCl$_3$) δ 7.39 – 6.45 (40H, m, Ar*H*), 2.40 – 1.68 (30H, m, C*H$_3$*), 1.31 – 1.15 (90H, m, ^{t}Bu*H*); ^{13}C NMR (125 MHz, CDCl$_3$) δ 148.1 – 147.9 (m), 147.5 – 147.2 (m), 146.79 – 146.78 (m), 146.5, 146.4, 146.2 – 146.1 (m), 145.9, 145.0 – 144.5 (m), 144.3, 139.7 – 139.6 (m), 137.0 – 136.7 (m), 136.0, 135.8, 121.8 – 121.4 (m), 120.2 – 119.8

(m), 117.8 − 117.5 (m), 117.13 − 117.07 (m), 110.3 − 109.9 (m), 48.4 − 48.1 (m), 34.9 − 34.8 (m), 31.7, 13.9 − 13.7 (m) (^{19}F-^{13}C coupling not assigned, extra carbons due to regioisomeric nature); ^{19}F NMR (282 MHz, CDCl$_3$) δ -111.3 − -112.5 (1F, cluster of singlets, ArF); LRMS (MALDI, *m/z*) calc. for C$_{171}$H$_{160}$FN$_3$O$_{10}$: 2435.21 (M$^+$), found 2434.75; GPC analysis (CHCl$_3$) M_n = 2147, M_w = 2214 g mol^{-1} relative to polystyrene, M_w/M_n = 1.031; BET surface area = 651 m^2 g^{-1}; total pore volume = 0.47 cm^3 g^{-1} at *p/p^o* = 0.98.

Penta-[cy6-triptycene-2,3-diol] terphenyl adduct

4,4',4''-Tricyano-2,2',2'',3,3'',5,5',5'',6,6',6''-undecafluoro-[1,1':3',1''-terphenyl] (0.0326 g, 0.0656 mmol), cy6-triptycene-2,3-diol (0.180 g, 0.355 mmol) and potassium carbonate (0.150 g, 1.09 mmol) were reacted together in anhydrous DMF (10 ml) in accordance with general procedure 1. Purification was achieved using column chromatography (7/2/1 hexane/DCM/toluene, R_f = 0.3) to give the penta-[cy6-triptycene-2,3-diol] terphenyl adduct (0.144 g, 77 %) as a yellow powder (mp > 300 °C); IR (DCM film) 2959, 2925, 2860, 2238, 1473, 1443, 1284, 1139, 1008 cm^{-1}; ^{1}H NMR (500 MHz, CDCl$_3$) δ 7.29 (2H, s, Ar*H*), 7.24 − 7.21 (13H, m, Ar*H*), 7.15 (2H, s, Ar*H*), 7.11 (4H, s, Ar*H*), 7.01 (2H, s, Ar*H*), 7.00 (2H, s, Ar*H*), 6.82

(3H, s, Ar*H*), 6.74 (2H, s, Ar*H*), 5.24 (1H, s, C*H*), 5.17 (2H, s, C*H*), 5.15 (2H, s, C*H*), 5.120 – 5.115 (4H, m, C*H*), 5.04 (1H, s, C*H*), 1.62 – 1.54 (40H, m, C*H*$_2$), 1.29 – 1.10 (120H, m, C*H*$_3$); ^{13}C NMR (125 MHz, CDCl$_3$) δ 143.9, 143.7, 143.4 – 143.3 (m), 141.9 – 141.5 (m), 139.9, 139.4, 137.9, 137.5, 137.3, 137.2, 137.1, 136.8, 136.0, 135.6, 121.8 – 121.5 (m), 113.1, 112.7, 112.6, 122.2, 111.9, 110.5, 109.8, 92.6, 91.9, 91.3, 91.0, 53.1 – 53.0 (m), 52.74, 52.68, 35.4, 34.49, 34.45, 34.41, 34.40, 32.8, 32.6, 32.51, 32.46, 32.32, 32.29, 32.2, 32.1 – 32.0 (m) (^{19}F-^{13}C coupling not assigned); ^{19}F NMR (282 MHz, CDCl$_3$) δ -112.6 (1F, s, Ar*F*); LRMS (MALDI, *m/z*) calc. for C$_{201}$H$_{200}$FN$_3$O$_{10}$: 2836.53 (M$^+$), found 2838.54; GPC analysis (CHCl$_3$) *M*$_n$ = 1973, *M*$_w$ = 2043 g mol^{-1} relative to polystyrene, *M*$_w$/*M*$_n$ = 1.036; BET surface area = 698 m^2 g^{-1}; total pore volume = 0.44 cm^3 g^{-1} at *p/p*^{o} = 0.98.

Penta-[ucy6-triptycene-2,3-diol] terphenyl adduct
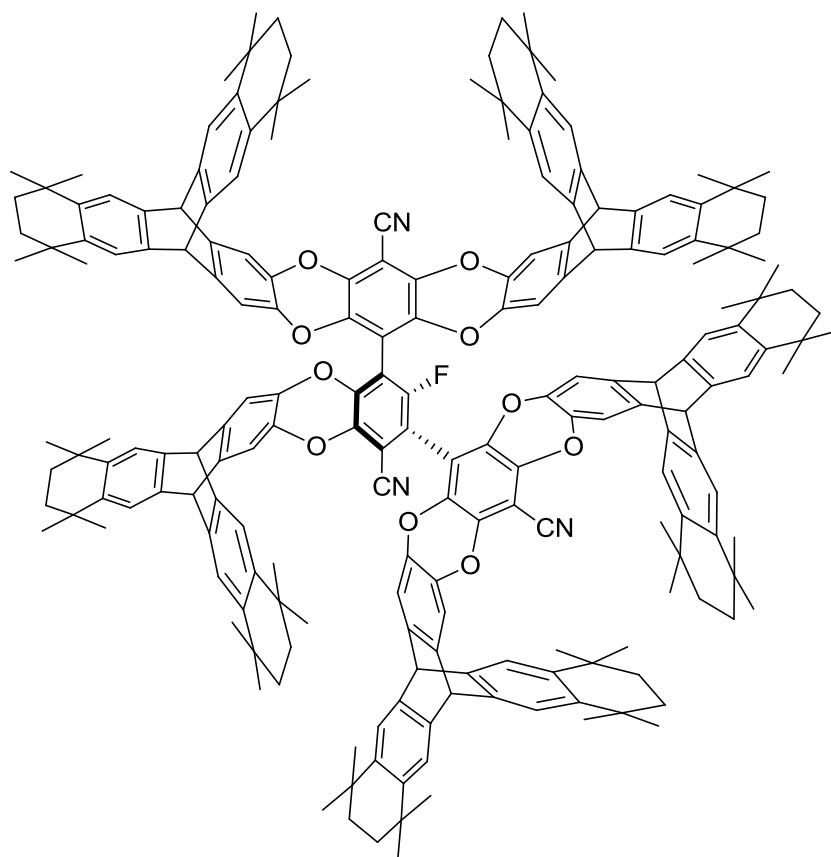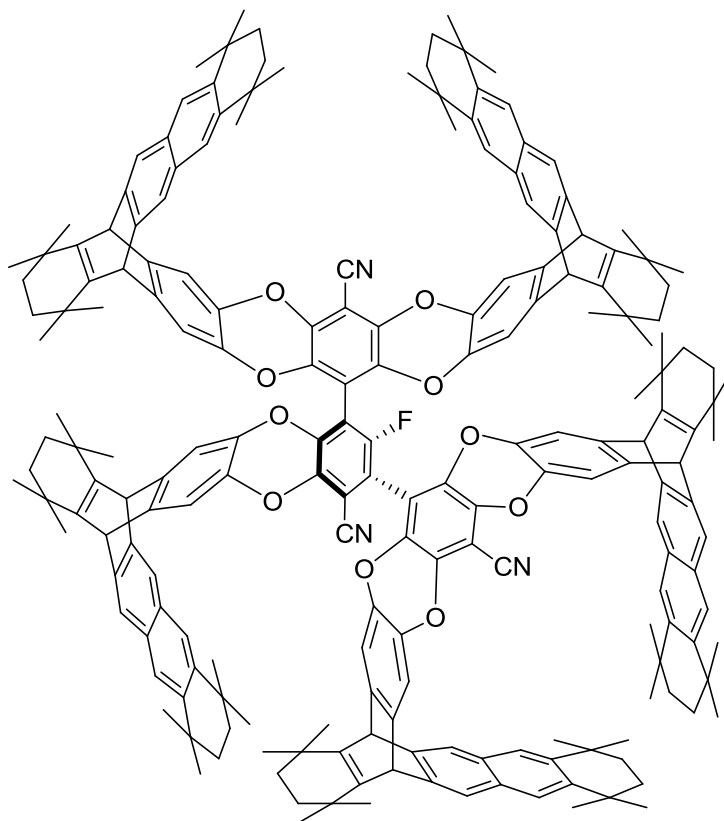

4,4',4''-Tricyano-2,2',2'',3,3'',5,5',5'',6,6',6''-undecafluoro-[1,1':3',1''-terphenyl] (0.0363 g, 0.0721 mmol), ucy6-triptycene-2,3-diol (0.201 g, 0.397 mmol) and potassium carbonate (0.165 g, 1.19 mmol) were reacted together in anhydrous DMF (10 ml) in accordance with general procedure 1. Purification was achieved using column chromatography (7/2/1 hexane/DCM/toluene, *R*$_f$ = 0.3) to give the penta-[ucy6-triptycene-2,3-diol] terphenyl

adduct (mixture of regioisomers) (0.160 g, 78 %) as a yellow powder (mp > 300 °C); IR (DCM film) 2957, 2925, 2861, 2237, 1610, 1447, 1284, 1141, 1009 cm^{-1}; ^{1}H NMR (500 MHz, CDCl$_3$) δ 7.96 – 7.20 (20H, m, ArH), 7.11 – 6.37 (10H, m, ArH), 5.07 – 4.44 (10H, m, CH), 1.74 – 1.67 (20H, m, CH_2), 1.39 – 0.30 (140H, m, CH_2/CH_3); ^{13}C NMR (125 MHz, CDCl$_3$) δ 146.9 – 146.4 (m), 144.1 – 143.5 (m), 142.8 – 142.4 (m), 140.2 – 140.1 (m), 137.7 – 137.1 (m), 130.2 – 130.0 (m), 124.9 – 124.7 (m), 119.6 – 119.4 (m), 111.7 – 111.5 (m), 91.5, 91.3, 50.1 – 49.7 (m), 35.5 – 35.4 (m), 34.7 – 34.6 (m), 34.2 – 34.0 (m), 32.8 – 32.6 (m), 27.2 – 26.7 (m) (^{19}F-^{13}C coupling not assigned, extra carbons due to regioisomeric nature); ^{19}F NMR (282 MHz, CDCl$_3$) δ -109.9 – -112.2 (1F, cluster of singlets, ArF); LRMS (MALDI, m/z) calc. for C$_{201}$H$_{200}$FN$_3$O$_{10}$: 2836.53 (M$^+$), found 2861.81 (MNa$^+$); GPC analysis (CHCl$_3$) M_n = 2123, M_w = 2205 g mol^{-1} relative to polystyrene, M_w/M_n = 1.039; BET surface area = 591 m^2 g^{-1}; total pore volume = 0.49 cm^3 g^{-1} at p/p^o = 0.98.

5.2.3 Dendrimers of Intrinsic Microporosity (DIMs)

Tri-[R-catechol]-9,10-diethyltriptycene dendrimers

R = H, ^{t}Bu
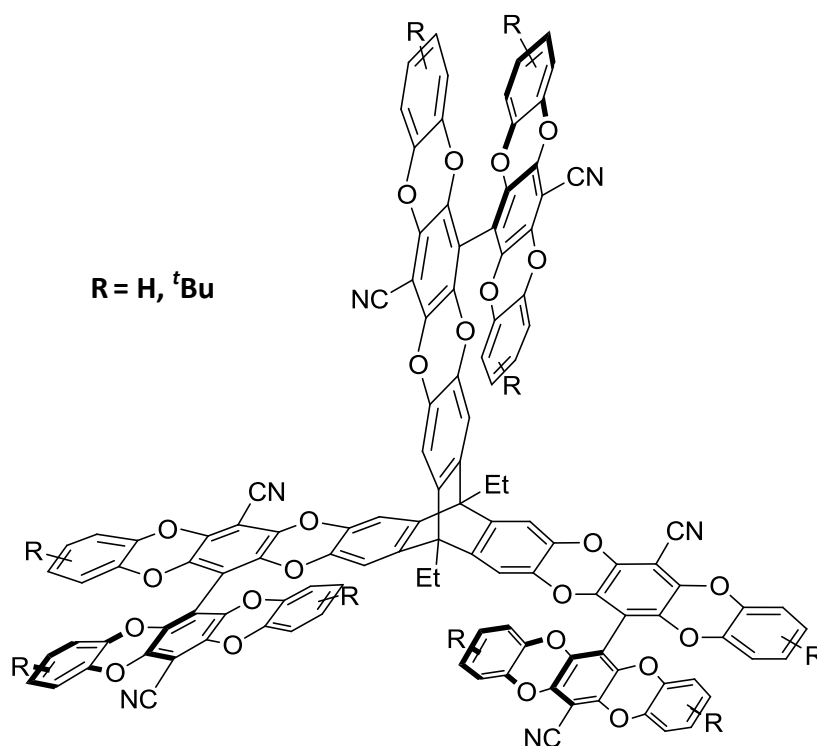
[R = H]: Tri-[catechol]-9,10-diethyltriptycene dendrimer

Tri-[catechol] biphenyl adduct (0.171 g, 0.306 mmol), 9,10-diethyltriptycene-2,3,6,7,13,14-hexaol (0.040 g, 0.098 mmol) and potassium carbonate (0.108 g, 0.782 mmol) were reacted together in anhydrous DMF (5 ml) in accordance with general procedure 1. Purification was achieved *via* trituration in chloroform (20 ml) to give the tri-[catechol]-9,10-diethyltriptycene dendrimer (mixture of regioisomers) (0.175 g, 91 %) as a yellow powder (mp > 300 °C); IR (DCM film) 2923, 2239, 1608, 1495, 1441, 1275, 1254 cm^{-1}; ^{1}H NMR (400 MHz, CDCl$_3$) δ 7.02 − 6.46 (42H, m, Ar*H*), Et protons not seen; LRMS (MALDI, *m/z*) calc. for C$_{120}$H$_{52}$N$_6$O$_{24}$: 1961.31 (M$^+$), found 1962.17 (MH$^+$); GPC analysis (CHCl$_3$) M_n = 1355, M_w = 1403 g mol^{-1} relative to polystyrene, M_w/M_n = 1.035; BET surface area = 330 m^2 g^{-1}; total pore volume = 0.44 cm^3 g^{-1} at *p/p^o* = 0.98.

[R = ^{t}Bu]: Tri-[4-*tert*-butylcatechol]-9,10-diethyltriptycene dendrimer

Tri-[4-*tert*-butylcatechol] biphenyl adduct of (0.316 g, 0.435 mmol), 9,10-diethyltriptycene-2,3,6,7,13,14-hexaol (0.057 g, 0.140 mmol) and potassium carbonate (0.155 g, 1.12 mmol) were reacted together in anhydrous DMF (5 ml) in accordance with general procedure 1. Purification was achieved using column chromatography (hexane/DCM 3/2, R_f = 0.3) to give the tri-[4-*tert*-butylcatechol]-9,10-diethyltriptycene dendrimer (mixture of regioisomers) (0.198 g, 57 %) as a yellow powder (mp > 300 °C); IR (DCM film) 2963, 2870, 2238, 1605, 1513, 1436, 1274, 1000 cm^{-1}; ^{1}H NMR (400 MHz, CDCl$_3$) δ 7.04 − 6.46 (33H, m, Ar*H*), 1.22 − 0.99 (81H, m, ^{t}Bu*H*), Et protons not seen; ^{13}C NMR (125 MHz, CDCl$_3$) δ 149.2, 149.04, 148.99, 148.91, 148.86, 140.4, 140.3, 140.0, 138.7, 138.3, 138.2, 138.1, 136.4, 136.3, 136.1, 136.0, 135.9, 128.19, 128.16, 128.0, 126.9, 121.9, 121.7, 116.2, 114.3, 114.2, 114.11, 114.05, 114.0, 111.6, 111.5, 111.3, 110.8, 93.1, 91.6, 91.5, 91.38, 91.35, 91.2, 34.8, 34.72, 34.65, 34.6, 31.5, 31.3, 31.2 (extra carbons due to regioisomeric nature); LRMS (MALDI, *m/z*) calc. for C$_{156}$H$_{124}$N$_6$O$_{24}$: 2465.87 (M$^+$), found 2466.85 (MH$^+$); GPC analysis (CHCl$_3$) M_n = 2358, M_w = 2458 g mol^{-1} relative to polystyrene, M_w/M_n = 1.043; BET surface area = 320 m^2 g^{-1}; total pore volume = 0.30 cm^3 g^{-1} at p/p^o = 0.98; elemental analysis calc. C: 75.96, H: 5.07, N: 3.41, found C: 75.79, H: 5.15, N: 3.25.

Tri-[3,5-di-*tert*-butylcatechol]-9,10-diethyltriptycene dendrimer
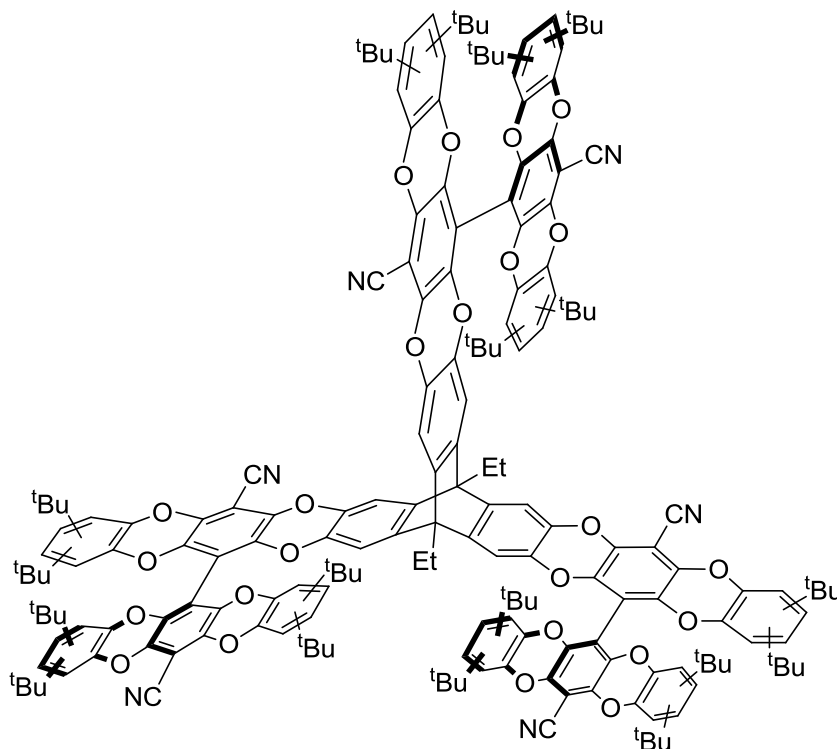
Tri-[3,5-di-*tert*-butylcatechol] biphenyl adduct (0.178 g, 0.199 mmol), 9,10-diethyltriptycene-2,3,6,7,13,14-hexaol (0.026 g, 0.0640 mmol) and potassium carbonate (0.070 g, 0.507 mmol) were reacted together in anhydrous DMF (5 ml) in accordance with general procedure 1. Purification was achieved using column chromatography (hexane/DCM 3/2, R_f = 0.3) to give the tri-[3,5-di-*tert*-butylcatechol]-9,10-diethyltriptycene dendrimer (mixture of regioisomers) (0.072 g, 39 %) as a yellow solid (mp > 300 °C); IR (DCM film) 2962, 2871, 2237, 1442, 1413, 1304, 1277, 1036, 1016 cm^{-1}; ^{1}H NMR (400 MHz, CDCl$_3$) δ 6.93 – 6.49 (24H, m, Ar*H*), 1.53 – 0.98 (172H, m, ^{t}Bu*H*), Et protons not seen; ^{13}C NMR (125 MHz, CDCl$_3$) δ 147.44, 147.41, 147.37, 147.33, 147.26, 140.7, 140.4, 140.3, 140.1, 140.0, 139.8, 139.3, 137.6, 137.4, 137.1, 137.0, 136.8, 136.7, 136.3, 136.1, 135.9, 132.7, 131.1, 119.8, 119.7, 119.6, 119.5, 112.7, 112.5, 112.4, 112.2, 90.8, 90.6, 35.40, 35.35, 35.3, 34.9, 34.8, 31.5, 31.42, 31.40, 30.2, 30.1, 29.9, 29.5, 29.4, 29.3 (extra carbons due to regioisomeric nature; LRMS (MALDI, *m/z*) calc. for C$_{192}$H$_{196}$N$_6$O$_{24}$: 2971.44 (M$^+$), found 2971.44; GPC analysis (CHCl$_3$) M_n = 2481, M_w = 2548 g mol^{-1} relative to polystyrene, M_w/M_n = 1.027; BET surface area = 346 m^2 g^{-1}; total pore volume = 0.27 cm^3 g^{-1} at *p/p^o* = 0.98; elemental analysis calc. C: 77.60, H: 6.65, N: 2.83, found C: 78.86, H: 7.10, N: 2.57.

Tri-[R-naphthalene-2,3-diol]-9,10-diethyltriptycene dendrimers

R = H, *t*Bu, Ad
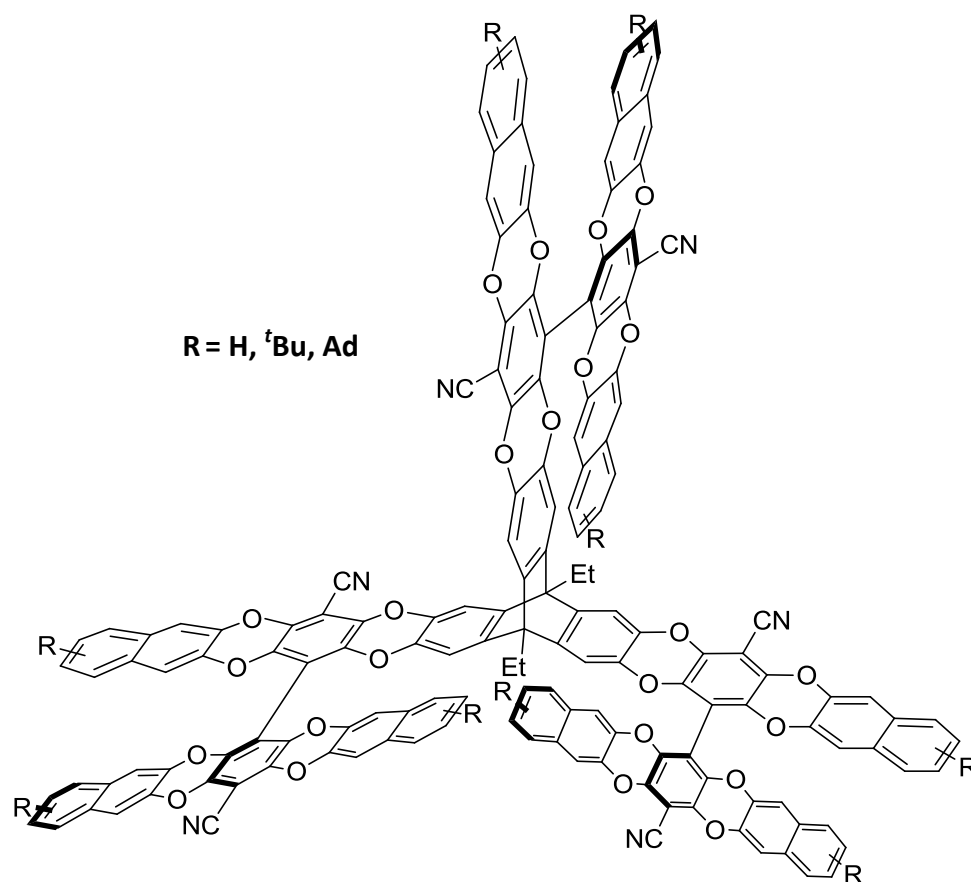
[R = H]: Tri-[naphthalene-2,3-diol]-9,10-diethyltriptycene dendrimer

Tri-[naphthalene-2,3-diol] biphenyl adduct (0.227 g, 0.321 mmol), 9,10-diethyltriptycene-2,3,6,7,13,14-hexaol (0.042 g, 0.103 mmol) and potassium carbonate (0.113 g, 0.818 mmol) were reacted together in anhydrous DMF (5 ml) in accordance with general procedure 1. Purification was achieved *via* trituration in chloroform (50 ml) to give the tri-[naphthalene-2,3-diol]-9,10-diethyltriptycene dendrimer (mixture of regioisomers) (0.124 g, 50 %) as a yellow powder (mp > 300 °C); IR (DCM film) 3056, 2236, 1514, 1431, 1258, 1168, 1000 cm^{-1}; LRMS (MALDI, *m/z*) calc. for $C_{156}H_{70}N_6O_{24}$: 2412.45 (M$^+$), found 2412.60; GPC analysis (CHCl$_3$) M_n = 1725, M_w = 1810 g mol^{-1} relative to polystyrene, M_w/M_n = 1.049; BET surface area = 300 m^2 g^{-1}; total pore volume = 0.33 cm^3 g^{-1} at *p/p^o* = 0.98.

[R = *t*Bu]: Tri-[6-*tert*-butylnaphthalene-2,3-diol]-9,10-diethyltriptycene dendrimer

Tri-[6-*tert*-butylnaphthalene-2,3-diol] biphenyl adduct (0.374 g, 0.427 mmol), 9,10-diethyltriptycene-2,3,6,7,13,14-hexaol (0.056 g, 0.138 mmol) and potassium carbonate (0.150 g, 1.09 mmol) were reacted together in anhydrous DMF (5 ml) in accordance with general procedure 1. Purification was achieved using column chromatography (hexane/DCM 3/2, R_f = 0.35) to give the tri-[6-*tert*-butylnaphthalene-2,3-diol]-9,10-diethyltriptycene dendrimer (mixture of regioisomers) (0.328 g, 81 %) as a yellow powder (mp > 300 °C); IR (DCM film) 2961, 2926, 2868, 2237, 1514, 1435, 1282, 1247, 1004 cm^{-1}; ^{1}H NMR (400 MHz, CDCl$_3$) δ 7.66 – 7.27 (36H, m, Ar*H*), 7.08 – 6.35 (15H, m, Ar*H*), 1.41 – 1.11 (81H, m, *t*Bu*H*), Et protons not seen; ^{13}C NMR (125 MHz, CDCl$_3$) δ 149.2, 149.10, 149.07, 149.0, 140.22, 140.20, 140.17, 140.09, 140.05, 140.0, 139.80, 139.76, 139.73, 139.68, 139.1, 139.6, 139.52, 139.49, 139.44, 139.38, 137.62, 137.59, 137.5, 136.0, 135.9, 135.84, 135.79, 135.74, 135.71, 135.67, 135.5, 135.4, 131.2, 131.1, 129.3, 129.24, 129.22, 129.17, 129.1, 127.1, 127.0, 125.2, 122.53, 122.48, 122.4, 122.3, 114.3, 113.32, 113.27, 113.2, 112.9, 112.80, 112.76, 112.7, 111.47, 111.46, 111.4, 110.7, 110.6, 91.8, 91.7, 34.99, 34.96, 34.9, 34.8, 31.4, 31.3, 31.2, 31.1 (extra carbons due to regioisomeric nature; LRMS (MALDI, *m/z*) calc. for C$_{192}$H$_{142}$N$_6$O$_{24}$: 2917.01 (M$^+$), found 2919.34; GPC analysis (CHCl$_3$) M_n = 2047, M_w = 2114 g mol^{-1} relative to polystyrene, M_w/M_n = 1.033; BET surface area = 665 m^{2}g^{-1}; total pore volume = 0.58 cm^{3}g^{-1} at p/p^o = 0.98.

[R = Ad]: Tri-[6-(1-adamantyl)naphthalene-2,3-diol]-9,10-diethyltriptycene dendrimer

Tri-[6-(1-adamantyl)naphthalene-2,3-diol] biphenyl adduct (0.238 g, 0.214 mmol), 9,10-diethyltriptycene-2,3,6,7,13,14-hexaol (0.028 g, 0.0689 mmol) and potassium carbonate (0.080 g, 0.579 mmol) were reacted together in anhydrous DMF (5 ml) in accordance with general procedure 1. Purification was achieved using column chromatography (hexane/DCM 1/1, R_f = 0.4) to give the tri-[6-(1-adamantyl)naphthalene-2,3-diol]-9,10-diethyltriptycene dendrimer (mixture of regioisomers) (0.163 g, 65 %) as a yellow powder (mp > 300 °C); IR (DCM film) 2905, 2849, 2237, 1514, 1439, 1265, 1243, 1004 cm^{-1}; ^{1}H NMR (500 MHz, CDCl$_3$) δ 7.58 – 6.39 (51H, m, Ar*H*), 2.09 – 1.24 (135H, m, Ad*H*) Et protons not seen; ^{13}C NMR (500 MHz, CDCl$_3$) δ 149.3, 140.1, 139.7, 139.54, 139.51, 139.4, 131.4, 131.32, 131.29, 131.25, 129.3, 127.0, 126.91, 126.85, 124.6, 124.5, 122.4, 113.3, 113.2, 91.8, 91.7, 43.22, 43.18,

43.12, 43.06, 37.02, 36.98, 36.6, 36.5, 29.19, 29.15, 29.12, 29.07 (extra carbons due to regioisomeric nature, some carbons missing); LRMS (MALDI, *m/z*) calc. for $C_{246}H_{196}N_6O_{24}$: 3619.44 (M$^+$), found 3621.41; GPC analysis (CHCl$_3$) M_n = 2679, M_w = 2785 g mol^{-1} relative to polystyrene, M_w/M_n = 1.040; BET surface area = 461 m^2 g^{-1}; total pore volume = 0.38 cm^3 g^{-1} at p/p^o = 0.98.

Tri-[R$_1$,R$_2$-triptycene-2,3-diol]-9,10-diethyltriptycene dendrimers

R$_1$ = H, ^{t}Bu

R$_2$ = H, Me
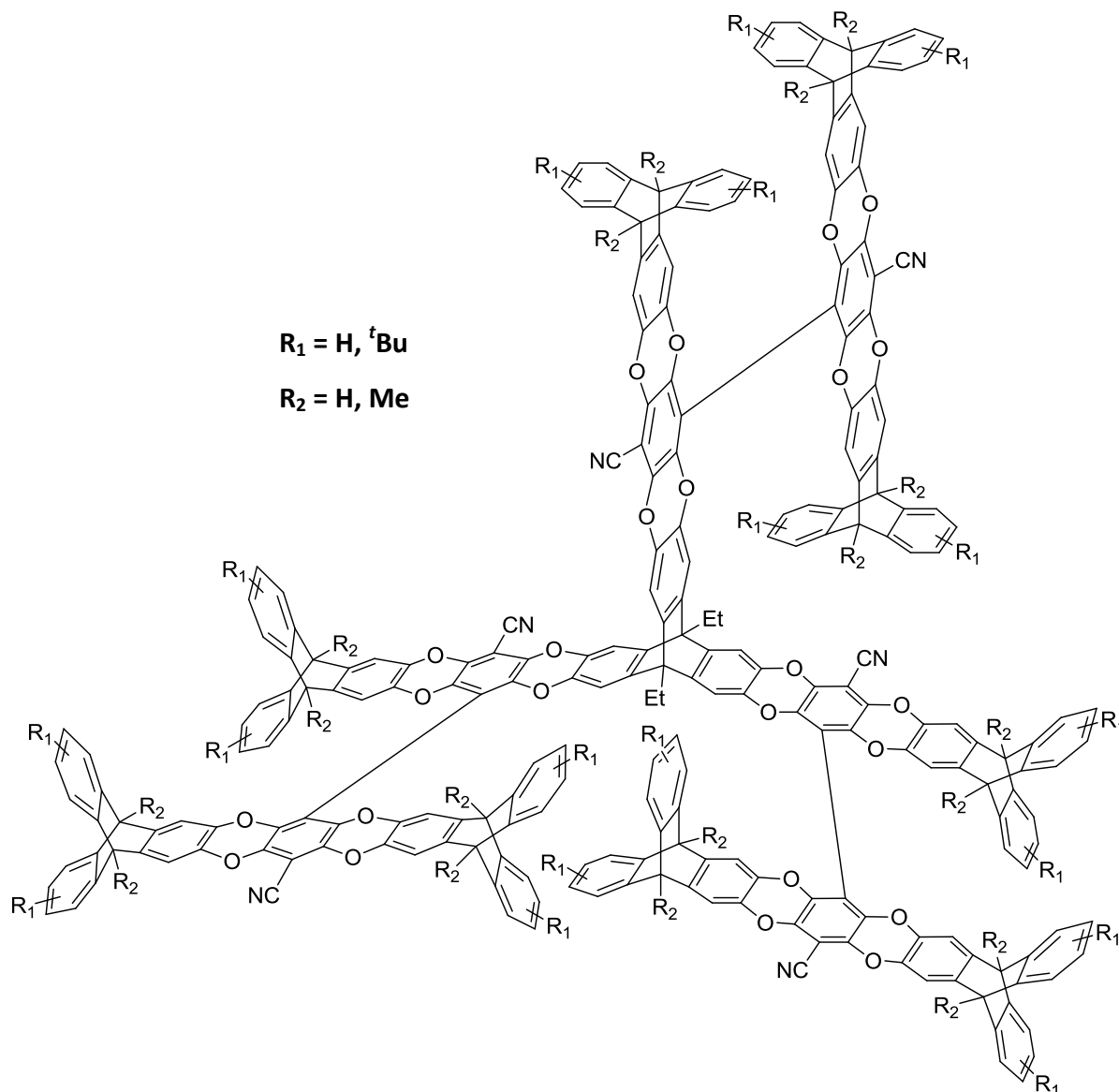
[R$_1$, = ^{t}Bu, R$_2$ = H]: Tri-[7,14-di-*tert*-butyltriptycene-2,3-diol]-9,10-diethyltriptycene dendrimer

Tri-[7,14-di-*tert*-butyltriptycene-2,3-diol] biphenyl adduct (0.194 g, 0.136 mmol), 9,10-diethyltriptycene-2,3,6,7,13,14-hexaol (0.0178 g, 0.0438 mmol) and potassium carbonate

(0.060 g, 0.434 mmol) were reacted together in anhydrous DMF (5 ml) in accordance with general procedure 1. Purification was achieved using column chromatography (hexane/DCM 3/2, R_f = 0.3) to give the tri-[7,14-di-*tert*-butyltriptycene-2,3-diol]-9,10-diethyltriptycene dendrimer (mixture of regioisomers) (0.124 g, 62 %) as a yellow powder (mp > 300 °C); IR (DCM film) 2961, 2906, 2869, 2239, 1608, 1440, 1284, 1139, 1001 cm^{-1}; ^{1}H NMR (500 MHz, CDCl$_3$) δ 7.40 – 6.48 (78H, m, Ar*H*), 5.26 – 4.99 (18H, m, C*H*), 1.29 – 0.85 (162H, m, ^{t}Bu*H*), Et proton not seen; ^{13}C NMR (500 MHz, CDCl$_3$) δ 148.5, 148.4, 148.32, 148.27, 144.52, 144.48, 144.42, 144.39, 142.91, 142.85, 142.7, 142.6, 141.7, 141.61, 141.55, 141.5, 139.5, 139.3, 137.2, 137.1, 137.0, 136.9, 135.63, 135.60, 135.5, 123.0, 122.91, 122.87, 122.8, 121.9, 121.82, 121.79, 120.8, 120.73, 120.67, 120.6, 112.6, 110.3, 110.0, 95.1, 90.9, 53.30, 53.25, 53.2, 53.11, 53.05, 34.54, 34.52, 34.4, 31.6, 31.5 (extra peaks due to regioisomeric nature); LRMS (MALDI, *m/z*) calc. for C$_{318}$H$_{268}$N$_6$O$_{24}$: 4557.00 (M$^+$), found 4558.97; GPC analysis (CHCl$_3$) M_n = 3237, M_w = 3352 g mol^{-1} relative to polystyrene, M_w/M_n = 1.036; BET surface area = 722 m^2 g^{-1}; total pore volume = 0.76 cm^3 g^{-1} at p/p^o = 0.98.

### [R$_{1,}$ = H, R$_2$ = Me]: Tri-[9,10-dimethyltriptycene-2,3-diol]-9,10-diethyltriptycene dendrimer

Tri-[9,10-dimethyltriptycene-2,3-diol] biphenyl adduct (0.400 g, 0.342 mmol), 9,10-diethyltriptycene-2,3,6,7,13,14-hexaol (0.0450 g, 0.111 mmol) and potassium carbonate (0.125 g, 0.905 mmol) were reacted together in anhydrous DMF (8 ml) in accordance with general procedure 1. Purification was achieved using column chromatography (hexane/DCM 1/1, R_f = 0.3) to give the tri-[9,10-dimethyltriptycene-2,3-diol]-9,10-diethyltriptycene dendrimer (mixture of regioisomers) (0.220 g, 52 %) as a yellow powder (mp > 300 °C); IR (DCM film) 3064, 2972, 2239, 1611, 1436, 1289, 1000 cm^{-1}; ^{1}H NMR (500 MHz, CDCl$_3$) δ 7.39 – 6.28 (96H, m, Ar*H*), 2.38 – 1.85 (54H, m, C*H$_3$*), Et protons not seen; ^{13}C NMR (125 MHz, CDCl$_3$) δ 147.7, 147.6, 147.54, 147.50, 147.2, 145.90, 145.87, 145.8, 145.73, 145.67, 139.8, 139.7, 139.6, 139.5, 139.4, 139.2, 137.5, 137.4, 137.33, 137.28, 137.2, 137.1, 136.98, 136.95, 136.82, 136.76, 136.1, 136.0, 135.81, 135.75, 135.7, 135.6, 125.5, 125.2, 125.0, 124.8, 124.6, 120.74, 120.65, 120.6, 120.5, 120.4, 120.1, 111.32, 111.28, 110.9, 110.8, 110.5, 110.43, 110.41, 110.31, 110.26, 110.2, 110.1, 91.24, 91.22, 91.16, 91.08, 91.05, 48.43, 48.41, 48.37, 48.36, 48.3, 48.23, 48.19, 13.8, 13.61, 13.60, 13.5, 13.42, 13.40 (extra peaks due to regioisomeric nature); LRMS (MALDI, *m/z*) calc. for C$_{246}$H$_{160}$N$_6$O$_{24}$: 3800.16 (M$^+$), found 3802.51; GPC analysis (CHCl$_3$) M_n = 2684, M_w = 2786 g mol^{-1} relative to

polystyrene, M_w/M_n = 1.038; BET surface area = 528 m^{2}g^{-1}; total pore volume = 0.45 cm^{3}g^{-1} at p/p^o = 0.98.

[R$_1$, = ^{t}Bu, R$_2$ = Me]: Tri-[7,14-di-*tert*-butyl-9,10-dimethyltriptycene-2,3-diol]-9,10-diethyltriptycene dendrimer

Tri-[7,14-di-*tert*-butyl-9,10-dimethyltriptycene-2,3-diol] biphenyl adduct (0.111 g, 0.0736 mmol), 9,10-diethyltriptycene-2,3,6,7,13,14-hexaol (0.0096 g, 0.0236 mmol) and potassium carbonate (0.026 g, 0.188 mmol) were reacted together in anhydrous DMF (5 ml) in accordance with general procedure 1. Purification was achieved using column chromatography (DCM/hexane, 2/1, R_f = 0.3) to give the tri-[7,14-di-*tert*-butyl-9,10-dimethyltriptycene-2,3-diol]-9,10-diethyltriptycene dendrimer (mixture of regioisomers) (0.067 g, 59 %) as a yellow powder (mp > 300 °C); IR (DCM film) 3066, 2966, 2904, 2869, 2240, 1611, 1443, 1290, 1002 cm^{-1}; ^{1}H NMR (500 MHz, CDCl$_3$) δ 7.43 – 6.53 (78H, m, Ar*H*), 2.35 – 2.14 (54H, m, C*H*$_3$), 1.30 – 0.88 (162H, m, ^{t}Bu*H*); ^{13}C NMR (500 MHz, CDCl$_3$) δ 148.0, 147.90, 147.88, 147.8, 147.42, 147.39, 147.36, 147.32, 147.28, 147.2, 146.9, 146.3, 146.1, 146.1, 146.01, 145.99, 144.82, 144.79, 144.77, 144.7, 139.6, 137.3, 137.24, 137.17, 136.8, 136.0, 135.8, 121.7, 121.64, 121.60, 121.56, 120.23, 120.17, 120.12, 120.06, 120.0, 117.8, 117.73, 117.71, 117.66, 111.4, 110.9, 110.4, 110.2, 110.0, 104.2, 91.1, 90.9, 48.22, 48.16, 48.1, 34.99, 34.97, 34.95, 34.81, 34.79, 34.77, 34.73, 34.70, 31.8, 31.7, 13.9, 13.79, 13.77 (extra peaks due to regioisomeric nature); LRMS (MALDI, *m/z*) calc. for C$_{336}$H$_{304}$N$_6$O$_{24}$: 4810.03 (M$^+$), found 4838.20 (MNa$^+$); GPC analysis (CHCl$_3$) M_n = 3358, M_w = 3532 g mol^{-1} relative to polystyrene, M_w/M_n = 1.052; BET surface area = 663 m^{2}g^{-1}; total pore volume = 0.58 cm^{3}g^{-1} at p/p^o = 0.98.

5.2.4 Sulfur-based Ladder Polymers of Intrinsic Microporosity (sPIMs)

sPIM-0
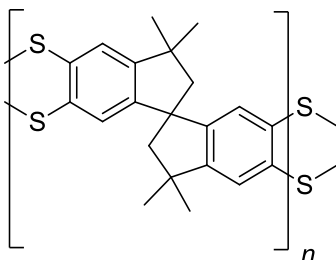
5,5'-Dibromo-6,6'-dithiol-3,3,3',3'-tetramethyl-1,1'-spirobisindane (0.400 g, 0.802 mmol), copper (I) bromide (0.046 g, 0.321 mmol), caesium carbonate (1.05 g, 2.98 mmol) and anhydrous DMSO (5 ml) were added to an oven dried flask and left to stir at 120 °C for 72 hrs. After cooling to RT, the crude reaction mixture was poured into water (200 ml), acidified with 2N HCl (50 ml) and stirred for 2 hrs. The resultant precipitate was collected by filtration, washed with 12N HCl (50 ml), water (2 x 200 ml) and methanol (100 ml), treated with boiling methanol (100 ml) for 12 hrs, filtered and dried under vacuum to give sPIM-0 (0.263 g, 97 %) as an off-white powder (mp > 300 °C); IR (DCM film) 2920, 2856, 1444, 1361, 1277, 1093, 1022 cm^{-1}; BET surface area = 438 m^2 g^{-1}; total pore volume = 0.38 cm^3 g^{-1} at p/p^o = 0.98. TGA (nitrogen): Initial weight loss due to thermal degradation commences at ~ 390 °C.

sPIM-1
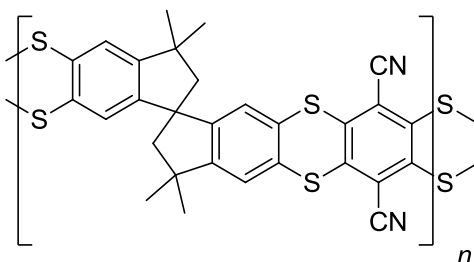
5,5',6,6'-Tetrathiol-3,3,3',3'-tetramethyl-1,1'-spirobisindane (0.537 g, 1.33 mmol), 2,3,5,6-tetrafluoroterephthalonitrile (0.266 g, 1.33 mmol), potassium carbonate (0.733 g, 5.30 mmol) and anhydrous DMF (14 ml) were added to an oven dried flask and stirred at 65 °C for 72 hrs. After cooling to RT, the crude reaction mixture was poured into water (300 ml), acidified with 2N HCl (50 ml) and left to stir for 2 hrs. The resultant precipitate was collected

by filtration, washed with water (300 ml) and methanol (50 ml), treated with boiling methanol (100 ml) for 12 hrs, filtered and dried under vacuum to give sPIM-1 (0.446 g, 95 %) as an orange/yellow powder (mp > 300 °C); IR (DCM film) 2956, 2926, 2864, 2227, 1454, 1364, 1252 cm^{-1}; ^{1}H NMR (500 MHz, CDCl$_3$) δ 7.38 (2H, br s, ArH), 6.88 (2H, br s, ArH), 2.35 – 2.22 (4H, m, CH_2), 1.39 – 1.31 (12H, m, CH_3); ^{13}C NMR (500 MHz, CDCl$_3$) δ 154.5, 151.8, 141.4, 131.4, 125.5, 125.4, 123.7, 123.6, 110.1, 110.0, 107.2, 59.4, 57.3, 44.0, 31.7, 30.0 (one carbon missing); elemental analysis calc. C: 66.38, H: 3.84, N: 5.43, S: 24.44, found C: 60.99, H: 3.73, N: 4.72, S: 22.33; GPC analysis (CHCl$_3$) M_n = 1578, M_w = 6877 g mol^{-1} relative to polystyrene, M_w/M_n = 4.351; BET surface area = 353 m^2 g^{-1}; total pore volume = 0.25 cm^3 g^{-1} at p/p^o = 0.98; TGA (nitrogen): Initial weight loss due to thermal degradation commences at ~ 380 °C.

sPIM-2-diketone
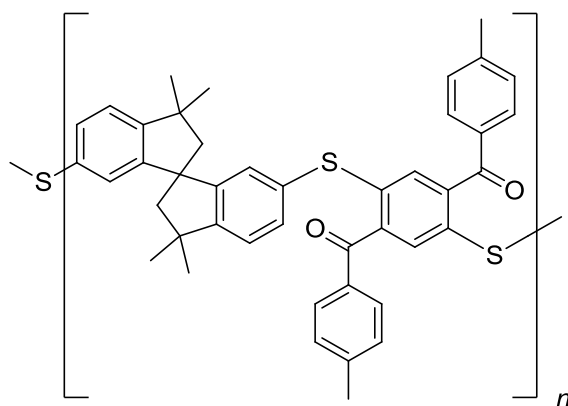
1,4-Dichloro-2,5-bis(4'-methylbenzoyl)benzene (1.129 g, 2.95 mmol), 6,6'-dithiol-3,3,3',3'-tetramethyl-1,1'-spirobisindane (1.003 g, 2.95 mmol) and anhydrous DMAC (5 ml) were heated to 90 °C to form a solution. Potassium carbonate (0.41 g, 2.97 mmol) was then added and the reaction mixture left to stir at 110 °C for 4 days. After cooling to RT, the viscous reaction mixture was poured into water (300 ml), acidified with 2N HCl (50 ml) and left to stir for 2 hrs. The resultant precipitate was collected by filtration, washed with water (300 ml) and methanol (50 ml), treated with boiling methanol (100 ml) for 12 hrs, filtered and dried under vacuum. The crude polymer was purified further by dropwise addition of a concentrated chloroform solution into acetone. After stirring for 2 hrs the resultant precipitate was collected, dried and the re-precipitation process repeated a second time to give sPIM-2-diketone (0.652 g, 34 %) as a yellow powder (mp > 300 °C); IR (DCM film) 2954,

2922, 2862, 1665, 1605, 1458, 1238, 1180, 1091 cm^{-1}; ^{1}H NMR (500 MHz, CDCl$_3$) δ 7.61 – 7.35 (4H, br m, ArH), 7.24 – 6.97 (10H, br m, ArH), 6.60 (2H, br m, ArH), 2.37 – 2.31 (6H, br m, PhCH_3), 2.07 (2H, br m, CH_2), 1.88 (2H, br m, CH_2), 1.18 (6H, br m, CH_3); ^{13}C NMR (500 MHz, CDCl$_3$) δ 194.8, 152.8, 151.3, 144.4, 140.7, 140.7, 135.5, 134.2, 132.4, 131.9, 131.1, 130.4, 130.2, 129.7, 129.6, 129.3, 129.2, 123.3, 110.2, 59.5, 57.6, 43.4, 31.6, 30.2, 22.0, 21.9; elemental analysis calc. C: 79.35, H: 5.88, S: 9.85, Cl: 0.00, found C: 77.50, H: 5.64, S: 10.04, Cl: 0.82; GPC analysis (CHCl$_3$) M_n = 13970, M_w = 21089 g mol^{-1} relative to polystyrene, M_w/M_n = 1.510; BET surface area = 2 m^2 g^{-1}; total pore volume = 0.02 cm^3 g^{-1} at p/p^o = 0.98; TGA (nitrogen): Initial weight loss due to thermal degradation commences at ~ 350 °C.

sPIM-2-diol

A solution of sPIM-2-diketone (0.285 g, 0.438 mmol) in anhydrous THF (15 ml) was added slowly *via* a dropping funnel to a solution of lithium aluminium hydride (0.11 g, 2.90 mmol) in anhydrous THF (12 ml) at RT. Once addition was complete, the solution was allowed to stir for a further 6 hrs at RT, poured over crushed ice (100 ml), stirred for 30 mins, acidified with 2N HCl (100 ml), stirred for 15 mins and extracted into chloroform (3 x 100 ml). The combined organic extracts were washed with 2H HCl (50 ml), water (50 ml) and brine (50 ml) then dried over anhydrous magnesium sulfate and reduced to give sPIM-2-diol (0.280 g, 97 %) as a yellow powder (mp > 300 °C); IR (DCM film) 3434, 2954, 2924, 2863, 2819, 1512, 1472, 1263, 1091 cm^{-1}; ^{1}H NMR (400 MHz, CDCl$_3$) δ 7.45 – 6.71 (16H, br m, ArH), 5.99 (2H, br s, CH), 2.28 – 2.21 (10H, br m, PhCH_3/CH_2), 1.28 (12H, br m, CH_3); ^{13}C NMR (500 MHz, CDCl$_3$) δ 151.4, 137.7, 137.1, 130.4, 129.1, 127.6, 127.6, 123.1, 81.6, 59.7, 59.7, 57.8, 57.7, 57.1, 57.0, 43.5, 31.9, 30.3, 21.4; elemental analysis calc. C: 78.86, H: 6.46, S: 9.79, found C: 77.24, H: 6.53, S: 9.65; GPC analysis (CHCl$_3$) M_n = 14270, M_w = 23900 g mol^{-1} relative to

polystyrene, M_w/M_n = 1.675; BET surface area = 0.00 m^2 g^{-1}; total pore volume = 0.01 cm^3 g^{-1} at p/p^o = 0.98; TGA (nitrogen): Initial weight loss due to thermal degradation commences at ~ 350 °C.
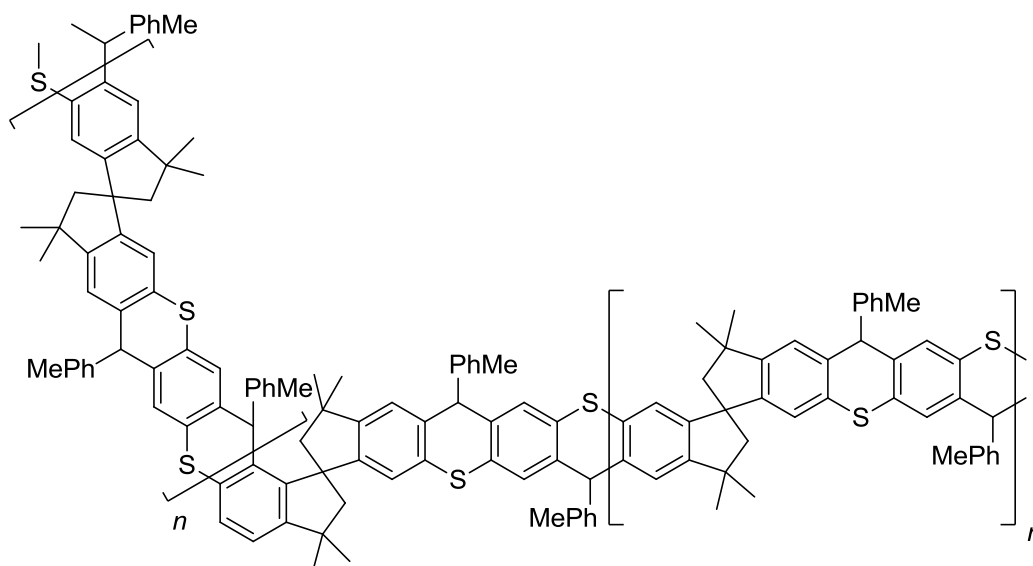
sPIM-2

A solution of sPIM-2-diol (0.165 g, 0.252 mmol) in anhydrous chloroform (15 ml) was added slowly *via* a dropping funnel to a solution of tin (IV) chloride (0.10 ml, 0.86 mmol) in anhydrous chloroform (15 ml) at RT. Once addition was complete, the solution was allowed to stir for a further 3 hrs at RT, 2N HCl (10 ml) added, and stirred for a further 2 hrs. The product was then extracted into chloroform (3 x 50 ml) and the combined organic extracts washed with 2N HCl (100 ml), 1N aqueous sodium hydrogen carbonate solution (100 ml), water (200 ml) and brine (100 ml), dried over anhydrous magnesium sulfate and reduced to give sPIM-2 (0.150 g, 92 %) as a purple solid (mp > 300 °C); IR (DCM film) 3049, 2955, 2924, 2863, 1510, 1467, 1264, 1092 cm^{-1}; ^{1}H NMR (500 MHz, CDCl$_3$) δ 7.58 – 6.75 (14H, br m, ArH), 5.27 (2H, br s, CH), 2.25 (10H, br s, PhCH_3/CH_2), 1.33 (12H, br s, CH_3); ^{13}C NMR (500 MHz, CDCl$_3$) δ 151.4, 136.8, 136.5, 136.1, 135.8, 131.9, 131.4, 129.0, 128.3, 128.0, 128.0, 127.8, 127.7, 125.6, 123.1, 122.9, 59.6, 53.5, 52.7, 43.3, 34.2, 31.8, 31.0, 30.4, 30.3, 29.7; elemental analysis calc. C: 83.45, H: 6.19, S: 10.36, Cl: 0.00, found C: 80.90, H: 6.28, S: 10.00, Cl: 0.71; GPC analysis (CHCl$_3$) M_n = 13158, M_w = 21311 g mol^{-1} relative to polystyrene, M_w/M_n = 1.620; BET surface area = 470 m^2 g^{-1}; total pore volume = 0.43 cm^3 g^{-1} at p/p^o = 0.98; TGA (nitrogen): Initial weight loss due to thermal degradation commences at ~ 410 °C.

6. Bibliography

[1]   J. Rouquerol, D. Avnir, C. W. Fairbridge, D. H. Everett, J. M. Haynes, N. Pernicone, J. D. F. Ramsay, K. Sing, S. W. and K. K. Unger; *Pure Appl. Chem.*, **1994**, 66, 1739.

[2]   F. A. L. Dullien; *Porous media. Fluid transport and pore structure* (Academic Press, **1992**).

[3]   J. Rouquerol, G. Baron, R. Denoyel, H. Giesche, J. Groen, P. Klobes, P. Levitz, A. V. Neimark, S. Rigby, R. Skudas, K. Sing, S. W., M. Thommes and K. Unger; *Pure Appl. Chem.*, **2012**, 84, 107.

[4]   S. Biniak, G. Szymański, J. Siedlewski and A. Świątkowski; *Carbon*, **1997**, 35, 1799.

[5]   L. J. Abbott, A. G. McDermott, A. Del Regno, R. G. D. Taylor, C. G. Bezzu, K. J. Msayib, N. B. McKeown, F. R. Siperstein, J. Runt and C. M. Colina; *J. Phys. Chem. B*, **2013**, 117, 355.

[6]   G. S. Larsen, P. Lin, K. E. Hart and C. M. Colina; *Macromolecules*, **2011**, 44, 6944.

[7]   S. Brunauer, P. H. Emmett and E. Teller; *J. Am. Chem. Soc.*, **1938**, 60, 309.

[8]   I. Langmuir; *J. Am. Chem. Soc.*, **1917**, 39, 1848.

[9]   I. M. K. Ismail; *Carbon*, **1990**, 28, 423.

[10]   K. S. W. Sing, D. H. Everett, R. A. W. Haul, L. Moscou, R. A. Pierotti, J. Rouquerol and T. Siemieniewska; *Pure Appl. Chem.*, **1985**, 57, 603.

[11]   O. Carmody, R. Frost, Y. Xi and S. Kokot; *Surf. Sci.*, **2007**, 601, 2066.

[12]   A. W. Van Den Berg and C. O. Arean; *Chem Commun (Camb)*, **2008**, 668.

[13]   N. B. McKeown, P. M. Budd and D. Book; *Macromol. Rapid Commun.*, **2007**, 28, 995.

[14]   J. Y. Lee, L. Pan, S. P. Kelly, J. Jagiello, T. J. Emge and J. Li; *Adv. Mater. (Weinheim, Ger.)*, **2005**, 17, 2703.

[15]   N. B. McKeown and P. M. Budd; *Chem. Soc. Rev.*, **2006**, 37, 675.

[16]   N. B. McKeown, P. M. Budd, K. J. Msayib, B. S. Ghanem, H. J. Kingston, C. E. Tattershall, S. M. Makhseed, K. J. Reynolds and D. Fritsch; *Chem.-Eur. J.*, **2005**, 11, 2610.

[17]   R. M. de Vos and H. Verweij; *J. Membr. Sci.*, **1998**, 143, 37.

[18]   C.-Y. Sun, S.-X. Liu, D.-D. Liang, K.-Z. Shao, Y.-H. Ren and Z.-M. Su; *J. Am. Chem. Soc.*, **2009**, 131, 1883.

[19]   M. P. Tsyurupa and V. A. Davankov; *React. Funct. Polym.*, **2006**, 66, 768.

[20]   H. van Bekkam, E. M. Flanigen, P. A. Jacobs and J. C. Jansen; *Introduction to zeolite science and practice* (Elsevier, **2001**).

[21]   A. F. Cronstedt; *Akad. Handl. Stockholm*, **1756**, 17, 120.

[22]   A. Corma, M. J. Diaz-Cabanas, J. Martinez-Triguero, F. Rey and J. Rius; *Nature*, **2002**, 418, 514.

[23]   C. C. Freyhardt, M. P. Tsyurupa, R. F. Lobo, K. J. Balkus and M. E. Davis; *Nature*, **1996**, 381, 295.

[24]   O. Lahav and M. Green; *Water Res.*, **1998**, 32, 2019.

[25]   S. M. Robinson, W. D. Arnold and C. H. Byers; *AIChE J.*, **1994**, 40, 2045.

[26]   M. Kuronen, R. Harjula, J. Jernstrom, M. Vestenius and J. Lehto; *Phys. Chem. Chem. Phys.*, **2000**, 2, 2655.

[27]   E. Álvarez-Ayuso, A. García-Sánchez and X. Querol; *Water Res.*, **2003**, 37, 4855.

[28]   F. Su, C. Lu, S.-C. Kuo and W. Zeng; *Energy Fuels*, **2010**, 24, 1441.

[29]   P. Cosoli, M. Ferrone, S. Pricl and M. Fermeglia; *Chem. Eng. J. (Lausanne)*, **2008**, 145, 86.

[30]   K. Smith, A. Musson and G. A. DeBoos; *J. Org. Chem.*, **1998**, 63, 8448.

[31]   K. Smith and G. A. El-Hiti; *Green Chem.*, **2011**, 13, 1579.

[32]   A. Corma; *Chem. Rev. (Washington, DC, U. S.)*, **1997**, 97, 2373.

[33]   J. C. Jansen, J. H. Koegler, H. van Bekkum, H. P. A. Calis, C. M. van den Bleek, F. Kapteijn, J. A. Moulijn, E. R. Geus and N. van der Puil; *Micropor. Mesopor. Mater.*, **1998**, 21, 213.

[34]   M. Boronat, P. M. Viruela and A. Corma; *J. Am. Chem. Soc.*, **2004**, 126, 3300.

[35]   A. Corma; *J. Catal.*, **2003**, 216, 298.

[36]   H. Li, M. Eddaoudi, M. O'Keeffe and O. M. Yaghi; *Nature*, **1999**, 402, 276.

[37]   K. Koh, A. G. Wong-Foy and A. J. Matzger; *J. Am. Chem. Soc.*, **2009**, 131, 4184.

[38]   O. K. Farha, I. Eryazici, N. C. Jeong, B. G. Hauser, C. E. Wilmer, A. A. Sarjeant, R. Q. Snurr, S. T. Nguyen, A. Ö. Yazaydın and J. T. Hupp; *J. Am. Chem. Soc.*, **2012**, 134, 15016.

[39]   O. M. Yaghi, H. Li, C. Davis, D. Richardson and T. L. Groy; *Acc. Chem. Res.*, **1998**, 31, 474.

[40]   C. J. Kepert and M. J. Rosseinsky; *Chem. Commun. (Cambridge, U. K.)*, **1999**, 0, 375.

[41]   SciFinder, **2013**, Search performed 17/06/13. Search criteria: [year = 1999, research topic = 'metal organic framework(s)' - 11 references containing concept found]. [year = 2012, research topic = 'metal organic framework(s) - 2496 references containing concept found].

[42]   N. L. Rosi, J. Eckert, M. Eddaoudi, D. T. Vodak, J. Kim, M. O'Keeffe and O. M. Yaghi; *Science*, **2003**, 300, 1127.

[43]   Y. He, W. Zhou, R. Krishna and B. Chen; *Chem. Commun. (Cambridge, U. K.)*, **2012**, 48, 11813.

[44]   J.-R. Li, R. J. Kuppler and H.-C. Zhou; *Chem. Soc. Rev.*, **2009**, 38, 1477.

[45]   K. K. Tanabe and S. M. Cohen; *Angew. Chem., Int. Ed.*, **2009**, 48, 7424.

[46]   B. Chen, S. Xiang and G. Qian; *Acc. Chem. Res.*, **2010**, 43, 1115.

[47]   P. Horcajada, T. Chalati, C. Serre, B. Gillet, C. Sebrie, T. Baati, J. F. Eubank, D. Heurtaux, P. Clayette, C. Kreuz, J.-S. Chang, Y. K. Hwang, V. Marsaud, P.-N. Bories, L. Cynober, S. Gil, G. Ferey, P. Couvreur and R. Gref; *Nat. Mater.*, **2010**, 9, 172.

[48]   O. K. Farha and J. T. Hupp; *Acc. Chem. Res.*, **2010**, 43, 1166.

[49]   H. Furukawa and O. M. Yaghi; *J. Am. Chem. Soc.*, **2009**, 131, 8875.

[50]   H. M. El-Kaderi, J. R. Hunt, J. L. Mendoza-Cortés, A. P. Côté, R. E. Taylor, M. O'Keeffe and O. M. Yaghi; *Science*, **2007**, 316, 268.

[51]   P. Kuhn, M. Antonietti and A. Thomas; *Angew. Chem., Int. Ed.*, **2008**, 47, 3450.

[52]   F. J. Uribe-Romo, J. R. Hunt, H. Furukawa, C. Klöck, M. O'Keeffe and O. M. Yaghi; *J. Am. Chem. Soc.*, **2009**, 131, 4570.

[53]   K. S. Novoselov, A. K. Geim, S. V. Morozov, D. Jiang, Y. Zhang, S. V. Dubonos, I. V. Grigorieva and A. A. Firsov; *Science*, **2004**, 306, 666.

[54]   Y. Tian, B. Xu, D. Yu, Y. Ma, Y. Wang, Y. Jiang, W. Hu, C. Tang, Y. Gao, K. Luo, Z. Zhao, L.-M. Wang, B. Wen, J. He and Z. Liu; *Nature*, **2013**, 493, 385.

[55]   X. Feng, X. Ding and D. Jiang; *Chem. Soc. Rev.*, **2012**, 41, 6010.

[56]   S. S. Han, H. Furukawa, O. M. Yaghi and W. A. Goddard; *J. Am. Chem. Soc.*, **2008**, 130, 11580.

[57]   C. J. Doonan, D. J. Tranchemontagne, T. G. Glover, J. R. Hunt and O. M. Yaghi; *Nature Chem.*, **2010**, 2, 235.

[58]   S.-Y. Ding, J. Gao, Q. Wang, Y. Zhang, W.-G. Song, C.-Y. Su and W. Wang; *J. Am. Chem. Soc.*, **2011**, 133, 19816.

[59]   Y. Zhou, Z. Wang, P. Yang, X. Zu and F. Gao; *J. Mater. Chem.*, **2012**, 22, 16964.

[60]   S. Wan, J. Guo, J. Kim, H. Ihee and D. Jiang; *Angew. Chem., Int. Ed.*, **2008**, 47, 8826.

[61]   A. P. Côté, A. I. Benin, N. W. Ockwig, M. O'Keeffe, A. J. Matzger and O. M. Yaghi; *Science*, **2005**, 310, 1166.

[62]   L.-P. Ma, Z.-S. Wu, J. Li, E.-D. Wu, W.-C. Ren and H.-M. Cheng; *Int. J. Hydrogen Energy*, **2009**, 34, 2329.

[63]   S. Cheng; *Catal. Today*, **1999**, 49, 303.

[64]   P. J. Florey; *Principle of polymer chemistry* (Cornell Univ. Press, Ithaca, NY, **1953**).

[65]   G. Couderc, T. Hertzsch, N. R. Behrnd, K. Krämer and J. Hulliger; *Micropor. Mesopor. Mater.*, **2006**, 88, 170.

[66]   P. Sozzani, S. Bracco, A. Comotti, L. Ferretti and R. Simonutti; *Angew. Chem., Int. Ed.*, **2005**, 44, 1816.

[67]   T. Hertzsch, C. Gervais, J. Hulliger, B. Jaeckel, S. Guentay, H. Bruchertseifer and A. Neels; *Adv. Funct. Mater.*, **2006**, 16, 268.

[68]   T. Tozawa, J. T. A. Jones, S. I. Swamy, S. Jiang, D. J. Adams, S. Shakespeare, R. Clowes, D. Bradshaw, T. Hasell, S. Y. Chong, C. Tang, S. Thompson, J. Parker, A. Trewin, J. Bacsa, A. M. Z. Slawin, A. Steiner and A. I. Cooper; *Nat. Mater.*, **2009**, 8, 973.

[69]   M. J. Bojdys, M. E. Briggs, J. T. A. Jones, D. J. Adams, S. Y. Chong, M. Schmidtmann and A. I. Cooper; *J. Am. Chem. Soc.*, **2011**, 133, 16566.

[70]   Y. Jiao, F. H. Stillinger and S. Torquato; *Phys. Rev. E*, **2009**, 79, 041309.

[71]   M. Mastalerz, M. W. Schneider, I. M. Oppel and O. Presly; *Angew. Chem., Int. Ed.*, **2011**, 50, 1046.

[72]   T. M. Long and T. M. Swager; *Adv. Mater. (Weinheim, Ger.)*, **2001**, 13, 601.

[73]   B. S. Ghanem, M. Hashem, K. D. M. Harris, K. J. Msayib, M. Xu, P. M. Budd, N. Chaukura, D. Book, S. Tedds, A. Walton and N. B. McKeown; *Macromolecules*, **2010**, 43, 5287.

[74]   B. S. Ghanem, K. J. Msayib, N. B. McKeown, K. D. M. Harris, Z. Pan, P. M. Budd, A. Butler, J. Selbie, D. Book and A. Walton; *Chem. Commun. (Cambridge, U. K.)*, **2007**, 0, 67.

[75]   Y.-C. Zhao, Q.-Y. Cheng, D. Zhou, T. Wang and B.-H. Han; *J. Mater. Chem.*, **2012**, 22, 11509.

[76]   M. M. Forde, C. G. Bezzu, R. Armstrong, R. L. Jenkins, M. H. A. Rahim, A. F. Carley, N. Dimitratos, J. A. Lopez-Sanchez, S. H. Taylor, N. B. McKeown and G. J. Hutchings; *J. Catal.*, **2012**, 290, 177.

[77]   N. B. McKeown, S. Makhseed, K. J. Msayib, L.-L. Ooi, M. Helliwell and J. E. Warren; *Angew. Chem., Int. Ed.*, **2005**, 44, 7546.

[78]   M. S. Park, W. Joo and J. K. Kim; *Langmuir*, **2006**, 22, 4594.

[79]   A. F. Bushell, P. M. Budd, M. P. Attfield, J. T. A. Jones, T. Hasell, A. I. Cooper, P. Bernardo, F. Bazzarelli, G. Clarizia and J. C. Jansen; *Angew. Chem., Int. Ed.*, **2013**, 52, 1253.

[80]   H. Marsh and F. Rodríguez-Reinoso; *Activated carbon* (Elsevier, **2006**).

[81]   S. M. Manocha; *Sadhana*, **2003**, 28, 335.

[82]   N. N. Greenwood and A. Earnshaw; *Chemistry of the elements* (ed. Elsevier) (**1997**).

[83]   M. Jordá-Beneyto, F. Suárez-García, D. Lozano-Castelló, D. Cazorla-Amorós and A. Linares-Solano; *Carbon*, **2007**, 45, 293.

[84]   M. Rattier, J. Reungoat, W. Gernjak, A. Joss and J. Keller; *J. Water Reuse Desal.*, **2012**, 2, 127.

[85]   M. N. Eshtiaghi, J. Kuldiloke and N. Yoswathana; *J. Food, Agric.Environ.*, **2013**, 10, 178

[86]   F. Zhang and J. Yu; *Bioprocess Engineering*, **2000**, 23, 295.

[87]   D. Lennon, D. T. Lundie, S. D. Jackson, G. J. Kelly and S. F. Parker; *Langmuir*, **2002**, 18, 4667.

[88]   D. Hulicova-Jurcakova, M. Seredych, G. Q. Lu and T. J. Bandosz; *Adv. Funct. Mater.*, **2009**, 19, 438.

[89]   G. I. Rosenberg, A. S. Shabaeva, V. S. Moryakov, T. G. Musin, M. P. Tsyurupa and V. A. Davankov; *Reactive Polymers, Ion Exchangers, Sorbents*, **1983**, 1, 175.

[90]   J. Germain, J. Hradil, J. M. J. Fréchet and F. Svec; *Chem. Mater.*, **2006**, 18, 4430.

[91]   J. Germain, J. M. J. Frechet and F. Svec; *J. Mater. Chem.*, **2007**, 17, 4989.

[92]   J.-H. Ahn, J.-E. Jang, C.-G. Oh, S.-K. Ihm, J. Cortez and D. C. Sherrington; *Macromolecules*, **2005**, 39, 627.

[93]   J. D. Fowler, S. Virji, R. B. Kaner and B. H. Weiller; *J. Phys. Chem. C*, **2009**, 113, 6444.

[94]   K. Roßberg, G. Paasch, L. Dunsch and S. Ludwig; *J. Electroanal. Chem.*, **1998**, 443, 49.

[95]   T. Ben, H. Ren, S. Ma, D. Cao, J. Lan, X. Jing, W. Wang, J. Xu, F. Deng, Jason M. Simmons, S. Qiu and G. Zhu; *Angew. Chem., Int. Ed.*, **2009**, 48, 9457.

[96]   T. Yamamoto, S. Wakabayashi and K. Osakada; *J. Organomet. Chem.*, **1992**, 428, 223.

[97]   J. R. Holst and A. I. Cooper; *Adv. Mater. (Weinheim, Ger.)*, **2010**, 22, 5212.

[98]   T. Ben and S. Qiu; *CrystEngComm*, **2013**, 15, 17.

[99]   H. Ren, T. Ben, E. Wang, X. Jing, M. Xue, B. Liu, Y. Cui, S. Qiu and G. Zhu; *Chem. Commun. (Cambridge, U. K.)*, **2010**, 46, 291.

[100]   H. Ren, T. Ben, F. Sun, M. Guo, X. Jing, H. Ma, K. Cai, S. Qiu and G. Zhu; *J. Mater. Chem.*, **2011**, 21, 10348.

[101]   J. Lan, D. Cao, W. Wang, T. Ben and G. Zhu; *J. Phys. Chem. Lett.*, **2010**, 1, 978.

[102]   Y. Yuan, F. Sun, H. Ren, X. Jing, W. Wang, H. Ma, H. Zhao and G. Zhu; *J. Mater. Chem.*, **2011**, 21, 13498.

[103] P. M. Budd, B. S. Ghanem, S. M. Makhseed, N. B. McKeown, K. J. Msayib and C. E. Tattershall; *Chem. Commun. (Cambridge, U. K.)*, **2004**, 230.

[104] P. M. Budd, B. Ghanem, K. Msayib, N. B. McKeown and C. Tattershall; *J. Mater. Chem.*, **2003**, 13, 2721.

[105] N. B. McKeown, S. Makhseed and P. M. Budd; *Chem. Commun. (Cambridge, U. K.)*, **2002**, 0, 2780.

[106] N. B. McKeown, S. Hanif, K. Msayib, C. E. Tattershall and P. M. Budd; *Chem. Commun. (Cambridge, U. K.)*, **2002**, 0, 2782.

[107] S. Ogasawara and S. Kato; *J. Am. Chem. Soc.*, **2010**, 132, 4608.

[108] L. M. Robeson; *J. Membr. Sci.*, **1991**, 62, 165.

[109] L. M. Robeson; *J. Membr. Sci.*, **2008**, 320, 390.

[110] M. Carta, R. Malpass-Evans, M. Croad, Y. Rogan, J. C. Jansen, P. Bernardo, F. Bazzarelli and N. B. McKeown; *Science*, **2013**, 339, 303.

[111] H. Liu and E. Min; *Green Chem.*, **2006**, 8, 657.

[112] C. G. Bezzu, M. Helliwell, J. E. Warren, D. R. Allan and N. B. McKeown; *Science*, **2010**, 327, 1627.

[113] H. J. Mackintosh, P. M. Budd and N. B. McKeown; *J. Mater. Chem.*, **2008**, 18, 573.

[114] K. J. Balkus, M. Eissa and R. Levado; *J. Am. Chem. Soc.*, **1995**, 117, 10753.

[115] P. Karandikar, A. J. Chandwadkar, M. Agashe, N. S. Ramgir and S. Sivasanker; *Appl. Catal., A*, **2006**, 297, 220.

[116] D. Wöhrle and B. Schulte; *Macromol. Chem. Phys.*, **1988**, 189, 1229.

[117] M. Hashem, C. Grazia Bezzu, B. M. Kariuki and N. B. McKeown; *Polym. Chem.*, **2011**, 2, 2190.

[118] B. Meunier; *Chem. Rev. (Washington, DC, U. S.)*, **1992**, 92, 1411.

[119] J. S. Lindsey, I. C. Schreiman, H. C. Hsu, P. C. Kearney and A. M. Marguerettaz; *J. Org. Chem*, **1987**, 52, 827.

[120] K. M. Kadish, B. C. Han, M. M. Franzen and C. Araullo-McAdams; *J. Am. Chem. Soc.*, **1990**, 112, 8364.

[121] G. Kestemont, V. d. Halleux, M. Lehmann, D. A. Ivanov, M. Watson and Y. Henri Geerts; *Chem. Commun. (Cambridge, U. K.)*, **2001**, 0, 2074.

[122] A. S. Lindsey; *J. Chem. Soc (Resumed)*, **1965**, 0, 1685.

[123] A. Collet; *Tetrahedron*, **1987**, 43, 5725.

[124] N. B. McKeown, B. Gahnem, K. J. Msayib, P. M. Budd, C. E. Tattershall, K. Mahmood, S. Tan, D. Book, H. W. Langmi and A. Walton; *Angew. Chem., Int. Ed.*, **2006**, 45, 1804.

[125] J. Tellenbröker and D. Kuck; *Angew. Chem., Int. Ed.*, **1999**, 38, 919.

[126] J. Vile, M. Carta, C. G. Bezzu and N. B. McKeown; *Polym. Chem.*, **2011**, 2, 2257.

[127] H. Hart, A. Bashir-Hashemi, J. Luo and M. A. Meador; *Tetrahedron*, **1986**, 42, 1641.

[128] R. E. Morris and P. S. Wheatley; *Angew. Chem., Int. Ed.*, **2008**, 47, 4966.

[129] J. Tian, P. K. Thallapally, S. J. Dalgarno, P. B. McGrail and J. L. Atwood; *Angew. Chem., Int. Ed.*, **2009**, 48, 5492.

[130] H. Kudo, R. Hayashi, K. Mitani, T. Yokozawa, N. C. Kasuga and T. Nishikubo; *Angew. Chem., Int. Ed.*, **2006**, 45, 7948.

[131] J. H. Chong, S. J. Ardakani, K. J. Smith and M. J. MacLachlan; *Chem.-Eur. J.*, **2009**, 15, 11824.

[132] S. Jiang, J. T. A. Jones, T. Hasell, C. E. Blythe, D. J. Adams, A. Trewin and A. I. Cooper; *Nat Commun*, **2011**, 2, 207.

[133] J. Tian, S. Ma, P. K. Thallapally, D. Fowler, B. P. McGrail and J. L. Atwood; *Chem. Commun. (Cambridge, U. K.)*, **2011**, 47, 7626.

[134] T. Hasell, X. Wu, T. A. JonesJames, J. Bacsa, A. Steiner, T. Mitra, A. Trewin, D. J. Adams and A. I. Cooper; *Nature Chem.*, **2010**, 2, 750.

[135] C. D. Meyer, C. S. Joiner and J. F. Stoddart; *Chem. Soc. Rev.*, **2007**, 36, 1705.

[136] N. B. McKeown; *J. Mater. Chem.*, **2010**, 20, 10588.

[137] N. B. McKeown and P. M. Budd; *Macromolecules*, **2010**, 43, 5163.

[138] A. I. Kitaigorodsky; *Molecular cystals and molecules* (Academic Press, New York and London, **1973**).

[139] Y. Jiao, F. H. Stillinger and S. Torquato; *Phys. Rev. Lett.*, **2008**, 100, 245504.

[140] B. S. Ghanem; *Polym. Chem.*, **2012**, 3, 96.

[141] J. K. E. Walker, **2010**, Thesis: *Novel polymers and dendrimers of intrinsic microporosity derived from triptycene and other monomers of high internal free volume*, Cardiff University.

[142] 1. Sigma-aldrich, *http://www.sigmaaldrich.com/catalog/product/aldrich/362662?lang=en&region=GB*.

[143] T. Kaneko, **2005**, Patent No. JP 2006273766, *Preparation of 2,2',3,3',5,5',6,6'-octafluoro-4,4'-biphenyldicarbonitrile from pentafluorobenzonitrile*.

[144] P. M. Budd, E. S. Elabas, B. S. Ghanem, S. Makhseed, N. B. McKeown, K. J. Msayib, C. E. Tattershall and D. Wang; *Adv. Mater. (Weinheim, Ger.)*, **2004**, 16, 456.

[145] J. Huang and M. Kertesz; *J. Am. Chem. Soc.*, **2007**, 129, 1634.

[146] A. Stepakov, A. Molchanov and R. Kostikov; *Russ. J. Org. Chem.*, **2007**, 43, 538.

[147] X.-X. Peng, H.-Y. Lu, T. Han and C.-F. Chen; *Org. Lett.*, **2007**, 9, 895.

[148] B. H. Klanderman and T. R. Criswell; *J. Org. Chem*, **1969**, 34, 3426.

[149] N. Herron, M. A. Guidry, V. Rostovtsev, V. J. North, J. A. Merlo and K. Dogra, **2008**, Patent No. WO 2008150828, *Green luminescent aminoanthracene derivatives and photoactive devices using them*.

[150] E. Yagodkin and C. J. Douglas; *Tetrahedron Lett.*, **2010**, 51, 3037.

[151] P. P. Fu and R. G. Harvey; *J. Org. Chem*, **1977**, 42, 2407.

[152] X.-Z. Zhu and C.-F. Chen; *J. Am. Chem. Soc.*, **2005**, 127, 13158.

[153] C. E. Wagner, P. W. Jurutka, P. A. Marshall, T. L. Groy, A. van der Vaart, J. W. Ziller, J. K. Furmick, M. E. Graeber, E. Matro, B. V. Miguel, I. T. Tran, J. Kwon, J. N. Tedeschi, S. Moosavi, A. Danishyar, J. S. Philp, R. O. Khamees, J. N. Jackson, D. K. Grupe, S. L. Badshah and J. W. Hart; *J. Med. Chem.*, **2009**, 52, 5950.

[154] J. Bouffard, R. F. Eaton, P. Müller and T. M. Swager; *J. Org. Chem*, **2007**, 72, 10166.

[155] N. Nakamura; *Chem. Lett.*, **1983**, 12, 1795.

[156] C. E. Godinez, G. Zepeda, C. J. Mortko, H. Dang and M. A. Garcia-Garibay; *J. Org. Chem*, **2004**, 69, 1652.

[157] M. Rybáčková, M. Bělohradský, P. Holý, R. Pohl, V. Dekoj and J. Závada; *Synthesis*, **2007**, 2007, 1554.

[158] Lionxi, *https://rcc.its.psu.edu/resources/hpc/lionxi*.

[159] T. Düren, F. Millange, G. Férey, K. S. Walton and R. Q. Snurr; *J. Phys. Chem. C*, **2007**, 111, 15350.

[160] Interactive structure analysis of amorphous and crystalline systems, *http://isaacs.sourceforge.net/*.

[161] C. G. Bezzu, K. J. Msayib, R. G. D. Taylor, J. Walker, L. J. Abbott, C. M. Colina, A. G. McDermott, J. Runt, L. Maynard-Atem, P. M. Budd, M. Helliwell and N. B. McKeown; *In preparation*

[162] P. J. Flory; *J. Am. Chem. Soc.*, **1941**, 63, 3083.

[163] P. J. Flory; *J. Am. Chem. Soc.*, **1952**, 74, 2718.

[164] D. A. Tomalia, H. Baker, J. Dewald, M. Hali, G. Kallos, S. Martin, J. Roeck, J. Ryder and P. Smith; *Polym. J. (Tokyo, Jpn.)*, **1985**, 17, 117.

[165] O. A. Matthews, A. N. Shipway and J. F. Stoddart; *Prog. Polym. Sci.*, **1998**, 23, 1.

[166] R. Esfand and D. A. Tomalia; *Drug Discovery Today*, **2001**, 6, 427.

[167] D. A. Tomalia and J. M. J. Fréchet; *J. Polym. Sci. A Polym. Chem.*, **2002**, 40, 2719.

[168] E. Buhleier, W. Wehner and F. Vögtle; *Synthesis*, **1978**, 1978, 155.

[169] C. J. Hawker and J. M. J. Frechet; *J. Am. Chem. Soc.*, **1990**, 112, 7638.

[170] Y. V. Shklyaev and Y. V. Nifontov; *Russ. Chem. Bull.*, **2002**, 51, 844.

[171] N. Schweigert, A. J. B. Zehnder and R. I. L. Eggen; *Environmental Microbiology*, **2001**, 3, 81.

[172] P. M. Budd, S. M. Makhseed, B. S. Ghanem, K. J. Msayib, C. E. Tattershall and N. B. McKeown; *Materials Today*, **2004**, 7, 40.

[173] P. M. Budd, N. B. McKeown and D. Fritsch; *J. Mater. Chem.*, **2005**, 15, 1977.

[174] N. Du, H. B. Park, G. P. Robertson, M. M. Dal-Cin, T. Visser, L. Scoles and M. D. Guiver; *Nat. Mater.*, **2011**, 10, 372.

[175] N. Du, G. P. Robertson, M. M. Dal-Cin, L. Scoles and M. D. Guiver; *Polymer*, **2012**, 53, 4367.

[176] C. R. Mason, L. Maynard-Atem, N. M. Al-Harbi, P. M. Budd, P. Bernardo, F. Bazzarelli, G. Clarizia and J. C. Jansen; *Macromolecules*, **2011**, 44, 6471.

[177] M. A. Hickner, H. Ghassemi, Y. S. Kim, B. R. Einsla and J. E. McGrath; *Chem. Rev. (Washington, DC, U. S.)*, **2004**, 104, 4587.

[178] M. A. Gauthier, M. I. Gibson and H.-A. Klok; *Angew. Chem., Int. Ed.*, **2009**, 48, 48.

[179] S. Hosoya; *Acta Crystallogr.*, **1963**, 16, 310.

[180] C. L. Aitken, W. J. Koros and D. R. Paul; *Macromolecules*, **1992**, 25, 3651.

[181] B. Zhang, G. Shen, Y. Wu, T. Wang, J. Qiu, T. Xu and C. Fu; *Ind. Eng. Chem. Res.*, **2009**, 48, 2886.

[182] N. Du, G. P. Robertson, J. Song, I. Pinnau, S. Thomas and M. D. Guiver; *Macromolecules*, **2008**, 41, 9656.

[183] N. Du, G. P. Robertson, I. Pinnau and M. D. Guiver; *Macromolecules*, **2009**, 42, 6023.

[184] N. Du, G. P. Robertson, I. Pinnau and M. D. Guiver; *Macromolecules*, **2010**, 43, 8580.

[185] M. S. Newman and H. A. Karnes; *J. Org. Chem*, **1966**, 31, 3980.

[186] H. Kwart and E. R. Evans; *J. Org. Chem*, **1966**, 31, 410.

[187] J. N. Harvey, J. Jover, G. C. Lloyd-Jones, J. D. Moseley, P. Murray and J. S. Renny; *Angew. Chem., Int. Ed.*, **2009**, 48, 7612.

[188] G. C. Lloyd-Jones, J. D. Moseley and J. S. Renny; *Synthesis*, **2008**, 2008, 661.

[189] H. Meier and N. Rumpf; *Tetrahedron Lett.*, **1998**, 39, 9639.

[190] D. M. Giolando and K. Kirschbaum; *Synthesis*, **1992**, 1992, 451.

[191] W.-F. Chen, H.-Y. Lin and S. A. Dai; *Org. Lett.*, **2004**, 6, 2341.

[192] T. Sugioka and A. S. Hay; *J. Polym. Sci., Part A: Polym. Chem.*, **2001**, 39, 1040.

[193] E. Block, V. Eswarakrishnan, M. Gernon, G. Ofori-Okai, C. Saha, K. Tang and J. Zubieta; *J. Am. Chem. Soc.*, **1989**, 111, 658.

[194] H. Goto and Y. Komata, **1991**, Patent No. JP 03148232, *Preparation of 5,6,5',6'-tetrahydroxy-1,1'-spirobisindans as materials for color photography image stabilizers*.

[195] A. Dei and L. Sorace; *Dalton Trans.*, **2003**, 0, 3382.

[196] T. Shinichi and S. Michio, **1995**, Patent No. JP 07173130, *Production of ortho-benzenedithiol*.

[197] C. L. Hilton, C. R. Jamison, H. K. Zane and B. T. King; *J. Org. Chem*, **2008**, 74, 405.

[198] R. Adams, W. Reifschneider and A. Ferretti; *Org. Synth.*, **1962**, 42, 22.

[199] A. Ferretti; *Org. Synth.*, **1962**, 42, 54.

[200] R. Gleiter and J. Uschmann; *J. Org. Chem*, **1986**, 51, 370.

[201] L. R. C. Barclay and R. A. Chapman; *Can. J. Chem.*, **1964**, 42, 25.

[202] K. Li, Z. Xu, H. Xu and J. M. Ryan; *Chem. Mater.*, **2005**, 17, 4426.

[203] Z. Xu, K. Li, J. C. Fettinger, J. Li and M. M. King; *Cryst. Growth Des.*, **2004**, 5, 423.

[204] D. Coucouvanis, A. R. Paital, Q. Zhang, N. Lehnert, R. Ahlrichs, K. Fink, D. Fenske, A. K. Powell and Y. Lan; *Inorg. Chem.*, **2009**, 48, 8830.

[205] K. E. Hart, L. J. Abbott, N. B. McKeown and C. M. Colina; *Macromolecules*, **2013**,

[206] S. V. Ley and A. W. Thomas; *Angew. Chem., Int. Ed.*, **2003**, 42, 5400.

[207] M. C. Bagley, M. C. Dix and V. Fusillo; *Tetrahedron Lett.*, **2009**, 50, 3661.

[208] M. H. Ali and M. McDermott; *Tetrahedron Lett.*, **2002**, 43, 6271.

[209] Y. Ding and A. S. Hay; *Macromolecules*, **1996**, 29, 6386.

[210] D. E. Pearson, R. D. Wysong and C. V. Breder; *J. Org. Chem*, **1967**, 32, 2358.

[211] S. Sharma, J. Rajaram and J. C. Kuriacose; *Indian J. Chem., Sect. B: Org. Chem. Incl. Med. Chem.*, **1977**, 15B, 274.

[212]   A. K. Verma, J. Singh and R. Chaudhary; *Tetrahedron Lett.*, **2007**, 48, 7199.
[213]   Y. Li, X. Li, H. Wang, T. Chen and Y. Xie; *Synthesis*, **2010**, 2010, 3602.
[214]   Y. Feng, H. Wang, F. Sun, Y. Li, X. Fu and K. Jin; *Tetrahedron*, **2009**, 65, 9737.
[215]   Y. Yuan, I. Thomé, S. H. Kim, D. Chen, A. Beyer, J. Bonnamour, E. Zuidema, S. Chang and C. Bolm; *Adv. Synth. Catal.*, **2010**, 352, 2892.
[216]   T. Freund, K. Muellen and U. Scherf; *Macromolecules*, **1995**, 28, 547.
[217]   U. Scherf and K. Müllen; *Die Mackromol. Chem. Rapid. Comm.*, **1991**, 12, 489.
[218]   Q. Xiao, R. Lui, H. Chen, J. Chang and H. Zhu; *Nanjing Gongye Daxue Xuebao*, **2010**, 32, 81.
[219]   2. Sigma-aldrich, *http://www.sigmaaldrich.com/catalog/product/aldrich/s437174?lang=en&region=GB*.
[220]   G. A. Eller, V. Wimmer and W. Holzer; *Chem. Heterocycl. Compd. (N. Y., NY, U. S.)*, **2007**, 43, 1060.
[221]   S. N. Tverdomed, A. V. Dogadina and B. I. Ionin; *Russ. J. Gen. Chem.*, **2006**, 76, 663.
[222]   D. M. McKinnon and A. A. Abouzeid; *J. Heterocycl. Chem.*, **1991**, 28, 445.
[223]   F. F. Shcherbina, I. A. Ral'chuk, A. V. Yazlovitskii, S. D. Rudenko, N. M. Khrinyuk and A. A. Grigor'ev; *Zh. Prikl. Khim. (Leningrad)*, **1990**, 63, 467.
[224]   H. Kakinuma, T. Oi, Y. Hashimoto-Tsuchiya, M. Arai, Y. Kawakita, Y. Fukasawa, I. Iida, N. Hagima, H. Takeuchi, Y. Chino, J. Asami, L. Okumura-Kitajima, F. Io, D. Yamamoto, N. Miyata, T. Takahashi, S. Uchida and K. Yamamoto; *J. Med. Chem.*, **2010**, 53, 3247.
[225]   J. P. Gunning, J. W. Levell, M. F. Wyatt, P. L. Burn, J. Robertson and I. D. W. Samuel; *Polym. Chem.*, **2010**, 1, 730.
[226]   J. M. Birchall, R. N. Haszeldine and M. E. Jones; *J. Chem. Soc. C*, **1971**, 0, 1343.
[227]   A. Alberola, R. Less, F. Palacio, C. Pask and J. Rawson; *Molecules*, **2004**, 9, 771.
[228]   L. E. Marinina, V. I. Alekseeva, L. P. Sawina and E. A. Luk'yanets; *Chem. Heterocycl. Compd. (N. Y., NY, U. S.)*, **1988**, 24, 220.
[229]   K. Gong, X. Zhu, R. Zhao, S. Xiong, L. Mao and C. Chen; *Anal. Chem.*, **2005**, 77, 8158.
[230]   J. Wang, W. Wan, H. Jiang, Y. Gao, X. Jiang, H. Lin, W. Zhao and J. Hao; *Org. Lett.*, **2010**, 12, 3874.
[231]   G. S. Bajwa, K. D. Berlin and H. A. Pohl; *J. Org. Chem*, **1976**, 41, 145.
[232]   K. Y. Tsang, S. Sinha, X. Liu, S. Bhat and R. Chandraratna, **2005**, Patent No. US 20050148590, *Disubstituted chalcone oximes as selective agonists of rar retinoid receptors*.
[233]   M. T. Rahman, S. L. Saha and A. T. Hansson; *J. Organomet. Chem.*, **1980**, 199, 9.
[234]   A. Hoffman; *J. Am. Chem. Soc.*, **1929**, 51, 2542.
[235]   R. Adams, W. Reifschneider, A. Ferretti, W. E. Parham, W. E. Noland and J. R. Throckmorton; *Org. Synth.*, **1962**, 42, 22.
[236]   M. Cachia; *Bull. Soc. Chim. Fr.*, **1956**, 1234.
[237]   A. S. Wheeler and I. V. Giles; *J. Am. Chem. Soc.*, **1922**, 44, 2605.